An assessment of the effects of pozzolanic activity on the behaviour of fly ash

Andrew Adams

An Assessment of the effects of Pozzolanic Activity on the Behaviour of Fly Ash

by

Andrew Adams, M.Sc

submitted to

University of Durham, School of Engineering

for the degree of Doctor of Philosophy

2000

ABSTRACT

This research used the ideas and methods, employed in previous studies of residual and weakly bonded soils, to help understand the shear strength and yielding characteristics of pozzolanically reacted fly ash. Samples of lagoon fly ash were supplemented by manufactured samples of fly ash/lime mortar. These were necessary to address the problem of wide variations and lack of observed bonding found in early tests on lagoon fly ash. The manufactured samples proved to be stronger and stiffer with a greater consistence between specimens, although their internal structure proved to be clumpy and the de-bonding method failed to remove all the bonding. The two forms of fly ash showed that the pozzolanic bonding was affected by confining pressure and axial strains. Under undrained conditions the build up of pore water pressures was shown to reduce the influence of pozzolanic bonding in stress space. The critical state line derived for the lagoon fly ash was linear to the extent of tsing conditions and also adequately described those of the mortar fly ash. As no one method for analysing the yielding characteristics could be found, a number of methods were cross-referenced in this research. Both forms of fly ash showed multiple yields that could be resolved to match the classic First and Second yield model. The loci of yields identified demonstrated the isotropic and anistropic nature of the mortar and lagoon fly ashes respectively. Despite the variations seen in the lagoon fly ash samples and the difference with the mortar samples the results point to common critical state parameters for unbonded fly ash and limiting condition for pozzolanic bonding within stress space.

Table of Contents

List of Figures

List of Plates

List of Tables

1. Introduction

This research is based on a man-made waste product called Fly Ash (sometimes known as Pulverised Fuel Ash (PFA)). Fly ash is a member of a group of materials known as 'Pozzolans', which have the ability to form a cementing medium with lime in the presence of moisture. This is termed a pozzolanic reaction. It is similar to the hydration of Portland cement but not as strong. The aim of this research was to understand the shear strength and yield behaviour of weak bonding formed in pozzolanically reacted fly ash. This information could further the understanding of the fundamental behaviour of weakly bonded material.

Most pozzolans are man-made siliceous ash products from furnaces, but some do occur naturally such as volcanic ash. These naturally occurring pozzolans were discovered by the Romans and used to form the first cements. The term pozzolan derives from the town Pozzolini, in Italy, where the Romans found the best volcanic ashes. The pozzolanic reaction occurs at room temperature and appears to rely on the fineness of the material and the amorphous nature caused by rapid cooling. Fly ash is relatively unique in the group of pozzolans due to the occasional occurrence of aluminium in the silicon dioxide glass. The aluminium enables the formation of many more complex compounds in the hydration paste.

Fly ash grading is similar to silt sized soils but the ash has a low specific gravity and dry density. It has also proved to be more workable and easier to lay as a fill material. Fly ash is produced from coal-fired power stations. It is collected from the flue gases exiting the furnaces, by electrostatic precipitation, before they are released to the

atmosphere. It has large variations in both its chemical and physical compositions. This is due mostly to different primary coals producing ashes of varying composition. In addition, variations within the furnaces used to burn the coal can affect the ash produced. Some fly ashes are rich in CaO due to high $CaCO_3$ contents of the parent coal. These fly ashes require only the presence of moisture to undergo self-cementation. As a result the CaO content of fly ash is a major factor in its classification. In the lagoon environment the conditions are sufficient for fly ashes with high lime contents to self-cement, potentially changing the behavioural characteristics. The cementing together of the fly ash grains is analogous to weakly bonded residual soils found in nature. The study of weakly bonded soils has helped to identify the features associated with weak bonding. Such research may prove useful in understanding self-cemented fly ash.

This research used two different fly ash sources. The lagoon fly ash originated from samples taken during a site investigation of settlement lagoons, used by Ferrybridge Power Station, at Brotherton Ings. They were collected by Soil Mechanics as part of a road-widening scheme planned for the A1 (supervised by Bullens & Partners). It was hoped that these samples would provide a sufficient number of self-cemented specimens for study. This proved not to be the case, so pozzolanic specimens were manufactured from a mortar of fly ash (with a low CaO content) and hydrated lime. The fly ash used for the mortar was taken directly from the electrostatic precipitators at Drax Power Station in N. Yorkshire.

The primary testing of the fly ash specimens was with triaxial equipment. The triaxial machines were fitted with internal strain devices for measuring local strains, as well as small pore probes for measuring the specimens' mid height pore water pressure directly. All the machines were controlled and logged by computers. The specimens were tested at a range of confining pressures up to 800 kPa to assess their behaviour through stress space. Specimens were also tested under one-dimensional consolidation conditions.

2. Literature Review

An important part of this research is based on the pozzolanic nature of fly ash and its potential for self-cementation. Previous studies involving the use of fly ash for geotechnical purposes have used soil mechanics to derive its properties. The self-cementing properties arising from bonding cannot be analysed satisfactorily by the use of traditional soil mechanics alone. To help study the bonding properties the approach used in the study of structured soils has been adopted. This is the first time such an approach has been used, to the author's knowledge, in the study of fly ash. This review of previous research has been split into three sections. The first section reviews the development over the last 50 years in the analysis of structured soils. These studies recognise the unique features of such soils and help to define how bonding influences their behaviour. The second section follows the development of critical state soil mechanics. An understanding of this is needed to help differentiate the behaviour of soil bonding from the similar behaviour of unbonded soils. The third section summaries research into fly ash, and its pozzolanic nature. The review considers the uses of fly ash for geotechnical purposes as well as developments in the understanding of its pozzolanic activity.

2.1 Structured Soils

Structured soils are found all round the world in different environments. They occur quite often in engineering projects and as such a lot of experience in dealing with these types of soils has been gained. The problems associated with them are generally minor when compared to sedimentary soils. This is probably associated with the nature of the structuring. Little effort was originally made to model their engineering properties. Normally the models of traditional soil mechanics (largely developed from remoulded material) were adapted to fit the observations. Today more is known about soils from a variety of different geneses, and it will be seen that a framework for these soils is emerging that describes their engineering properties more closely than traditional soil mechanics.

The beginning of the study of structured soils was the identification that some soils posed problems, when they were characterised using traditional soil mechanics parameters. Vargas (1953) observed from oedometer tests the presence of additional strength in natural samples, when compared to remoulded samples, and defined this as ' virtual pre-consolidation pressure'.

Ingles (1962) studied the potential for bonding in soils, and concluded that the electrostatic forces of flocculation are insufficient to cause anything more than only slight cohesion. Instead Ingles suggested that a covalently bonded macro-lattice, capable of being formed from most soil components, has the potential to create

considerable strength. This led to his proposal of a mechanism of bond formation based on alternate wetting and drying cycles.

Not all soils containing structures are formed in the same way. Sangrey (1972) indicated a number of possible cements that may occur naturally in soils. Despite this variety, they all exhibit some common characteristics. At low stresses, these soils appear to be stronger than expected, with less strain being required prior to yield. It is the structure of the soil that dominates its pre-yield behaviour. Post-yield behaviour shows a more usual response to loading.

Wallace (1973) noticed the low sensitivity of coarse cemented soils from the continuously wet highlands of Papua New Guinea. He recognised the limitation of applying this observation to other residual soils, because soils formed under continuously wet conditions will be different from those soils formed under seasonal climates. Wallace also called for some simple working generalisation of the behaviour of soil structure to aid residual soil engineering.

Uriel & Serrano (1973) wrote on the collapse phenomena caused by the yielding of cementation in cemented soils, due to tensile stress, compressive stress, and shear stress. He gave a simple view on how the collapse of a cemented structure occurs, commenting that any reliance on the strength due to the soil structure might have catastrophic consequences, if the structural strength is lost by over-stressing.

Saxena and Lastrico (1978) performed triaxial tests on lightly cemented sands from the Vincetown Formation, New Jersey. They obtained results demonstrating the variability of calcite-cemented sand. Samples showing similar index properties were found to have a large variation in friction angle. Some lower density samples were found to have higher strengths, and in the stress-strain plots no correlation could be observed between strain at failure and confining stress. These observations demonstrated the heterogeneous nature of strength in the material, a problem found with many other residual soils. Despite the variability, it was obvious that at low confining pressures, the strength was dominated by cementation, and at higher stresses, frictional resistance controlled the strength, as suggested by Sangrey (1972).

On the Californian coast near San Francisco deposits of cemented sand, which exhibited slopes typically of 60°, were studied by Clough *et al.* (1981). In these sands the cementing agents were found to be silicates and iron oxide. Again the same characteristics of brittle failure at lower confining pressures were seen.

As the stress history of a residual soil appears to have little influence on behaviour compared to its structure, Vaughan & Kwan (1984) devised a theory, for lower confining pressures, relating weathering to a weakening process in residual soils. They argue that the changes in stiffness are due to changes in the compression modulus for the soil skeleton assuming the whole system remains elastic. It is the porosity and structure of the residual soils that are important rather than the insitu stress history. The influence of the soil's stress history is reduced leaving the structure to control the strength.

In an attempt to stimulate the production of a framework of engineering properties for residual soils, sufficient for prediction, Vaughan (1985) laid out the unique features of residual soils, and the problems of using normal soil mechanics, suggesting that the presence and influence of weak bonding in soils may be common in many more soils than was at first supposed. Such a framework for weakly bonded soils would allow the study of stress-strain and strength characteristics to be correlated. He encourages the use of their characteristics and origins, such as the presence of weak bonding, which affects their properties independently of density and stress history. Following the suggestion of previous research by Sangrey (1973) and Uriel & Serrano (1973) he recommends that the representation of the yield stress of the weakly bonded soil be defined in stress space, as well as the use of comparisons between structured and destructured soils to qualify the effects of bonding. He warned against the reliance on oedometer tests, because of the unknown stress-path, and the possibility of misinterpreting true collapse

A framework for the interpretation of the engineering properties of structured soils was proposed by Vaughan *et al* (1988), who also suggested methods of engineering classification. As the testing of residual soils is problematic (due to sampling problems, as outlined by Bressani & Vaughan (1989), and inherent variability and weakening from the weathering processes as decribed by Vaughan & Kwan (1984)) they promoted the use of artificial samples instead of specific soil types, where the grading, grain strength, void ratio, and bond strength could be controlled and varied. They showed that the yield in artificial samples can be mapped in 'deviatoric stress/mean stress/void ratio space' similar to the yield of sedimentary soils. Vaughan

et al noted that with residual soils, two yields are often observed. The first yield is at the onset of bond breakdown, and the second is at the point when bond strength equals increasing bond stress. Yielding is a function of initial bond strength and initial void ratio. Thus a bonded soil may exist in a 'stress/void ratio space' stable field of the structured material or in a meta-stable state, outside the stable field of the destructured material. In this meta-stable state significant creep may occur.

As bond strength is difficult to determine, and can be very variable, Vaughan *et al* proposed a classification based on initial void ratio. Two methods of classification were suggested. The first method uses in situ stress related to two standard index tests, of either the liquid limit, plastic limit or compaction tests. The second method involves the use of the oedometer tests on de-structured soils to establish the meta-stable/stable boundary. They warned that field trials would also be required to establish practicality and usefulness of the classification.

The development of artificial samples as suggested by Vaughan *et al* (1988) to study the mechanical behaviour of weakly bonded soils was initiated by Maccarini (1987), and later followed up by Bressani (1990) and Malandaki (1994).

Maccarini (1987) developed a method for producing artificial samples, the properties of which could be varied, with a repeatability of a few percent. The samples were formed of a uniform sand mixed with a Kaolin slurry. The mixture was air-dried, so the clay slurry could recede into the areas of contacts between neighbouring sand grains. The samples were fired so that the clay started to undergo vitrification

towards a ceramic state. This enabled the bond strength to be varied, by altering the firing time and temperature. To simulate particles which themselves degrade during loading fired Kaolin slurry was crushed to the same grading as the quartz sand and mixed with the quartz sand. To obtain samples of low density, wax particles were incorporated. These left larger voids in the samples when they were fired as the wax was burnt off.

Triaxial tests on the artificial samples by Maccarini showed a consistent pattern. A similar pattern was also observed in a natural residual soil from Mauritius. Results indicated that deformations were controlled by bond strength, porosity and grading. Two yield loci were observed for all types of artificial material. The stress increments from first to second yield increased with decreasing porosity and decreased with increasing bond strength. It was possible from the results to derive a tentative framework describing the behaviour. One notable observation was the manner in which the bonding broke down only gradually with increasing stresses and strains.

Bressani (1990) continued Maccarini's work using loose artificial samples, but studying different densities and compositions. He identified the two yields on a plot of deviatoric stress against strain, using a log scale for both. Again he noted that the yield surface plotted in stress space was controlled by bond strength and void ratio, except that for samples of the same composition, changes in void ratio had more effect than changes in bond strength. He also noticed that mineralogy affected the shape of the yield surface when samples containing crushed fired Kaolin sand were compared against those containing only quartz sand.

At low stresses all samples behaved similarly, indicating that bond strength was very important to the samples' behaviour. However at higher stresses variation became apparent and these were related to the variation in the characteristics of the samples, such as mineralogy and void ratio, which seemed to have the greater influence.

Bressani was also concerned with the problems associated with the testing of weak samples (Bressani and Vaughan, 1989). He realised that methods used on normal soil samples were inappropriate when using weakly bonded samples, as the stresses and strains applied to the samples (e.g. during saturation procedures) could easily weaken or destroy the bonds.

The role of structure in natural soils and weak rocks was compiled by Leroueil & Vaughan (1990). By reviewing the varied nature of soil type and formation noted by other authors they concluded that structure was present in a wide range of geomaterials, as suggested by Vaughan (1985), and that the structuring has a similar effect on all of them. The concept of yielding, applied to the stress history of soft clays, could also be used for these materials with the exception that the yield curve controls the type, amount, and the development time of the structuring as well. The failure at yielding is a product of the breakdown of bonding and does not correspond to the maximum rate of dilation.

They noted that the structure increased the strength and stress domain, showing stiffer behaviour additional to that expected from the stress history, largely irrespective of the origins of the structure. They called for a separate framework and terminology to

highlight the role of structure, as both bond strength and density are reflected in the size and shape of the yield loci in stress space (Figure 2-1). The use of comparisons between structured and de-structured soils by using stress/void ratio states, showed the effects of soil structure most clearly. The void ratio influences the abruptness of yield, the shape of the yield, and the post-yield stiffness. Vaughan & Leroueil (1990) also commented that this unique feature of structure is irreversibly destroyed by large strains. It is possible that structure may be recovered, but on an unknown time scale, analogous to autogenous healing of damaged concrete

Some of the work undertaken at the Sience & Engineering Research Council (SERC) experimental research site at Bothkennar (on the bank of the Forth, midway between Edinburgh and Glasgow) has identified the occurrence of structure in samples, and its importance in understanding the soil's behaviour. A selection of relevant papers is detailed below.

Hight *et al* (1992) outlined the basic geological characteristics of the soil and its observed behaviour. The structure was suggested to have been formed from post-depositional bonding, ageing and leaching. Similar to the natural variability of soil features, it was found that the strength of structure also varied. From the use of different sampling techniques, it was noted that destructuring was caused by both shear and volumetric strain, especially during sampling and some test preparation techniques.

Smith *et al* (1992) used sophisticated stress-path triaxial equipment on the samples from Bothkennar, which was controlled by a micro-computer (Toll 1993), to help map the yielding characteristics. They identified three zones of yield (Figure 2-2) based upon the ideas presented by Jardine (1992). The first zone, where the soil behaved in a linear elastic manner, could be identified but proved to be too small to be mapped in stress space. The second zone, for non-linear elastic soil behaviour, gave surprisingly distinct yield points, allowing it to be mapped with reasonable confidence. The third zone, for inelastic behaviour prior to failure, was seen in all tests. The surface representing the initial boundary surface depended on the ratio of vertical to horizontal stresses (K) adopted and the magnitude of the stress changes involved.

Allman & Atkinson (1992) worked on establishing the basic characteristics of the reconstituted samples from Bothkennar. They characterised the behaviour by a simple state boundary surface, the shape of which demonstrated features usually found in soils with crushable and breakable grains. When comparing intact samples to the reconstituted samples, the intact samples initially plotted outside the state boundary then moved towards the critical state, outlined by the reconstituted samples, at large strains indicating the loss of structural influence.

Clayton *et al* (1992) commented on the effects of different sampling methods on samples from Bothkennar, and their effects on the structure, noting that volumetric strain probably accounted for more de-structuring than did shear strains. De-structuring in samples was also thought to occur during reconsolidation procedures designed to reduce the effects of sampling.

Coop & Atkinson (1993), working on cemented carbonate sands from Dog's Bay in Ireland, noticed that even at higher confining pressures, cementing had an influence on stiffness and stress-strain behaviour. However, they concluded that this influence was due to the effect of the cementing on specific volume, by the addition of fines to the matrix and partial filling of the voids. They stated that cementing only affects the soil strength at low confining pressure. At the higher confining pressures the strength is frictional, and the transition between the two is not fully understood.

Cuccovillo & Coop (1993) took the work of Coop & Atkinson (1993) further using carbonate soft rocks, and compared the behaviour of cemented and de-structured samples. The cemented samples achieved states outside the intrinsic state boundary surface. The extent of the movement outside the boundary surface was suggested to be due to bond strength and specific volume.

Tests on artificial samples with different bond strengths and the same specific volume showed that higher bond strength caused more movement. In natural calcarenites the influences were the same in general, but it was noted that increases in bond strength caused decrease in specific volume and tended to have counteracting effects. In fact the most pronounced movement was with lightly cemented samples with high specific volumes.

In studies on weakly cemented sedimentary rocks Leddra *et al* (1993) tried to characterise chalk, using soil mechanics to describe its behaviour. However the models did not accurately predict behaviour at lower confining pressures. This was

explained by the presence of bonded structures in the chalk, allowing it to pass outside the state boundary surface predicted by soil mechanics. Their results showed behaviour similar to previous work described above on structured soils.

Malandraki (1994) continued the work on artificial soils started by Maccarini (1987), and followed up by Bressani (1990). She worked on similar samples to those described by Maccarini, except using a stress-path cell linked to a PC (Toll 1993). The results from drained and undrained shear tests identified three zones of behaviour. Up to a mean stress of 115 kPa, the bonds controlled the soil's behaviour at failure. From 115 - 800 kPa, the bonds only partially controlled the soils behaviour, as yielding occurred before failure. Above 800 kPa mean stress, structured and destructured samples shared the same bounding surface. The testing went further, and examined the role of the stress-path on the samples, rotating them anti-clockwise in p'-q stress space, to follow paths of constant p' and constant σ_1'. The results showed that with an increase in anticlockwise direction of the stress-path, the second yield occurred at lower axial strains. Different yield loci were observed for different stress-paths. The development of radial and volumetric strains was thought to be able to account for the reduction in axial strain required for yielding. It was also noted that by changing the stress-path in a clockwise direction during a test (after reaching the point of yield for the initial stress-path direction), it was possible to encounter successive yields for each of the stress-paths followed.

Novelle & Johnston (1995) looked at the compression behaviour of a range of geomaterials from soils to hard rocks in a study that demonstrated the similarity of the

brittle-ductile transition in rock mechanics to the pre-consolidation pressure of soil mechanics. The basis for the work was the suggestion by Schoffield & Wroth (1968) that the concept of critical state soil mechanics may be applicable to other geotechnical materials. The similarity of behaviour among the several different geomaterials was also noted by Leroueil & Vaughan (1990) when considering the structure of natural soils. The porous nature of soft rocks showed a similarity with that of soils. The peak and ultimate failure states of normally consolidated rocks and the ultimate failure of over consolidated rocks could be described by the same locus, consistent with the critical state view of soil behaviour. In the case of hard rocks the identification of a frictional sliding envelope that appeared to form a brittle-ductile transition locus was shown to be equivalent to the critical state locus. Overall the results indicate that the differences between the different geomaterials are related more to traditional definition, rather than to rational patterns of behaviour.

Using samples artificially cemented with iron oxide (Haematite) prepared by a repeated wetting and drying process, Roa *et al* (1995) studied the collapse behaviour of cemented soils using oedometer tests. They cautioned against reliance on the additional strength of the soil gained from bond strength.

Das *et al* (1995) performed a feasibility study with Brazilian tensile strength tests on lightly cemented sands, using an optical imaging technique to measure the tensile strain. The tests demonstrated an increase in tensile strength with increasing cement content and a decrease in tensile strain at failure.

Zhu *et al* (1995) studied the at-rest lateral stress in artificially cemented sands and factors affecting it. Samples were tested in oedometers using a modified ring fitted with strain gauges to measure at-rest lateral stresses. They identified that K_o (coefficient of earth pressure at rest) was related to sand type, cement content, vertical stress, sand density, curing period and stress history. Results indicated that for cemented sands, cement content and stress history were the most important.

Cuccovillo & Coop (1997) studied the pre-failure behaviour of two structured sands in triaxial compression over a wide range of pressures. They noted that, in contrast to the typical strain hardening response of the unbonded reconstituted soils, bond degradation resulted in the progressive transition from a structured soil to a frictional material. They pointed out that the contribution of the component of structure to the shear stiffness is only relevant as long as yielding, which is indicated in sands by a rapid decrease in stiffness and a progressive deterioration of bonding resulting in the development of plastic strains, is prevented. The influence of structure depends on the state of the soil. Where the structure arises predominantly from bonding the value of shear stiffness after first yielding decreases as the bonding degrades. Conversely where the structure is due to a predominance of interlocking fabric the values of shear stiffness remain high despite the bond degradation.

Nagaraj et al (1998) looked at the compressibility of soft-cemented soils. The term "soft cemented" refers to the sensitivity of the soil, which is indicated by the ratio of the equilibrium void ratio to the void ratio to the liquid limit (e/e_L). By comparison of the calculated value with the measured field value the soil was considered to be soft

cemented when the field value was the larger. Using published data on sensitive soils they were able to predict compressibility from the insitu water content and the field vane strength, and are looking for more data for further confirmation of their findings.

Lui & Carter (1999) studied the virgin compression of structured soil, both natural and artificial, using data obtained by other authors. They define an equation [Equ 2-1] to calculate the effects of structure upon soil compression. The equation includes a new parameters, 'A' (structural compression factor) concerned with the additional void ratio of the structure during virgin compression with e (void ratio, the asterix indicating the reconstituted soil) and p' (mean effective stress). The equation was used to compare the results of 20 different soil types, approximations for the new parameters being made where there were insufficient data. They also define a virgin yield point for each soil marked by the onset of increased compression. However it is apparent that some soils may have already undergone some form of yielding where it is possible to see an increase in the compression of the soil prior to the virgin yield point. This indicates that the virgin yield point may approximate to the secondary yield point outlined in Vaughan *et al* (1988).

$$e = e^* + \frac{A}{p'} \qquad \text{Equ 2-1}$$

2.1.1 Summary of Studies of Structured Soils

An overview of the many studies of structured soils has identified the same quasi-preconsolidation characteristics, first reported by Vargas (1953) in a range of different

soil and rock types. The recognition of specific traits, which may be associated with the weak binding together of adjacent particles, has led to the development of a new approach to the understanding of such materials. Previous attempts to describe the behaviour of these materials by the use of either soil or rock mechanics alone can now be supplemented with this new approach. The development of a framework to describe bonded soils has been aided by the use of artificially bonded specimens. The creation of these artificial samples allows adjustment of their parameters during their formation, which allows the various influences of these parameters to be assessed more critically. The recognition of the bonding influence is facilitated by comparisons with the same material in an unbound form. Achieving such a material is still an area of interpretation for each soil and rock type. To date, apart from the artificial samples designed for the study of weak bonding, only naturally occurring soils have been studied. The approach has not been used in the assessment of man-made wastes, such as fly ash.

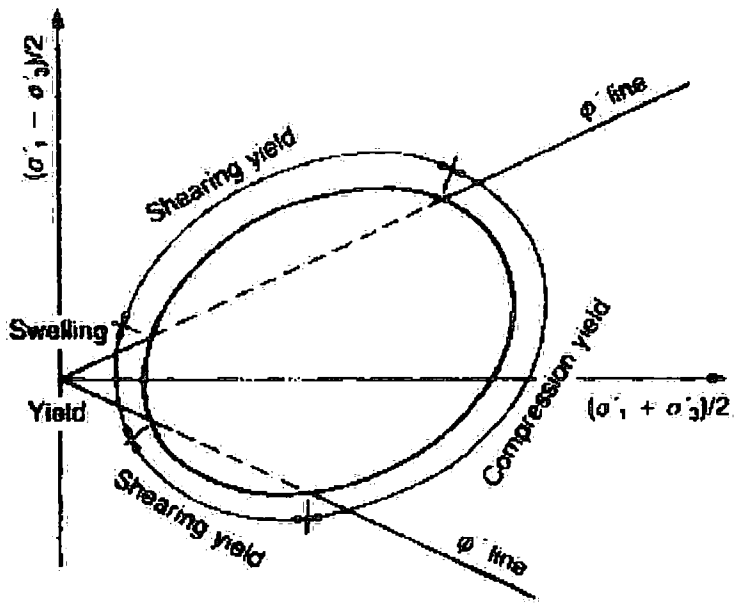

Figure 2-1 A typical yield loci within stress space showing different types of yield (Vaughan & Leroueil 1990)

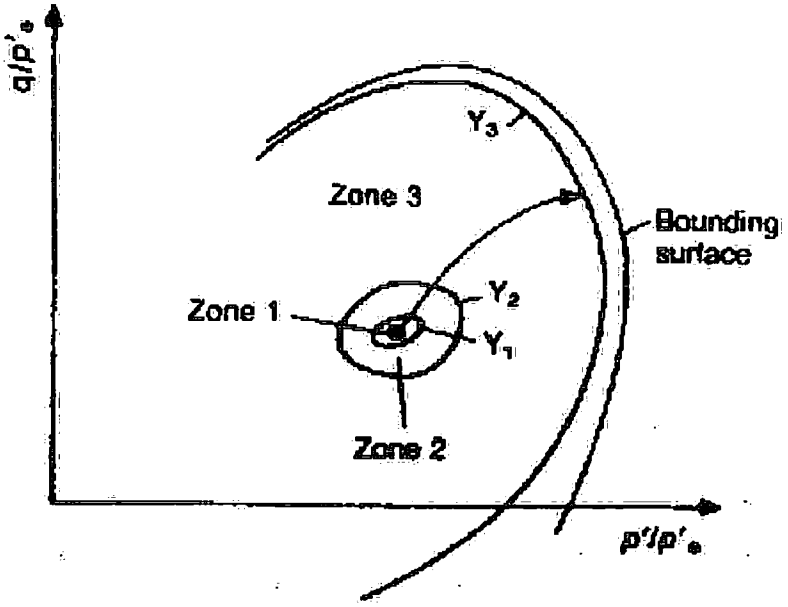

Figure 2-2 Definition of yield surfaces (Smith et al 1992)

2.2 Critical State

The concepts of critical state soil mechanics were first proposed by Roscoe *et al* (1958) and later developed by Schofield and Wroth (1968) in a slightly differently form. The first concept was of *yielding* of soil through progressive severe distortion, which alters the soil into an ultimate state that is explained by the second concept of *critical state*.

The kernel of the concept of critical state as stated by Schofield and Wroth (1968) is that soils and other granular materials, if continuously distorted until they flow as a frictional fluid, will come into a well-defined critical state of strength and volume as determined by two equations (Equ 2-2 & Equ 2-3

$$q = M\, p'_f \qquad \text{Equ 2-2}$$

$$v = \Gamma - \lambda \ln p'_f \qquad \text{Equ 2-3}$$

where M, Γ and λ represent basic soil properties and q, p' and v represent deviator stress, mean effective pressure and specific volume respectively. The first equation defines the deviator stress required to maintain a continuously flowing soil as a product of the frictional constant and effective pressure. The second equation indicates that the specific volume of a unit volume of flowing soil decreases with the logarithmic increase in effective pressure.

From these two equations it is possible to see that a critical state line in q-p'-v space can represent the critical state (Figure 2-3), and is unique for any one soil independent of its stress history. Normally consolidated or lightly overconsolidated clays and loose sands compress as shear stresses increase, resulting in the strain hardening of the soil, with the critical state occurring once it reaches a constant maximum shear stress where there are no more volumetric changes under drained conditions and constant pore water pressure for undrained condition. These are said to be on the Wet side of critical, Atkinson and Bransby (1978). Conversely heavily overconsolidated clays and dense sands dilate as shearing occurs and will usually reach a peak strength after which they undergo strain softening to a constant shear stress again with no changes in volume and pore water pressure for respective conditions. These are discussed by Atkinson and Bransby as being on the Dry side of critical. Independent of which side a soil specimen originates with continued shear the specimen will reach the same critical state, which is independent of the drainage conditions of the test.

Based upon these concepts Schofield and Wroth showed that the *total change* from initial state to an ultimate critical state could be precisely predicted, leaving only the problem of calculating how much of the total change can be expected to have occurred when the process is only progressed part way.

The critical state parameters are unique for each soil. However Schofield and Wroth (1968) noted that the critical state lines of many different soils pass through the same point they called the Ω point and give its approximate coordinates as $v_\Omega = 1.25$ and

p'_{Ω} =10Mpa (= 1500 lb/in^2). Wood (1991) considered this to be a bold generalisation but to the author's knowledge there is no research to challenge it.

The critical or ultimate state has been described by Atkinson (1993) as the essence of soil mechanics and its idealized behaviour has been supported by much experimental work notably by Atkinson and Bransby (1978) and by Wood (1991).

The majority of the work on the concept of critical state discusses separately the behaviour of normally and overconsolidated clays. A unifying model is the model of Cam-Clay, which displays recoverable but non-linear volumetric strains Equ 2-4. It can be used to predict experimental data. The application of critical state to sands was included in experiments by Atkinson and Bransby (1978) and Wood (1991) showing that the critical state concept can be applied to all soil types. However, its application to sands was found to be less successful by Wroth and Basset (1965) and by Stroud (1971) where it proved to be less successful. The lack of success was attributed to the problems associated with the definition of the virgin compression line for sands and the measurement of the critical state line. The difficulties in establishing the normal consolidation slope also raised problems in the normalisation of tests, as noted by Atkinson and Bransby (1978).

$$\frac{q'}{Mp'}+\left(\frac{\lambda}{\lambda-k}\right)\ln p'-\left(\frac{\Gamma-v}{\lambda-k}\right)=1 \qquad \text{Equ 2-4}$$

The measurement problems for sands were partially resolved in work by Castro (1969) using undrained stress-controlled triaxial tests on very loose sands. From these

tests he developed a *steady state line*. This steady state line was intended to be an equivalent to the critical state line but led to discussion as to how the two actually relate to one another, notably by Casagrande (1975), Poulos (1981), Sladen *et al* (1985) and Alarcon-Gurzon *et al* (1988). The distinction between the two is essentially the method of measurement, which has led to the two lines being classified with letters after Casagrande (1975). The steady state line derived from undrained tests on loose samples was termed the F-line, whilst critical state work using drained strain-controlled tests on dilatant samples was termed the S-line. Discussions by Poulos (1981), Sladen *et al* (1985), Alarcon-Gurzon *et al* (1988) based on the data set of one sand indicate that the results are consistent with the hypothesis that the two are the same. But other data by Castro (1969) and Alarcon-Gurzon *et al* (1988) show a significant difference between the S & F lines. Casagrande (1975) suggests that this difference between the two may be the result of strain rates, but Poulos (1981) points out that the difference lies in the definitions. The definition for steady state involves both the flow structure and the constant velocity neither of which are defined in the concepts of critical state.

Further study into the definition of the critical and steady state lines has led to the suggestion of non-uniqueness, which could result in the re-evaluation of the use of the concept. From Been *et al* (1991), Kuerbis *et al* (1988) and Vaid *et al* (1990) test data show that extension testing resulted in achieving a different steady state from compression testing. Also Alarcon-Gurzon *et al* (1988) suggested that the soil particle matrix structure could affect whether the soil reached the S or the F line.

Further investigation would be needed on different soils to corroborate these suggestions.

In addition to the previous discussions there has been some evidence that the assumption of a straight critical/steady state line in v–$\ln p'$ space does not hold true for granular soils. Data from Been and Jefferies (1985), Been *et al* (1991), Hardin (1987) and Tatsuoko *et al* (1986) suggest that this line deviates from its linear nature at high pressures of about 1000 kPa or more, possibly linked to a small amount of fracturing of grains at these pressures.

After more than four decades the critical state concept is now well established in soil mechanics, especially with respect to clay soils. However there remain some questions with regard to its application to granular soils due to problems in establishing the normal consolidation behaviour. Establishing the critical state for a de-structured soil is important for distinguishing between overconsolidation conditions and those due to bonding.

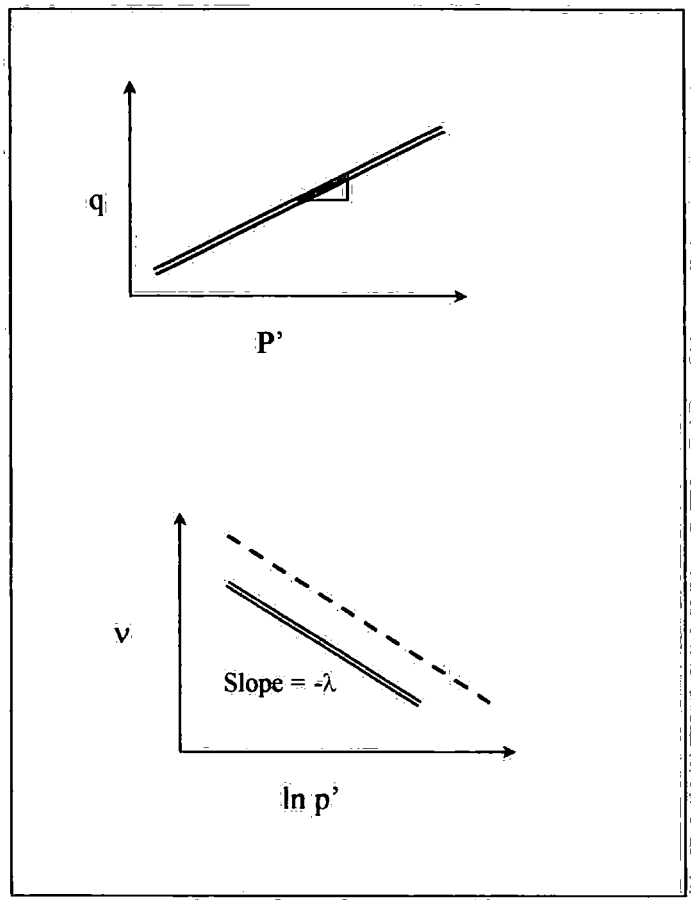

Figure 2-3 Critical State lines for Triaxial tests in a) q' – p' space, b) v - ln p' space

2.3 Fly Ash (Pulverised Fuel Ash)

Fly Ash, also know as Pulverised Fuel Ash (PFA), is a man-made waste material produced from coal-fired power stations. The processes of formation and extraction of the fly ash are documented by Helmuth (1987). As with all man-made wastes the disposal of the material has caused concern, and the usual method of disposal for fly ash was in storage lagoons adjacent to the producing power station.

The reported utilisation of the material for geotechnical purposes can be traced back to the 1950's. The use of fly ash with lime in the stabilisation of soil is described by Minnick and Miller (1952). The technique uses the pozzolanic nature to increase the compressive strength of the soil as well as improving its resistance to freeze-thaw and wetting and drying. One of the advantages of using fly ash was to lower the required amount of lime, and hence decrease costs. The use of fly ash with lime was found to be effective in two ways. The immediate benefit was the reduction in plasticity and improved shrinkage characteristics. In the long term the cementitious nature of the fly ash and lime led to enhanced compressive strength with ageing.

Sutherland *et al* (1968) list some early investigations into the use of fly ash as a fill material. In 1952 fly ash from Hams Hall power station was noted for its high bearing capacity. It was employed as a cheap convenient alternative material for filling a disused railway cutting at Packington for the construction of a trunk road. Despite the undesirable method of end tipping the ash directly into the cutting, the fly ash proved to have very good settlement properties. Subsequent employment of fly ash in

geotechnical projects were documented in 1955 by the Road Research Laboratory and in 1960 at the Coleshill-Tamworth road where its low dry density added to the evidence for the strongly beneficial properties of fly ash.

Since the 1960's fly ash has been used in many more applications. Some investigations into fly ash concentrated on the age hardening characteristics. Sutherland and Finlay (1964) studied fly ashes from four Scottish power stations. The development of cementious properties of the fly ash when placed in the wetted state was related to the chemical and physical properties. The strengths of cylindrical samples (cured for various periods of up to 3.4 years and tested by triaxial compression) were compared to various physical and chemical properties of the fly ash. These studies showed decreasing strength for increasing specific surface area, silica and alumina content, but increasing strength with increasing carbon content, and free lime. The percentage of free lime was most closely related to the age hardening characteristics.

Thorne & Watt (1965) identified the heterogeneous nature of fly ash by identifying eight types of particle based on 14 British fly ashes. The particles were predominantly rounded types I-III (Table 2-1), and irregular grains were the minority. Crystalline phases only composed 11-17% of the ash whilst glass phases made up 71-88%. In many investigations the density of fly ash has proved to vary widely. The density of the ash in this study was seen to relate to the content of the clear glass spheres.

Type	Shape	Colour	Crystallinity and texture	Characteristic size range, μ	Comments
1	Spherical and rounded	Colourless	a) Glassy, clear, solid b) Glassy, containing small bubbles c) Glassy, with crystal traces d) Predominantly crystalline, solid	0-20 0-20 0-20 10-50	
2	Spherical and rounded	Light brown to black	Lighter coloured ones glassy; all solid	5-30	Deepening colour suggests increasing iron content
3	Rounded	White in reflected light	Glassy, spongy	10-200	Small and large bubbles giving a range from foam to cenopheres
4	Irregular	Light brown	Partly crystalline, solid	10-100	Irregularity of profile and surface very marked
5	Irregular	Varicoloured in reflected light	Partly crystalline, solid	50-500	Agglomerated particles, apparently sintered; generally containing red particles and area
6	Irregular	Black	Solid or porous	20-200	Partially burnt coal particles, sometimes containing mineral matter
7	Angular	Colourless	Crystalline, solid	10-100	Probably quartz
8	Angular	Red	Crystalline. solid	5-50	Probably Haematite

Table 2-1 Type of fly-ash particles characterised by microscopic examination

In a second paper Thorne & Watt (1965) indicated that the crushing strength of small unconfined cubes of lime/ash mortar was related to carbon content, glass content, silica & alumina content, density, and specific surface, as identified in previous research. Investigations showed that for short curing periods of up to 91 days, none of the factors correlated closely, the best being the specific surface, calculated from particle size analysis. It is interesting to note that the specific surface calculated from air permeability had poor correlation to strength throughout. This is unlike the study of Sutherland and Finlay (1964) where increasing specific surface measured by air permeability was linked to increasing strength. For longer periods of curing of 1-2

years the contents of SiO_2 and (SiO_2 + Al_2O_3) had close correlations with increasing strength. Activity was observed to reside in the siliceous particles and was determined relative to particle size.

Watt & Thorne (1966), related the pozzolanic activity to chemical analysis using two methods. The first Feret-Florentin method was used on fragments from the crushing strength tests (Thorne & Watt 1965). Where fragments were not available a Lime Solution method was used. Both are based on estimating the percentage of acid-soluble material, which has been produced by the pozzolanic reaction. The important factors determining the fly ash activity from both methods agree with results from Thorne & Watt (1965). These tests showed that it was possible to relate the fly ash pozzolanic strength with the chemical reaction.

Another line of investigation was into the use of fly ash for geotechnical purposes. Grey & Lin (1972) studied the engineering properties of Michigan fly ash. They concluded that its low compacted density is advantageous when an embankment or fill needs to be constructed over soft compressible ground. The Michigan ash proved different from British ashes, as it did not exhibit any pozzolanic properties. The pozzolanic property would be expected to affect the extent of field settlement. However the lack of this reaction in the Michigan fly ash from field evidence did not seem to affect compressibility or settlement significantly.

Leonards & Bailey (1982) reported on the use of fly ash as structural fill in the foundations of a new generating station for the Indianapolis Power and Light

Company. The physical properties and characteristics of fly ash were discussed, including some scanning electron micrographs of different shaped particles. The observations concluded that untreated fly ash possessing no self cementing characteristics can successfully be used for structural fill, as long as the moisture content, and the inherent variability of fly ash is controlled. Long-term settlement cannot be estimated using conventional approaches, because they do not account for the effects of pre-stressing due to compaction. Plate load tests proved good indicators for observed settlements.

The importance of the moisture content in the stabilisation of soil using both lime and fly ash together was noted by Manz (1984). In a study of the addition of lime and fly ash to sand soils, in varying proportions and differing moisture contents it became apparent that the moisture content was important to the compressive strength of the stabilised soil (Figure 2-4).

The analysis of the pozzolanic nature of fly ash has been carried out mainly in the field of cement chemistry, where attempts have been made to define the chemical reactions better. Helmuth (1987) describes well the nature of fly ash and its role in its use with Portland cement. He also looks at the pozzolanic reaction and brings together different explanations for the reaction. All of these involves the gradual chemical breakdown of the fly ash glass particles with time. It is the material dissolved from the glass into solution that is re-precipitated out as calcium hydrates. The alumino hydrates require more calcium ions to form the hydrates than the siliceous hydrates. This seems to explain why the alumino hydrates tend to form in

the space between the fly ash particles, whilst the siliceous hydrates form closer to the surface of the glass.. It is obvious that the varied nature of the chemical constituents of the glass make the exact determinations of the reaction very difficult to ascertain, but the precipitation of the hydrates is a mechanism for the production of cementing mediums binding the grains together.

The mechanism of the pozzolanic reaction with lime is summarised by Helmuth (1987) as being similar to the corrosion of glass and alkali-aggregate reactions of reactive siliceous aggregates in concrete. The tetrahedral frame work of crystalline silica has a central Si[4+] ion surrounded be four O[2-] ions, with each O[2-]ion linking together two Si[4+] ions. However as the glass is amorphous and this balanced structure does not exist. This means that on the surface of the glass there are unsatisfied oxygen and silica bonds which can take up OH[-] ions from the water.

Further investigations into the pozzolanic activity of fly ash included the chemical variations of different ashes. Stevenson *et al* (1988) looked at the chemical variations between lignite ashes from different sources of central North America, comparing the major and minor element oxides. The study demonstrated the influence of geological units on the grain compositions and bulk chemistry by using ternary plots of Cao-SiO_2-Al_2O_3 and CaO-Na_2O-MgO. Grains rich in SiO_2 and Al_2O_3 were also seen to be rich in Na_2O, whilst grains rich in CaO had similar MgO and SO_3 contents.

The chemical analysis of Stevenson *et al* (1988) was continued by the x-ray powder diffraction study in McCarthy *et al* (1988). This study showed the large variation in

the fly ashes from across North America. The high calcium concentrations of these Lignite ashes were thought to make them more reactive than ashes derived from bituminous coal sources.

The heterogeneous nature of fly ashes was considered by Schlorholtz *et al* (1988). They suggested the variation could be due to production procedures as well as different geological sources. In a study of high calcium fly ashes produced at Ottumwa Generating Station in Iowa between 1985 and 1986 and noted the influence sodium carbonate feed rate (in the electronic precipitation of the fly ash from the flu gases) on the sodium content of the ash. The sodium content had been linked to the compressive strength of different ashes. Fly ashes with high sulphate-hydration products, typically Ettringite, tended to have low compressive strength, whilst those with high compressive strengths normally contained Stratlingite.

Toth *et al* (1988) compared the application of fly ash and Furnace Bottom Ash (FBA) material from Ontario Hydro coal-fired generating stations, which were identified as ASTM class F, (i.e. possessing no pozzolanic activity), in four case studies. The studies demonstrated that fly ash, as fill material, behaved in a similar manner to silt. It performed as well as or better than similar silt-sized natural material, being easy to handle with conventional plant. It had a wide range of moisture contents for compaction, and typically gave friction angles of 35° and 40° for fly ash and FBA respectively. Groundwater studies observed that leachate solutes did not exceed the Guidelines for Canadian Drinking Water Quality. Concern over the corrosion of

buried metals was shown to be unfounded, and the sulphates in the leachate were considered to have little or no detrimental effect on concrete structures.

An environmental study in Denmark by Hjelmar (1990) into the leachate from fly ash, using large-scale lycimeters, tried to show the relevance of laboratory based accelerated leachate tests. Ca^{2+} is one of the main components in the leachate from the fly ash used, becoming the dominant constituent with SO_4^{2-} after the initial flush out of Na^+ and K^+. The paper concluded that the results from the long-term field tests in lycimeters and laboratory tests, especially the column tests, produced a good correlation. Hence accelerated time laboratory tests can be useful tools for predicting the composition of leachate from fly ash. The most significant aspect for self reaction in Class C fly ash is the removal over time of CaO, which will diminish the potential for self cementation to reoccur, if the structure is broken from over stressing.

The tests commonly employed to determine the properties of fly ash are given by Wersche *et al* (1991), which also covers the use of fly ash in concrete. The tests cover the physical properties and those used to determine specific chemical properties, as well as tests to examine the activity of fly ash for use with concrete. The physical properties commonly associated with the activity of fly ash include the moisture content, carbon content, glass content, particle density, and fineness. The main chemical tests quantify the major element oxides of SiO_2, Al_2O_3, Fe_2O_3, CaO, MgO, SO_3, Na_2O and K_2O.

Indraratna *et al* (1991) looked at the reaction of fly ash with lime, with respect to using the mixture in construction fill. Results indicated that a curing period of only 2-3 weeks was necessary for the material to approach its maximum strength. The authors considered the results could be applied only to other ASTM class C lignite ashes and may not be applicable to types of fly ash from other coal types.

A study into the mechanical properties of self-cementing fly ash by Yang (1992), was specifically aimed at geotechnical applications. This study looked at the characteristics of self-cementation using soil mechanics approaches. However the assessment of stiffness and yield used by Yang are not as refined as the methods employed in the study of structured soils. The analysis of the binding processes occurring within the curing of the fly ash highlighted three different areas in which the self-cementing specimens gained their strength. Two types of binding agents were observed to be formed from the pozzolanic reaction. Gel Binding, formed in the contact areas of specimens cured for 6 months showed strength increase with time. In addition to the gel binding secondary crystals grow inside and outside the fly ash from the surface, some of which were identified by X-ray diffraction to be Ettringite. Secondary crystals that formed in clumps were not considered to cause any considerable gain to strength because they were scarce, whilst others only grew inwards. The gel binding was thought to be supplemented by crystals, which grew on the outer surface, and were more dispersed. They also added to the self-cementing strength by the interlocking of crystals from adjacent grains.

Sharma *et al* (1993) worked on assessing the lime reactivity of fly ash 'L' (Kg/cm^2). They proposed an empirical equation (Equ 2-5) based on observations from 25 Indian fly ash samples of ASTM class F, which do not possess self cementing properties.

$$L = \left(\frac{F}{1000}\right)^{0.85} \times S^{0.80} \qquad \text{Equ 2-5}$$

The equation is based on the fineness of the material 'F' (cm^2/g), and the soluble silica 'S' (%) in the fly ash, the soluble silica is the difference between total silica content and free silica content, determined after dissolution of the fly ash. The equation provided adequate estimation of the reactivity of samples, when compared with other fly ash samples.

Tashiro *et al* (1994) used an electric resistance measurement method to evaluate the reactivity of some different pozzolans, including fly ash, with portlandite. The method proved useful in assessing their variation in degree of reactivity, forming four distinct groups. The fly ash proved to be in a group of its own, as it demonstrated a delay of 24 hour before reacting. This behaviour is completely different from the other pozzolans. (Figure 2-5) This may have been a consequence of the aluminous content of fly ash.

Ma *et al* (1995) looked at the structure of fly ash, which had been activated with Ca Cl_2 and $CaSO_4{\cdot}H_2O$. The pores were identified as being mainly open ended wedge shaped voids. For samples reacted with $CaCl_2$ the surface area was found to be nearly 30 times that of the untreated fly ash and it was found that the volume of pores with

radii of 19Å increased with increasing temperature of thermal treatment. The form of the pore structure was considered to be important in assessing the physical and mechanical properties of concrete containing fly ash.

Indraratna *et al* (1995) performed a study on the use of fly ash as a stabilising agent on soft clays. The study used lime and cement as secondary additives to the fly ash. Triaxial tests confirmed that the addition of fly ash with lime or cement increased the shearing resistance of the specimens by improving the apparent frictional angle, whilst having marginal effects on the cohesion intercept.

Sivapullaiah *et al* (1995) looked at a test for determining the Optimum Lime Content (OLC) for fly ash. Three methods were used. One used the pH of the fly ash to determine the OLC. Another used the Liquid Limit of the lime/fly ash mixture. The third used the free swelling index. All three proved capable of identifying the OLC, with the easiest method being the free swelling index.

In an attempt to accelerate the hardening time for the pozzolanic reaction Shi & Day (1995) looked at the addition of Na_2SO_4, $CaCl_2$, and NaCl. Two different fly ash samples were studied, one with a low and the other with a high calcium content. With the exception of NaCl the chemical activators produced significant gain in rate of strength. The $CaCl_2$ worked best for the low calcium fly ash, whereas the Na_2SO_4 proved best for the high calcium fly ash. The different activators produced varying quantities and types of hydrates from the lime-ash pastes. Na_2SO_4 produced Ettringite, whilst $CaCl_2$ resulted in the solid solution of $[C_4AH_{13} - C_3A]\cdot CaCl_2\ 10H_2O$

2.3.1 Fly Ash Summary

Fly Ash was initially used in geotechnical projects on a 'trial & error' basis where it was conveniently available, usually in large quantities. Its strengthening properties were known but there were no guidelines or much anecdotal evidence as to how best to deploy the material. As geotechnical research began to investigate the major influences of the strengthening characteristics there were contradictory results due to a lack of understanding, specifically of the large variations possible for a variety of different reasons. The biggest advances in the understanding of the pozzolanic nature of fly ash came from research into cement chemistry. The benefits of using fly ash in cement were studied by understanding the cement reaction. Although there have been many attempts to characterise the pozzolanic reaction in fly ash, there is still no consensus as to the actual mechanisms involved. There is however a greater understanding of the influencing factors and the components of the reaction. In more recent years the variations in the composition of the fly ash have been revealed, ranging from the macro to the nano scale. These have helped to understand how the ash forms in the furnaces. Research has also looked at the use of fly ash for soil stabilisation, where it is rich in lime, as well as methods for manipulating its pozzolanic nature. By being able to control the reaction better the use of fly ash for its pozzolanic potential is advanced. Tests devised to assess the lime content and silica reactivity are such advances, helping to better predict the activity of the fly ash produced.

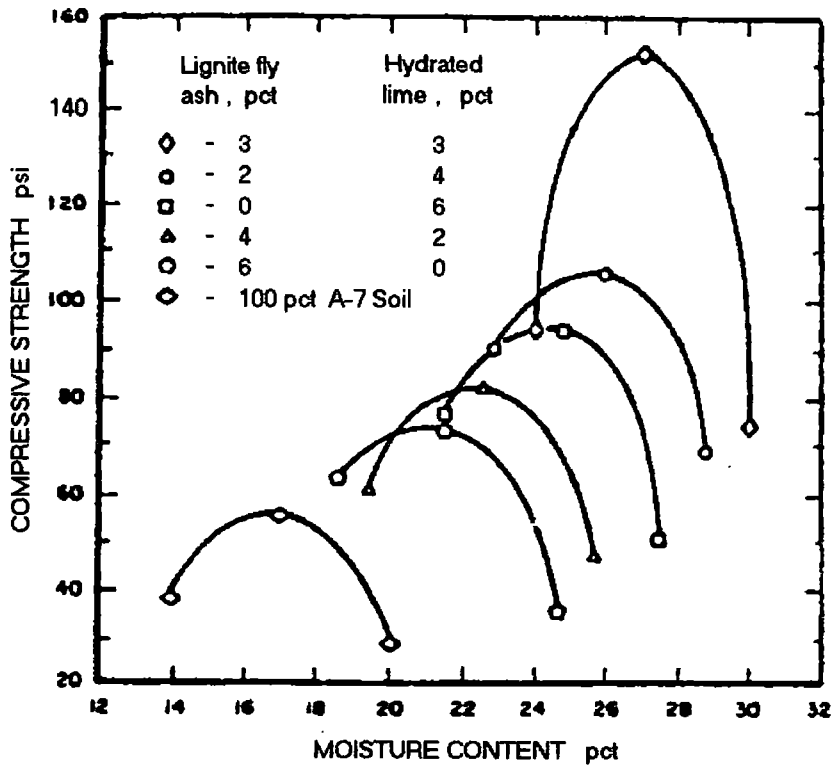

Figure 2-4 Compressive strength versus moisture content after 7 days moist curing (Manz 1984)

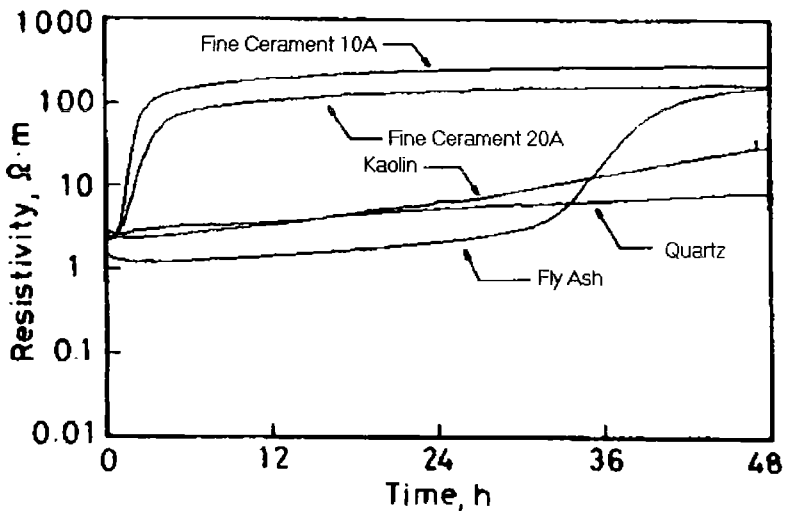

Figure 2-5 Variation of resistivity with time. The fly ash shows a retardation to its activity (Tashiro 1994)

3. General Properties of Fly Ash

3.1 Fly Ash

Fly ash is an artificial sandy to slightly sandy SILT soil, varying in colour from beige through brown to grey, dark grey and black. Classification test results are given in section 3.2. Fly ash from two different sources was used for this research, each being processed by different methods to analyse the pozzolanic activity. The first fly ash material originated from a settlement lagoon where the pozzolanic activity was due to the self-cementing nature of the fly ash disposed, and termed lagoon ash. The other fly ash was obtained fresh and dry from the precipitation hopper. It had been identified as having pozzolanic activity but lacked sufficient CaO to induce self-cementing. Hydrated lime and water were added to this dry fly ash to form a mortar which was allowed to cure before testing. Specimens formed from fly ash prepared in this way were termed mortar ash.

3.1.1 Lagoon Fly Ash Material

The original samples for the research were taken from lagoons at Brotherton Ings, Hook Moor (Figure 3-1) associated with Ferrybridge power station adjacent to the A1. The samples were taken as part of an investigation by Soil Mechanics Limited in 1995, under instructions from Bullen & Partners, Consultant Engineers to the Department of Transport. The investigation was based upon the proposed construction of a new offline section of the existing A1, part of which was to cross the Brotherton Ings lagoons. Lagoon 1 had previously been investigated by Foundations

and Explorations Services Limited in 1991 for Bullen & Partners (Figure 3-2) when the proposed route was to cross the north end of the site. Due to revisions to the planned route the investigation by Soil Mechanics Limited (Figure 3-3) looked at the lagoons just south of this lagoon No 1. Sampling in this investigation occurred predominantly in lagoons 2 and 5N. Two types of samples were taken from boreholes on the site by Soil Mechanics Limited. Delft samples were extracted to obtain a continuous record of the fly ash in the lagoon and piston samples were taken to identify the bottom layers and the lagoon liners. The Delft sampling method (section 3.1.1.1) was used to extract the fly ash, as this method causes minimal disturbance to the recovered material.

At the start of this study, samples from boreholes BS401 and BS402 (fig 3.3), on the western embankment of Lagoon 5N, were available for the project. The fly ash contained in these Delft tubes came from depths of between 10-12m. These samples had been covered by material used to build additional berms as the height of the lagoons was increased over time. The cross section of Figure 3-4 shows the west containment berms of lagoon 5N, down to the River Aire, with the relevant positions of BS401 and B402. As this research project progressed more samples were required, which were taken from boreholes BS408 and BS406, located closest to BS401 and BS402 in lagoon 5N. As nearly all of the Delft tubes extracted from BS406 were available for the research, this borehole was used to investigate the depth profile within the lagoon.

Coal mining in the region has extended underneath the location of the lagoons. Subsidence from mining has been reported by Clark et al (1985), who gave a brief

description of the site history and geology, as well as the expected surface subsidence as shown in Figure 3.5. Seepage problems identified by the analysis were cured by the introduction of impermeable membranes and geotextiles. The subsidence events add to an already complex stress history, which comes from the periodic fly ash placement and large phreatic fluctuation experienced by lagoon material used in the research.

3.1.1.1 Delft Sampling Method

The Delft samples obtained from the lagoons were of a 66mm diameter, and 1m in length. The samples were extracted by the Delft sampling system for obtaining a continuous undisturbed core. The method, devised by the Laboratorium Voor Grond Mechanica Delft in Holland (Begemann, 1961), is useful for the ground investigation of normally consolidated soils, which are soft and easily compressible. These types of samples can provide a permanent record of the soil profile and allow samples to be taken from a particular horizon of interest.

To reduce the friction on the outside of the sample the system uses a stocking, and a lubricating mud. The main disturbance of samples comes from the cutter. Normally samples are extracted from the tube containers by pulling on the stocking. Due to the lengthy period of time between extraction from the lagoon and being used for testing, most of the moisture in the lubricating mud was lost. Therefore this method was not possible and instead the tubes were cut open (section 4.2.2).

During the site investigation there were problems reported by the site engineer (Ball 1994). These problems occurred during drilling when occasional hard layers cut the stocking before the resistance depth was reached. On such occasions another hole was drilled at the same location. These harder layers were thought to be due to the pozzolanic activity of the fly ash and indicated the presence of a reaction occurring within the lagoons.

3.1.2 Fly Ash - Lime Mortar Material

The heterogeneous nature of the layering in the lagoon fly ash samples, and a possible limit to the supply of the material in the early stages of the project, led to the search for a controlled material of similar properties for a more rigorous test programme. It needed to have a similar composition, and to exhibit the features of pozzolanic cementing, but to allow homogeneous samples to be made. The ideal material would have been a self-cementing fly ash (ASTM Class C) which contains a high percentage of CaO (5-10%), and little or no free carbon. Alternatively, a fly ash with little or no free carbon but a low percentage of CaO (0-2%) (ASTM Class F) can be made reactive by the addition of lime. The fly ash obtained for this purpose came directly from the precipitator collecting hopper at Drax power station. Drax power station is located to the south east of the town of Selby in N.Yorkshire, about 20km due east of the Brotherton Ings site Its carbon content was low (2%), but so was its CaO content (>2%), putting it in ASTM class F.

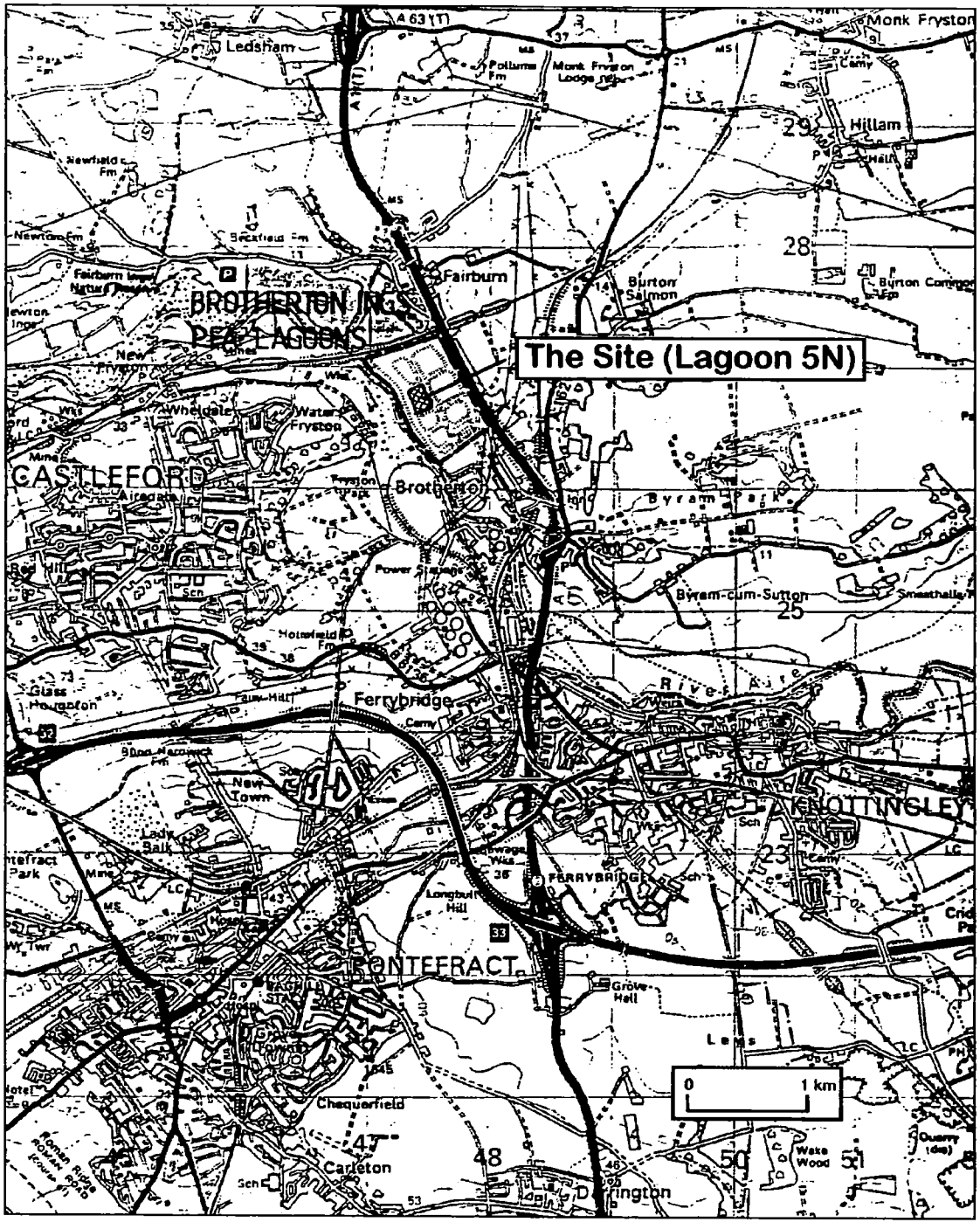

Figure 3-1 Location of the Fly Ash Lagoons at Brotherton Ings, adapted from Foundation & Exploration Services Contract 2045 Location Map figure 206

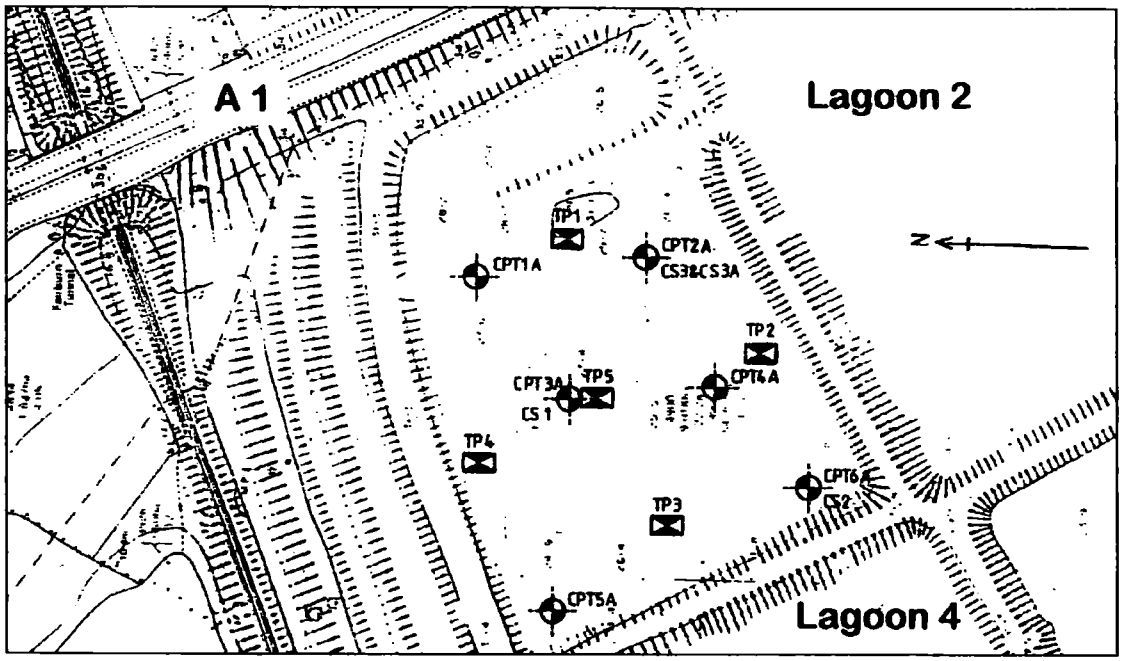

Figure 3-2 Foundation and Exploration Services Limited investigation of Lagoon 1 in 1991, adapted from from Foundation & Exploration Services Contract 2045 figure 207

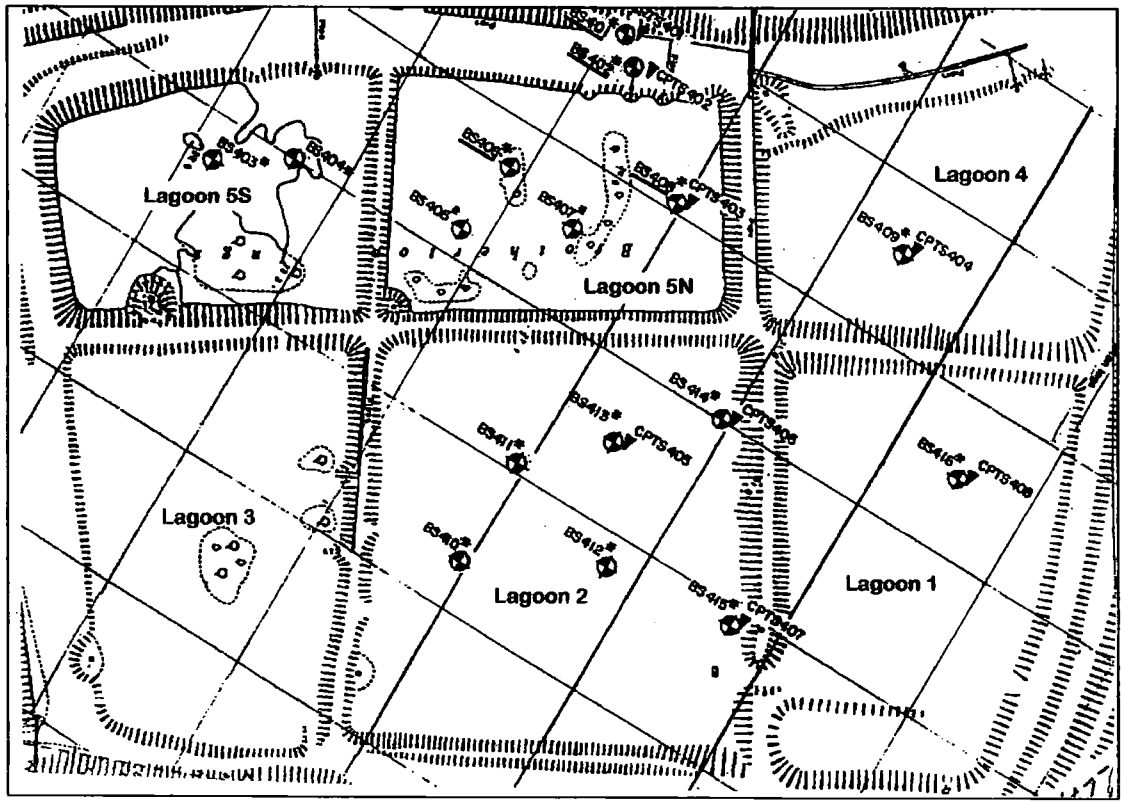

Figure 3-3 Investigation by Soil Mechanics in 1995 on the fly ash lagoons at Brotherton Ings, showing the location of the boreholes sunk, supplied by Bullen & Partner Consultants

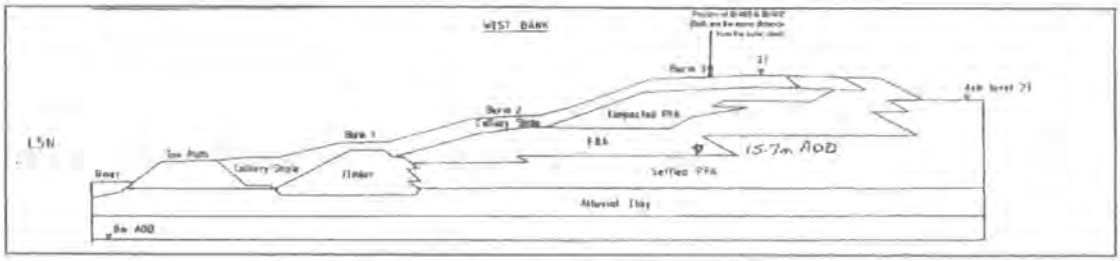

Figure 3-4 Cross section through the western bank of Lagoon 5N on the Brotherton Ings site, showing the location of boreholes BS401 and BS402, supplied by Bullen & Partners Consultants

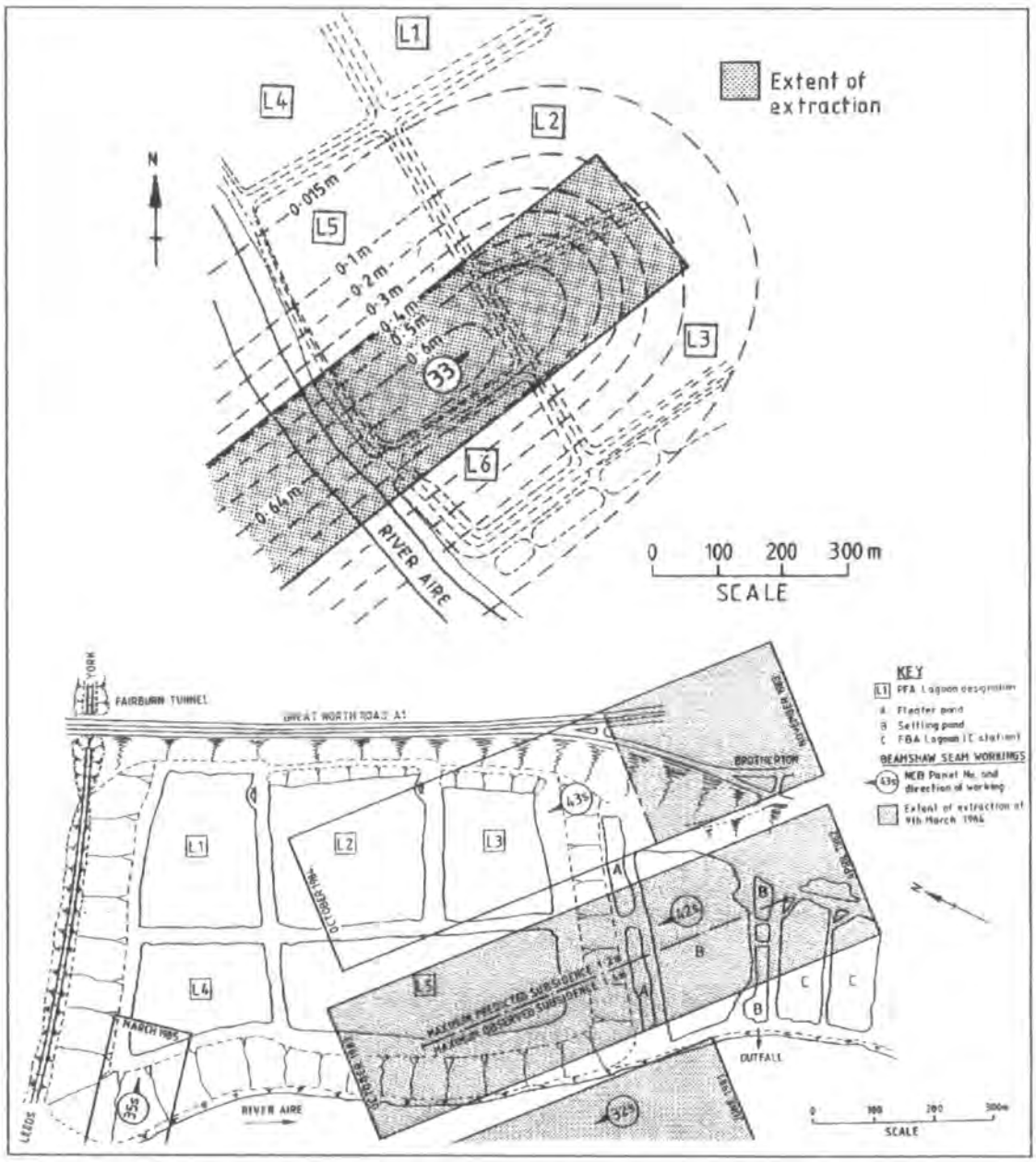

Figure 3-5 Areas of surface subsidence caused by coal mining beneath the lagoons at the Brotherton Ings site, adapted from Clark et al (1985)

3.2 Classification Tests

3.2.1 Specific Gravity

This test using small pyknometer bottles to determine the specific gravity of the fly ash particles followed the procedure laid out in BS1377 (1990) Part 2:8.3. Samples of different particle sizes from the same source were also tested to establish the presence of changes in specific gravity with change in particle size.

The lagoon fly ash was found to have large variations in its specific gravity, ranging from 1.96 to 2.42 with the majority of values falling between 2.10 and 2.25. Because of the wide distribution of values, additional tests were conducted on the trimmings cut from the outside of the undisturbed samples. Each batch of lagoon fly ash used to form moulded lagoon samples was also tested.

The fly ash used for the lime/ash mortar specimens was obtained directly from the power station dry hoppers, and came from the same furnace firing. A number of specific gravity tests performed on the fly ash revealed a uniform value of 2.10 throughout the batch.

Table 3-1 gives the range and average values for each borehole, plus results from a previous investigation on the Ferrybridge lagoon site.

Tests performed on samples from borehole 406 show a variation in specific gravity with variation in particle size. Tests carried out on silt-sized particles showed higher

specific gravities than tests performed on entire samples, and on other size fractions. The fine sand sized particles had the lowest values whilst the coarse sand sized grains had slightly higher values.

Sample	**Specific Gravity**		
DRAX Whole Sample	2.10		
FERRYBRIDGE Lagoon Ash	Min	Max	Ave
BS 401	2.13	2.15	2.14
BS 402	1.89	2.20	2.05
BS 406	1.99	2.35	2.17
BS406 passing 63μm	2.24	2.42	2.32
BS 408	2.21	2.26	2.23
Foundation & Exploration Associates (1991)	1.96	2.36	2.21
Soil Mechanics (1995)	2.06	2.33	2.20

Table 3-1 Specific Gravity values for different Fly Ash Samples

Tube Numbers	Specific Gravity				
	Sample Trimmings	Coarse Sand	Medium Sand	Fine Sand	Silt
2233	2.10	/	/	1.75	2.34
7642	2.08	/	/	1.55	2.27
7887	1.98	/	/	2.1	2.40
9351	2.24	2.25	/	1.85	2.33
9811	2.35	2.12	/	2.17	2.42
10179	2.14	/	/	1.93	2.30
10458	2.01	2.11	1.98	2.03	2.37
10522	2.24	/	/	1.66	2.24
10606	2.03	2.29	/	1.86	2.25

Table 3-2 Specific Gravities of different size fractions from Borehole BS406

3.2.2 Compaction

The determinations of the maximum dry density and optimum moisture content for the fly ash were performed using a Proctor compactor machine, and followed the

procedure laid out in BS1377 (1990) Part 4:3.3. The tests used a 2.5kg cylindrical hammer of diameter 50mm dropped from a height of 300mm. The material was compacted into a split mould with internal dimensions of 105mm diameter and 115mm height. These dimensions give the mould a volume of $1x10^6mm^3$ when completely filled. The mould was filled in three layers, each layer receiving 27 blows.

The results from Proctor compaction tests using a 2.5 kg hammer on lagoon fly ash are shown in Figure 3-6 and for Drax fly ash in Figure 3-7. The low specific gravity value of the ash means the fly ash has a low dry density. The maximum dry density of the Drax fly ash was 1.41 Mg/m^3 whilst that of the lagoon fly ash from BS 406 was only 1.22 yet they had similar optimum moisture contents. Estimation of the air void space at the maximum dry density showed that the Drax fly ash attained a state of only 5% air voids whilst the fly ash of BS 406 retained 18% air void space. The results of the fly ash from BS406 were not typical as demonstrated in Figure 3-8, which shows the results of other compaction tests from previous investigations at the Ferrybridge site (section 3.1.1).

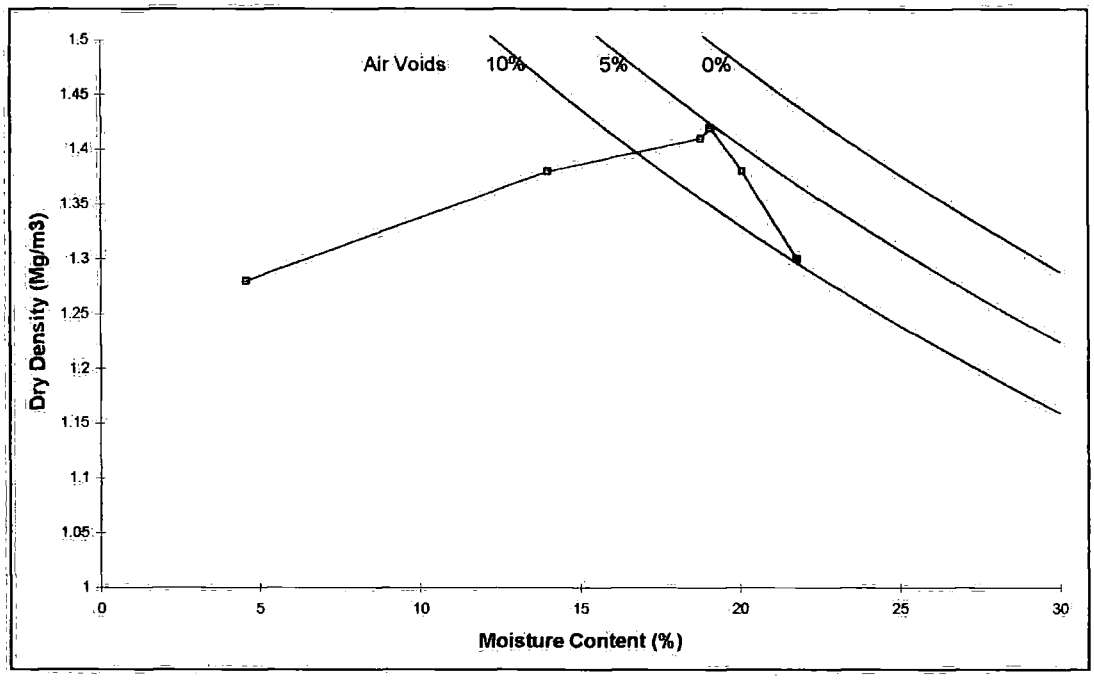

Figure 3-6 Compaction results on fly ash from Drax

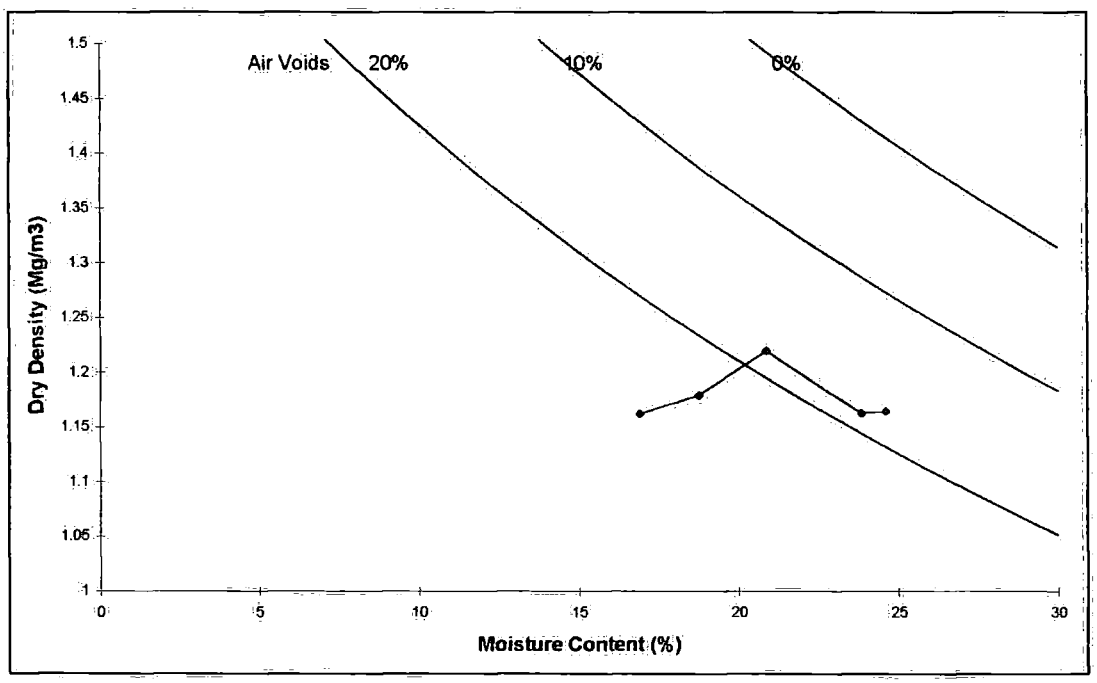

Figure 3-7 Compaction results on fly ash from BS 406

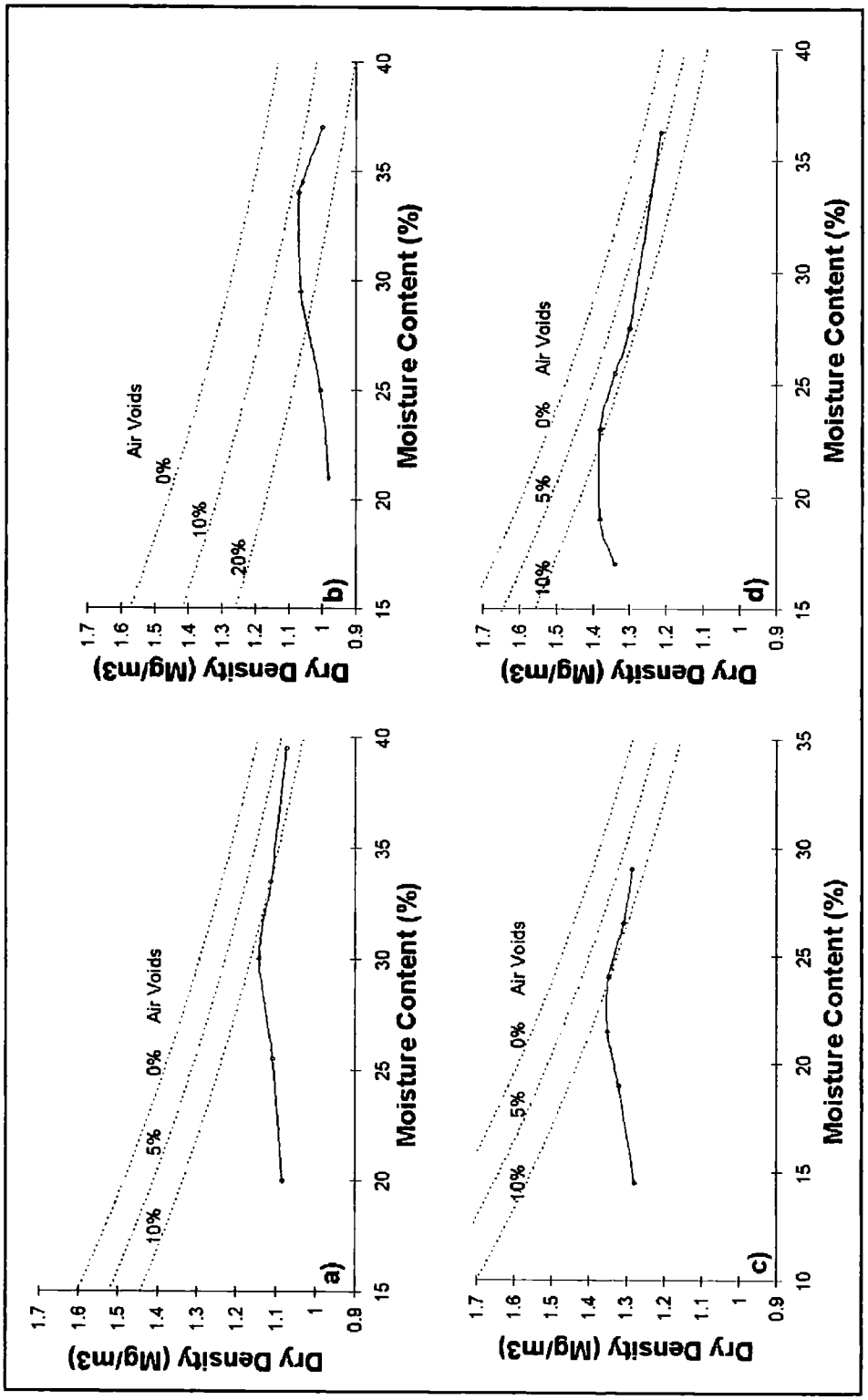

Figure 3-8 Compaction results on fly ash from a),b),& c) Trial Pit investigations(TP1, TP3, TP5) in Lagoon 1, by Foundation & Exploration Services Limited, and d) Bulk Surface Samples from Lagoon 5N, by Soil Mechanics.

3.2.3 Particle Distribution

3.2.3.1 Dry Sieving

This test to determine quantitatively the distribution of particle sizes followed the method laid out in BS1377 (1990) Part 2:9.3.

Samples for dry sieving were obtained from boreholes BS401 and BS406 as examples of the lagoon ash. The sample from BS401 consisted of the unused material from the Delft tube 10818. The samples from BS406 were the specimens recovered after triaxial testing. In the analysis of the lime/ash mortar, distributions were obtained for the dry unmixed Drax fly ash, as well as for samples of structured and de-structured mortars. The distribution for the structured material was obtained from the breakdown due to sieving action alone of an intact specimen (section 4.2.4). The de-structured material comprised specimens recovered from the triaxial and oedometer tests (section 4.2.5). Particle distribution from previous investigations on the lagoon ash by Soil Mechanics and Foundation & Exploration Associates are also included for comparison.

3.2.3.2 Sedimentation Analysis

This test used the pipette method defined in BS1377 (1990) Part 2:9.4 on material passing the 63μm sieve. Samples were taken from the suspension at a depth of 100mm at time intervals relating to the particle sizes 20μm, 6μm, & 2μm based on

their specific gravity. The specific gravity used was the value obtained from tests carried out on the same material passing the 63μm sieve.

The majority of the particles for lagoon fly ash samples passed through the 63 μm sieve, and required further differentiation of particle sizes which was achieved by a sedimentation analysis using the pipette method. The sedimentation analysis identified particles to sizes of 20 μm, 6 μm, and 2 μm. The pipette method assumes that all the particles possess the same specific gravity. The percentage of each size fraction is based on this assumption. Although evidence from larger sized particles suggests minor variation in specific gravity with size, the pipette results can be assumed to be representative of the distribution of fine material.

The range of particle distributions from investigation by Foundation & Exploration Associates (F&E) and Soil Mechanics Limited are plotted along with those of the dry Drax fly ash and a sample from BS401 in (Figure 3-9). Separate curves for each of the samples from BS 406 are plotted in (Figure 3-10). For the Drax fly ash used in the mortar samples, results for three different samples are plotted in (Figure 3-11): the unreacted ash, samples of de-structured material, and a structured sample broken down by hand. The dry fly ash used to produce the lime/ash mortar gives a curve, which falls within the typical range for the lagoon ashes. The lagoon and dry Drax ashes were composed predominantly of silt sized particles, with 60-90% passing the 63 μm sieve and 5% or less being clay sized. The curves obtained from reacted lime/ash mortar specimens show these to be formed of coarser material, with 75 % of the particles sand sized or greater. The curve for the de-structured material, correlates

well with the curve for the structured sample broken down by hand. The fly ash of Delft tube 10606 shows a greater number of large particles than other lagoon fly ash samples, most of which are composite grains made from an aggregation of much smaller spherical grains.

A majority of the distribution curves for the lagoon ashes show a hiatus for particle sizes of 212 μm. There were very few or no particles caught on the 212 and 300 μm sieves. For the samples with higher percentages of large particles (e.g.: sample 10606) their curves show a reduction in particles about this size indicated by the flattening of the curves at this point. This hiatus in the curves is also evident in distribution curves from previous investigations on the lagoon ash in (Figure 3.11).

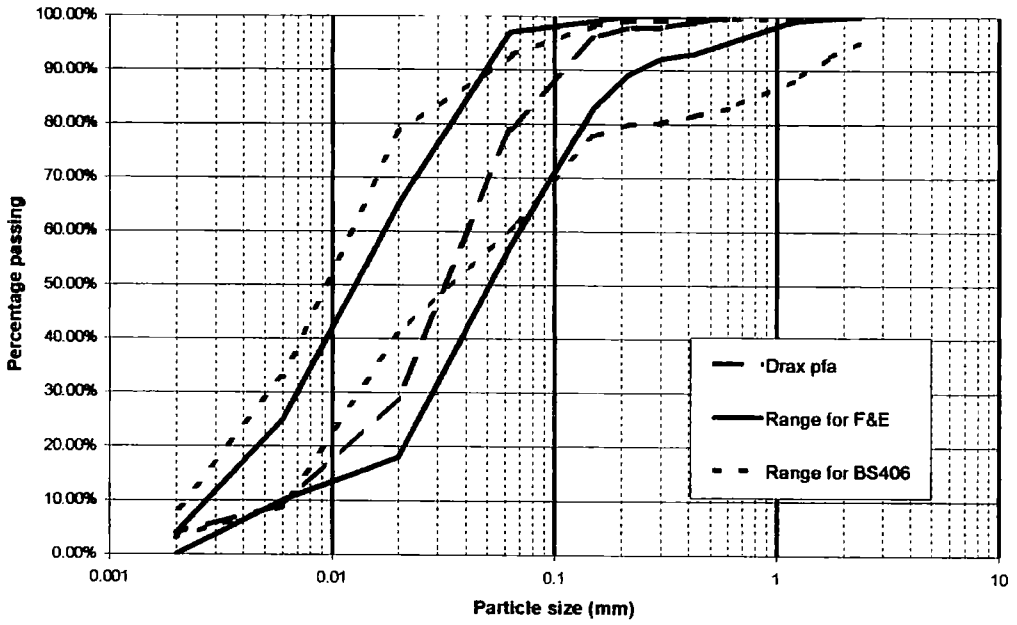

Figure 3-9 Typical ranges of fly ash particle distributions from different fly ash sources

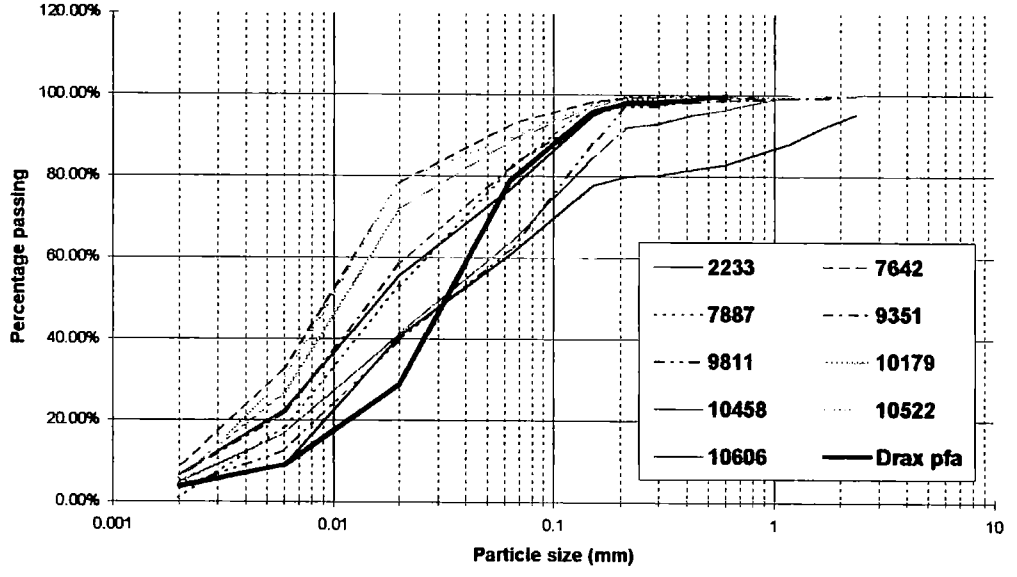

Figure 3-10 Particle distributions from BS406 and Drax fly ash. The numbers refer to tubes extracted from BS406 as shown in Table 3-2.

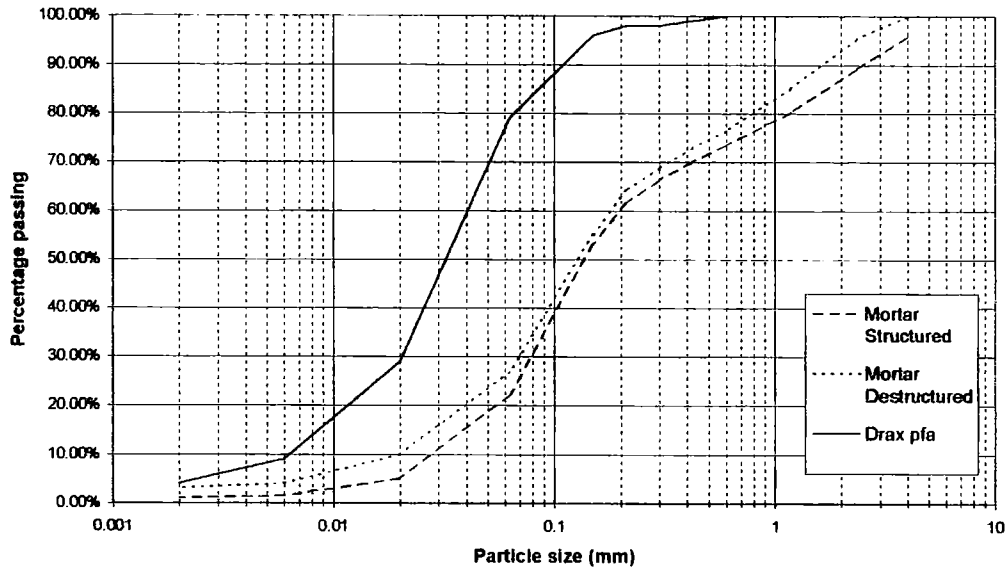

Figure 3.11 Particle Distributions for Drax fly ash on its own, and when mixed with lime

3.2.4 Sample Descriptions

3.2.4.1 Borehole BS401

The majority of the coarse to medium sand sized particles were speckled grey, and looked to be composed of aggregates of smaller particles. There were many white platy particles that were assumed to be the dried, lubricating mud found around the fly ash cores. The fine sand grains were mainly grey in colour with some darker grains, which increased in concentration, as the size of the particles grew smaller. The presence of the dark grains was reduced significantly in the silt-sized grains, which were grey in colour.

3.2.4.2 Borehole BS406

Tube 2233

The medium sand sized particles were a mixture of black, grey composite and light spherical grains. The fine sand grains contained a majority of black grains, accounting for approximately 75% of its makeup. The silt size grains were predominantly grey with very few black grains.

Tube 7642

Dark composite grains made up 60% of the coarse sand grains, with 25% nodule grains, and the remainder made up of grains of lighter colour. The medium sand grains were similarly composed, with a reduction in the black grains to 50% and the

lighter grains increased to 30%. In the fine sand grains the concentration of the black grains was reduced further to about 40% whilst the lighter grains were now dominant. The silt-sized grains once again were predominantly composed of the grey grains although they were slightly lighter in colour with very few dark grains visible.

Tube 7887

The medium sized sand grains in this sample were predominantly nodular grains with some black grains and some light grey grains. The fine sand sized grains however were predominantly dark coloured grains, with some grey composite grains and light-coloured spherical grains. The silt sized particles were similar to those of samples 2233 and 7642 and showed little or no dark grains.

Tube 9351

Nodular and rounded platy composite grains composed the coarse sand sized fraction. The medium sand sized grains showed a reduction in the nodular grains and an increase in the number of darker grains. The darker grains made up the majority of the grains in the fine sand size. Again, the silt-sized grains were composed predominantly of grey grains with very few dark grains.

Tube 9811

Similar to sample 9351 the coarse sand sized grains were made up of nodular and composite grains. The medium sand grains were composed of nodular, light coloured spherical grains with some rust colouring. There were some darker grains accounting

for about 30% of the fine sand grains, with the rest being grey or light grey in colour. The silt-sized grains were similar to other samples silt fractions

Tube 10178

The coarse sand grains were composed of nodular and dark composite particles in even quantities. The medium sand grains were similar with the additional presence of some light coloured grains. The fine grains were composed of dark and grey particles. The silt grains were the same as the other samples and lacked a significant number of dark grains as seen in the coarser fractions.

Tube 10458

The coarse grains were again a combination of dark composite and nodular particles. The nodular particles were not present in the medium sand grains. Their place has been taken by grey particles with the concentration of the darker particles increasing with fineness. The fine sand grains showed a similar distribution of particles types as the medium sand grains. The silt sized grains were the same as for the other samples.

Tube 10522

The coarse grains were composed mostly of dark particles with some grey composite, lighter coloured spherical, and nodular particles. The medium sand sized grains had an increased proportion of grey and light coloured particles and less dark and nodular

particles. The fine sand particles were similarly composed to the medium sand grains. The silt-sized grains were again similar to the other samples.

Tube 10606

The coarse grains were mostly grey composite particles platy and needle-like in shape, becoming more rounded and spherical with decreasing size. The medium sand size grains were mostly grey composite particles mostly needle-like or spherical in shape. The fine sand sized grains were predominantly grey coloured with about 25% of dark grain as well. The dark grains were not evident in the silt-sized grains, which were similar to the other samples.

3.2.5 Liquid Limit

This test using a cone penetrometer to determine liquid limit followed the procedure in BS1377 (1990) Part 2:4.3 using a standard cone described in BS4691. The liquid limit was determined as the moisture content for which the cone reaches a penetration of 20mm.

The liquid limit for the lagoon fly ash from borehole 401 averaged 28%, whilst the value obtained from dry Drax fly ash averaged 22.5%.

The liquid limit test was very difficult to perform on the ash samples, and liquefaction of the mixture was a major problem. The results are typical of an inorganic silt soil of low plasticity. No Plastic Limit was obtained.

Test	Liquid Limit (%)
Lagoon 1	29.0
Lagoon 2	26.9
Drax 1	23.0
Drax 2	21.9

Table 3-3 Moisture contents corresponding to a cone penetration of 20mm

3.2.6 Chemical Composition

The fly ash was analysed for major and minor metal oxides using an X-ray diffraction (XRD) machine. Specimens were formed from dry powdered fly ash mixed into a paste with a 4% solution of Mowiol glue. The paste was then compressed under a weight of 7-10 tonnes, into 20mm diameter tablet, and allowed to dry before being examined in the machine.

The amount of carbon within the fly ash is an important factor in its pozzolanic activity. The carbon content of the ash was determined using the loss on ignition test following the procedure outlined in BS1377 Part 3:4.3.

3.2.6.1 X-Ray Diffraction Analysis

3.2.6.1.1 Major Elements

A summary of the major element oxides is given in Table 3-4. The fly ashes from both the Ferrybridge lagoons and Drax hopper were composed predominantly of silicon and aluminium oxides probably combined together in the glass. Iron was the next most common element, some of which was in the form of magnetite, which was identified within the samples by using a magnet. Both sources had low levels of calcium content, which would affect their potentials for self-cementation. Potassium was present in both samples at over 3.5%, whilst concentrations of other metal oxides was less than 2%.

Element Oxides	*Ferrybridge Lagoon Fly Ash (%)*	*Drax Dry Hopper Fly Ash Only (%)*
SiO_2	45.5	47.66
Al_2O_3	28.15	27.21
Fe_2O_3	9	6.44
MgO	1.48	1.25
CaO	1.67	1.67
Na_2O	.93	1.66
K_2O	3.73	3.64
TiO_2	0.92	0.99
MnO	0.06	0.05
P_2O_5	0.18	0.19
CARBON	**1.00**	**1.15**

Table 3-4 Major Element Oxide concentrations from XRF analysis plus Carbon content (%) from Loss on Ignition test.

3.2.6.1.2 Minor Elements

The trace elements found using the X-ray diffraction are listed in Table 3-5 and account for only 0.3% of the samples. There are seven elements listed in Table 3-6, whose levels of concentration would be of concern if these levels were observed in natural soils. In both the Drax and lagoon ashes the levels of nickel and vanadium were high enough to be classified as contaminated, whilst chromium, copper and barium were only slightly contaminating. The levels of lead and zinc were too low to cause any contamination.

Metal ***Toxic***	*Drax Fly Ash (ppm)*	*Lagoon Fly Ash (ppm)*
Barium Ba	909.1 - 917.9	723.3 - 824
Chromium Cr	143.2 - 155.8	152.2 - 160.6
Copper Cu	154 - 197	214 - 274.5
Nickel Ni	111	111.8 - 127.9
Lead Pb	98.9	**144.8 - 133.4**
Vanadium V	**300.2 - 317.7**	**295.3 - 351.8**
Zinc Zn	**146 - 156**	**95.2 - 120.6**
Non-toxic		
Cerium Ce	126.7	130.4 - 168.0
Cobalt Co	34.2 - 40.1	38.0 - 45.4
Gallium Ga	37.2	30.6 - 34.2
Lanthanum La	74.6	66.4 - 72.3
Niobium Nb	21.6	22.0 - 23.2
Neodymium Nd	65.2 - 71.0	64.7 - 73.2
Rubidium Rb	134.7	140.9 - 141.9
Scandium Sc	**9.7 - 12.3**	**12.1 - 16.2**
Strontium Sr	**300.3**	**261.7 - 273.4**
Thorium Th	**17.3**	**13.4 - 14.1**
Uranium U	**6.4**	**6.1 - 7.1**
Yttrium Y	**52.4**	**48.2 - 53.3**
Zirconium Zr	**217.5**	**205.9 - 212.5**

Table 3-5 Concentration of Trace Elements

Element	*Uncontaminated*	*Slightly Contaminated*	*Contaminated*	*Heavily contaminated*
Cr	0-100	100-200	200-500	500-2500
Cu	0-100	100-200	200-500	500-2500
Pb	0-200	200-500	500-1000	1000-5000
Ni	0-20	20-50	50-200	200-1000
Zn	0-250	250-500	500-1000	1000-5000
Ba	0-500	500-1000	1000-2000	2000-1.0%
V	0-100	100-200	200-500	500-2500

Table 3-6 The relative degree of contamination for different trace elements, taken from Carson & Mumford (1994)

3.2.6.2 Loss on Ignition

The presence of carbon within the ash has been reported (Indraratna 1995) to reduce the potential for the ash to undergo the pozzolanic reaction. The levels of carbon concentration in fly ash samples from the lagoon and Drax are 1.00% and 1.15% respectively. At these concentrations, the carbon would not impede the pozzolanic reaction.

3.2.7 Fly Ash Composition

Different fractions from the dry sieving were analysed, using an optical microscope at 10 - 40 x magnifications, to identify variation in grain type. A number of distinctly different groups of grains were identified. These different groups are related to the classification for grains by Thorne & Watt (1964) in Table 3-7.

3.2.7.1 Grain Types

Spherical Grains

These are light beige and light grey in colour and look like small glass spheres, which can be hollow or solid, as indicated by broken grains. They make up most of the smaller grains (<65 μm) but can be larger than 1mm diameter.

Nodular Grains

Those observed under the microscope vary in size from 300 μm to over 2mm and are irregular in shape. The surface is smooth except on broken surfaces which are angular. Their colour is grey to dark grey, and they contain smaller grains of varying colour within their matrix.

Pumice Grains

Similar to the nodular grains these appear to be formed of the same material, but contain many more air voids resembling froth. Other smaller grains are also contained within the glass matrix around the air voids.

Black Grains

These are black or dark grey in colour and can be angular to rounded with occasionally shiny surfaces. Most probably composed of carbon, they appear to have

a much lower specific gravity than the glassy grains and some float on water. They are mostly found in the larger particle size fractions.

Composite Grains

These are composed of agglomerates of smaller grains, the majority of which are the spherical grains. They are rounded but vary in shape and most are greater than 212 μm in size. The larger grains are usually platy or needle like in shape whilst the smaller ones tend to be more spherical.

Magnetite Grains

These are black or dark grey in colour and are normally rounded to a sub-spherical shape. Some are magnetic and can be separated from other grains by this means. The magnetite grains will have a greater specific gravity than the glassy grains.

3.1.2.1.1 Grain Types	Classification from Thorne & Watt (1965)
Spherical	Types 1&2
Nodular	Type 4
Pumice	Type 3
Black Magnetite	Type 6
Composite	Type 5

Table 3-7 Relationship of grain types to the classification given by Thorne & Watt (1965) (Table 2-1)

3.2.8 Scanning Electron Microscope (SEM) Images

Some samples of fly ash were examined using a scanning electron microscope to examine the microscopic structure of the ash particles. Specimens of dry powdered fly ash were fixed to 10mm studs using double sided adhesive carbon disks, before being coated with a thin layer of gold to ensure a good conduction across the stud.

3.2.8.1 Drax Flay Ash

Plates 3-1& 3-2 show images of dry Drax fly ash with Plate 3-2 showing an enlargement of the area marked on Plate 3-1. Nearly all of the grains visible are spherical in shape, with a large irregular grain enlarged in Plate 3-2. These images demonstrate well the variation in size of the fly ash particles. The large central particle measures 170μm whilst some of the smaller grains are less than 1μm, a difference of over 2 orders of magnitude. Despite the difference in size, the grains have the same smooth spherical shape. The non-spherical grain in Plate 3-2 appears to be composed of the same glass as the spheres but it contains many vesicles similar to pumice. Some of the vesicles are large enough to be filled with the smaller spherical grains.

3.2.8.2 Lagoon Fly Ash

The image in Plate 3-3 is of material taken from the broken down specimen LUS10606, which originated from Tube 10606 extracted from BS406. These are the same variation in grain sizes observed in the Drax fly ash, with smaller grains

clumped around the outside of larger grains. There is also a fuzzy material in-between grains in some of the clumps. This may be part of the bonding material, binding the grains together, although the resolution is insufficient to give much more than an indication. This image shows more irregular grains than the plates of Drax ash, most notably at the bottom of the image.

3.2.8.3 Mortar Cured Fly Ash

The image in Plate 3-4 has been taken from a broken piece of cured lime-ash mortar from a structured specimen. There are spherical grains ranging in size from 1-5μm covered in a matrix of thin crystals that coat the exterior of grains and partially fill the interparticulate voids. This material may be assumed to be responsible for the binding together of the fly ash grains in this and similar samples. There appears to be little deformation to the grains themselves despite being the source of some of the raw materials used in the pozzolanic reaction in the growth of the interlocking crystals. The growth of the fine needle like crystals appears to be uniform throughout the image.

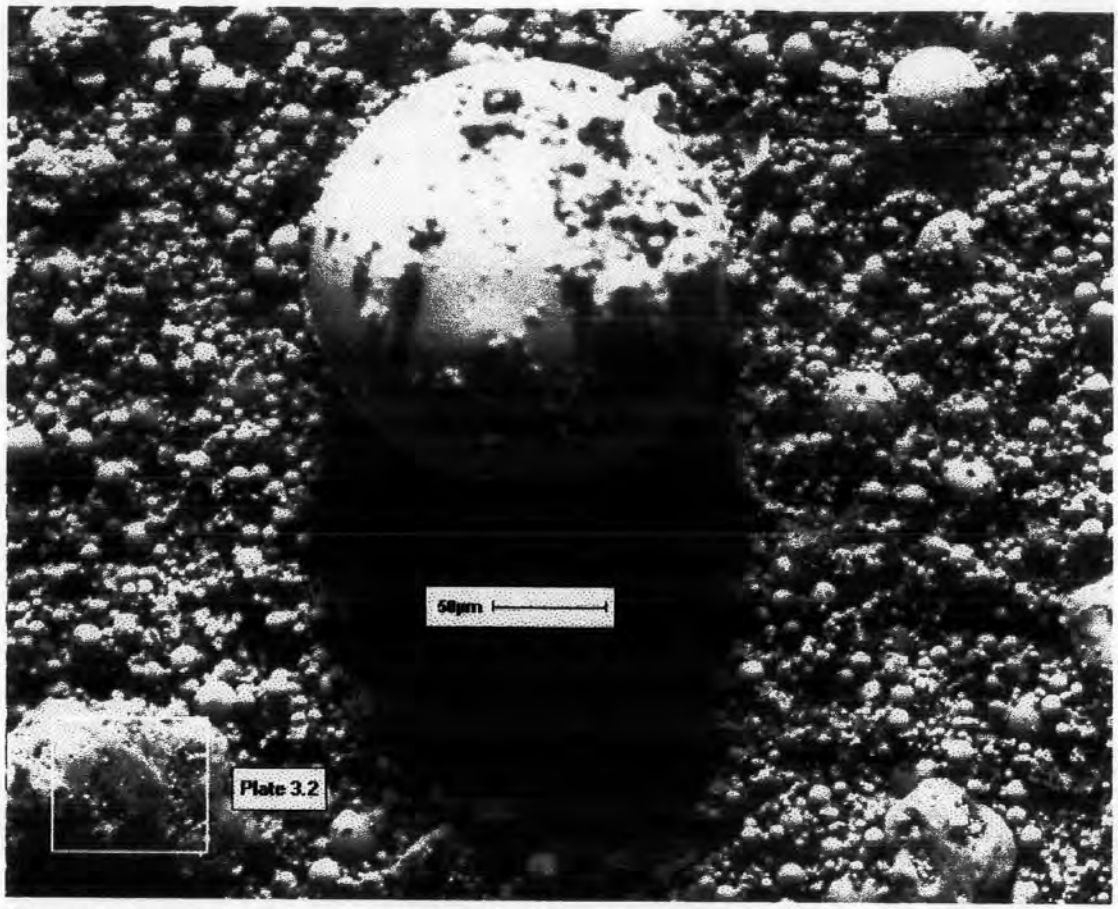

Plate 3-1 Drax view showing very different grain sizes

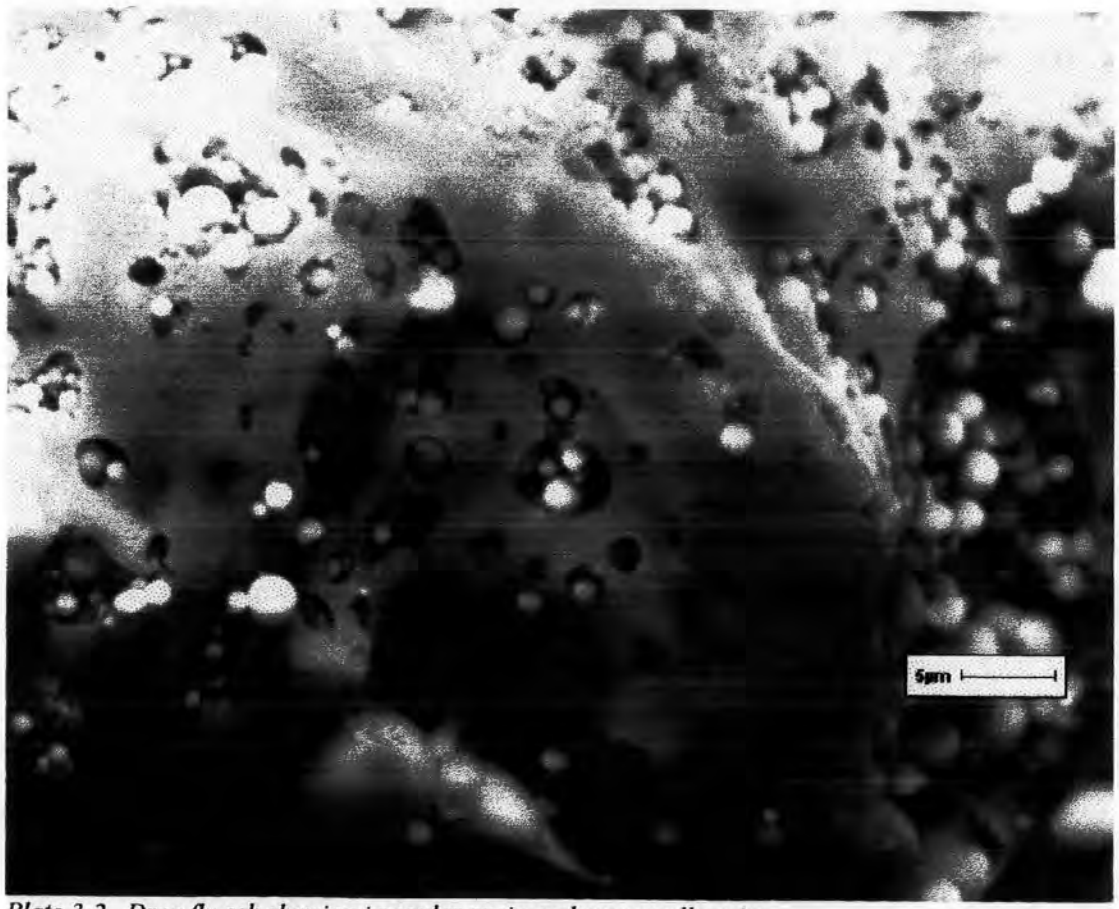

Plate 3-2 Drax fly ash showing irregular grain and very small grains

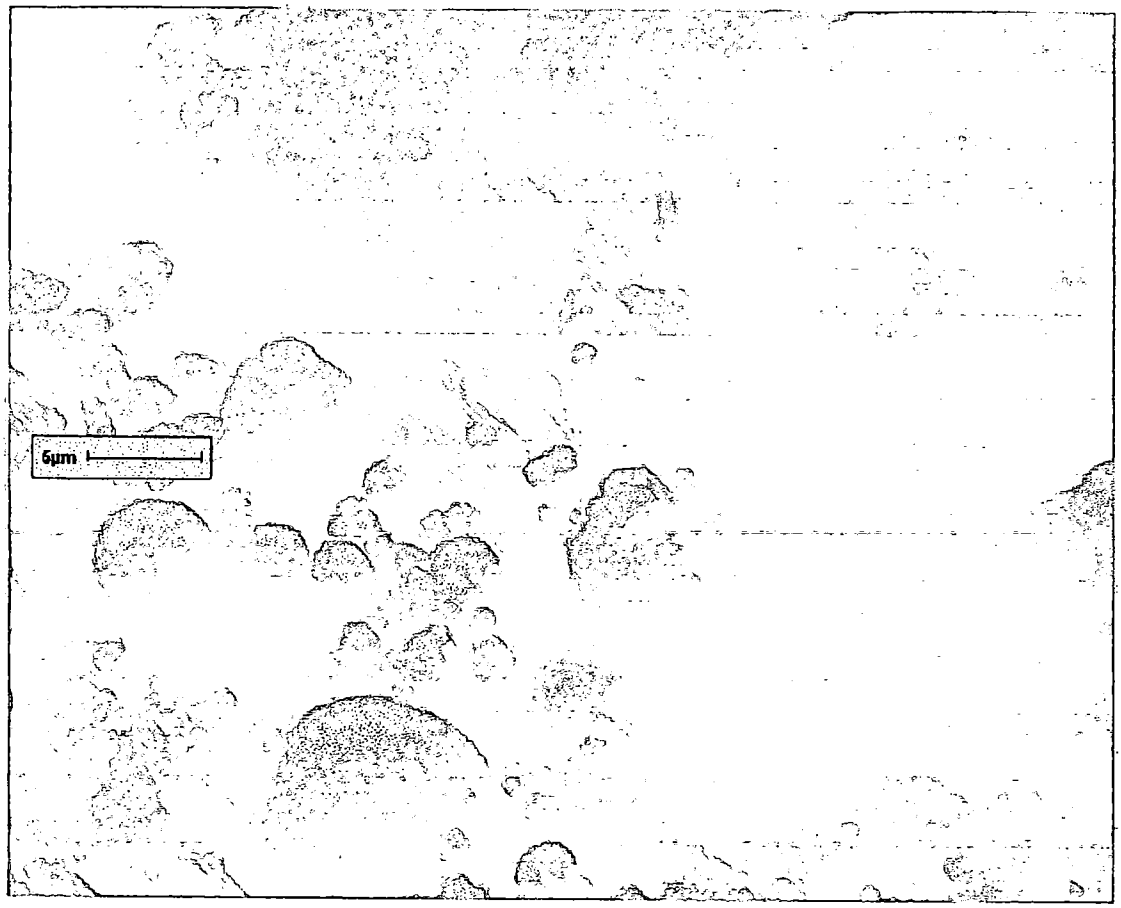

Plate 3-3 Lagoon fly ash showing various grains and the indication of a binding medium

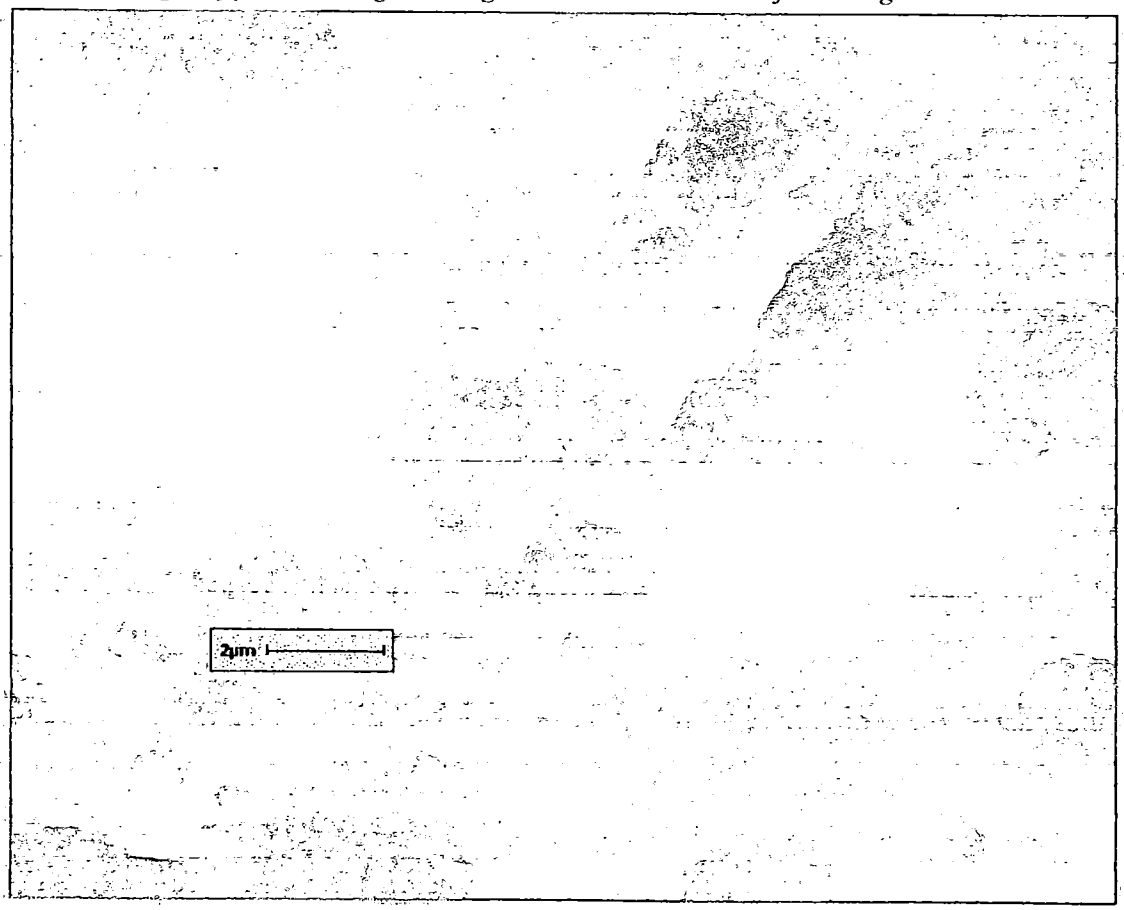

Plate 3-4 Mortar specimen showing the binding medium of very fine crystals inbetween the grains.

3.3 Discussion

The results of the above tests on the Lagoon fly ash and Drax fly ash indicates that both are non-plastic sandy silts with low dry densities containing some trace elements in toxic concentrations. Despite it's uniform appearance, the fly ash is composed of a number of different characteristics. The variations within the fly ash occur on a number of different levels from the macro scale, with the variety of grain types, down to the nanoscale and variations in the chemical compositions in the glass.

The fly ash is a by-product of the burning of pulverised coal and is composed of the incombustible, and non-combusted particles. The incombustible material mostly originates from flood events that deposit sediment whilst the peat is growing, as well as, mineral veins from circulating hydro-thermal fluids. In the fierce furnace temperatures of the power station, the incombustible material melts, allowing the mixing and concentration of elements. The droplets of molten incombustible material within the flue gases solidify on exiting the furnaces, preserving their compositions. Air bubbles form glass spheres, which make up the majority of the fly ash grains.

There is a wide variation in the specific gravity of fly ash from the tests. Looking at the specific gravity of different size fractions shows an increase in value with decreases in size. This is to be expected when the majority of particles contain air, and the ratio of air to glass decreases as their size decreases. However, the variation of specific gravity is not due to the changes in air content alone. The variation in the content of other minerals has a noticeable effect. The unburned carbon content will

tend to decrease the specific gravity as the percentage increases, whilst the increase in iron content will tend to increase the value. The variations due to particle types are amplified by their distribution whilst filling the settlement lagoons. It is the lagoon samples that show the widest variation.

The majority of the grains are silt sized, with some fine and coarse sand sized grains, but very few of medium sand size. Particle size distributions for previous investigations also indicate a lack of these particle sizes in most tests. Grains of greater size tend to be composite or nodular whilst those smaller tend to be the glass spheres and dark grains. This may be a limit imposed by the amount of glass needed to maintain an air bubble. Large bubbles tend to break down on cooling very easily. There is evidence from scanning electron microscope (SEM) to show larger spheres broken whilst smaller grains remain intact. The composite grains held together and the nodular grains have sufficient glass to maintain their shape on cooling and retain the air within. The larger grains have a different character to the smaller grains but there are few of each with the intermediate size, which causes the hiatus.

There is evidence from the particle distribution results of the pozzolanic potential within the lagoon ash. The particle size distribution for the structured and de-structured mortar samples show a reasonable correlation with each other, distinct from the other ash samples. Their flatter curves are spread more consistently over a range of particle size. The lagoon ash samples tend to have steeper curves and can be defined by the same region on the plot, although, their paths may wander within it. The exception is the curve for sample 10606, who's distribution curve falls at the edge of the region of other ash samples below silt size, but shows a higher proportion of

coarse sand particles. Again there are very few medium sand grains. The large grains were platey or needle-like in shape indicating a possible origin of a single bonded layer.

The lack of plasticity shown by the Liquid Limit test indicates that interparticulate electrostatic forces are weak, and another bonding force is occurring. As the layers within the lagoon specimens represent different outwash events, which can have different chemical compositions, it may be assumed that the bonding may be caused by the presence of a specific element not present in the same concentrations in other layers. As CaO_2 varies in fly ash 1-10%, and is known to produce the pozzolanic reaction, this may be the bonding force between the particles.

Looking closely at grains of lagoon ash, most are clean glassy spheres. However on occasion, the surface of the spheres appears rough and there are signs of needle shaped mineralisation appearing which is easily visible in the mortar samples. These needles are believed to be composed of ettringite and are an alumino calcium hydrate product of the pozzolanic reaction, as suggested by Helmuth (1987) & Yang (1992). The complex reaction uses the glass as a source of react material. The area between the glass spheres is where the resultant pozzolanic paste is produced. The siliceous calcium hyrates that form at the surface of glass allows for the binding of adjcent particles at their contacts. This is similar to the binding of the sand grains by the kalin clay in the artificial specimen first described by Maccarini (1987) and later used by Bressani (1990) and Malandraki (1994). The presence of the ettringite suggests that there is another mechanism contributing to the surface binding. The interlocking and intergrowth of the ettringite needles, in the void space between particles, adds an

additional binding structure. It also suggests that the bonding is rigid where compounds physically join grains, but also possibly elastic where the strength comes from the interlocking of the ettringite needles. The bonding characteristics will thus be a function of the interaction of the various binding mechanisms present within the reactions fly ash. To separate out the various different mechanism involved in the bonding would require extensive compound and chemical analysis, using a variety of different pozzolans other than fly ash, and hence outside the scope of this research.

4. Triaxial and Oedometer tests - Equipment and Procedures

A series of tests was designed to evaluate the strength and deformation properties of the fly ash along similar lines to those employed for other structured soils. The majority of these tests were performed using triaxial testing equipment although some one-dimensional consolidation tests were also carried out. An extensive series of drained and undrained tests was performed on both structured and de-structured samples at confining pressures ranging from 25 kPa to 800kPa. The higher confining pressures were possible after modifications were made to the testing equipment, extending the maximum working pressures from 750kPa to 1000kPa.

In addition to the triaxial tests, one-dimensional tests were performed on structured and de-structured samples for both the mortar and lagoon fly ash, as well as, some tests on very loose samples of lagoon fly ash. These tests were designed to quantify the consolidation behaviour over a wide range of conditions.

A series of tests was carried out on samples of lagoon fly ash obtained at different depths from the same borehole. These tests were conducted to establish patterns of behaviour associated with depth in the lagoon.

4.1 Triaxial Compression Equipment

The majority of fly ash samples examined in this research were tested using a computer controlled triaxial machine.

4.1.1 Axial Shearing

Two of the three machines employed in triaxial tests were standard triaxial machines supplied by Wykeham Farrance [Load capacity 5000kg]. The third machine was a hydraulic triaxial cell from Imperial College, University of London (Bishop & Wesley, Geotechnique 1975). The Wykeham Farrance machines used a multi-speed motorised drive unit to control the rate of strain, raising or lowering a pedestal upon which the whole cell sits. The hydraulic cell used a hydraulic ram to raise or lower the bottom seating of the sample from within the cell. A screw pump run by a computer controlled stepper motor controlled the hydraulic ram for these tests.

4.1.2 Cell and Back Pressure Systems

The cell and back pressure systems were controlled by the computer (Section 4.1.4.2). However, the Wykeham Farrance machines retained the ability to be manually controlled if necessary. Both systems originally used air/water interfaces to control the pressure limited to the maximum stable air pressure from the compressor of 750 kPa. To increase the useable confining pressure systems of the cells, modifications were made to allow them to be independent of air pressure. Screw pumps similar to those employed in the control of the hydraulic ram of the stress path cell were fitted to the cell pressure system in between the air water interface and the cell, as shown in

Figure 4-1. As the screw pump consisted essentially of only variable void space, the cell pressure could still be maintained by the air pressure if desired or increased to higher pressures using the screw pump when tap 'A' was closed.

It was hoped that the screw pumps could provide pressures close to the maximum limits of the cells of 1700kPa. Pressure transducers PII (Table 4-1) were installed to cope with the extended pressure range. However, initially the screw pumps only extended the range to 1200 kPa, which decreased during the testing program to only 800kPa. The reductions in pressure obtained from the screw pump were considered to be due to frictional resistance within the screw mechanism. The screw pumps did provide sufficient extension of the pressure range for the analysis of the material.

The back pressure system used computer controlled pressure valves and remained dependent on the air pressure for all the tests.

4.1.3 Transducers

Measurements of the different pressures and strains within the triaxial were taken using the several types of transducer detailed in Table 4-1 with their relative locations shown in Figure 4-2. The cell pressure was measured externally using either type PI or PII transducers. The same devices were fitted externally to the cell in the back pressure system, measuring the pressure at the base of the specimen. Pore water pressures at mid-height of the specimens were measured using a pore water probe type PIII.

The volume change in the back pressure system was measured by an Imperial College volume change device (Head, 1982).

The strain of a specimen was measured using three types of transducers. Two external displacement transducers, types DI & DII, were used in the conventional way to measure the change in height of the specimen. These were subject to the seating effects in the initial stages of the test and did not measure the true strain within a sample during this time (Jardine et al, 1984). A pair of electrolytic level internal strain gauges, types DIIIa&b described in Jardine et al (1984), were mounted on the specimen. Attached directly on opposing sides, they measured the strain of the central portion of the specimen, and were not subject to the end effects and movement within the cell that hindered the external devices initially. They were calibrated absolutely to give a true distance between the two footings when they were on a vertical surface.

The axial load applied to the sample was measured using submersible load cells, types LI a&b, contacting with the sample through a ball end sitting within a cup in the top cap as suggested by Bressani & Vaughan (1990) to avoid non-uniform loading due to tilting of the top surface during compression.

4.1.4 Computer Control System

The TRIAX program (Toll, 1993) was used to control the tests. Each of the triaxial machines was controlled by its own computer, which was used to monitor and control the environment of the test. In the case of the hydraulic cell, the computer controlled all aspects of the test (cell pressure, back pressure and axial load). The Wykeham

Farrance machines that were adapted for computer control for this research had only the pressure systems computer controlled. The motorised ram for applying a constant rate of strain could only be manually controlled.

4.1.4.1 Data Logging

All transducers on each machine were connected to a data-logging unit which transmitted the voltage information to the computer. Measurement Systems Ltd units (DataScan 70 & 72 series) were used. These units use a 16 bit analogue to digital converter and also provide auto-ranging to match the measurement range to the input voltage. At the lowest voltage range (20mV) the converter has a resolution of 0.6μV. The TRIAX program provides facilities for calibration for each of the transducers, from which it calculates a regression, used to convert the voltages into the necessary units

4.1.4.2 Control Boxes

The same computer used to take readings from the transducers also adjusts the relevant pressures within the triaxial machine through control boxes, which contain stepper motors. The computer can operate pressure valves and screw pumps by sending signals to the associated stepper motors. The pressure control units, supplied by Imperial College, have a resolution of 0.07kPa per step, and the screw pumps have a resolution of 0.694mm^3 per step of the motor, providing very precise control.

4.1.4.3 Stages

Taking information from the transducers through the data logger, the computer can use this information to adjust the control boxes to carry out complex stress path tests. The necessary information and commands are written down in 'Stages' (Toll 1993). A test may require only one stage to perform a certain task such as raising the cell pressure between two pressures, or a combination of many stages linked together for more complex tasks as in the K_o (lateral earth pressure at rest) tests.

	Transducer	Range	Resolution	Machine
Pressure (kPa)				
	PI	0-750	±0.02	T2
	PII	0-2000	±0.03	S-P & T1
Piezometer Probes	PIII	0-750	±0.04	ALL
Volume (cc)				
	VIa	50	±0.01	S-P
	VIb	100	±0.01	T1 & T2
Displacement (mm)				
External {	DI	25	±0.0005	S-P
	DII	75	±0.0012	T1 & T2
Internal	DIII	31-47	±0.002	ALL
Load (N)				
	LIa	4400	±0.05	S-P
	LIb		±0.35	T1 & T2

Table 4-1 Different types of Transducers used with the Triaxial machines.

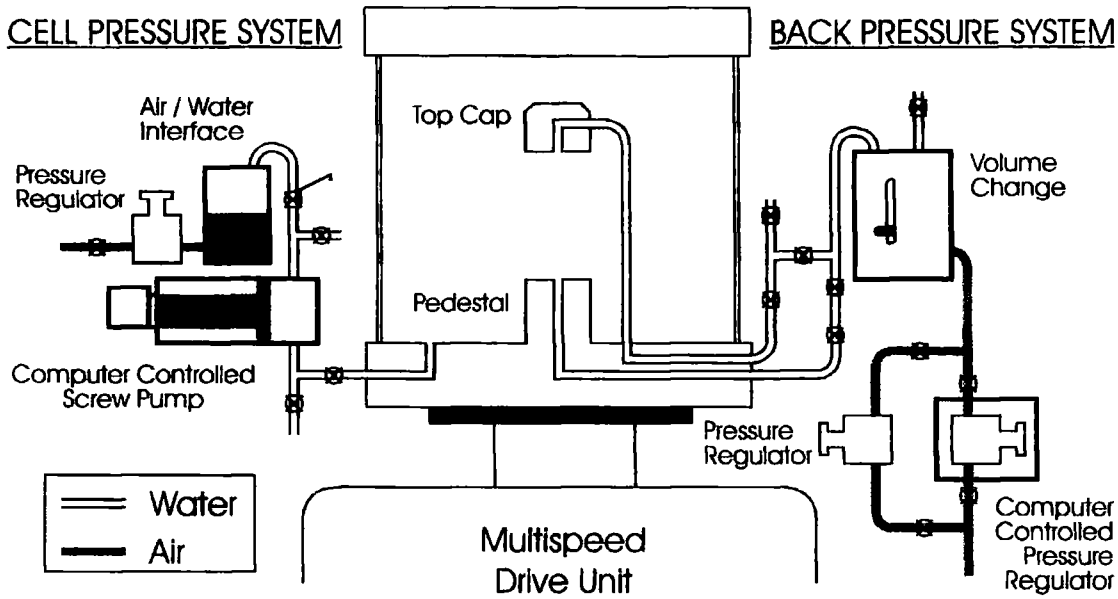

Figure 4-1 The insertion of computer controlled devices in to the Cell and Back pressure systems of the Wickham and Farrance machines.

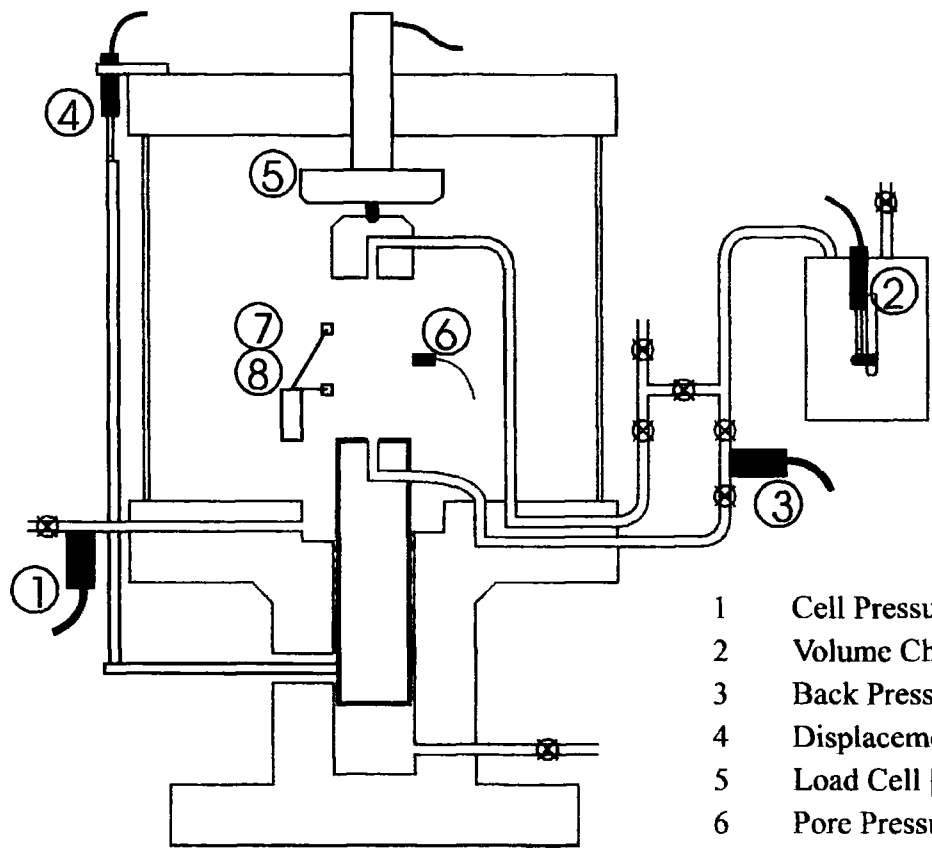

Figure 4-2 The location of transducers used in the Stress Path Cell

4.2 Samples

4 2.1 Nomenclature of Specimens

Each specimen was uniquely identified using a system of three letters followed by a number that describe the material and the testing conditions. The initial three letters describe the material and pore water environment. The first letter identifies the type of fly ash used (Lagoon Ash 'L', or Mortar Ash 'M'), the second describes the drainage conditions under which the specimen was tested (drained 'D', or undrained 'U'), and the final letter indicates the potential state of the pozzolanic structure (undisturbed & structured 'S', or remoulded & de-structured 'D'). The number suffix normally represents the effective confining stress (kPa) applied during the consolidation stage of the triaxial test, except for the lagoon specimens from BH406. These specimens were tested at similar confining pressures and to avoid confusion the Delft tube numbers from which the fly ash originated were used instead.

4.2.2 Undisturbed Lagoon samples

The Delft tubes were opened by using a drillsaw to cut the plastic lining along its length on both sides. This was performed whilst the sample tubes rested in a frame canted at 60°. The casing was then removed from one side, and the internal stocking was cut off. Then the length of the core was photographed and logged.

The cores of fly ash were well laminated from the numerous outwash events from the power station. It was not possible to divide the cores up into measured lengths for testing because of narrow silt and fine sand horizons along which the core pared

easily. It was necessary to first identify the more competent segments of the core between these horizons and use those with an axial length greater than 76mm to prepare undisturbed samples for triaxial testing.

The Delft core samples of 60mm diameter were trimmed to 38mm diameter for use in triaxial compression tests with the use of a soil lathe shown in Figure 4-3; the design was based on the lathe by Wykeham Farrance. Only the central portion of the cores considered to be the least affected by the sampling processes were used for specimens. The edges of the soil lathe were designed to allow the cutting instrument to pass up and down at a distance of 19mm from the vertical axis to give a final specimen. The samples were trimmed using a fine cheese-wire or a sharp knife by cutting off vertical slivers. The platform was rotated slightly between each cut until a cylindrical specimen had been formed. After the specimen was cut to the correct size, the trimmings created were used to obtain moisture contents and specific gravities for the specimens.

During trimming of the core segments it became obvious that different layers possessed different strengths. Most layers were cut easily with the cheese wire. However, there were more resistant layers requiring trimming with a knife. Samples containing resistant layers were of more interest in this research where it was the properties of the pozzolanic activity that were being observed. They were also the hardest to prepare and were not present in some cores.

The self-cementing characteristics of fly ash rely on certain chemical and physical characteristics of the ash, which are dependant largely on the parent coal, as well as

the ash production and processing. The weak material probably lacks the pozzolanic activity and structure of interest. Some horizons contained many gravel sized particles, probably Furnace Bottom Ash (FBA) used to construct the berms around the lagoons for containment of the fly ash slurry (Figure 3-4). Samples found to contain these were discarded, as were samples containing rootlets.

Undisturbed lagoon specimens used in the oedometer test were cut from the central portion of the Delft core to the approximate size of the oedometer ring, which was then used to trim off the excess (see Section 4.2.6.3).

4.2.3 Remoulded Lagoon Samples

The term "remoulded" refers to the reconstitution of broken down fly ash from Delft core samples to the same moisture content, removing any internal fabric that may be present. The remoulding removes the layering as well as potential bonding between particles. The fly ash used came from trimmings cut from around undisturbed samples. Additional material was obtained from the same region of the sample. The material was left to air dry and was then broken down by hand to a powder in a similar manner to that described by Sivapullaiah et al (Unpublished). The powder was oven dried and allowed to cool before being mixed with distilled water to a moisture content of 24% and left in an air tight bag to equilibrate for 48 hours. A moisture content of 24% was chosen to match the moisture contents observed in the undisturbed samples. The samples were then formed to the required void ratio of about 0.95 using the technique described in Section 4.2.6.

4.2.4 Structured Mortar Samples

Samples were prepared by sieving the mixture of dry fly ash and 5% slaked lime (Ca(OH)2) together, before adding distilled water to the optimum moisture content of 19%, observed from compaction tests. The fly ash and lime were mixed for half an hour by hand to an even consistency, and formed into samples with a void ratio of about 0.9 using the method described in Section 4.2.6. Once formed, they were weighed and fitted with a rubber membrane and left in a humid environment to cure before being tested. In this way the bonds formed in the first 48 hours of the curing process were not broken down by the remoulding of the fly ash during the formation of the cylindrical samples from the mixture. Specimens remained in the humid environment for the desired curing period before being tested. The optimum length of 6-8 weeks was established by comparing compressive strength against curing time (see Section 6.1).

4.2.5 De-structured Mortar Samples

The de-structured mortar samples were formed from a mixture of lime and fly ash formed in the same manner as the mixture used for the structured mortar samples. The mixture was not formed into specimens but was left in a sealed environment for 8 weeks before being broken down by hand to a powder. To remove the potential for this powder to react further with any unreacted lime in its composition, the de-structured material was processed as follows. To remove the lime rich moisture of curing, the loose cured material was washed with distilled water over filter paper to retain the fines. It was then oven dried before being mixed with distilled water to a moisture content of 19%. The mixture was left for 48 hours to equilibrate and allow

for any re-reaction of the lime and fly ash, which would increase the strength of the uncompacted clumps and be noticeable during the specimen formation in the moulding process. Samples were formed immediately prior to testing using the split mould (Section 4.2.6) to achieve a void ratio of about 0.9, mimicking the structured samples. Because the unstructured material consisted of broken down structured mortar, the term de-structured has been adopted to emphasise that the material has undergone the pozzolanic reaction in its formation.

4.2.6 Moulded Samples

4.2.6.1 Preparation of Material

The materials used for the formation of remoulded lagoon, structured mortar and de-structured mortar samples were in powdered form. Distilled water was added to the powder to achieve the required moisture content and they were then mixed together. In the case of the de-structured samples the mixture was left in a sealed plastic bag for a minimum of 48 hours before being used to construct samples. This was not possible in the case of the structured mortar samples, where the formation of samples could cause the breakdown of any bonds formed during this time. These samples were formed immediately after mixing to an even consistency.

4.2.6.2 Formation of Moulded Samples

Samples were made in a split mould of approximate dimensions, 76mm high and 38mm in diameter. The samples were constructed in six layers, containing an equal amount of material, to reduce the effect of compaction differential from top to bottom

of a sample (if it were composed of a single layer). When using more than six layers it proved difficult to control the compaction needed to produce equal layering throughout the sample. Each layer was statically loaded to achieve a height of 13.0mm, with the top of the preceding layer being heavily scored to improve the bonding between successive layers. The samples were statically loaded to reduce the potential for particle breakdown under dynamic loading, and because of the high void ratios to be achieved. These were in the region of 0.9 to 0.95 to match the lagoon undisturbed samples and the low force required to compact each layer to the desired thickness was best achieved by hand.

The mould used was a brass split mould fitted with an extension collar to accommodate loose material prior to compaction. The ram, also made of brass, was made to fit the mould loosely, and was marked along its length with the heights required to form a six layer specimen.

4.2.6.3 Oedometer Samples

Moulded oedometer specimens were formed directly into the oedometer ring in only three layers. The same method of static loading was used to compact each layer. In the case of the Lagoon fly ash an additional remoulded sample was tested with the fly ash in a very loose state. This sample was formed by filling the ring with a known weight of dry lagoon ash poured in up to the level of the ring top, without any compaction.

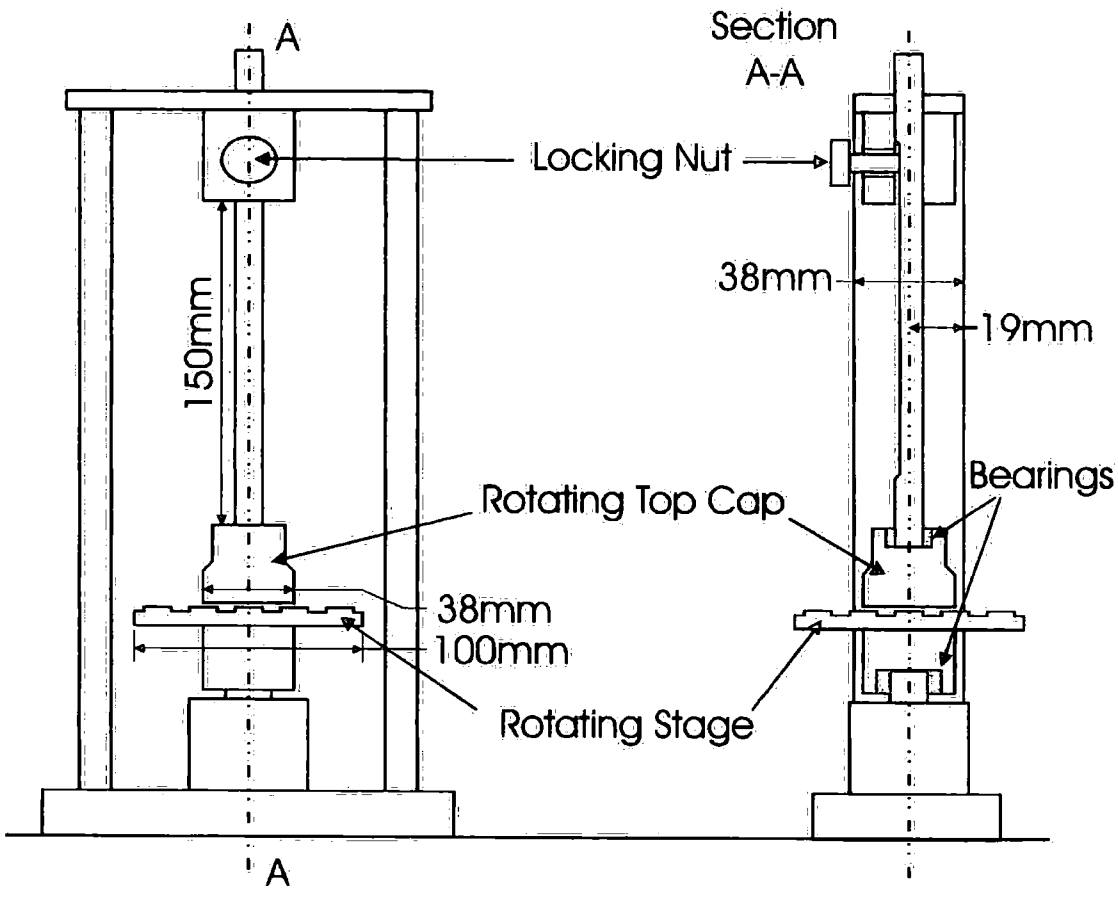

Figure 4-3 Soil Lathe for trimming undisturbed material into 38mm cylindrical specimens

4.3 Procedure for triaxial testing

4.3.1 Specimen preparation

The specimens were weighed wet to within ±0.01g and dimensions were measured to an accuracy of ±0.1mm. All specimens tested in the triaxial machines were fitted with latex membranes to keep the cell and back pressure systems separate. A membrane former was used to fit the latex membrane around the specimens without causing damage, and suction was used to expand the membrane before it was placed over the sample. For normal triaxial tests the former needed to be only a few mm larger in diameter than the sample. However, in tests using a mid height pore water probe a larger former with special adaptations was needed to accommodate the pore probe rubber holder. The installation procedure described in Hight (1982) covers the modifications required when such devices are used. The larger diameter of this type of former can cause some difficulty when the membrane is released, as the membrane is under greater tension and can damage delicate samples. Most notably, the remoulded and de-structured specimens could be damaged upon release.

The samples were set up in the machine as shown in Figure 4-4 with a porous disk at each end and the membrane secured top and bottom by O-rings. Any internal strain gauges were glued to the outside of the membrane on opposing sides with super glue. A good bond between the membrane and footing was needed, as the cell water could affect the super glue after long periods of immersion. This may result in one or both of the gauges becoming detached. It was found that liquid super glue proved better than those in a gel form.

4.3 2 Saturation

All triaxial samples were saturated using a two-stage method. The first stage involved slowly flowing water through the sample under a slight head of pressure, of up to 5kPa, to remove any large bubbles. Then the pore water in the sample was pressurised to dissolve any remaining air bubbles within the soil.

For the first stage the cell was filled with water and the pressure raised to 30kPa whilst freshly de-aired distilled water was allowed to flow through the sample from a head pressure of 25kPa to remove any visible air bubbles. Through flowing was stopped when no more air bubbles were observed. For the undisturbed lagoon samples this was 24 hours but samples formed in the mould required only 1-2 hours. The flow was then stopped by sealing the back pressure system and both the cell and back pressures increased up to 300 kPa at a rate of 100kPa per hour. The cell pressure was always maintained at 5kPa above the back pressure, thus keeping a small effective positive stress. The 5kPa was maintained by using the computer to slowly control both the back and cell pressures. B-tests were performed to establish the degree of saturation of the sample. If a B-test is performed on a sample with only partial saturation it will affect its state, which is particularly important for structured soils shown by Bressani & Vaughan (1990). To prevent this, the volume change was plotted with time giving a measure of the amount of water passing into samples as the air dissolved into the pore water. B-tests were taken once the graph levelled off. The sample was considered saturated once a B-value greater than 0.95 was reached, following the recommendations in Head (1998:52).

4.3 3 Isotropic Consolidation

Samples were isotropically consolidated to a specific confining pressure ranging from 25-800 kPa. The cell pressure was applied rapidly to the desired amount to establish the required effective stress whilst maintaining a constant back pressure. This method allowed the assessment of the permeability of the undisturbed lagoon specimens. The other specimens were also subjected to the same conditions to allow for comparison between the results. The shearing stage of testing was only started when consolidation was completed and the volume remained steady within ±0.01cc. The consolidation of the sample was calculated using the volume change measurement. The change in volume was used to calculate the reduction in the length of the specimen, assuming the sample was a right cylinder.

4.3.4 Shearing

Most tests were run to 25% strain or greater and all were carried out under constant rate of displacement conditions of 13.72 mm/hour, (or 0.009ins/min for the Wykeham Farrance machines). Samples fitted with internal strain gauges used the devices to measure strains at the start of compression, up to 2% axial strain, after which the external displacement transducers measured the strain to the end of the test. This exploited the benefits of both transducer types. The internal strain gauges measured the direct strain on the sample at the start of the test when seating movement in the equipment affected the external transducer. After all the seating effects of the machine had finished and the samples began to bulge, reducing the accuracy of the internal strain gauges, the external displacement transducer took over to measure the axial strain for the remainder of the test.

Samples fitted with a pore water probe used the device to measure pore water but the external pressure transducers were still recorded for comparison, as well as to control the back pressure control system during drained tests.

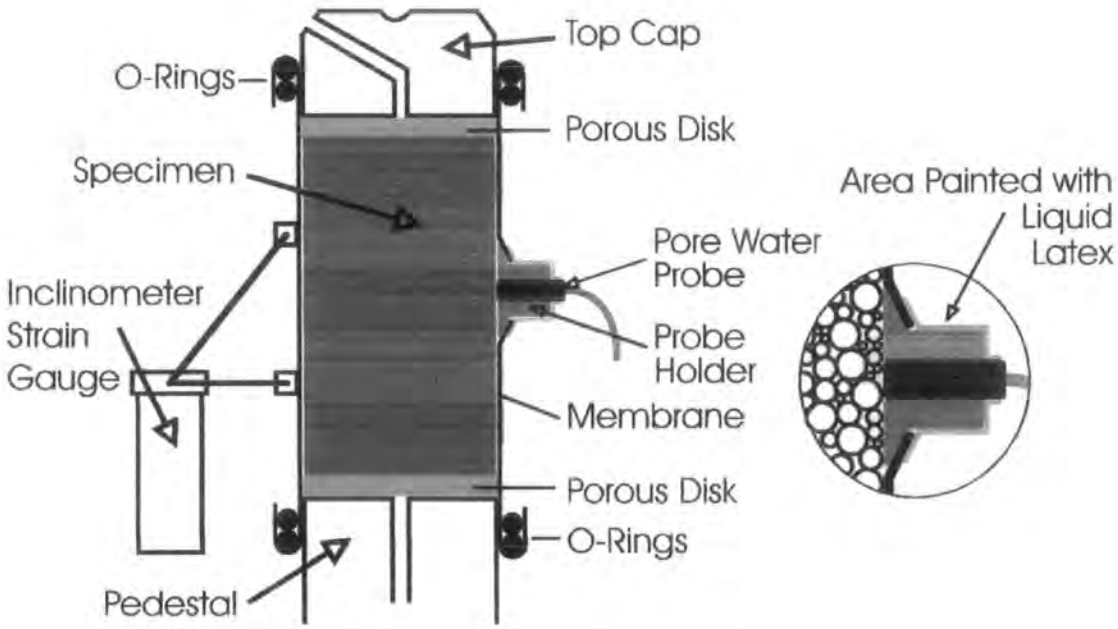

Figure 4-4 The completed setup of a specimen fitted with direct strain measurement and pore water probe devices prior to immersion

4.4 Procedures for Consolidation Testing

4.4.1 Oedometer

One-dimensional consolidation tests were carried out on both the Lagoon and Mortar fly ash materials, looking at the response of both the structured and de-structured forms. These tests were performed using a standard oedometer following the procedure outlined in BS1377 (1990) Part 5:3 using multiple stages on a 50mm diameter cylindrical samples of approximately 20mm height. The samples were flooded at the beginning of consolidation with the first load. Samples were tested to the maximum load of 785 kPa and 2355 kPa, due to limit of the weights available.

5. Triaxial Results on Lagoon Fly Ash

5.1 Drained Tests

5.1.1 Remoulded Samples

Samples composed of remoulded lagoon fly ash were compacted to achieve void ratios of 1.0 -0.9 using the technique described in Section 4.2.3. They were tested under drained triaxial conditions at confining pressures ranging from 25 to 800 kPa. These tests were designed to study the de-structured behaviour of the remoulded lagoon material.

All tests were performed at a rate of 0.009 inch/min (13.716 mm/hour). This was the closest speed on the Wykeham Farrance machines, which have fixed gear ratios, to the rate suggested from early tests. The pore water pressures during the drained tests presented fluctuated by less than 1kPa based upon pore probe reading. The different batches of remoulded fly ash material are indicated in Table 5.1 along with initial moisture content, specific gravities and void ratios.

Plots of deviator stress ($q = \sigma_1-\sigma_3$) against axial strain are shown in Figure 5-1. The axial strains were measured using internal devices for tests LDD25, LDD100 and LDD800. Where the information from these devices was unavailable in tests LDD50, LDD200 and LDD400, the axial strains were measured using traditional external devices. The plots show that maximum strengths were reached at axial strains of 10%

or higher, except for LDD25, which was carried out at a confining stress of 25kPa. The other test results showed a very gradual decrease in sample stiffness as they approach maximum strength, followed by a sharper decrease in strength. LDD25 reached a peak strength at 1% axial strain, and showed a significant decrease in post peak strength.

Test	*(batch number)*	M/C %	SG	$e_{initial}$	e_{consol}
LDD25	*(4)*	25.74	2.26	0.984	0.945
LDD50	*(1)*	26.74	2.14	0.932	----
LDD100	*(1)*	30.00	2.14	0.949	0.880
LDD200	*(1)*	28.57	2.14	0.946	0.867
LDD400	*(1)*	26.98	2.14	0.906	0.838
LDD800	*(4)*	25.74	2.26	1.074	0.969

Table 5-1 Specimen information and parameters for LDD tests

The specimens after testing are shown in Plate 5-1. Sample LDD25 demonstrated the formation of multiple slip surfaces not seen in any of the other samples. LDD200 was the only other sample to show a slip surface to develop, but in this sample it was more of a zone of shear and not a well-defined surface. All other samples barrelled in the middle, which is consistent with a ductile deformation upon loading.

The plots of volumetric strain with axial strain (Figure 5-2) showed an initial contraction for each of the samples (volume strain is defined as positive for contraction). After compression, sample LDD25 started to dilate at a high rate that

decreased after 2% axial strain. The peak strength occurred at the point of maximum rate of dilation of the sample. There was a general trend of an increasing amount of reduction in volume with increasing confining stress. However, tests at 200kPa and 400kPa did not follow this general trend. LDD200 showed a greater contraction than LDD400. Tests LDD50 to LDD400 reached a state of near constant volume by 10% axial strain. However, LDD800 was still contracting at 28% axial strain.

The effective stress paths in p'-q space are shown in Figure 5-3 where p' is the mean effective stress ($p'=(\sigma 1+2\sigma 3)/3$) and q is the deviator stress. The maximum strengths for each test at confining pressures of 50 kPa and above could be used to define a linear failure envelope with a stress ratio q/p' of 1.15 (equivalent to an angle of friction φ' of 28°, calculated from $\sin \varphi' = 3n/(6+n)$: where n=q/p'). The close correlation between the tests consolidated at 50 kPa and above could be seen in the plots of stress ratio against axial strain in Figure 5-4. The plot of test LDD25 was again very different from the rest in the group and shows a peaked curve followed by a much higher residual ratio of 1.40 by 20% axial strain.

Figure 5-5 shows a plot of void ratio (e) against mean effective stress plotted on a logarithmic scale (log p'). The tests at 100kPa confining pressure and above all demonstrated a reduction in void ratio indicating that these tests started with their void ratios on the wet side of critical. There was no plot for LDD50 due to the lack of reliable information from the consolidation stage of the test. The plot of LDD25 showed an increase in void ratio, which would indicate the specimen originated on the

dry side of critical. The end points of the tests tend towards a linear relationship that can be drawn in e-logp' space. The plot from LDD25 helped to define the lineation as it approaches from a different direction to the other tests and provided a lower limit. As the specimens are close to a state of constant volume by the end of the tests, from Figure 5-2, the lineation is probably a good approximation of the Critical State Line (CSL) for the lagoon fly ash in its remoulded state.

5.1.1.1 LDD Group Discussion

The results, with the exception of LDD25, show a near consistent pattern with increasing stress. They define a boundary surface in stress space and have comparable stress ratios. Test LDD25 exhibits a different behaviour to the other tests. Its peak strength occurs at a lower strain with a significant decrease in post peak strength, which may be associated with the formation of the slip surface. The volumetric change shows significant dilation after an initial contraction of the sample and the stress path extends above the boundary surface obtained from the other tests. As the specimens are made of de-structured material, these results indicate that specimen LDD25 was in an overconsolidated state. The void ratio of an overconsolidated specimen would be expected to plot on the dry side of the CSL, which is why the path of LDD25 in e-log p' space is different to the other paths which all plot above the line on what would be the wet side. The CSL is reasonably well defined by the results of these tests and can be used in the analysis of the bonded undisturbed specimens.

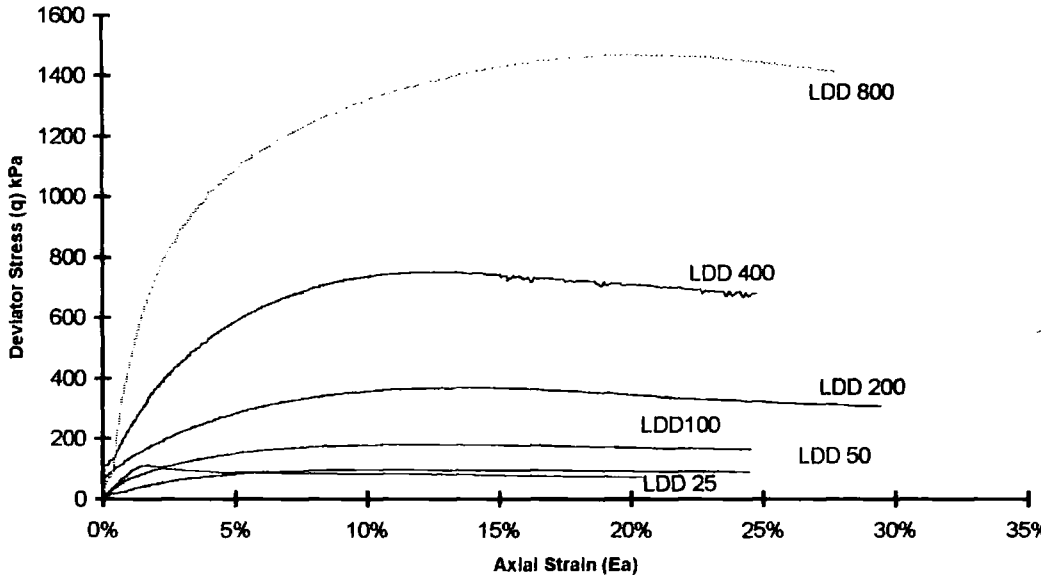

Figure 5.1 Stress against Strain plot for LDD tests

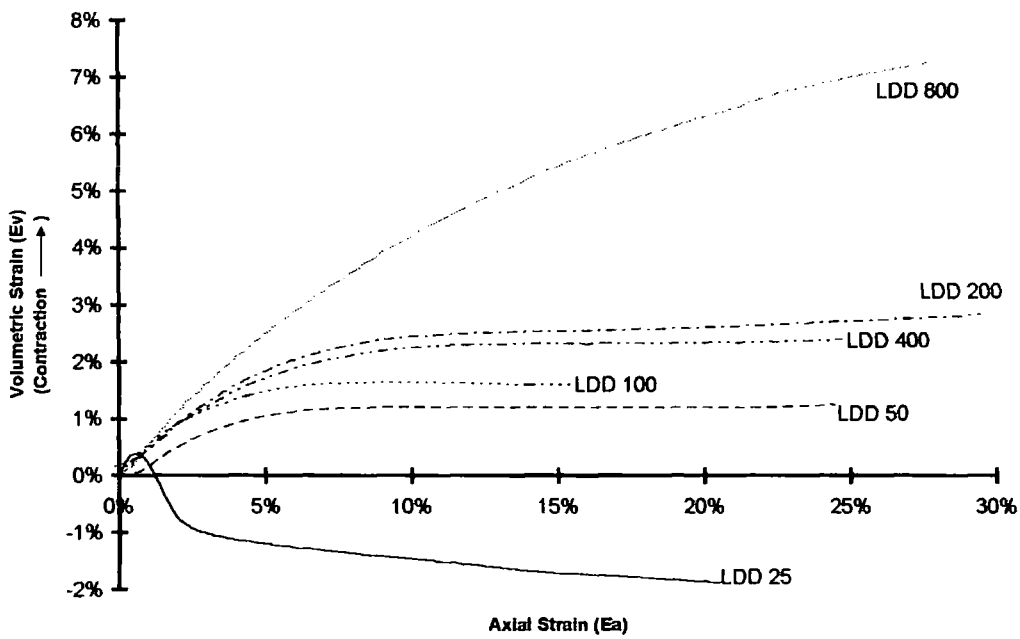

Figure 5.2 Volumetric Strain versus Axial Strain plot for LDD tests

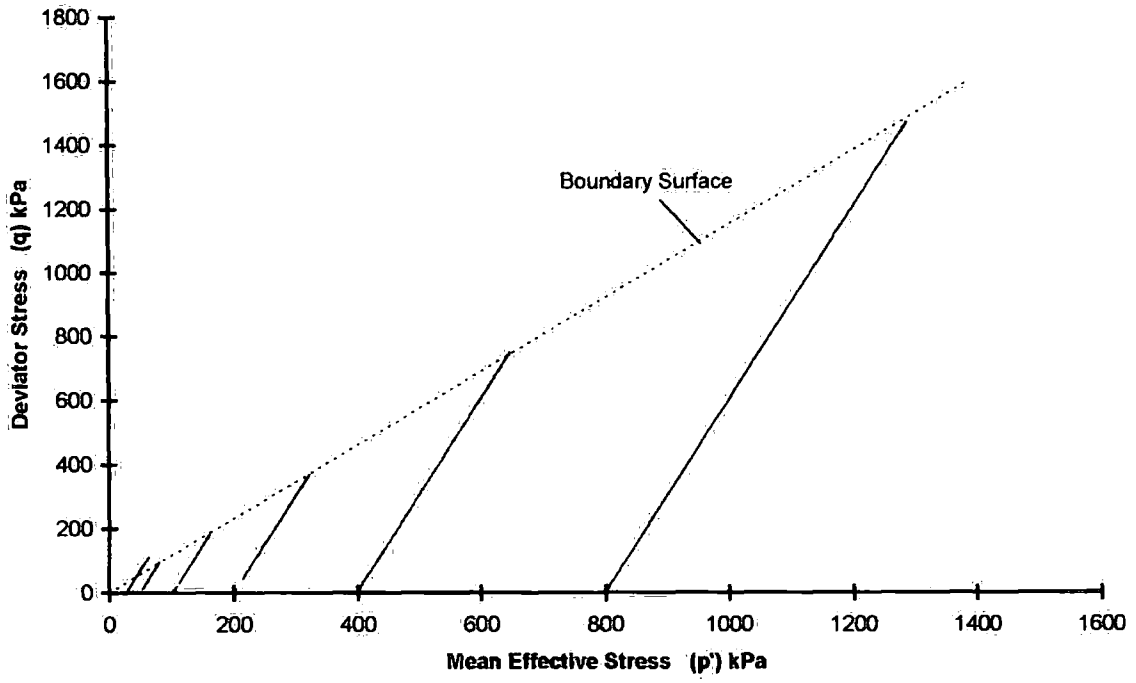

Figure 5.3 Effective stress paths for the LDD tests

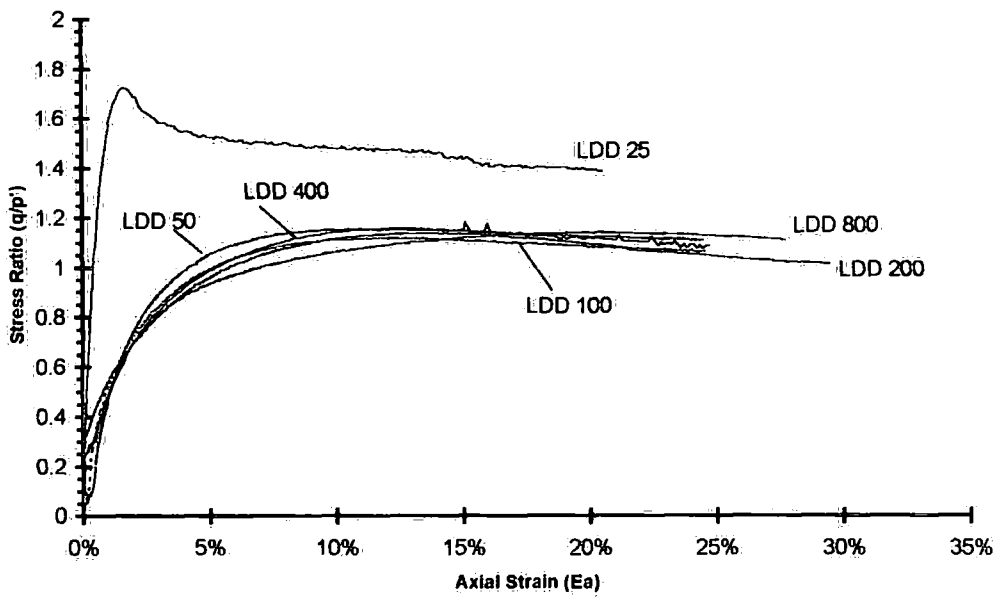

Figure 5.4 Stress ratio against strain plot for LDD tests

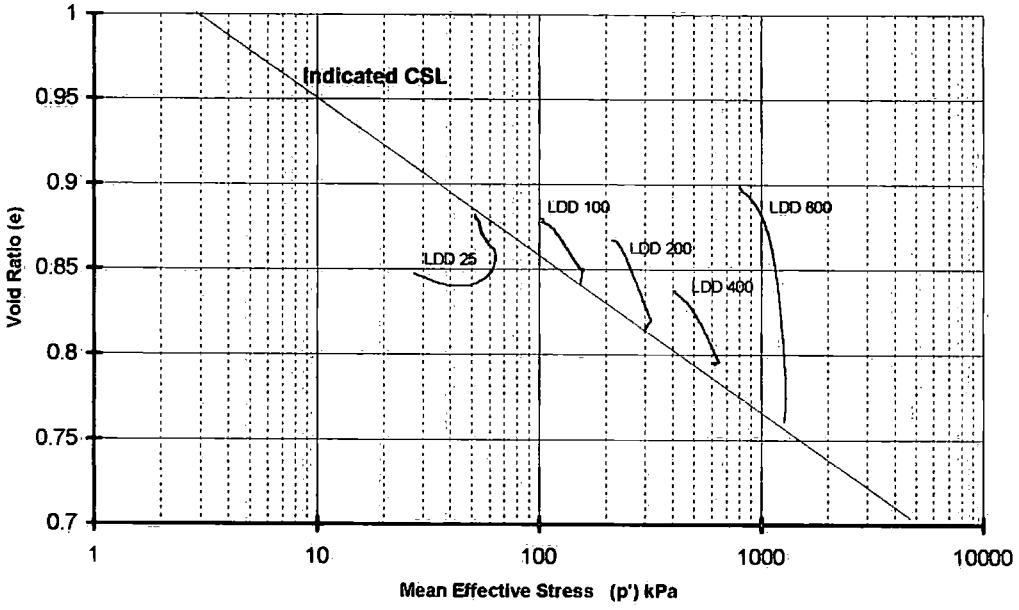

Figure 5.5 Plot of void ratio changes against mean effective stress for LDD tests

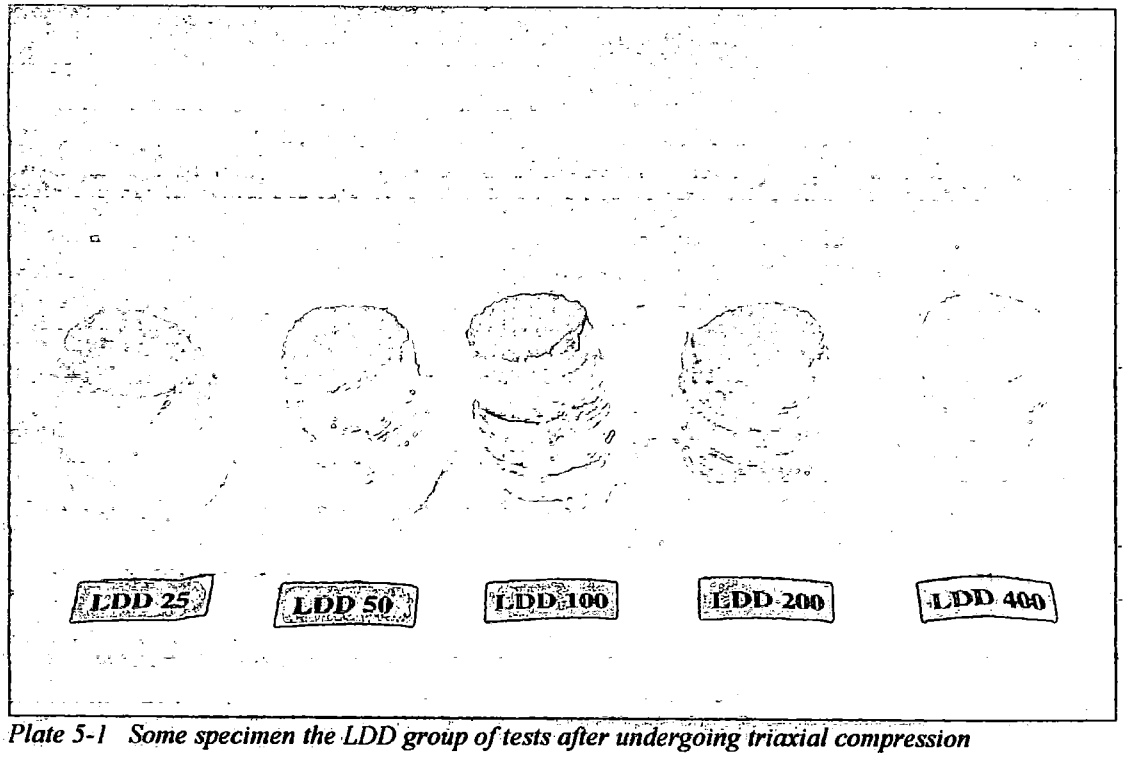

Plate 5-1 Some specimen the LDD group of tests after undergoing triaxial compression

5.1.2 Undisturbed Samples

Samples of undisturbed materials were cut from the central portions of the Delft samples. Six specimens were tested under drained triaxial conditions with a range of confining pressures from 25 to 800 kPa. This was to match the conditions of the tests performed on the remoulded samples. These tests were performed at the same rate of axial strain, again showing no significant pore water pressure changes above 1kPa.

Test	Tube	[Borehole] Depth(m)	*M/C (%)*	*SG*	$e_{initial}$	e_{consol}
LDS25	12022	[402] 11-12	37.39	2.20	0.830	0.821
LDS50	12022	[402] 11-12	41.67	2.06	0.858	0.838
LDS100	10818	[401] 12-13	33.60	2.13	0.843	0.789
LDS200	10818	[401] 12-13	37.63	2.22	0.883	0.839
LDS400	10194	[402] 16-17	37.97	1.89	0.826	0.806
LDS800	10540	[408b] 5-6	52.10	2.22	1.194	0.990

Table 5-2 Specimen information and parameters for LDS tests

The stress strain plots for the tests are shown in Figure 5-6. The first plot (Figure 5-6a) showed the tests where internal devices were available. The second (Figure 5-6b) showed all tests with the strain measurement based on external displacement devices. For tests LDS25, LDS50 and LDS700 there was little difference between the two methods of strain measurement. In LDS200 the measurement by internal devices did show a significant difference. The internal devices showed a significantly stiffer

response to loading. Failure occurred at only 1% axial strain compared to 6% axial strain for the external displacement devices. For LDS100 and LDS400, where there were no internal devices, the external displacement devices showed failure at about 5% axial strain, similar to the other lower pressure tests. LDS700 has a maximum strength at a significantly higher axial strain near the end of the tests at 23%. This test showed strain hardening throughout and did not have a peak strength.

The specimens seen in Plate 5-2 show a variety of deformations. Failure surfaces are seen clearly in LDS50, LDS400 and LDS800. The failure surface in LDS100 is visible due to its orientation. A more complicated series of failure surfaces is seen in LDS200, where there appear to be multiple surfaces concentrated in the centre region of the specimen. LDS25 shows a significant increase in its diameter with a suggestion of failure surfaces at the base.

Figure 5-7a shows the plot of volumetric strain against axial strain for the tests at 400kPa confining pressure and below. LDS800 is plotted in Figure 5-7b along with LDS400 for comparison. Tests at lower confining pressures, including LDS400, showed initial contraction followed by dilation. At the lowest confining pressures (LDS25 and LDS50) the contraction is small followed by a larger dilation. The rate of dilation reduces around 7% axial strain once a maximum strength has been reached. This point coincides with a change in the deviator stress versus axial strain plot (Figure 5-6 a&b), where the smooth curve changes to more erratic response as the specimens underwent strain softening. The initial contraction and subsequent dilation of test

LDS100 was smaller than at lower pressures. No significant volume change (± 0.1% volumetric strain) was demonstrated by the sample throughout the test. Tests LDS25, LDS50 and LDS100 all showed a further change when the sample begins to contract again at a similar point with respect to axial strain. Tests LDS200 and LDS400 both showed similar initial contractions followed by a smaller amount of dilation, with LDS200 dilating more. The dilation was followed by further compression, similar to test LDS 100.

Test LDS700 (Figure 5-6b) reached peak strength by the end of the test at 24% axial strain. It underwent continued compression throughout the test, approaching, but not reaching, a state of constant volume. Its behaviour was very different to the other tests in the group but is very similar to the remoulded tests.

From the plot of effective stress paths in p'-q stress space (Figure 5-8) it was possible to identify a failure envelope which represents a boundary for the undisturbed material. The boundary surface for the undisturbed material approximates to the boundary of the remoulded samples, with a slight increase in strength for low-pressure tests. The increase was lost by test LDS400.

The boundary surface of the undisturbed material could be confirmed from the plot of stress ratio against axial strain Figure 5-9. Here the plots of the low-pressure tests showed a decrease in the peak ratio with increasing confining pressure. The plot showed that for the higher pressures there was a grouping at 1.1 for ultimate stress

ratios similar to the stress ratio seen in the remoulded specimens (Figure 5-4). All but LDS700 showed a peaked stress ratio curve. For test LDS25 and LDS50 the stress ratios are higher with ultimate stress ratio around 1.4.

5.1.2.1 Identifying Bonding

As both overconsolidated and bonded soils tended to show a peak strength followed by strain softening it was necessary to identify behaviour, which distinguishes between bonded specimens and overconsolidated specimens. There were a number of features of the results that could used to determine whether the specimens were bonded and to represent its influence on the soil matrix, that have been used in previous research by Malandraki (1994), Maccarini (1984), Bressani (1990), and Vaughan(1985). Additionally any bonding found in the undisturbed specimens will help to determine the pattern of pozzolanic activity within the lagoon.

5.1.2.2 Maximum Dilation Rate and Maximum Stress

Previous research on structured soils (Vaughan et al, 1988), has identified that the dilatancy seen in the low pressure tests on undisturbed material may be caused by the bonding between the particles, as well as by the dense packing of unbonded sands and silts. Taylor's Model (Atkinson and Bransby, 1978), based on initial work by Taylor (1948) and later expanded by Schofield and Wroth (1968), considered the behaviour of coarse granular materials in shear box tests. It shows that when the strength of the material is due to particle interlocking and inter-particulate friction, the point of

maximum stress $(q/p')_{max}$ coincides with the point of maximum rate of dilation $(dEv/dEa)_{max}$ (Figure 5-10). The maximum rate of dilation refers to the maximum rate of change in the plot of volumetric strain against shear strain. Where bonding between particles influences the maximum strength, the dilation would be expected to occur after the bonding has yielded and so the two points would not be expected to coincide. Malandraki (1994) adopted this approach in her study of artificial structured specimens of sand and kaolin clay. In her study the maximum rate of dilation was defined from a plot of dEv/dEa plotted against Ea, where the shear strain is replaced by axial strain. By plotting these points in relation to the stress-strain curves, some indication is given as to the presence of bonding within the sample.

The points of maximum stress ratio and maximum rate of dilation are plotted on the stress-strain curves in Figure 5-11. For both LDS25 & LDS50 the points of maximum stress ratio coincide with maximum dilation of the sample, indicating a lack of structure in these specimens. The point of maximum stress ratio occurred prior to that of maximum dilation for tests LDS100, LDS200 and LDS400 indicating a structural influence to their strengths. The difference in strain between the two points was larger in LDS100 and LDS200 than LDS400. This reduction may be an indication of structural breakdown with increased stress. Also, as the two points occurred at the same stress levels this may indicate a ductile nature to their behaviour. There was no dilation in LDS700 and no corresponding maximum dilation point to compare to the maximum stress ratio.

5.1.2.3 Volume change in relation to the Critical State Line

A good indication of the presence of bonding used by other investigators was the comparison of each test against the critical state line (CSL) as shown by Malandraki (1994). As unbonded specimens approach the critical state, discussed in Section 2.2 on the critical state of soils, they will either dilate or contract. This depends on whether they plot on the wet or the dry side of the critical state line (i.e. normally or over consolidated). For bonded specimens this general pattern will not necessarily be the case for as long as the bonding is influencing the specimen's behaviour. This was best seen in specimens of high void ratio that plot above the CSL on the wet side. Whereas unbonded specimens on the wet side will tend to undergo consolidation those with bonding will tend to dilate towards failure (or the breakdown of bonding influence) before consolidating as the structure is progressively broken-down and the specimens become de-structured. The CSL used in the analysis of the undisturbed specimens could be defined from the results of the remoulded specimens as shown in Figure 5-5.

The plot of e vs. log p' in Figure 5-12 shows the CSL defined from the LDD tests. There appeared to be four different responses of void ratio change to the increased axial strain. For the lower pressure tests of LDS25 and LDS50, where the void ratio of the specimen started on the dry side of the CSL, there was continuous movement towards the CSL. Initially this movement was an increase in p' changing to increasing void ratio as the tests progress. For LDS100, which also originates on the dry side of

the critical, there was minimal change in void ratio as it moves towards the CSL. The higher-pressure tests, LDS200 and LDS400, start very close to the CSL and show trends that parallel the CSL. LDS700 started at a much higher void ratio than the other tests, probably due to the consolidation method used, which was similar to LDD800. It showed a large void ratio change towards the CSL, crossing it at the bottom.

5.1.2.4 Bond yielding

Some concepts on yielding originate from studies on sedimentary clay stress history by Roscoe et al (1958) and Schofield & Wroth (1968).

Yielding of a soil can be used to chart its response to loading as shown by Jardine (1992), who studied the kinematic nature of some soils, and described three zones of soil behaviour separated by two yield loci. The yield loci were obtained by combining the yield points observed in a number of tests, with the same origin, following different stress paths. These yield loci mark the changes in behaviour and hence the response of the specimen to loading within stress space. He found that with increased loading the response changed from elastic deformations to plastic deformations with irrecoverable straining. The first and second zones represented recoverable deformations, which were linear and non-linear respectively. The third zone marked the change to plastic deformation, suggesting that the load columns within the soil are continually deformed and reformed whilst accommodating the increased loading.

Previous research into bonded soils, Malandraki (1994), Bressani (1990), Sangrey (1972), Vaughan (1985) had demonstrated that the behaviour of the samples before they failed could be studied by their yield characteristics. Since the emergence of the study of structured soils, after Vargas (1953), significant points of pre-failure yielding in bonded soils have been recognised. Vaughan (1985) studied the relevance of yielding to structured soils, highlighting the similarities among three different materials: cemented Canadian soft clay (Sangrey 1972), altered volcanic agglomerate (Uriel & Serrano 1972) and weak silty mudstone (Ohtsuki *et al* 1981). All were able to identify significant yield points from stress/strain data. Sangrey (1972) postulated further on the presence of yield surfaces for a soil that could be mapped in stress space Figure 5-13a. This was demonstrated by the results of Uriel & Serrano (1972) in Figure 5-13b. Further work by Vaughan led to a 'tentative explanation' for two yield points (Vaughan et al 1988) and is shown in Figure 5-14. Some of the applied stress is carried by the soil's bonding and termed 'Bond Stress'. The 'Bond Strength' refers to the stress carried by the bonds in excess to the stress carried by the de-structured material (at the same void ratio). The first yield occurs at the onset of bond breakdown after which the bond strength begins to decrease with continued loading and straining. Bond stress however continues to increase, with increasing applied stress, until the bond stress equal the bond strength. As the bond stress cannot exceed the bond strength the two then decrease together at an increased rate; as the bonds are broken down they can no longer support the stress applied to them, which increases the stress applied to the unbonded soil matrix. This suggests two significant yielding

events in the breakdown of bonded soils, which researchers such as Macarrini (1988), and Vaughan *et al* (1988) have reported to be more distinct at higher void ratios.

The recognition of the two yield points in the pre-failure behaviour had been developed further in research with sand/clay artificial specimens (Malandraki 1994, Bressani 1990, Macarrini 1988). The first yield was usually associated with the first changes in slope of the stress-strain curve at small strains. Defining the second yield point from graphical data has proved more difficult. Macarrini (1988) used the point of maximum curvature of the pre-failure stress strain curve, whilst Vaughan (1988) suggested the use of log-log plots of the stress-strain curve Figure 5-15a. Bressani (1990) in his PhD thesis compared both approaches and found that they both produced similar results. These methods were examined further by Malandraki (1994) and Malandraki & Toll (1994). They proposed an improved method based on the features of the tangential stiffness of the sample. Using log-log plots of tangential stiffness against axial strain Malandraki defined the first yield as 'the first change in stiffness', and the second yield as 'the point where the major drop takes place' as demonstrated in Figure 5-15b.

To identify the yield points for the undisturbed specimens, selected as possibly being bonded, all of the above methods were employed and are plotted in Figures 5-16 to 5-18. Generally they showed good agreement, with the stiffness methods allowing for an easier identification of indistinct yield points. However no one method proved itself to be more effective than the others.

A first yield between 0.1% - 0.2% axial strain could best be identified for LDS100 from the stiffness plots (Figure 5.16 c&d). However the identification of the second yield point was more of a problem. Using the log-log stiffness plots, as recommended by Malandraki & Toll (1994) leads to some ambiguity as the plot shows a drop in stiffness at about 0.5% axial strain. However on non-log scales this appears as a consistent continuous drop in stiffness suggesting a consistent breakdown of structure after the initial yielding. This raised a question about the reliance on log-log stiffness plots. A negative slope will always be converted into a steepening curve when a log scale is applied to the axes (Figure 5-19). The consistent loss in stiffness might suggest that the second yield had already occurred, close the point of initial yield. The stiffness plots in this test did not clearly show a second yield point. However both plots of stress against axial strain (Figure 5-16 a&b) did show a significant yield point at about 0.86% axial strain.

In the case of LDS200 (Figure 5-17) the first yield again occurs very early in the test. All four methods were able to identify an initial yield. The second yield was less distinct than in for the stress-strain plots (a&b), but the stiffness plots (c&d) showed a drop in stiffness at 0.1% axial strain. It was notable that after this second yield there appears to be subsequent yield points at 0.18% and 0.60% axial strains.

In LDS400 (Figure 5-18) the first yield occurred again at very low strains and the determination of the second yield was more difficult. The non-log scaled stress-strain plot showed an initial yield at about 0.2% axial strain and a less obvious yield at

0.85%. The log-log plot was less convincing. From the log-log stiffness plot there were no obvious yields other than the initial yield due to fluctuations masking any potential yields. The non-log stiffness plot however also indicated a yield at 0.8% axial strain, as well as other less noticeable yields at axial strains of 1.43%, 1.93% and 2.71%.

Analysis of the axial strain against time checked the possibility of cyclical characteristics of the drive mechanisms causing multiple yield points, but no influences were observed. This meant that the multiple yields were probably due to the de-structuring of the pozzolanic bonding.

The yield points were plotted in Figure 5-20 with reference to the stress paths for each test. In LDS100 the first yield occurred at a low stress level whilst the second yield occurs close to the remoulded boundary line. In LDS200 the two yields were much closer together, although there was another yield just higher. The first yield occurred at higher stress than in LDS100 but the second yield was not much higher. All yields were below the remoulded boundary. In LDS400 the yields occurred at similar levels to those of LDS100 and LDS200 but at an increasing distance below the remoulded boundary.

5.1.2.5 Comparison of Test Results of Bonded and Unbonded Specimens

Comparison of the test results from undisturbed lagoon ash samples with remoulded lagoon ash samples should help to highlight any structural characteristics present in the lagoon ash, which are removed by the remoulding process. The results of the remoulded samples helped to define the material behaviour of the lagoon ash in an unbonded state. It was against this framework of information that any influences from the presence of bonding could be judged. From the analysis of the yielding patterns described above (Section 5.1.2.4) there was no certainty as to whether all the undisturbed samples contain a bonded structure.

Plotting the tests for the remoulded and undisturbed specimens, for the same confining pressures together, helped to show the difference between them (Figure 5-21). The tests on undisturbed bonded soils demonstrated a stiffer response to loading, and maximum stress occurred at much lower axial strains, compared to the results of remoulded samples. At high axial strains the undisturbed specimens showed strain softening which converged with the maximum stress levels of the remoulded samples.

Combining the boundary surface from the remoulded samples with the points of yielding and maximum stress of the bonded undisturbed samples, it was possible to indicate a framework for the pozzolanic bonding under drained conditions (Figure 5-22). The first yield occurred at a low level in all the tests. The second yield locus was

relatively consistent showing a slight increase from LDS100 to LDS400. A yield in LDS700 might have helped to define the second yield locus with increased confining pressures.

Toll & Malandraki (1993) suggested that the breakdown of bonding can be represented by three zones in stress space, shown in idealised form in Figure 5-23. In zone 1 the bonds are not fully broken down until failure, which is represented by a close relationship between the limiting stress ratio and the second yield. As stress conditions are increased, some bonding begins to break down, but there is still a significant proportion of bonds remaining to effect the soils behaviour. This can be recognised by the occurrence of the second yield at stresses lower than the maximum stress.

The plot of yield loci (Figure 5-22) showed that the second yield although initially close to the boundary in LDS100 falls below it in LDS200 and further in LDS400. This would indicate that the transition from zone 1 to zone 2 occurs just below 100 kPa confining pressure for the lagoon fly ash. The transition between zone 2 and zone 3, which was suggested by Toll and Malandraki (1993) to occur at the coincidence of the bonded and unbonded boundaries, appears to exist above LDS400. The separate zones implied from these results are shown in Figure 5-24.

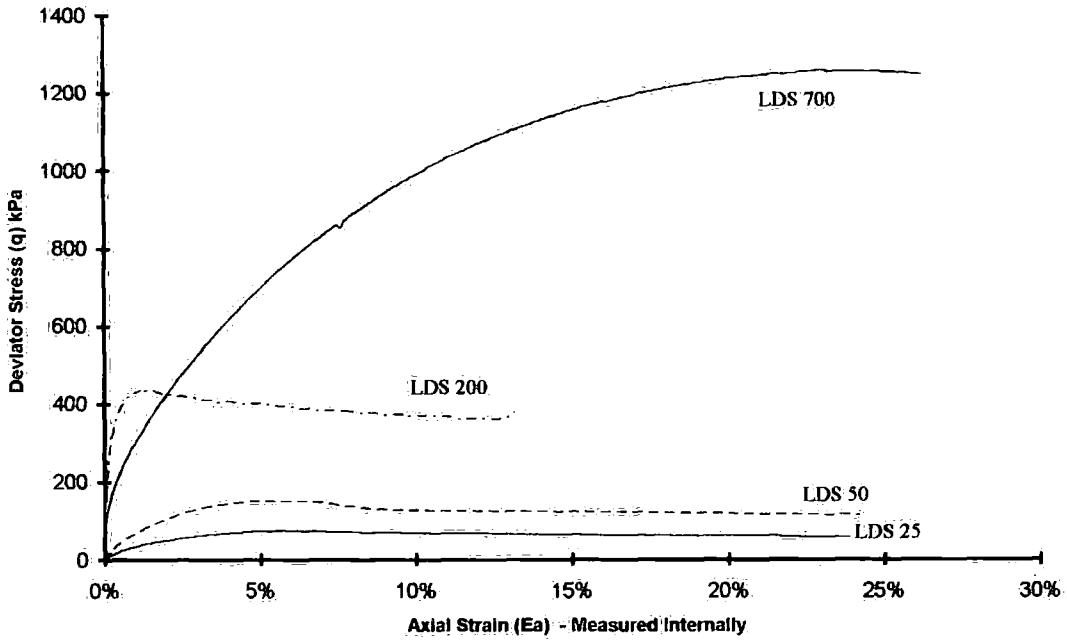

Figure 5.6a Stress against strain plot for LDS tests using direct strain measuring devices

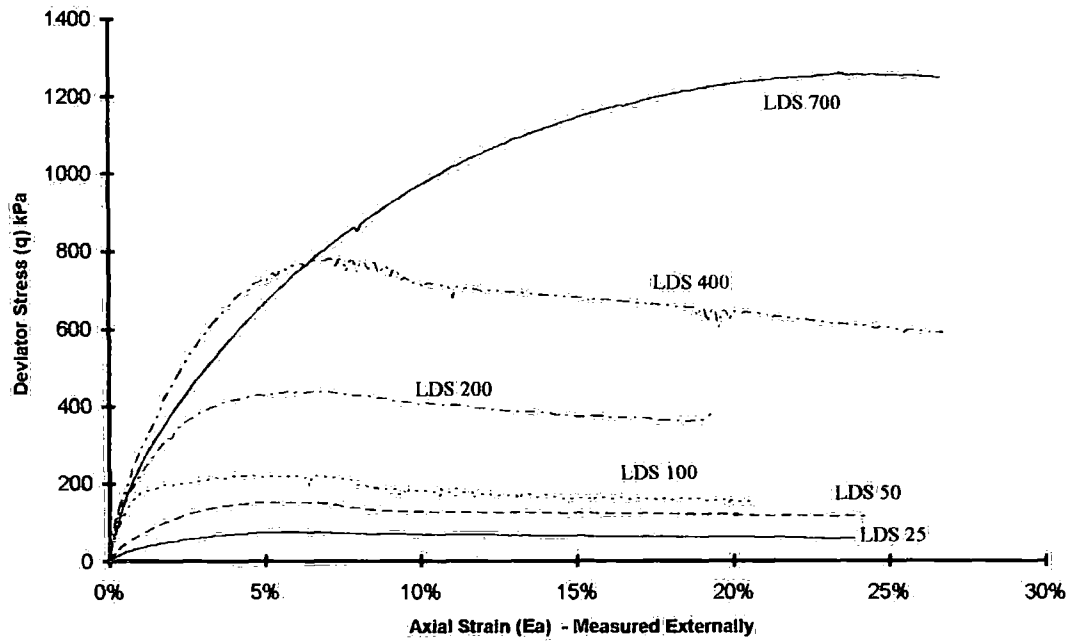

Figure 5-6b Stress against Strain plot for LDS tests using external strain measuring devices

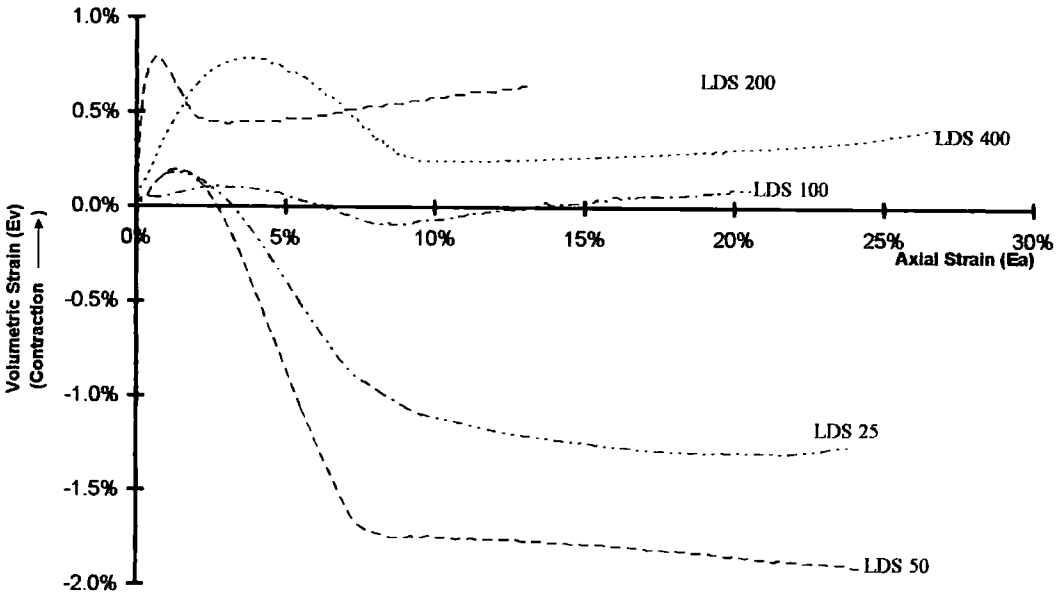

Figure 5.7a Volumetric strain versus axial strain plot for LDS tests up to 400kPa confining pressure

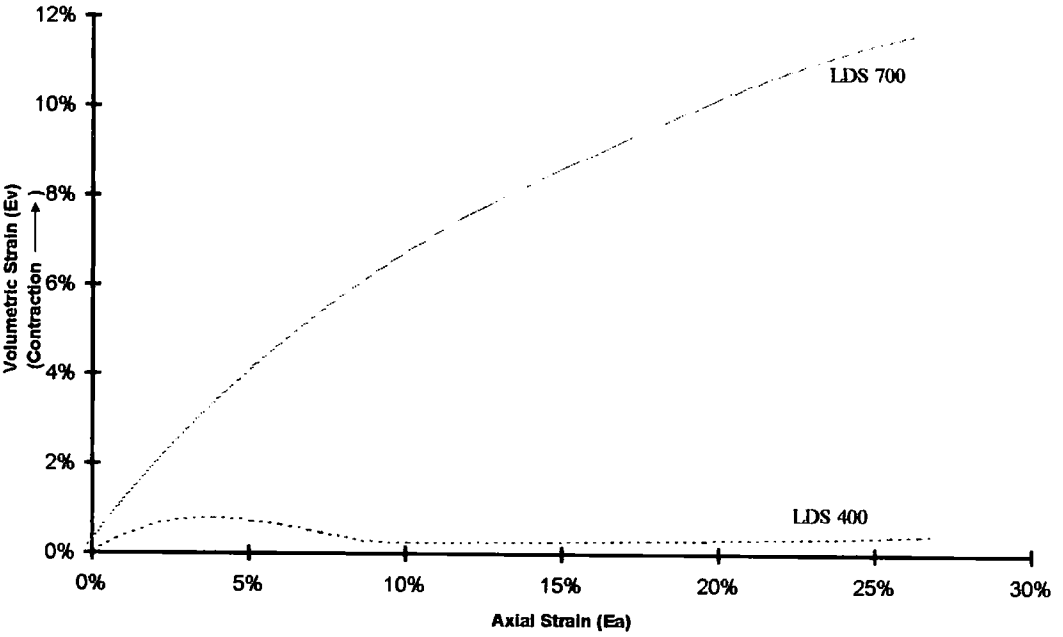

Figure 5-7b Volumetric strain versus axial strain for LDS tests at 400 & 700kPa confining pressure

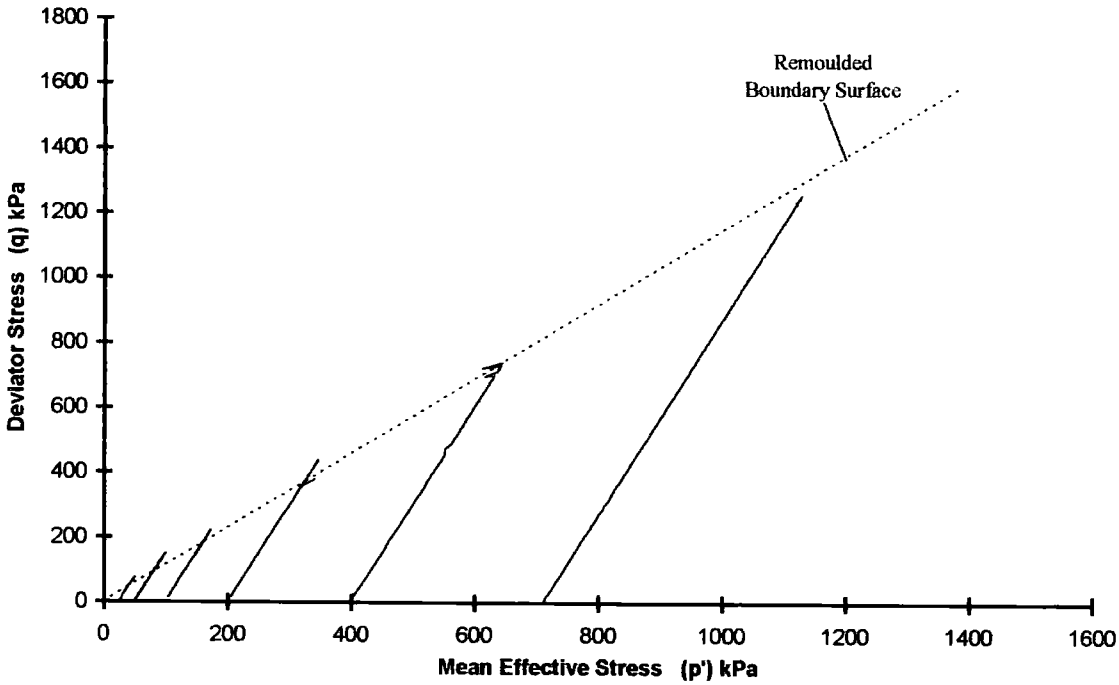

Figure 5.8 Effective stress paths for LDS tests

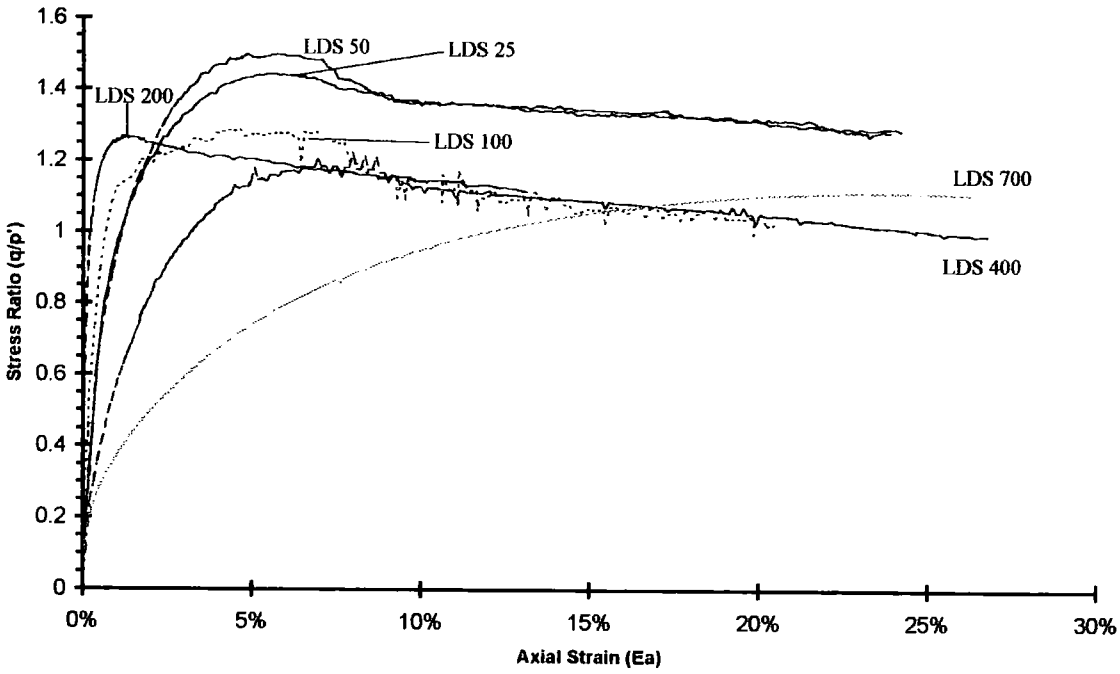

Figure 5.9 Stress ratio against strain plot for LDS tests

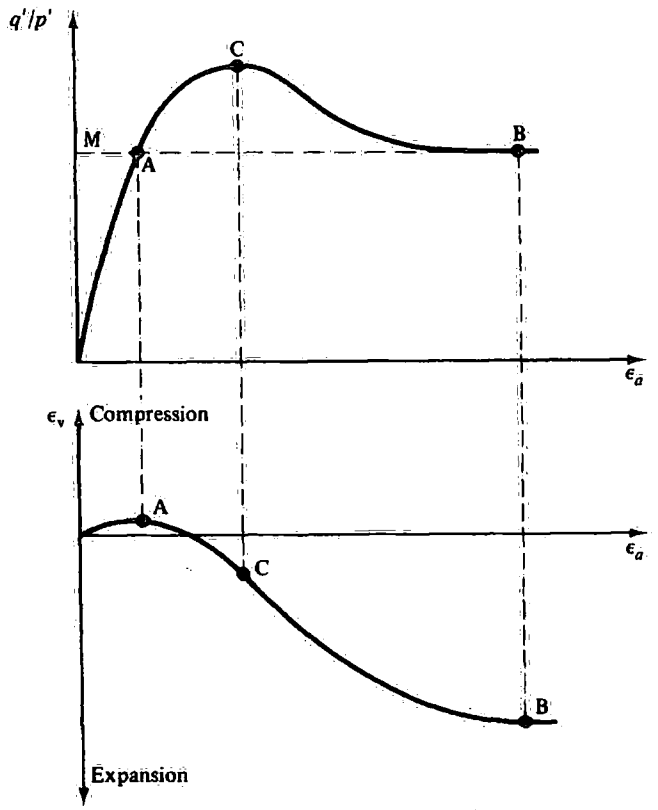

Figure 5.10 Typical relationship between stress ratio and volumetric strain for a drained triaxial test on dense sand (after Atkinson 1978)

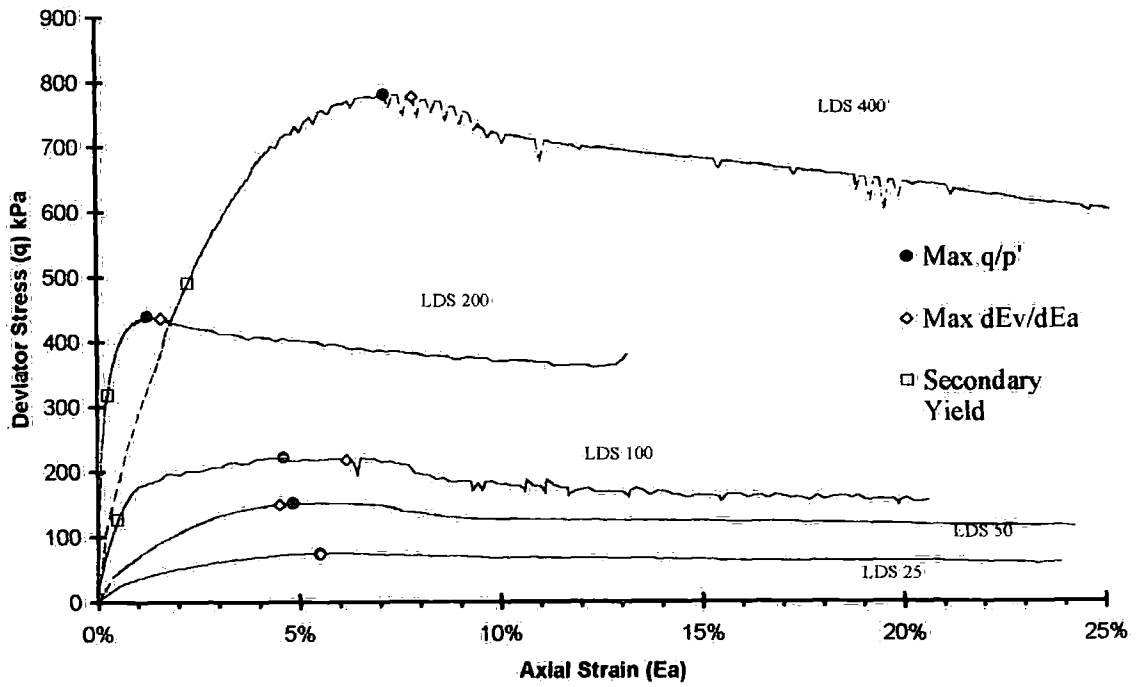

Figure 5.11 Relative position of $(q/p')_{max}$ and $(dEv/dEa)_{max}$ on stress-strain curves for LDS tests

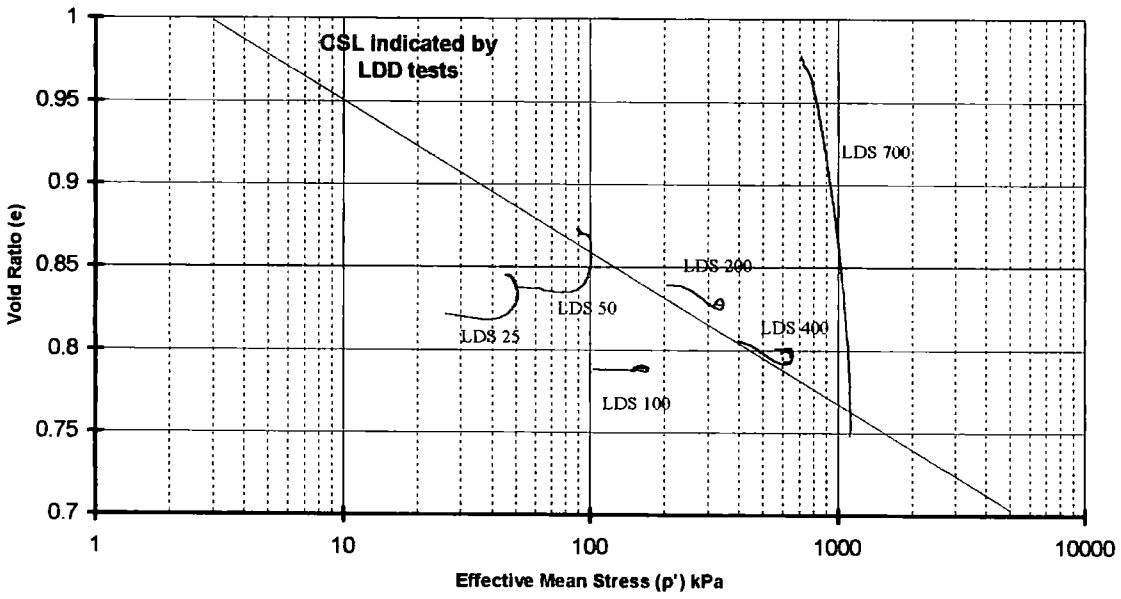

Figure 5-12 Void ratio changes against mean effective stress for LDS tests

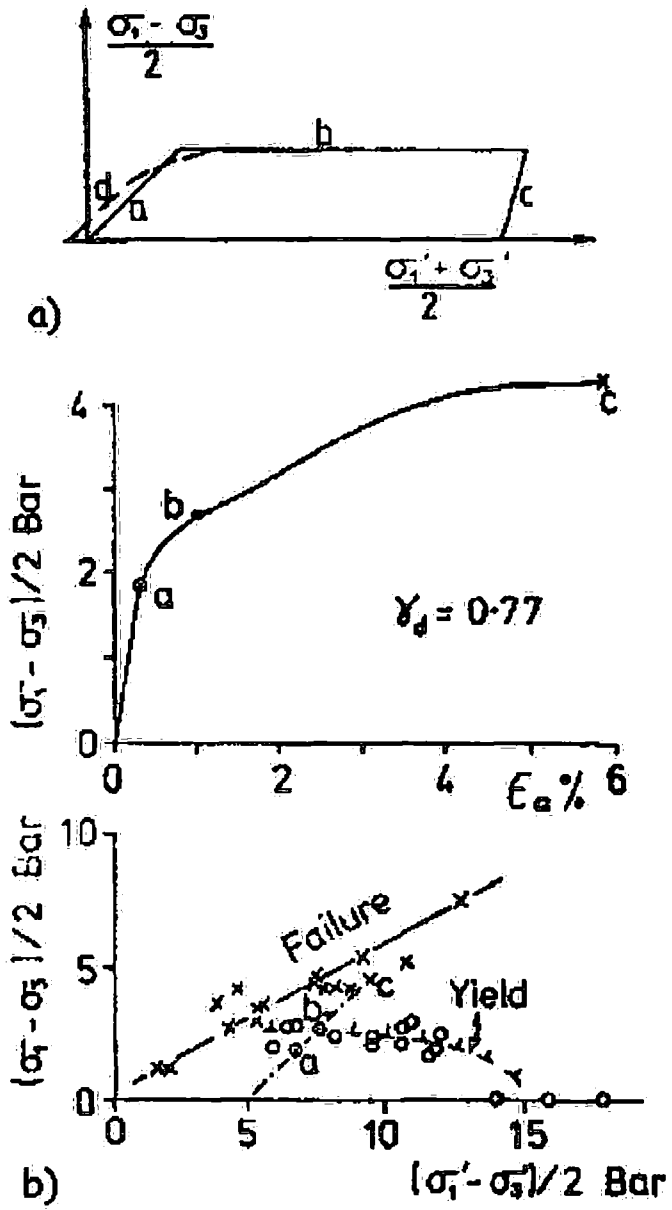

Figure 5-13 a)Sangrey(1972) postulated yield surface from Vaughan (1985) Fig.7
b) Yield surface for altered volcanic agglomerates by Uriel and Serrano (1972) from Vaughan (1985) Fig.8

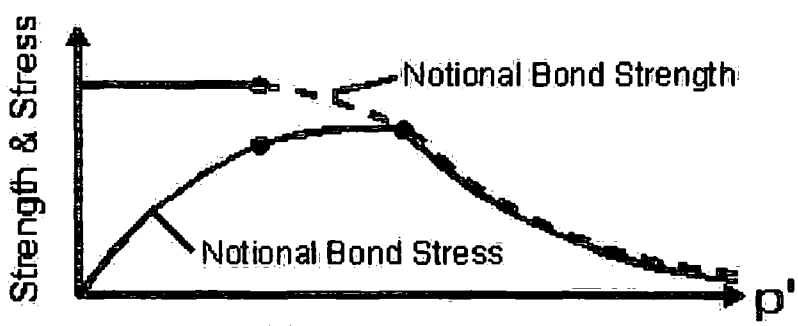

Figure 5-14 Vaughan's ideas on two yields

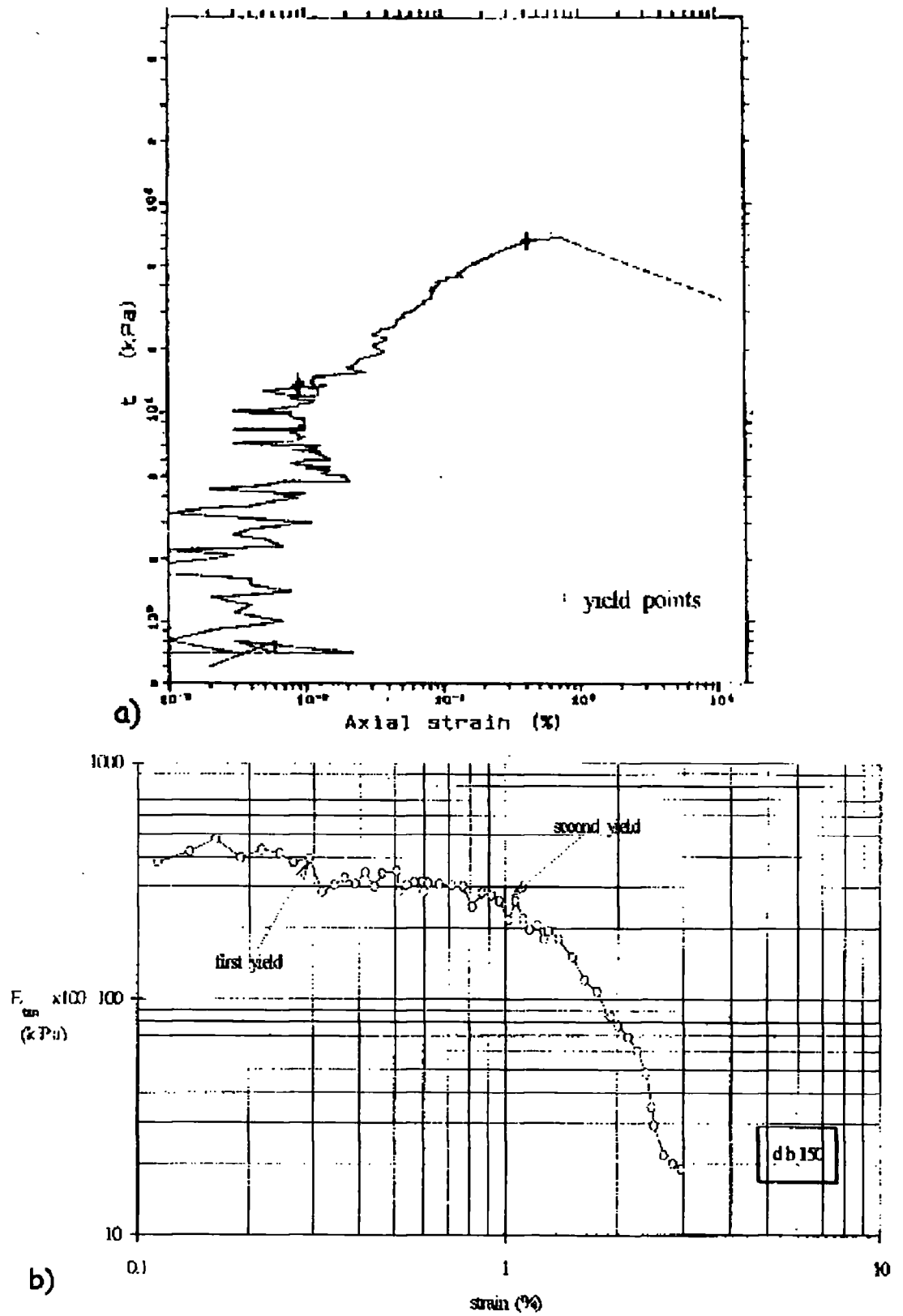

Figure 5.15 Definition of two yields by a) Vaughan (after Vaughan 1985) & b) Malandraki (after Malandraki 1994)

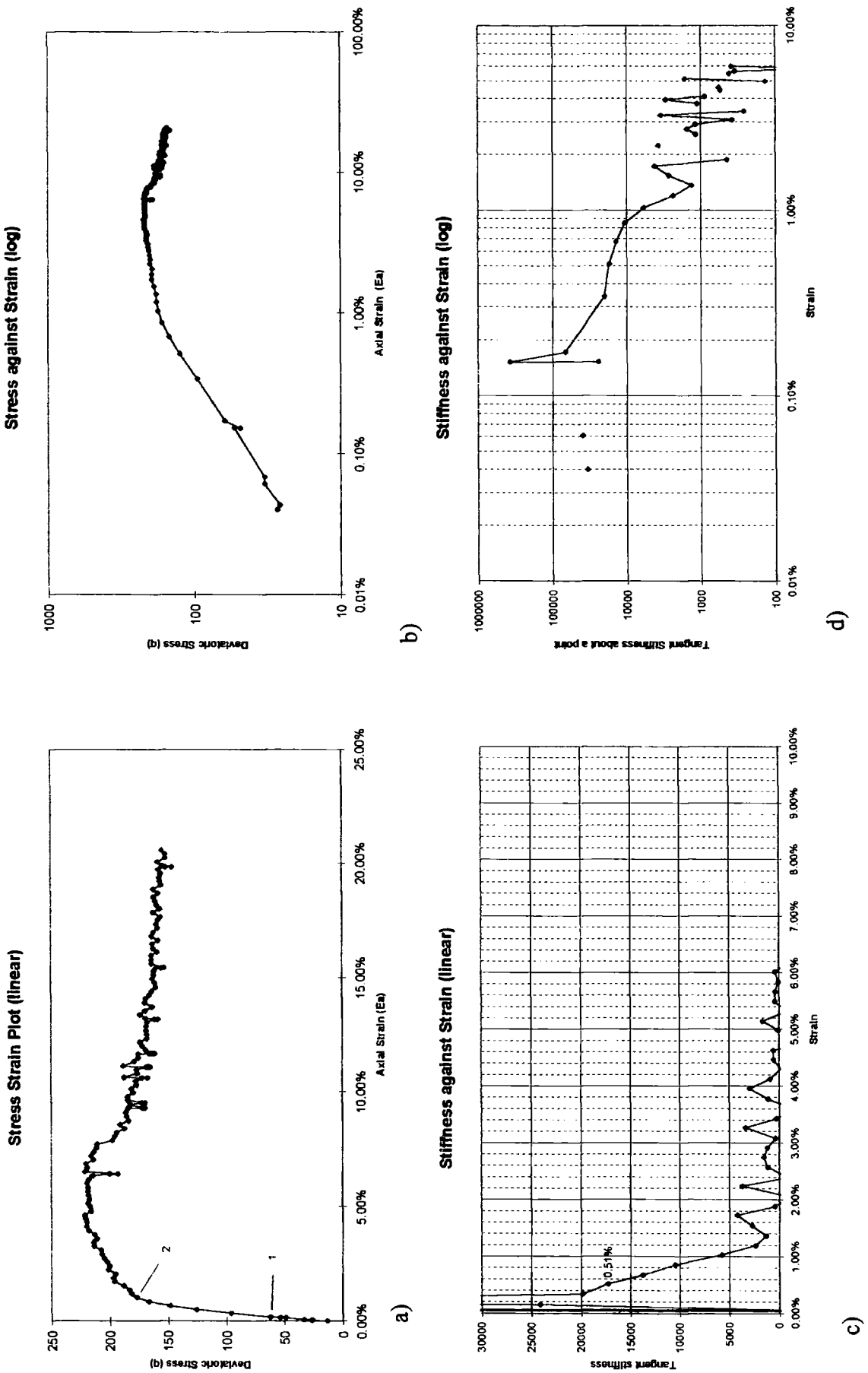

Figure 5-16 Plots of stress against strain (a) normal scales, b) log-log scales) and tangential stiffness against axial strain (c) normal scales, d) log-log scales) for LDS100

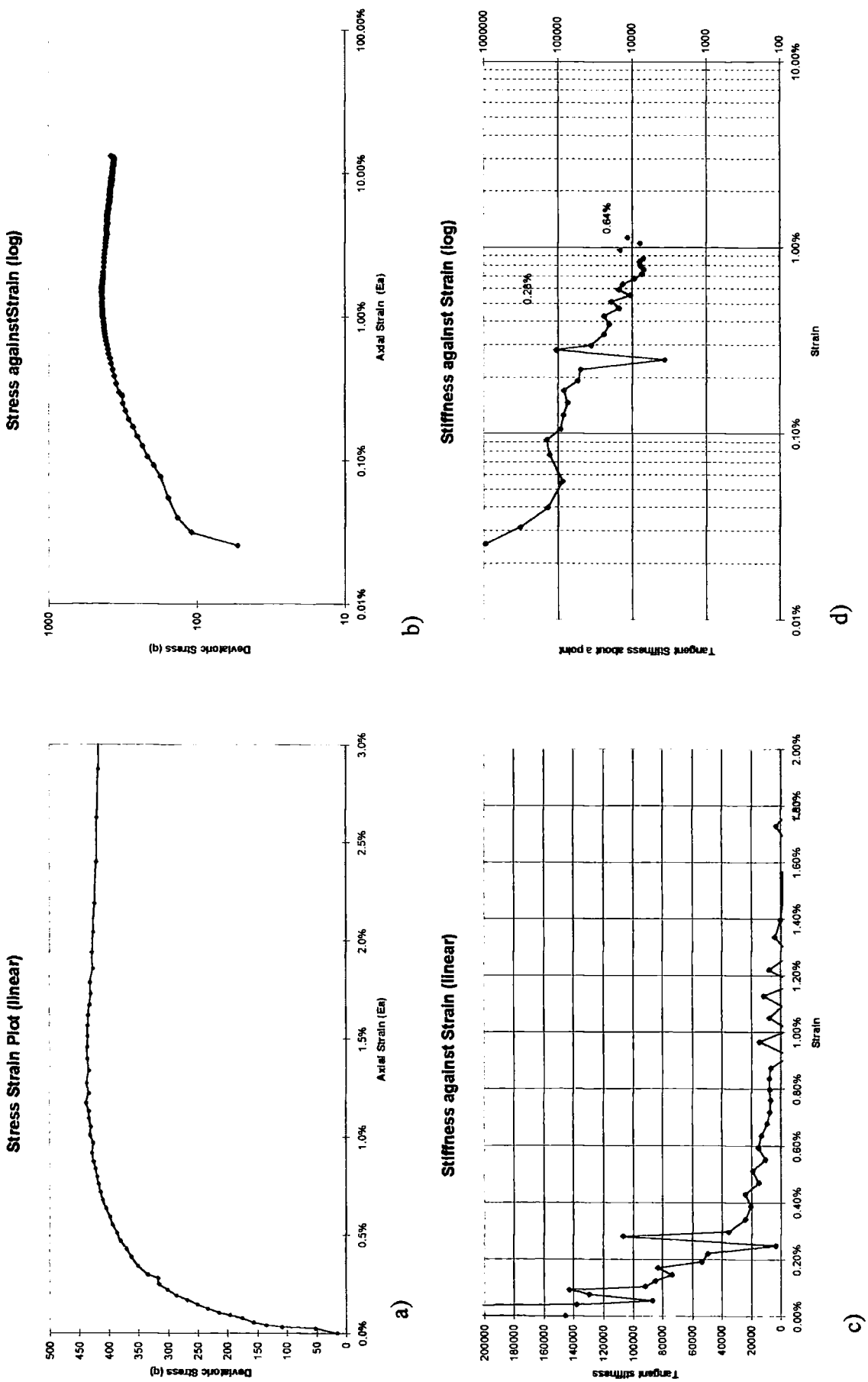

Figure 5-17 Plots of stress against strain (a) normal scales, b) log-log scales) and tangential stiffness against axial strain (c) normal scales, d) log-log scales) for LDS200

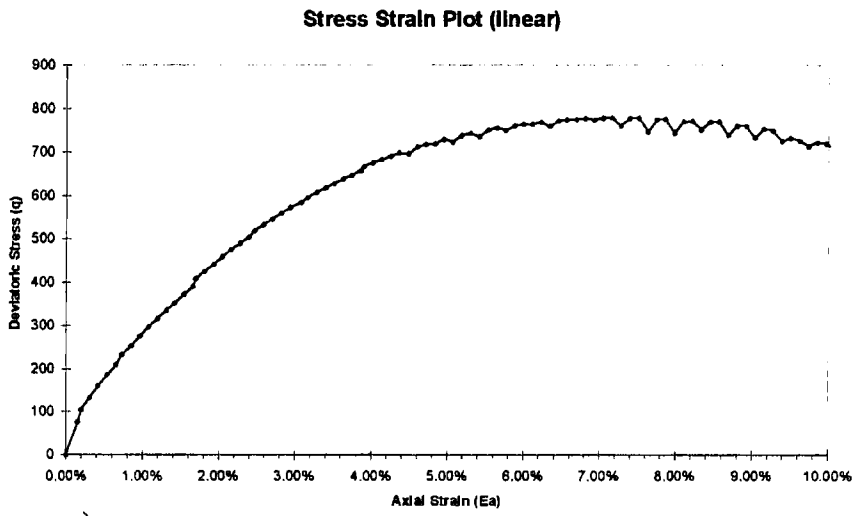

a)

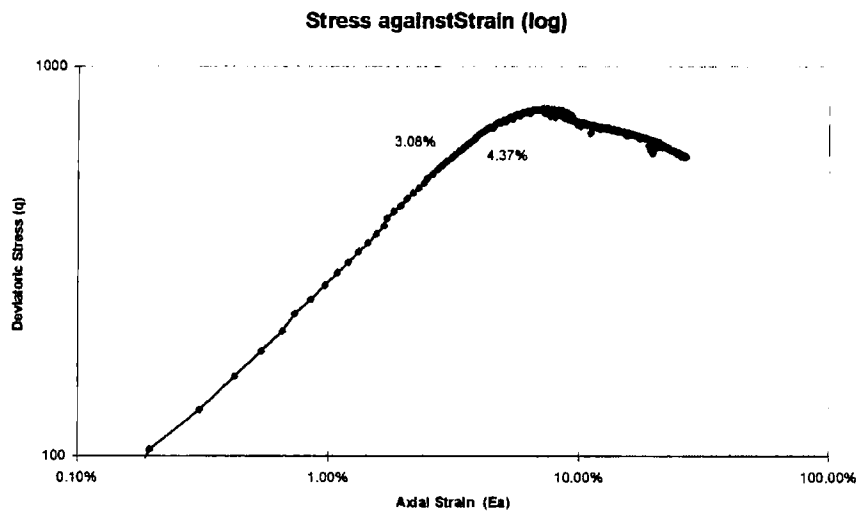

b)

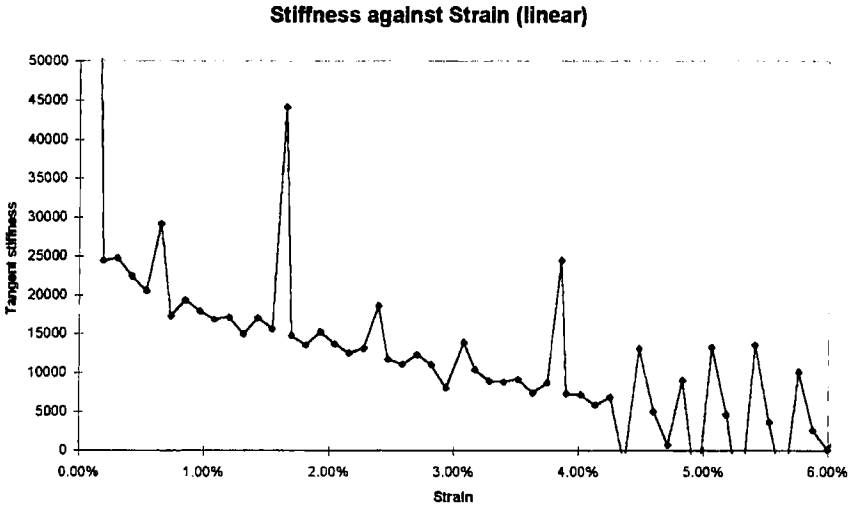

c)

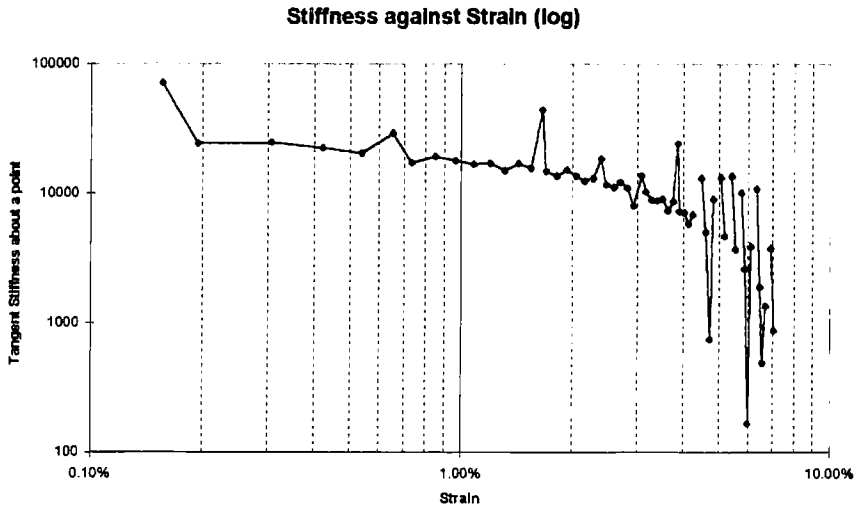

d)

Figure 5-18 Plots of stress against strain (a) normal scales, b) log-log scales) and tangential stiffness against axial strain (c) normal scales, d) log-log scales) for LDS400

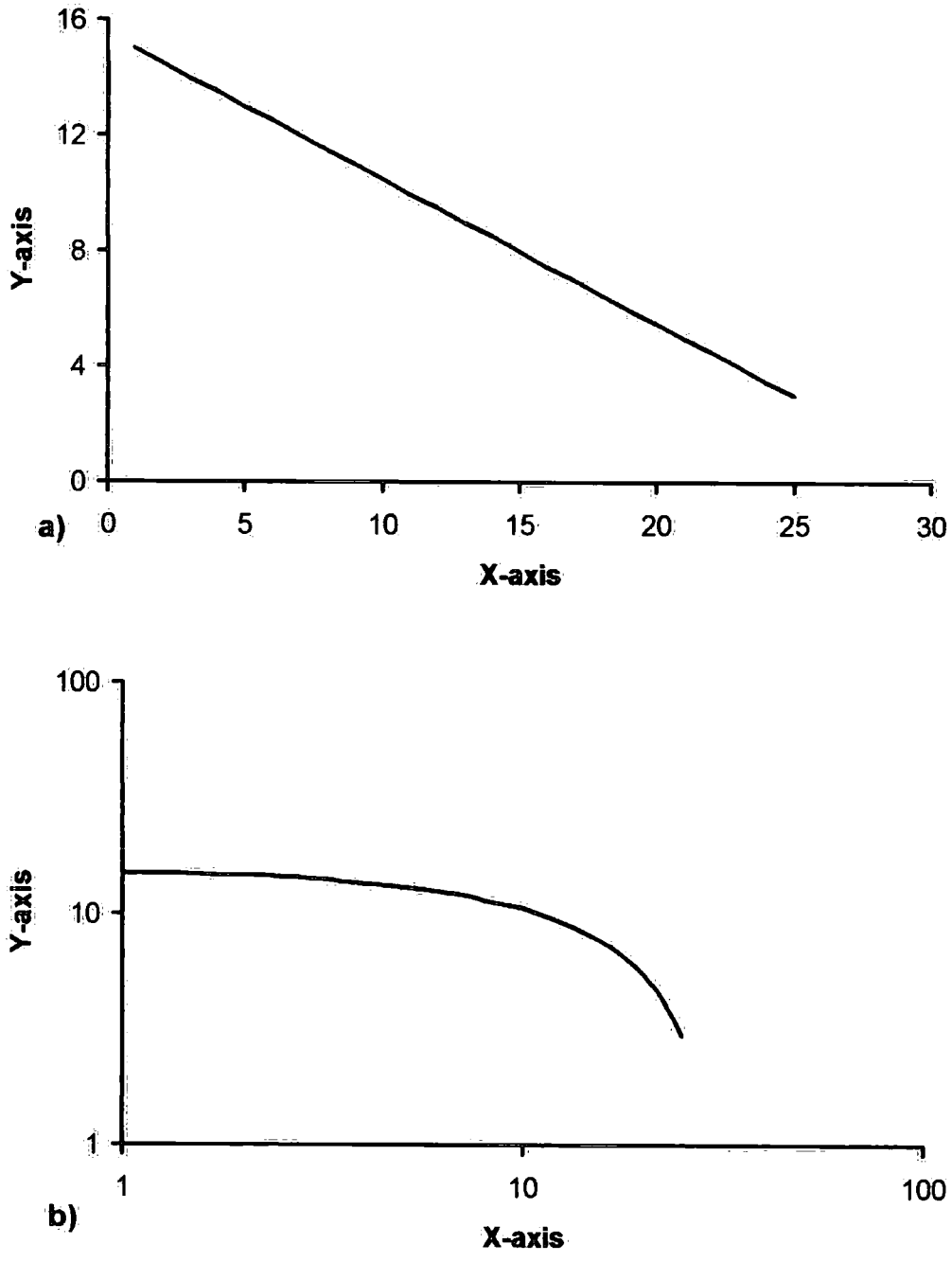

Figure 5-19 Effect of log scales on a negative slope

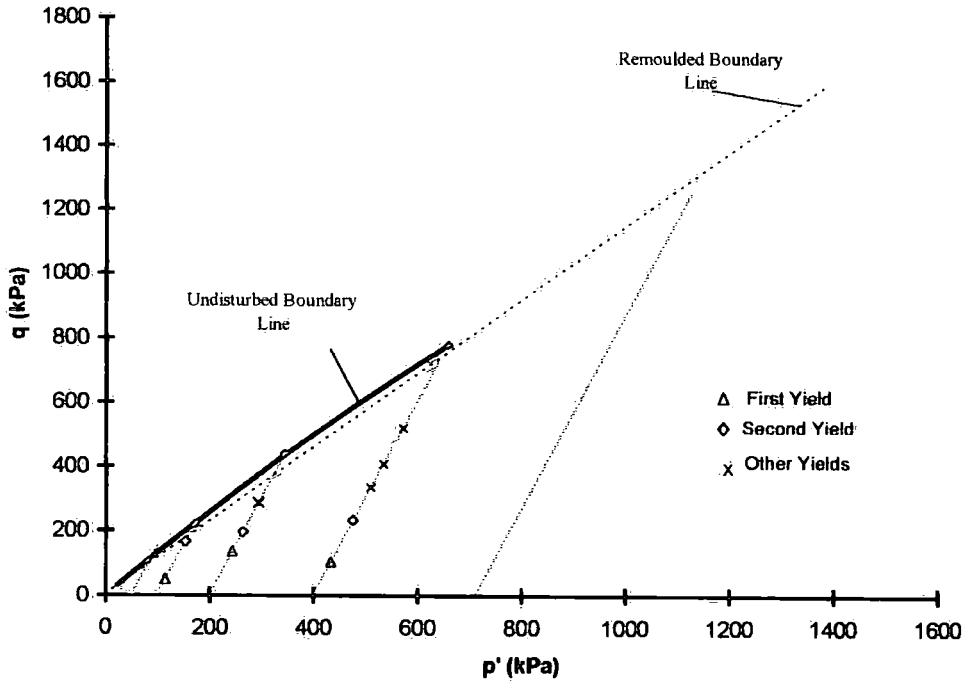

Figure 5.20 First and second yield points plotted in stress space with the boundary surfaces for LDD and LDS tests

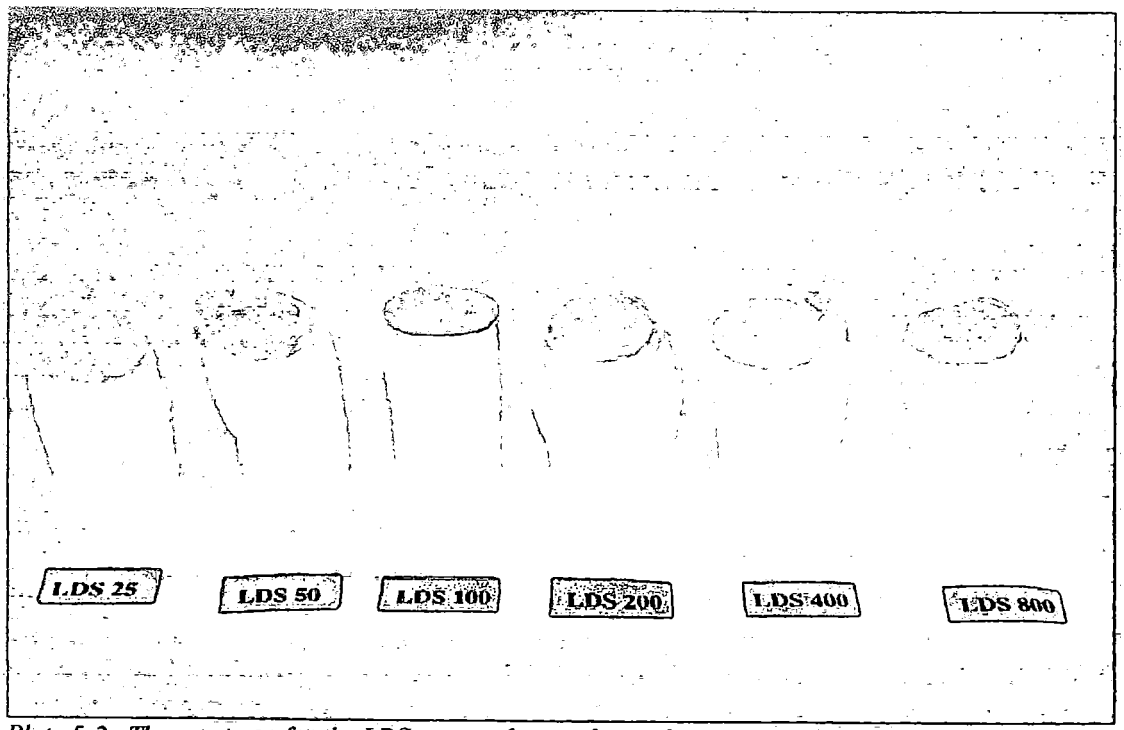

Plate 5-2 The specimen for the LDS group of tests after undergoing triaxial compression

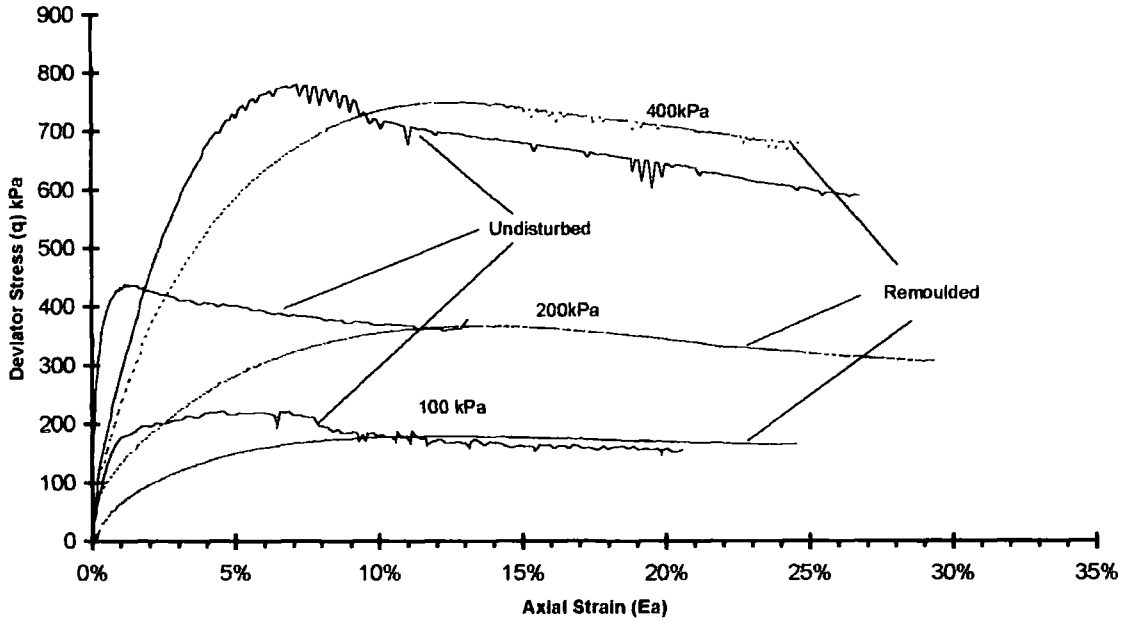

Figure 5.21 Comparison of stress-strain curves for undisturbed and remoulded specimen

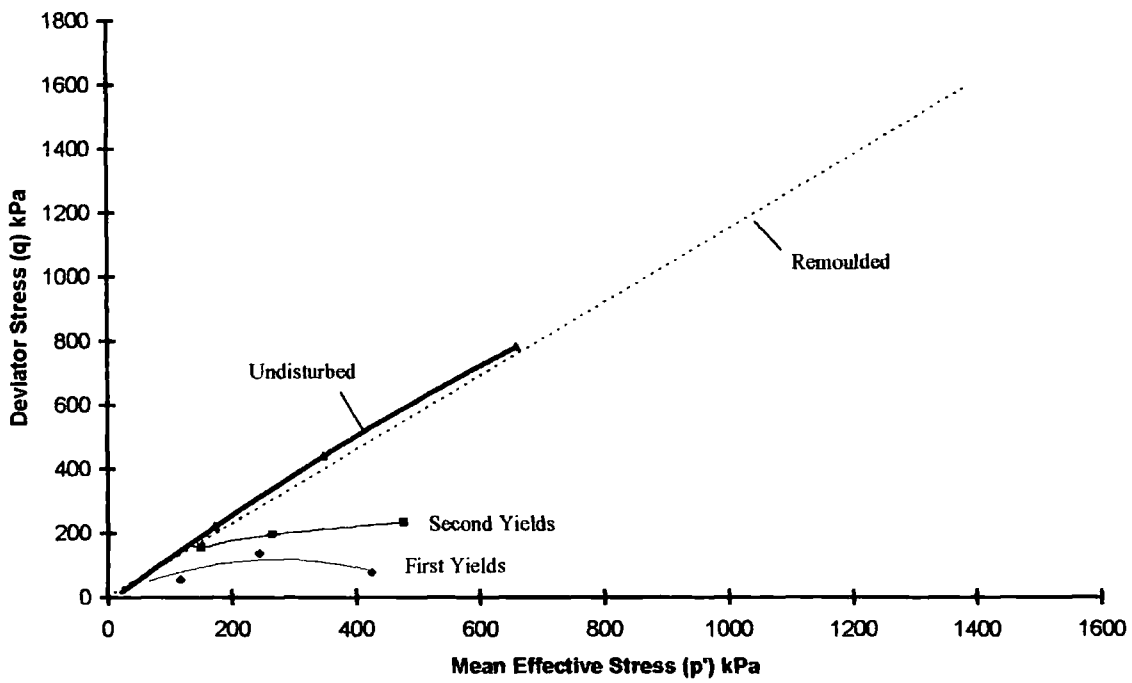

Figure 5.22 Frame work for drained triaxial tests on lagoon fly ash

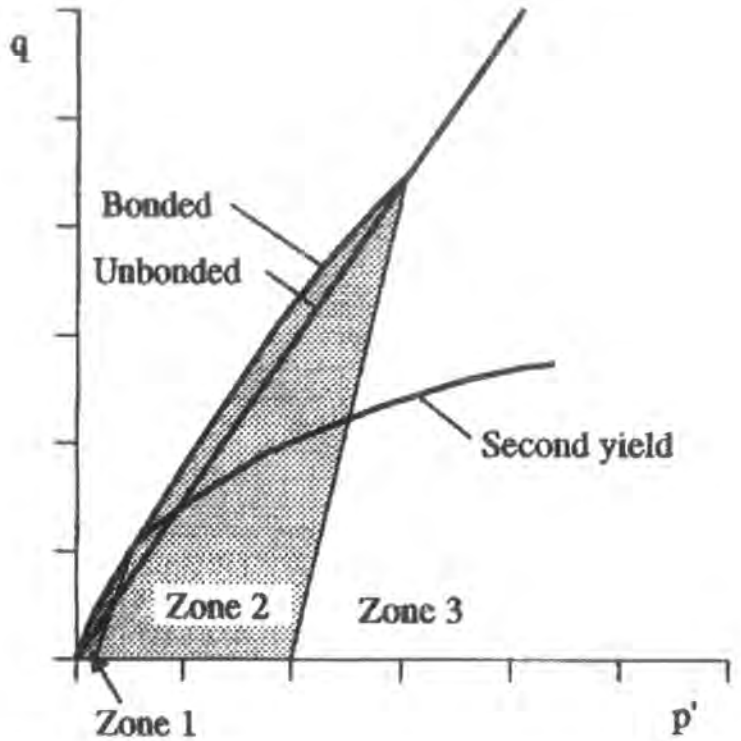

Figure 5.23 Idealised zones of behaviour for bonded soil (after Toll & Malandraki 1993)

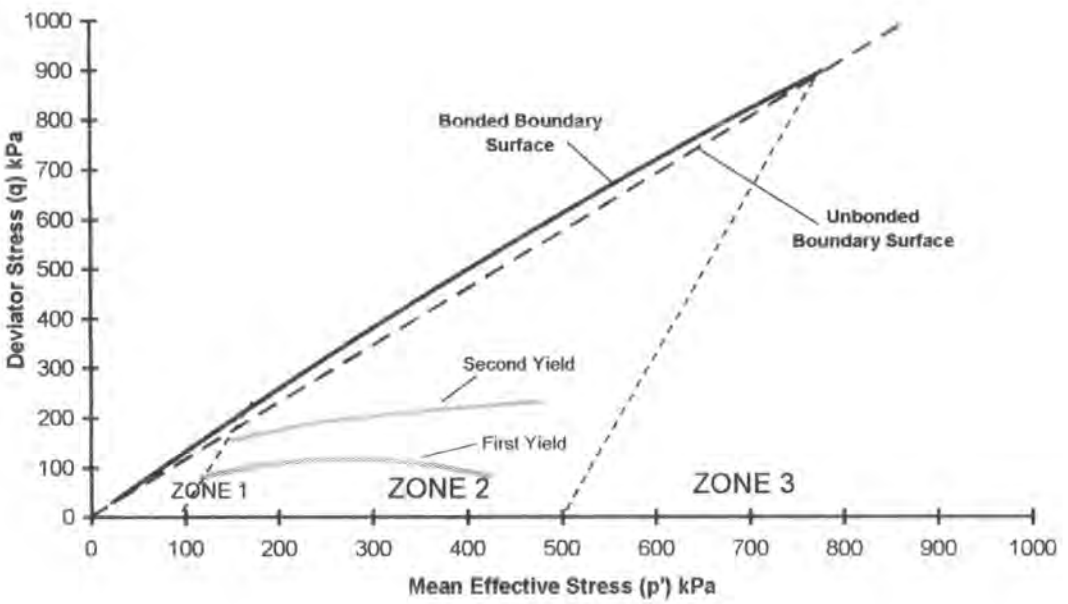

Figure 5.24 Zones of behaviour for drained triaxial tests on lagoon fly ash

5.2 Undrained Tests

5.2.1 Remoulded samples (LUD tests)

The remoulded samples were made in the same way as the tests under drained triaxial conditions, as well as to the same void ratio and dimensions. The moisture contents and specific gravities were obtained from the respective batch of remoulded material used to make the specimens. The initial conditions and consolidation parameters for each test are listed in Table 5-3.

Test (batch number)	*M/C (%)*	*SG*	$e_{initial}$	e_{consol}
LUD25 *(5)*	25.00	2.23	1.023	0.800
LUD50 *(2)*	25.51	2.15	0.959	0.904
LUD100 *(4)*	24.00	2.22	0.989	-
LUD200 *(3)*	25.51	2.15	0.920	0.879
LUD400 *(3)*	25.51	2.15	0.915	0.819
LUD800 *(4)*	25.43	2.22	1.014	0.843

Table 5-3 Specimen information and parameters for LUD tests.

From the plot of stress against axial strain (Figure 5-25a) it was possible to identify the tests where there were no direct sample strain measurements (LUD50, LUD200, LUD800), as the devices were unavailable for these tests. These were marked by a delay at low strains before there is a marked increase in deviator stress. There was little significant difference in stiffness between these tests and the tests where the

devices were available other than an initial shift with the external devices. The differences between strains calculated for internal and external devices (for tests with internal devices where fitted) were shown in Figure 5-25b.

Tests LUD400, LUD50 and LUD25 showed the maximum strength being reached at relatively high axial strains of around 10%, whilst the other tests showed a strain softening once a maximum strength, at 1-3% axial strain, has been reached. LUD25 had a higher maximum strength than LUD50, tested at twice the confining stress, whilst LUD100 had a similar maximum strength to LUD200. There was no correlation between the maximum strength of the sample and the confining pressure being applied as seen for LDD tests above 50kPa.

All of the specimens in the LUD group can be seen in Plate 5-3. Specimens LUD25 and LUD50 suggested relatively brittle failures with the development of shear zones. The shear zone in LUD25 appeared to be bounded by two separate parallel surfaces, whilst the zone in LUD50 did not have any specific surfaces indicating a more ductile deformation. The specimens tested at higher stresses all show an increase in ductile behaviour with no shear zones being developed, just barrelling.

The response of pore water pressure (pwp) to axial strain is shown in Figure 5-26, where tests reach a state of near constant pore pressure by 10% axial strain. Again it was possible to identify the tests where there was no direct strain information in tests LUD50, LUD200 & LUD800. With the exception of test LUD25, all showed an

increase in pore pressure, showing a tendency to contract, before reaching a state of near constant pressure. The increased pore pressures correlate well with the confining pressure applied in the tests. LUD25 showed an initial increase in pore pressure, followed by a decrease. This showed a tendency of the sample to dilate and resulted in an overall lowering of pore pressure over the test.

From plots of the effective stress paths for the tests in p'/q stress space (Figure 5-27), it was possible to identify a bounding surface for the remoulded lagoon ash tested with undrained conditions. The stress paths of the six tests showed a limiting stress ratio represented by a line in stress space passing through the origin at a stress ratio of 1.4 (equivalent to an angle of friction φ' of 34.6°). Tests LUD400 & LUD50 both approached this line almost perpendicularly, but stop upon meeting it. They did not pass into the stress space above it. The stress path for LUD25 showed increasing mean effective stress as it approached the line, then curved to travel up along the trend. The stress paths of LUD100, LUD200, & LUD800 all reached their maximum stress prior to meeting the line, from which they curved down and travel along the trend towards the origin.

The plots of stress ratio (q/p') against axial strain Figure 5-28 showed a spread of ultimate q/p' values from 1.1 to 1.4. Tests LUD200, LUD400 and LUD800 reached a steady ultimate stress ratio of 1.4 by 10% axial strain and remain at this ratio. These tests had formed the basis for the boundary surface marked in Figure 5-23. LUD100 and LUD25 attain a q/p' value of 1.25 initially at only 5% axial strain, followed by a

gradual reduction to values of 1.1 and 1.2 respectively. Test LUD50 had the lowest q/p' value of only 1.1 by 10% axial strain, increasing slightly to 1.15 by the end of the test.

The plots of e vs. log p' in Figure 5-29 show all tests in the LUD group except LUD100. Consolidation information for LUD100 was lost due to a corrupted data file and the actual volume change is unknown. The remaining tests identified a line in e – log p' space defined with the use of LDD tests as well. LUD25 plotted on the dry side of critical, whilst the other tests all plotted on the wet side. This helps to define the CSL better than the LDD tests where LDD25 approaches the CSL from a higher void ratio. LUD25 moved from the dry side and gave an indication of a lower limit for the line. LUD800 was the only test of the group not to finish close to the CSL. This was explained by the continued increase in pwp in Figure 5-26.

Despite the slightly varied reaction of the samples to axial loading, the remoulded samples demonstrated in stress space a common boundary surface for the lagoon ash. The over consolidated LUD25 traveled up the trend with a consistent relationship between decreasing pwp and increasing deviator stress. The other tests also showed a common relationship between pwp and deviator stress at the bounding surface they share with LUD25. None of the tests passed into the region of stress space above this boundary.

LUD25 showed behaviour distinct from the other tests in the group of remoulded samples, in a similar way to LDD25. The remoulded samples were prepared in the same way for both the Drained and Undrained Triaxial tests. The over-consolidation seen in LDD25, and in LUD25, showed a consistency in the sample preparation process. This indicated that tests below 50 kPa may show the overconsolidated response to loading.

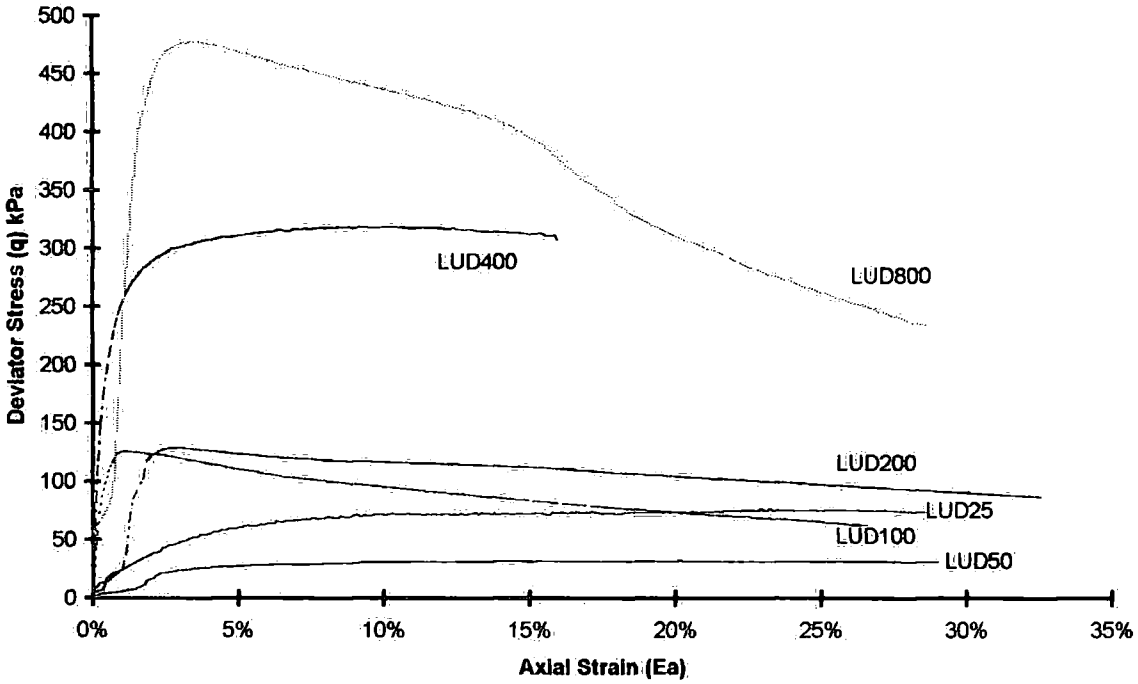

Figure 5-25a Stress against strain plot for LUD tests

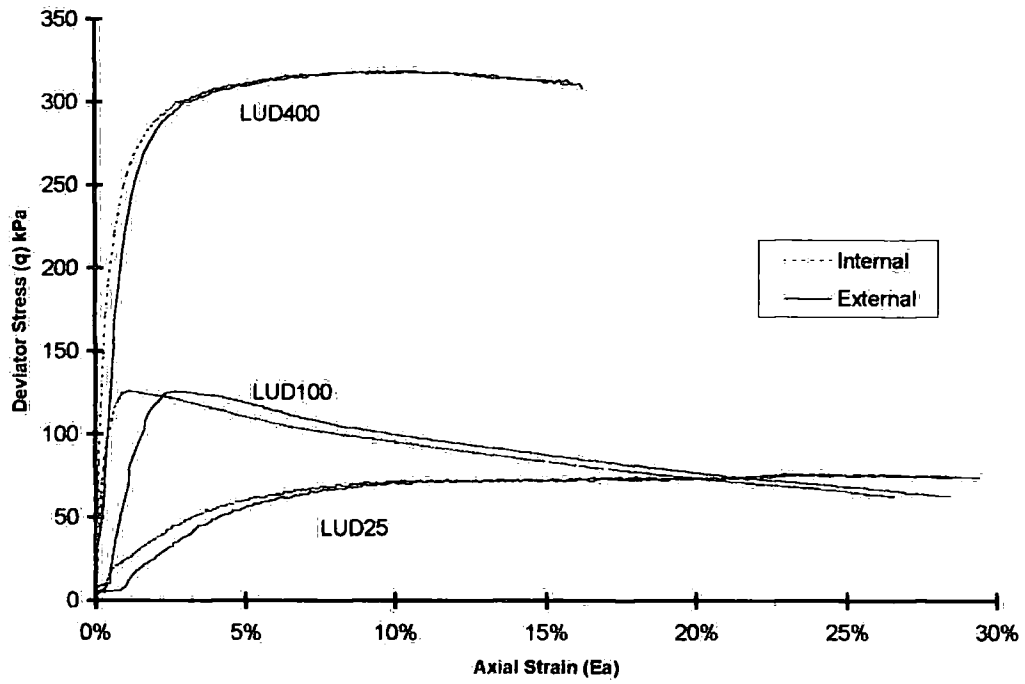

Figure 5-25b Comparison of axial strain measurement against stress for LUD test specimens fitted with internal strain measuring devices.

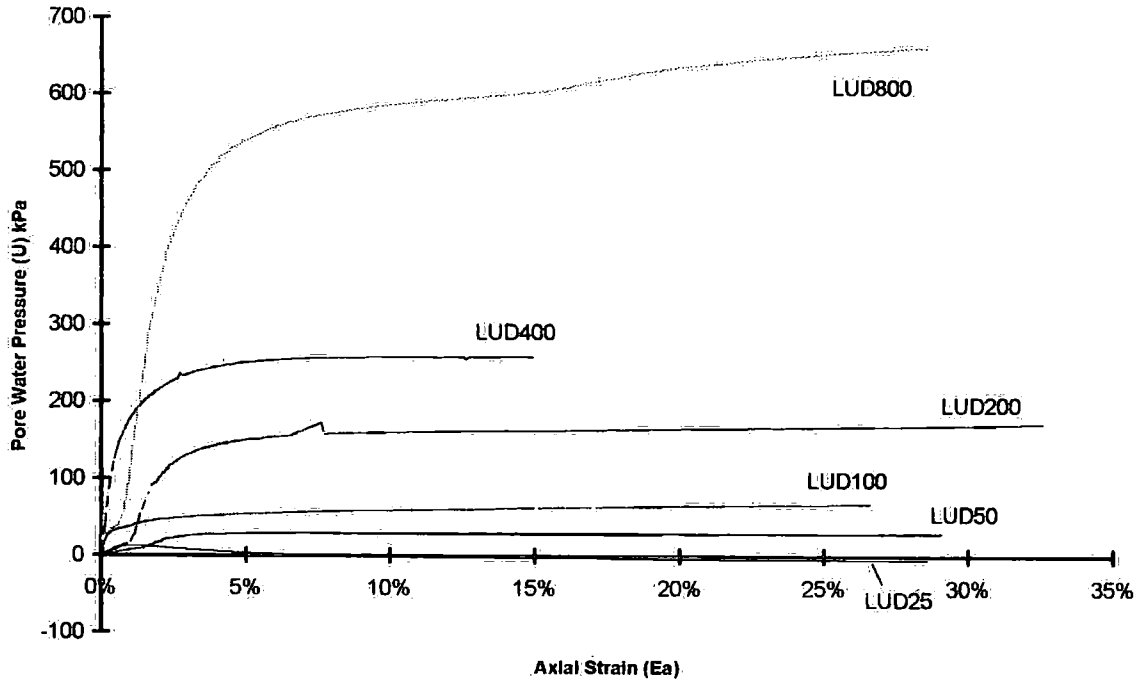

Figure 5-26a Change in pore water pressure versus axial strain plot for LUD tests

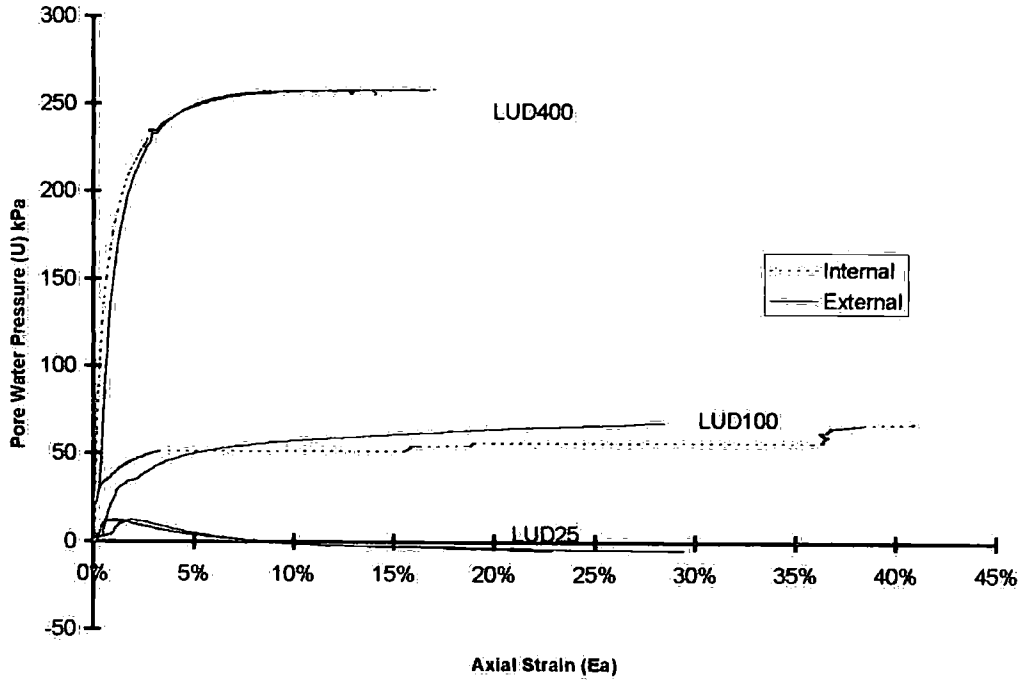

Figure 5-26b Comparison of axial strain measurement against change in pore water pressure for LUD test specimens fitted with internal strain measuring devices

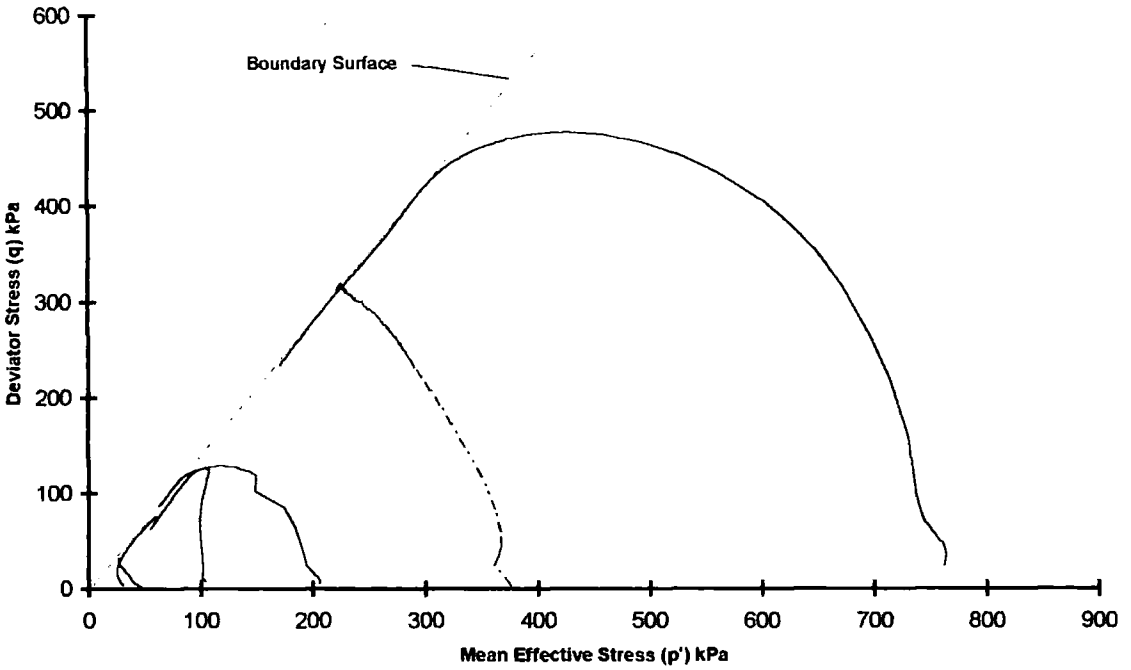

Figure 5-27 Effective stress paths for LUD tests

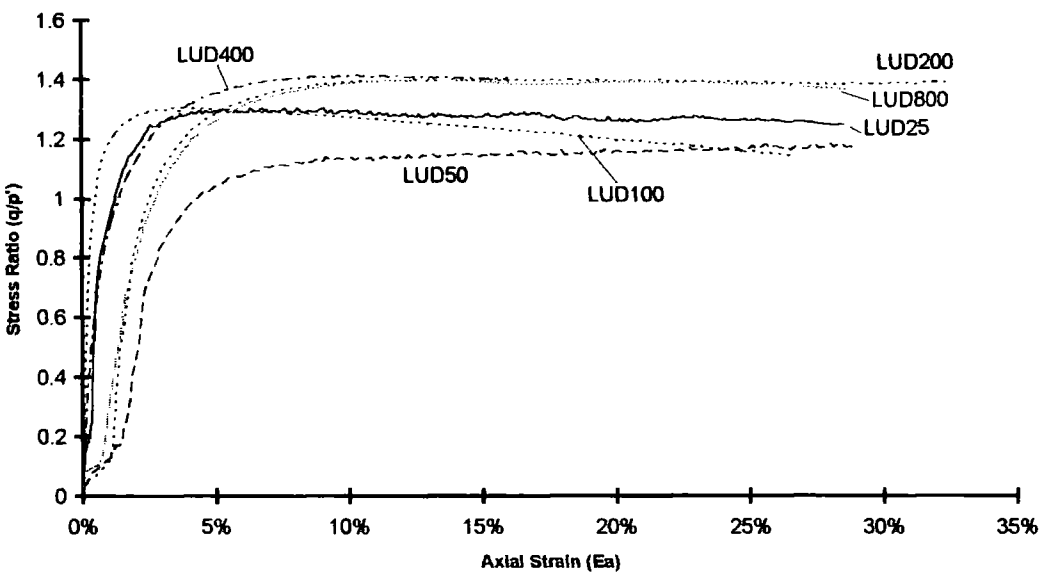

Figure 5-28 Stress ratio against strain plots for LUD tests

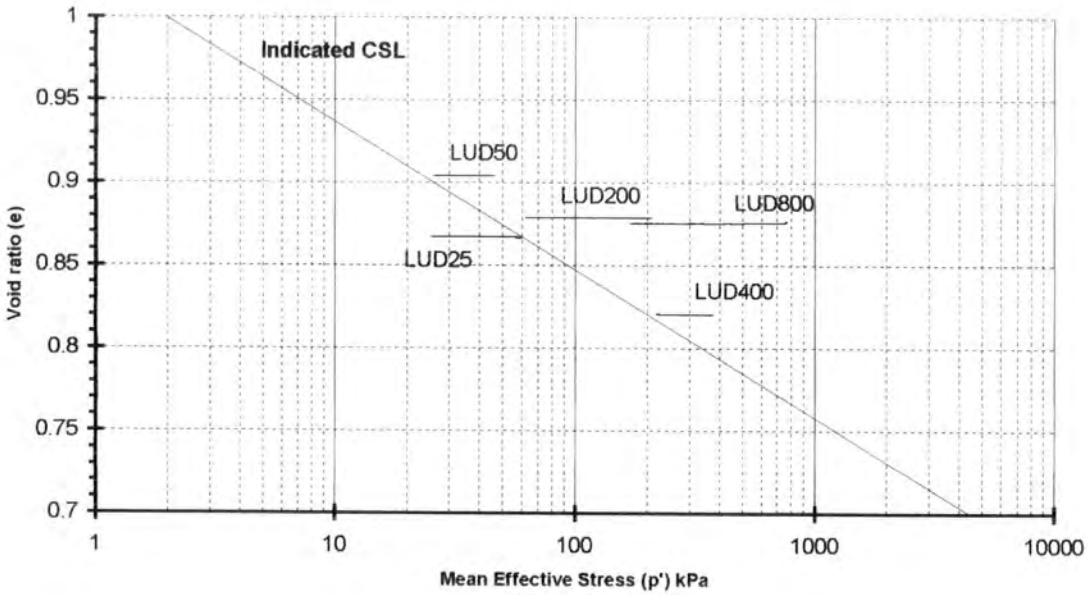

Figure 5-29 Void ratio changes against mean effective stress plot for LUD tests

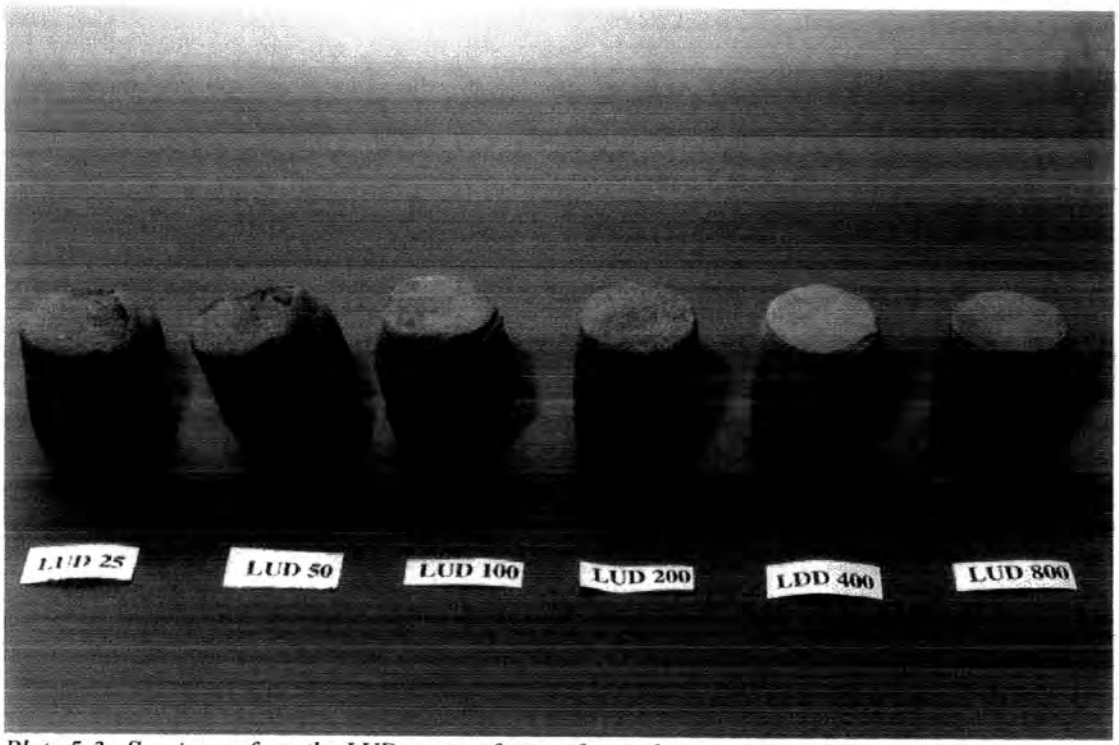

Plate 5-3 Specimens from the LUD group of tests after undergoing triaxial compression

5.2.2 Undisturbed Samples (LUS tests)

The undisturbed samples used in the undrained triaxial tests were cut directly from the Delft tubes in the same manner as the samples used in the drained triaxial tests section 5.1.2. The specimens originated from a number of different tubes, from three different boreholes. Undrained tests were initially carried out to identify the effect of increasing confining pressure on samples. They were also used in the tests designed to quantify the effect of increasing depth within the lagoon. The samples used for these tests were taken from tubes all originating from the same borehole BS406. BS406 was chosen because it was one of the deepest drilled and nine out of the ten tubes extracted were available for use.

Test	*Tube [b/h]*	*Depth (m)*	***M/C*** *(%)*	***SG***	$e_{initial}$	e_{consol}
LUS25	9546 [408_b]	2 - 3	-	-	-	-
LUS50	7642 [406]	2 - 3	41.75	2.25	0.805	0.800
LUS100	10052 [401]	11-12	37.19	2.15	0.852	0.801
LUS200	10540 [408_b]	5 - 6	38.97	2.23	1.060	1.005
LUS400	10540 [408_b]	5 - 6	41.87	2.21	1.112	1.067
LUS800	9855 [408_b]	3 - 4	14.54	2.26	1.110	0.813

Table 5-4 - Specimen information and parameters for LUS '25-800' tests

5.2.2.1 LUS '25-800' Tests

The first group of tests were performed over a range of consolidation stresses from 25kPa to 800kPa, to compare with the group of remoulded samples (Section 5.2.1). The origins for each are given in Table 5-4 along with the specimens' initial parameter and consolidation information.

The plots of stress against strain (Figure 5-30a) showed an increase in maximum strength with increasing confining pressure for tests carried out at 100kPa and below. There was a fall in strength between LUS100 & LUS200 followed by further increasing strength with increasing confining pressure above 200 kPa. Three tests: LUS200, LUS400, & LUS800 showed a stiff initial response to axial loading achieving most of their strength by 1% and a maximum by 3% axial strain. LUS25 had a stiff initial response followed by a continued increase in strength, at a much lower rate, attaining a maximum at 15% axial strain. The specimens for tests LUS50 and LUS100 were not fitted with internal strain devices. Therefore their stress strain plots could not be compared directly with those tests where the devices were used.

The difference between the internal and external strain measurements was shown in Figure 5-30b. They do not show any significant changes in stiffness observed in LUS50 and LUS100. The external strain measurements generally showed an axial strain of 1-2% before there was an increase in the applied stress. The stiffnesses for tests LUD25 and LUD200 were lower, whilst those of LUD400 and LUD800 changed

very little. Tests LUD50 and LUD100 showed behaviour different to the other tests. The external strain measurements showed lower stiffnesses than those seen for the internal gauges, reaching maximum strength at 6% and 8% respectively. A sharp reduction in strength followed with increased axial strain. Although strain softening is also seen in LUS200 and LUS800, there was not the same significant loss of strength seen in LUS50 and LUS100. The loss in strength might be associated with a bond yielding but the axial strains were large and the stiffness was low, which are opposite to the response seen by other structured soils (Sangrey 1972, Uriel & Serrano (1973) & Maccarini (1987) to name a few)

All specimens except LUS800 are shown in Plate 5-4. A notable feature was the variation in greyscale of the different specimens. The fly ash in LUS100 was considerably lighter in colour than LUS25. It was also worth noting the lamination in LUS25, along which the barrelled specimen was pared easily after drying. Shear surfaces were developed in LUS50, LUS200 and LUS400, with LUS400 demonstrating this feature best in the picture. The internal deformation was masked by the surface alterations due to the latex membranes.

The change in behaviour between (Figure 5-30a) 100 and 200 kPa noted in the stress strain plot could also be seen in the plot showing the change in pwp against axial strain Figure 5-31a&b. For the tests at 100kPa and below (Figure 5-31a) there was an initial increase in the pore pressure followed by a rapid decrease. LUS25 continued to decrease for the remainder of the test, with a change in the rate of decrease at 5% and

16% axial strain. Following the rapid decrease in pore pressure for tests LUS50 & LUS100, the pore pressure increased once more. This occurred at the point where the sample strength begins to fall off. This implied that these two features are linked. The response for the tests at 200kPa and above (Figure 5-31b) was an initial rapid increase in pore pressure followed by continued increase at a reduced rate. The increases in pore pressure for these tests could be related to the confining pressure being applied.

The stress paths are plotted in p'-q stress space (Figure 5-32) where the tails showed a trend for LUS25, LUS50, LUS200 & LUS800. This represented an upper limit for the lagoon material under these conditions. Tests LUS100 and LUS400 did not quite reach the line but instead identified a similar trend at a slightly reduced stress ratio. The same distinction between tests at 100kPa and below and 200kPa and above was shown. Those at lower pressures with paths that moved to the right showed reducing pore pressure to failure, before looping to the left. Here strength was lost and pore pressure began to increase again. The maximum strength was reached after the maximum stress ratio. Those at higher pressure moved to the left throughout the tests showing increasing pore pressures as the samples underwent axial strain. Maximum strength was reached at or near the boundary marked by the stress path tails.

The plots of stress ratio against axial strain (Figure 5-33) showed a change in behaviour linked to the confining pressure. The lower pressure tests below 100 kPa confining pressure have peaked curves, whilst those above showed a more gradual change. Most tests showed an ultimate stress ratio of 1.4, which matched the stress

ratio of the boundary surface used for the LUD tests. Two tests (LUS100 & LUS400) had lower stress ratios of 1.25. The variation in the ultimate stress ratio did not appear to be linked to the confining pressure. It was more likely to be a function of the specimens' original structure.

The stress strain plots (Figure 5-34) showed the relative positions of, the points of maximum stress ratio $(q/p')_{max}$ and maximum rate of change in pwp $(du/dEa)_{max}$. The point representing the maximum rate of change in pwp used in these undrained tests corresponded to the point of maximum dilation $(dEv/dEa)_{max}$ used for the drained tests, as suggested by Malandraki (1994). It should be noted that the ratio q/p' already reflects the change in pwp through effective stresses and it is the rate of change that is being compared. The relative positions of these points with respect to axial strain, may be of use as an additional indication for the presence of bonding by comparison between different tests. For tests LUS50 and LUS100 the point of $(du/dEa)_{max}$ occurred at a lower strain than the point of $(q/p')_{max}$. In LUS25 the point of $(q/p')_{max}$ occurred before that of $(du/dEa)_{max}$. For the tests above 100kPa the maximum stress ratio occurred after the rate of pwp change has been reduced. There was no development of negative pore pressures in these tests.

The plots of e vs. log p' (Figure 5-35) showed the change in void ratio for each test relative to the CSL defined by the remoulded tests (Figure 5-29). Test LUS25 was not plotted, as there was no information for the specimen's initial moisture content. Hence no accurate calculations of its void ratio could be made. The plots for LUS50 and

LUS100 were below the CSL, on the dry side. These tests showed dilation by the increase in p' during the applied stress as might be expected for densely packed grains. All the other tests plotted above the CSL, on the wet side. These all showed contraction during shearing by the decrease in p' as the lines move towards the CSL at their specific void ratios. They showed behaviour that might be predicted from knowledge of their void ratios and the position of the CSL. There were no anomalies that might indicate any of the specimens having bonding as part of the specimen's structure. The movement to the CSL took place at relatively large strains when any bonding could be expected to have been destroyed already.

Comparison of the sample stiffnesses, normalised with respect to the effective mean stress (Figure 5-36), showed the plots for the high pressure tests, LUS200, LUS400, & LUS800. These coincide with each other from 0.1% axial strain to the end of the test, showing a gradual decrease in stiffness. The stiffness response of LUS25 was much higher than the other tests and unlike their gradual loss of stiffness; LUS25 showed a sharp fall in stiffness over the first 1% of axial strain. A more constant level of stiffness follows this from 1.3 % axial strain for the remainder of the test. Tests LUS50 & LUS100 (not shown in Figure 5-36) had a later development of stiffness due to use of external strain measuring devices to evaluate their axial strains. From comparison of their stiffnesses with those of the other tests, by using their external strain results (Figure 5-37) it was evident that they have lower stiffnesses than the other tests at both higher and lower pressures. There was also a decrease in stiffness from LUS50 to LUS100 as the confining pressure was increased.

5.2.2.1.1 Evidence of Bonding within the specimens

The results from the tests above did not show a feature that definitely indicates these specimens had bonding as part of their structure. The evidence from the drained tests on undisturbed specimens showed that only half could be considered as being pozzolanic bonded. In the undrained tests there were two that show peaked strength, which might be an indication of bonding. However, these two tests (LUS50 and LUS100) appeared to be overconsolidated and it was the dense packing that gives rise to the peaked strength and the generation of negative pore pressures. LUS25 was the only other test in this LUS group to show dilation. Unfortunately as there was no calculated void ratio, it could not be compared to the CSL. However, there were other indications that suggest LUS25 is bonded. The first was its stiffness. The second was its different behaviour from LUS50 and LUS100, where it did not show a peaked strength. The third was the relative position of the points of $(q/p')_{max}$ and $(du/dEa)_{max}$, which were similar to those of other bonded sand/clay specimens by Malandraki (1994). The reverse relationship was seen in tests LUS50 and LUS100. The expected relationship for an unbonded specimen was a coincidence of the points in drained tests. Did the non-coincidence indicate that these also contained bonding, or that the irregular layering had produced a complex structure to the undisturbed specimens? The question was whether or not there was any influence due to pozzolanic activity. The low stiffness and high strains indicated that LUS50 and LUS100 probably did not contain bonding.

5.2.2.1.2Summary

The results of the six specimens tested demonstrate different behaviours, which appear to be linked to their confining pressures. LUS25, tested at the lowest pressure, appears to have the characteristics of a bonded specimen. At slightly higher pressures, LUS50 and LUS100 show overconsolidation behaviour, which may be masking bonded characteristics. A simpler explanation might be the presence of layering itself. Each layer was distinct from the others and may vary in specific gravity, grain size distribution and chemical properties. A stiffer layer due to a greater proportion of angular grains may easily occur. The variation can lead to a complex structure

At the higher pressures of 200kPa and above there was no evidence of bonding. Again, these specimens behave in a similar manner to the LUD group. Whether bonding was originally present and destroyed by consolidation, or the specimen never contained any bonding cannot be resolved by these tests alone. These results suggest that either the bonding was lost at very low confining pressures or bonding within the structure was an uncommon feature. The results of drained tests indicated bonding was still present at 400kPa and it appeared that the pozzolanic activity, which could be causing the bonding, was an uncommon feature of this lagoon.

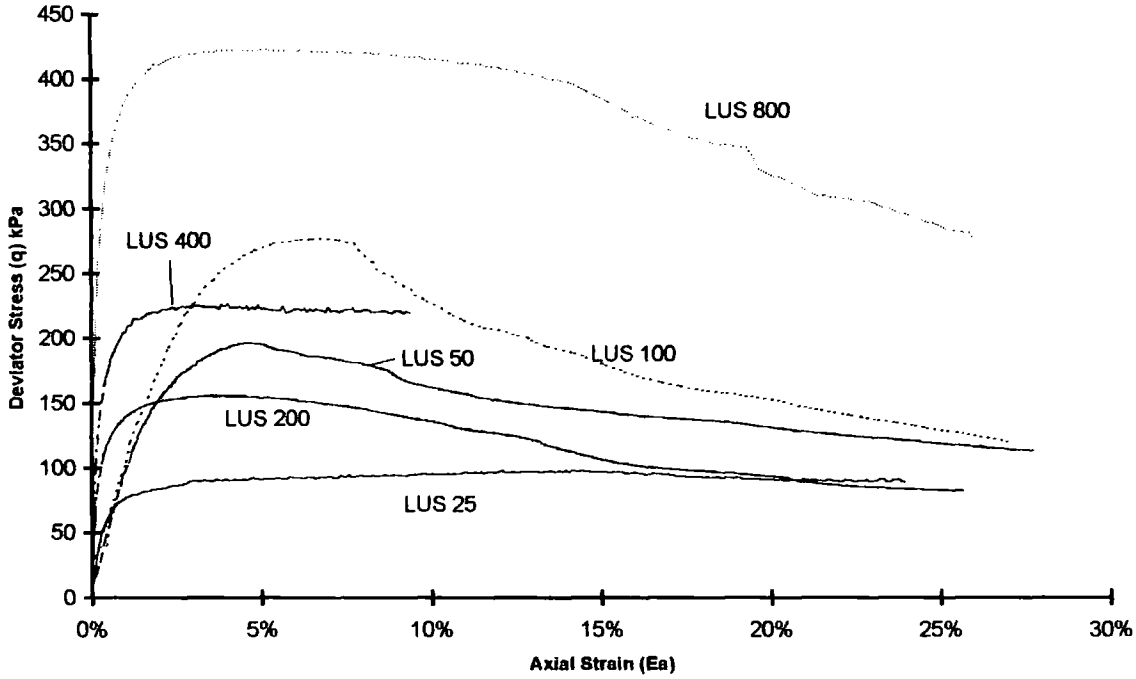

Figure 5-30a Stress against strain plot for LUS '25-800' tests using external measuring devices

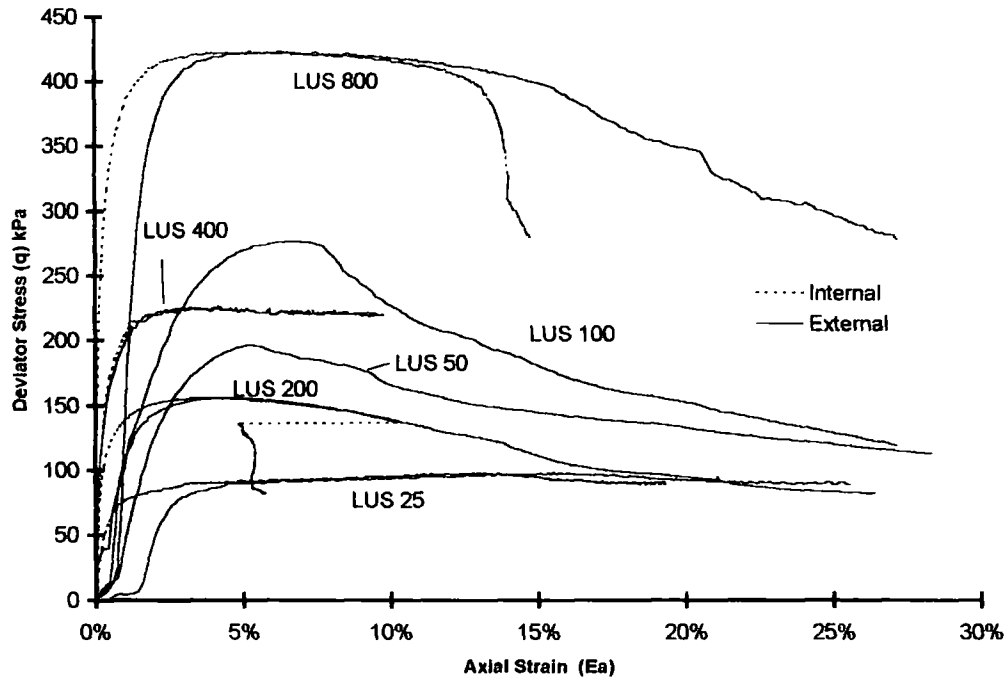

Figure 5-30b Stress again strain plots for LUS '25-800' tests showing the difference in strain measurement between internal and external devices

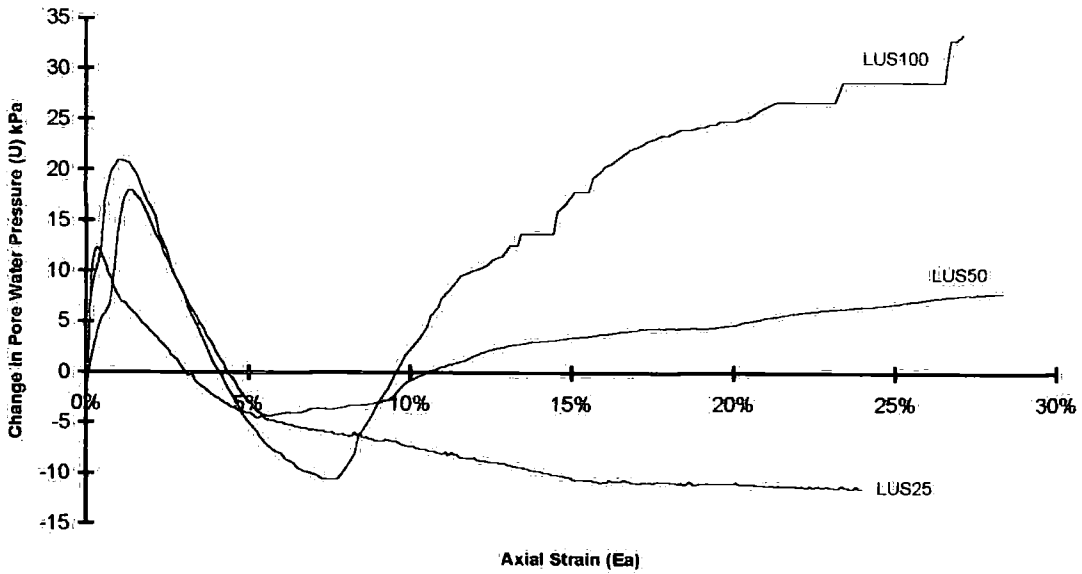

Figure 5-31a Changes in pore water pressure versus axial strain for LUS '25-800' tests at 100kPa confining pressure and below.

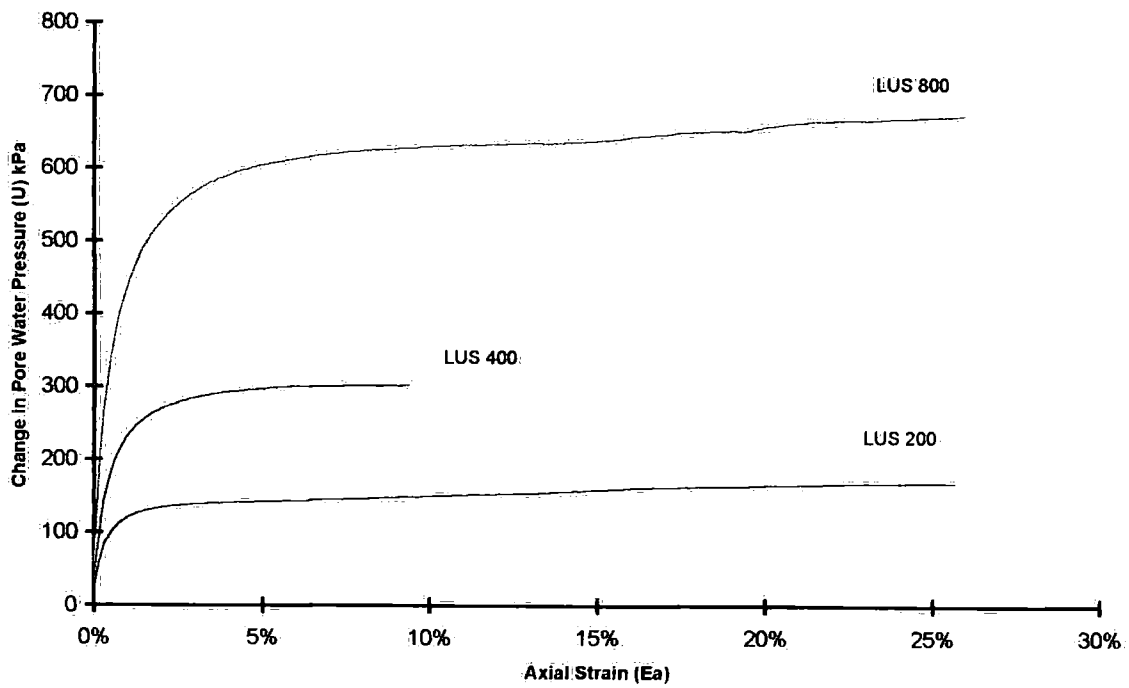

Figure 5-31b Changes in pore water pressure versus axial strain for LUS '25-800' tests at 200kPa confining pressure and above.

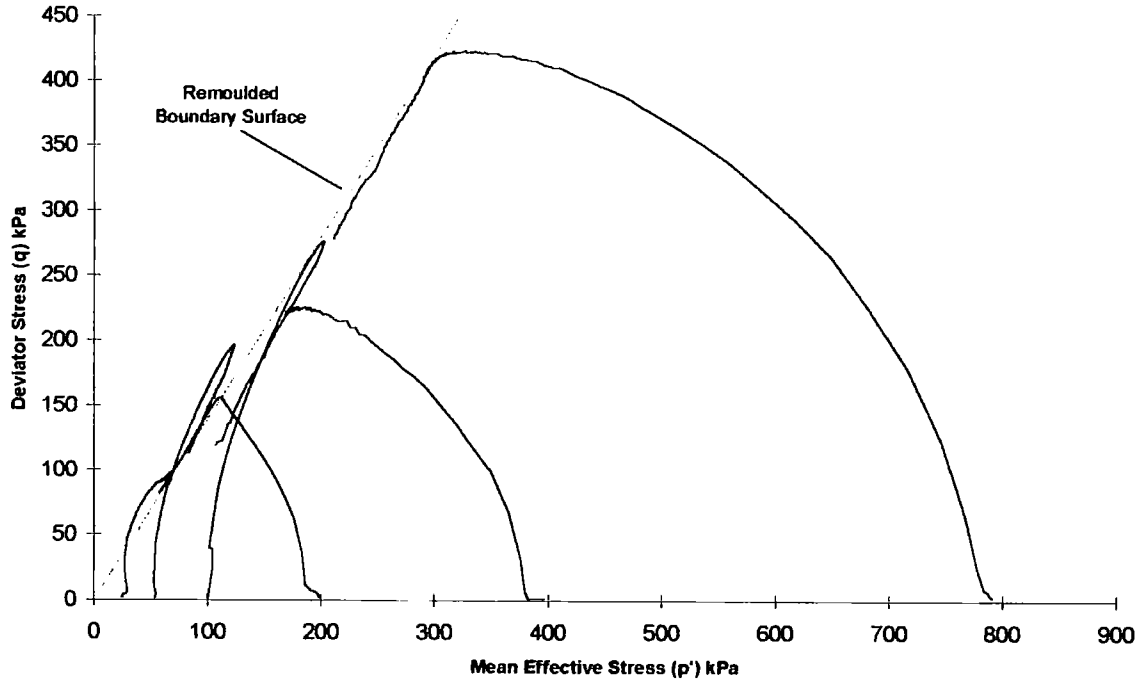

Figure 5-32 Effective stress paths for LUS '25-800' tests

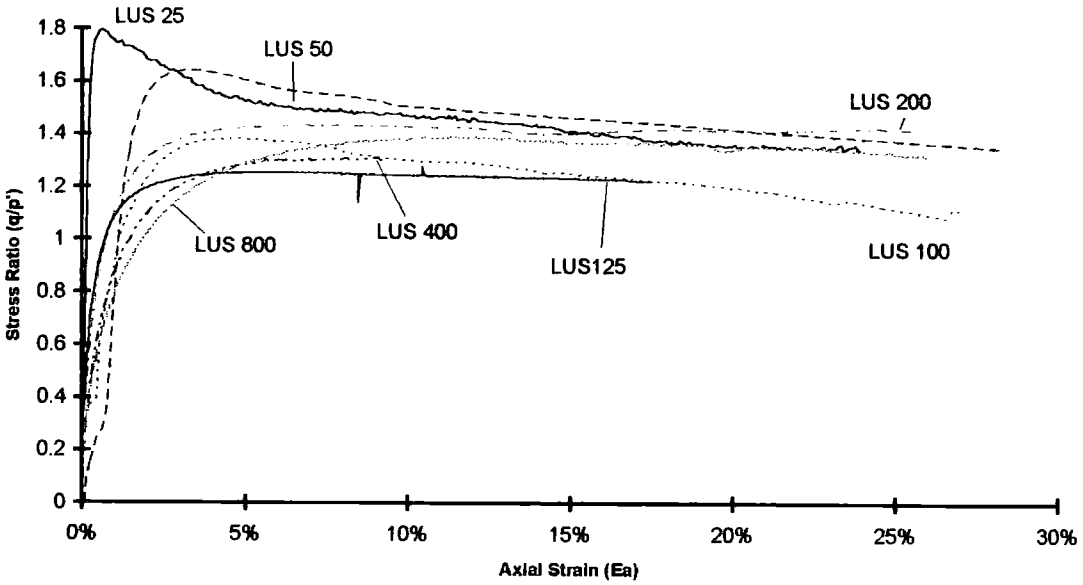

Figure 5-33 Stress ratio against strain plot for LUS '25-800' tests

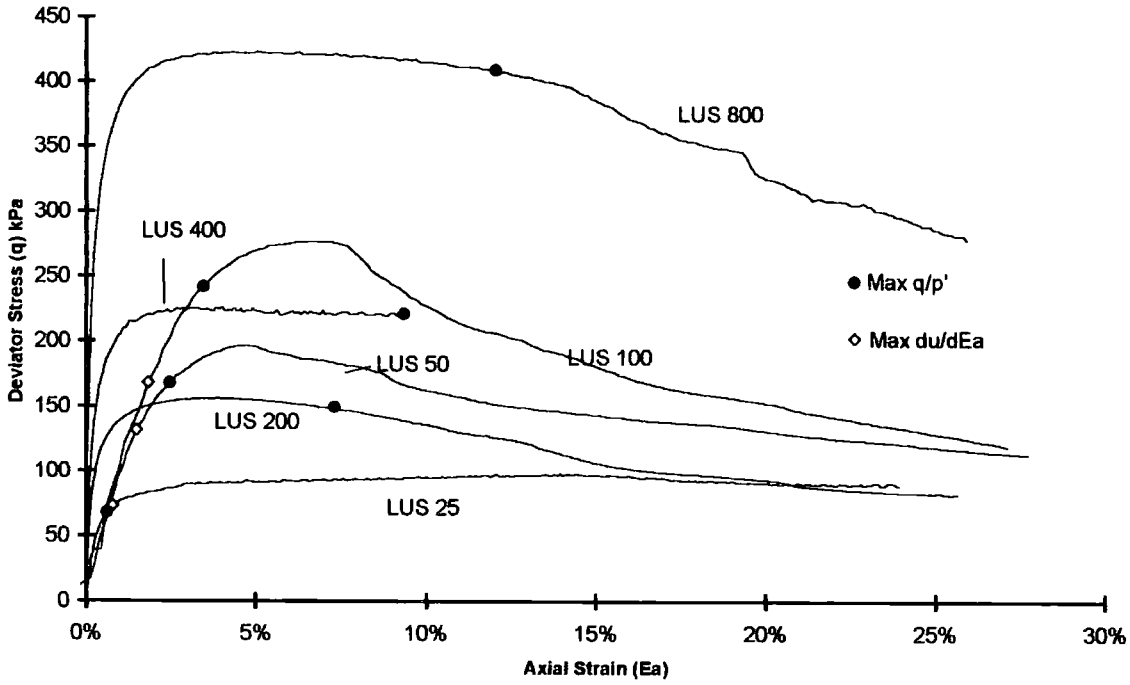

Figure 5-34 Relative position of the maximum points for LUS '25-800' test plotted stress-strain curves

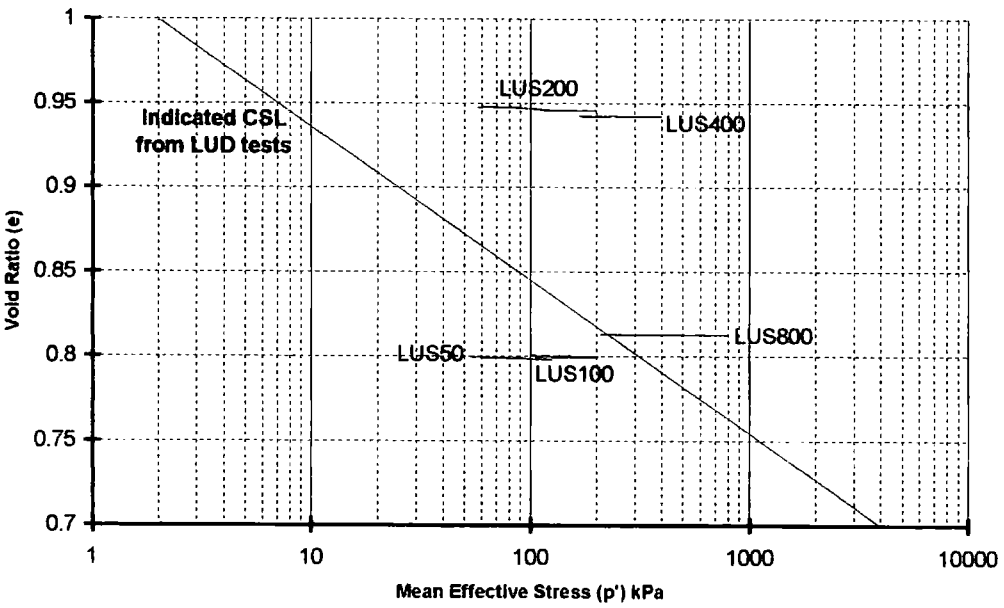

Figure 5-35 Void ratio changes against effective mean stress plot for LUS '25-800' tests

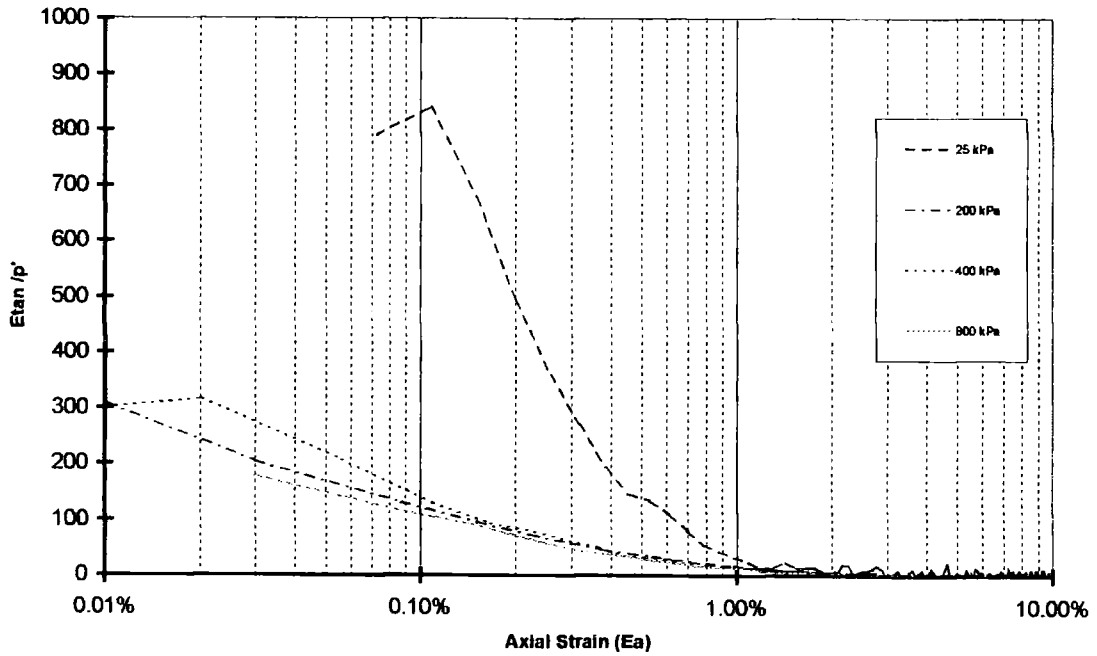

Figure 5-36 Plot of stiffness normalised with respect to the mean effective stress against strain for LUS '25-800' tests using internal strain measuring devices only

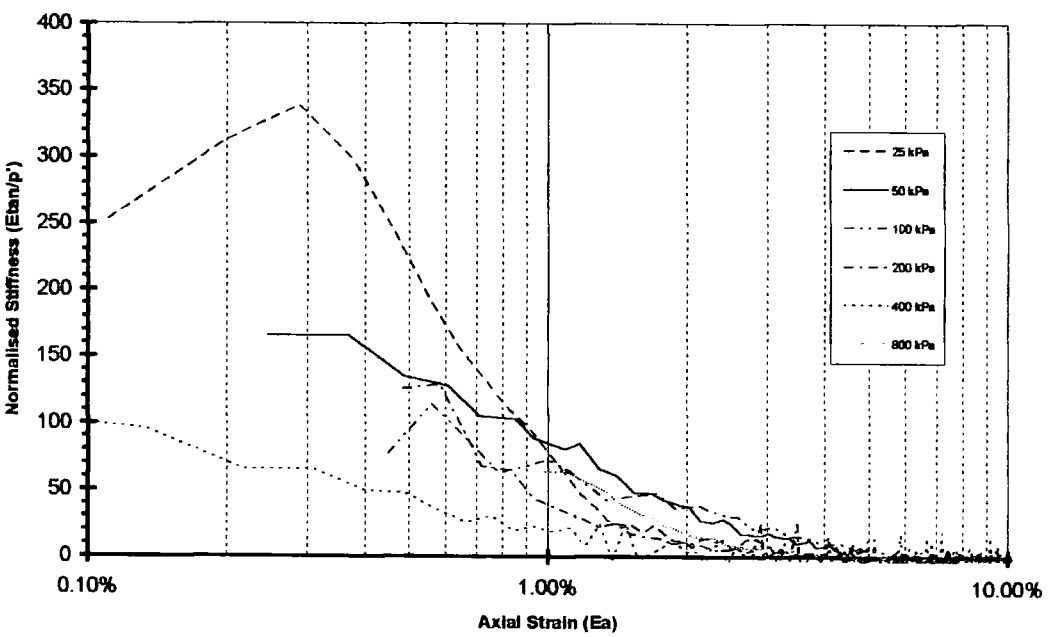

Figure 5-37 Plot of stiffness normalised with respect to the mean effective stress against strain for LUS '25-800' tests

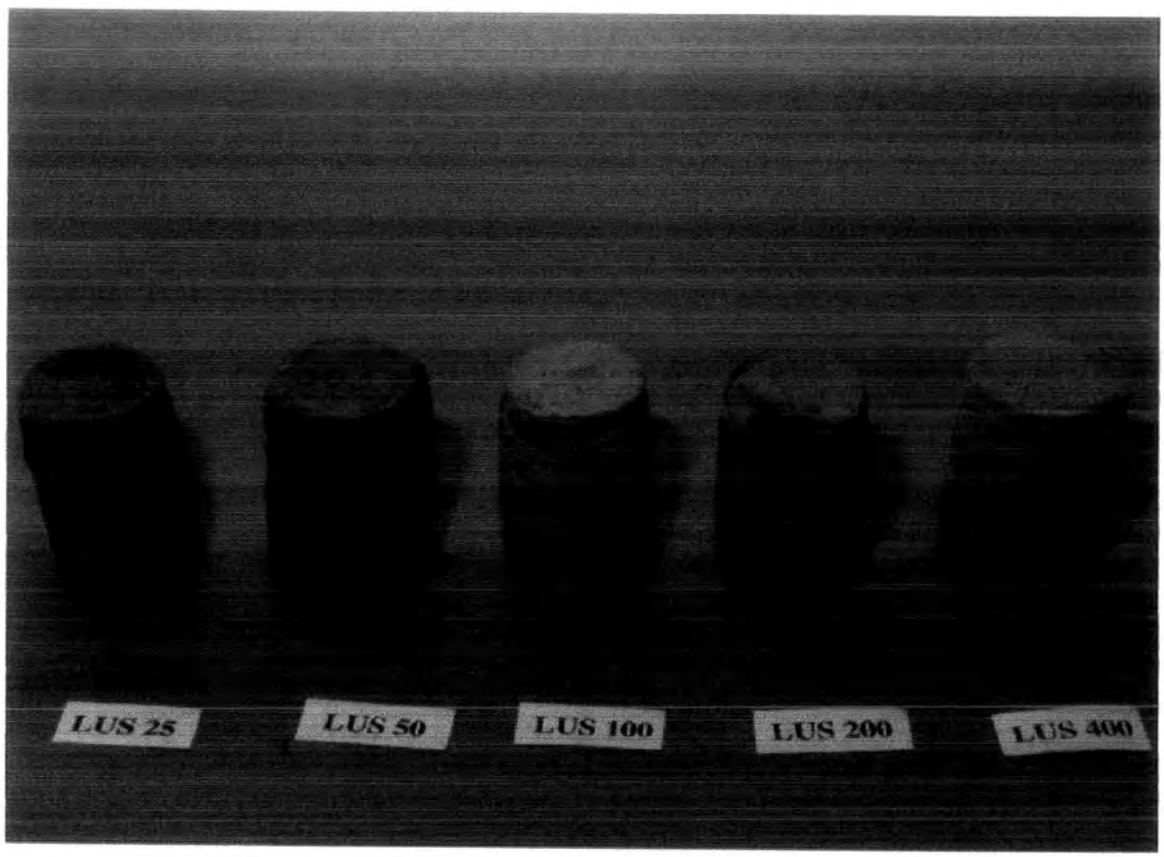

Plate 5-4 Some of the specimens from the LUS '25-800' group of tests after undergoing triaxial compression

5.2.2.2 LUS '100-200' Tests

The undisturbed tests of the '25-800' group highlighted significant change in behaviour related to the confining pressure. This group of tests ('100-200') was used to study this change more closely. All four of the specimens came from the same Delft tube, (Tube 10522 which was extracted from a depth of 8-9m in BS406). This tube unusually contained thick layers of a light coloured ash, producing long competent sections of Delft core. The thick layers represented single outwashes of ash and so a number of samples could be taken from the same or closely related sources of fly ash. This would allow a better correlation between results compared to results from a range of different tubes. These samples lacked the fine layering characteristic of many other undisturbed samples tested.

Test	*M/C (%)*	*SG*	$e_{initial}$	e_{consol}
LUS125	40.72	2.24	0.938	0.894
LUS150	37.15	2.09	0.902	0.859
LUS175	31.66	2.09	0.979	0.943
LUS200/2	-	-	0.867	0.864

Table 5-5 Specimen information and parameters for LUS '100-200' tests

The stress against axial strain plots, Figure 5-38, of these tests showed no correlation between the maximum strength and the confining pressure. All the tests showed a high stiffness to initial loading, achieving most of their strength by 1% axial strain. However LUS200/2, a repeat test at 200kPa, was the only test of the four to exhibit a significant drop in strength from its maximum strength at 1.5% axial strain, a much

lower strain than the other tests. The rest reached a maximum by 6-10% axial strain when there was a gradual rise and fall. Internal devices were fitted for all four tests.

All of the tests in the plots of pwp change with axial strain Figure 5-39 were dominated by increasing pwp similar to those in Figure 5-31 at 200kPa and above. Test LUS200/2 behaves in a very similar manner to LUS200. The other three tests showed a slight reduction in pwp at about 8% axial strain, before continuing to increase pore pressure at a low rate of change. The changes were small when compared to LUS100.

The stress paths plotted in p'-q stress space (Figure 5-40), showed a gradual change in behaviour with increasing confining pressure. All four tests showed a common trend for the tail of their respective stress paths, also shared by LUS100 plotted for comparison. As the confining pressure is increased from 100-125kPa there was a decrease in the extent of the stress path passing above the trend line. There was also an increase in the pore water pressure developed. By 150kPa confining pressure there was a further reduction in the travel of the stress path above the trend, linked to the reduction in pore water pressure in Figure 5-39. By 175kPa there was no movement above the trend-line. They all showed decreasing pore pressure as they approached the trend-line. Between 100kPa and 125kPa the initial stage of the stress path now showed large increases in pore pressure for only small increases in axial strain. The reduction in pore pressure occurred at a much later stage and to a lesser extent. LUS200/2, similar to LUS200, did not show this reduction in pore pressure as it

approaches the trend-line. The pore water pressure continued to increase as it changes direction upon meeting the trend-line and traveled down along it towards the origin.

The plot of q/p' vs. Ea (Figure 5-41) showed a very close relationship between the four specimens from tube 10522, when compared to LUS100 and LUS200. They all had similar initial increases, but only reached a maximum stress ratio of about 1.2, after which there is little change. The main difference between the curves was in the rate of change . LUS150 changed abruptly at 1.2, whilst the other tests demonstrated a gradual transition to their ultimate ratios.

The position of the points for $(q/p')_{max}$ and $(du/dEa)_{max}$ were plotted in relation to the q-Ea curve in Figure 5-42. For LUS125 and LUS175 these points were coincident at large axial strains of 5% and 7% respectively. Based on the work described in section 5.1.2 this coincidence was indicative of an unbonded specimen. For LUS150 the $(q/p')_{max}$ occurred prior to the $(du/dEa)_{max}$, indicating no relation between the two and hence that the strength of the specimen was related bonding and not just interparticulate friction.

The plot of e vs. log p' (Figure 5-43) showed that all the tests plotted close to each other just above the CSL defined by remoulded tests in Figure 5-29. LUS125 plotted closest to the CSL and showed very little change in p'. The other tests all showed greater changes in p'. The change in behaviour shown in the stress paths was due to changes in void ratio.

The plot of normalised stiffness Figure 5-44 showed LUS175 initially less stiff than the others, which wss due to its high void ratio. LUS150 & LUS200 coincide well, although the strength of only LUS150 may be attributed to bonding. LUS125 had a similar plot to LUS150 & LUS200/2 but maintains a higher stiffness with increased strain.

5.2.2.2.1 Yielding and Bonding

The four specimens from tube 10522 had a closer relationship compared to the other LUS tests. They had very similar ultimate stress ratio values and plotted close to each other above the CSL in Figure 5-43. As many of the others LUS tests did not appear to be bonded, it raised the question as to whether these specimens represent bonded or unbonded behaviour. LUS150 was the only test of the four to show variation from the other three that may be identified as having bonding characteristics. Despite having the lowest strength, it reached a maximum at 2.5% and retained this strength to 6.5% axial strain. It had the greatest negative change in pore water pressure of all four. The curve of stress ratio against axial strain showed a sharp change once it reaches its maximum. Also, the point of $(q/p')_{max}$ occurred at a lower strain than $(du/dEa)_{max}$. The different behaviour of LUS150 indicated this specimen may contain bonding as part of its structure, which was not present in the other three tests.

As LUS150 appeared to be a bonded specimen its results were analysed, in the same way as the bonded specimens identified in the drained tests (section 5.1.2), to identify any yield points. The same four plots of stress against axial strain and tangential

stiffness against axial strain, both on normal and log-log scales were used (Fig 5-45). Poor data at the beginning of the test meant that an initial yield point could not be identified, but there was a noticeable drop in the stiffness plots at 0.032% axial strain that may represent the second yield. The stiffness plots also showed a number of other yield events with continued loading. This was in agreement with the multiple yields identified in LDS200 and LDS400.

5.2.2.2.2 Summary

These four specimens were originally tested to explore the change in behaviour between LUS100 and LUS200. The specimens demonstrate similar behavioural characteristics as emphasised by the plot of q/p' vs. Ea (Figure 5-41). Tested at confining pressures spanning 100-200 kPa they showed the gradual change from dilatant to compacting behaviour due to their void ratios. The question of whether this was due to bond yielding or sample density was answered by the lack of evidence of bonding seen in most of the samples. Bonding did not appear to play a role in this change. These four highlight an important point concerned with undisturbed specimen. Despite the close association of these four specimens in behaviour and location, LUS150 appeared to be bonded while the others do not.

These specimens were distinct from the other undisturbed specimens in the thickness of the layering. Each specimen was formed from only one or two layers representing single outwash events. The undisturbed specimens of 'LUS25-800' were composed of many thinner layers (Plate 5-4 - LUS25) that vary in particle type and origins. The

thicker layers in tube 10522 indicated their relative closeness of the outwash pipe to the location of BS406 when these layers were deposited, whilst the thinner layers were from further away from the pipe when they were deposited.

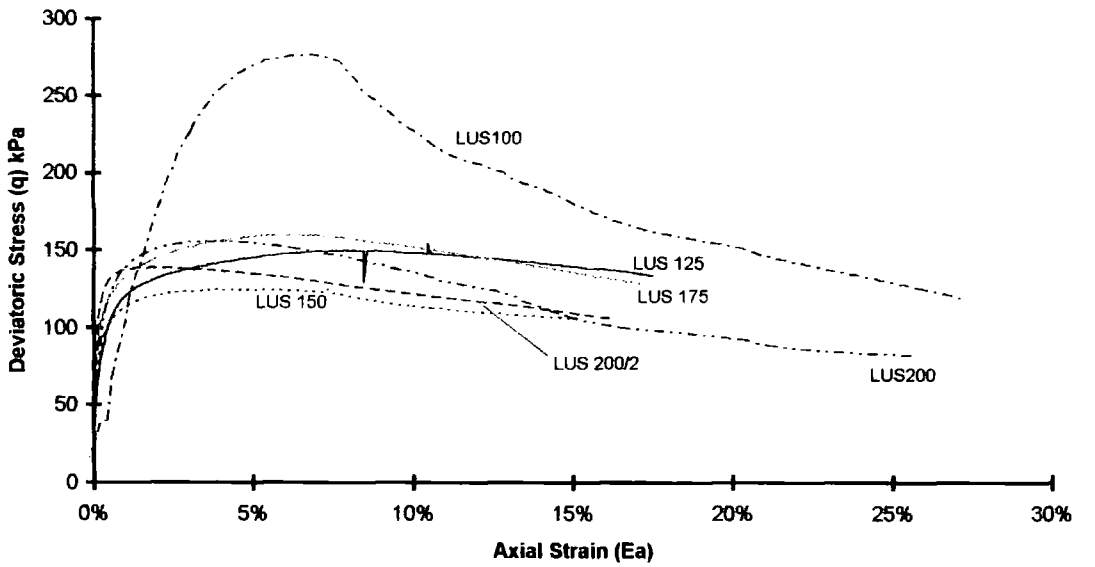

Figure 5-38 Stress against strain plot for LUS '100-200' tests, with LUS100 and LUS200

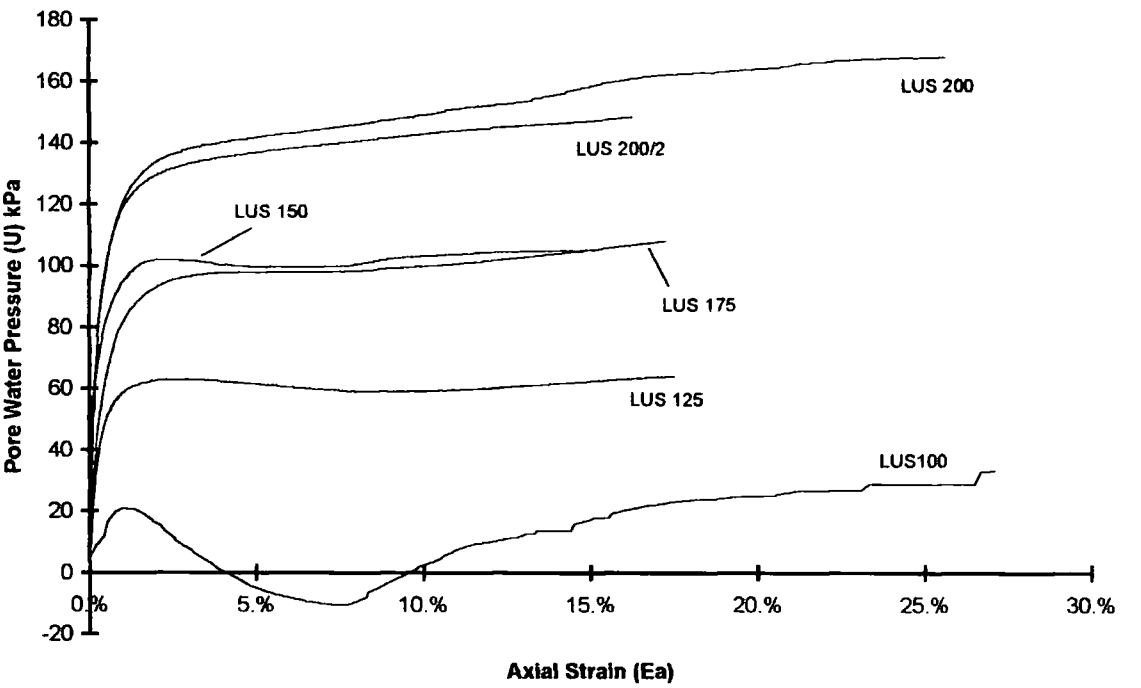

Figure 5-39 Changes in pore water pressure against axial strain for LUS '100-200' tests with LUS100 and LUS200 for comparison.

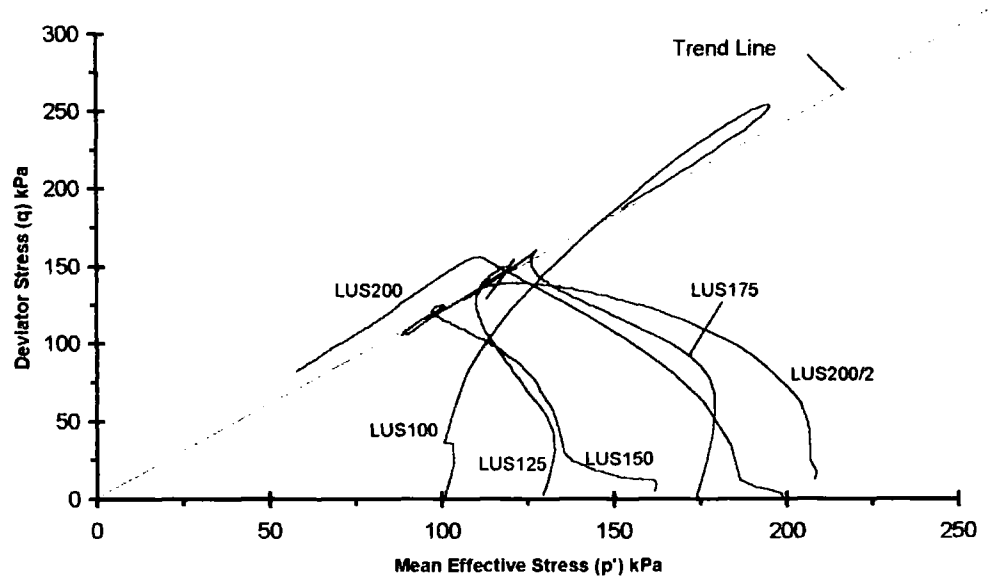

Figure 5-40 Effective stress paths for LUS'100-200' tests plotted with LUS100 and LUS200 against the boundary surface defined from LUD tests

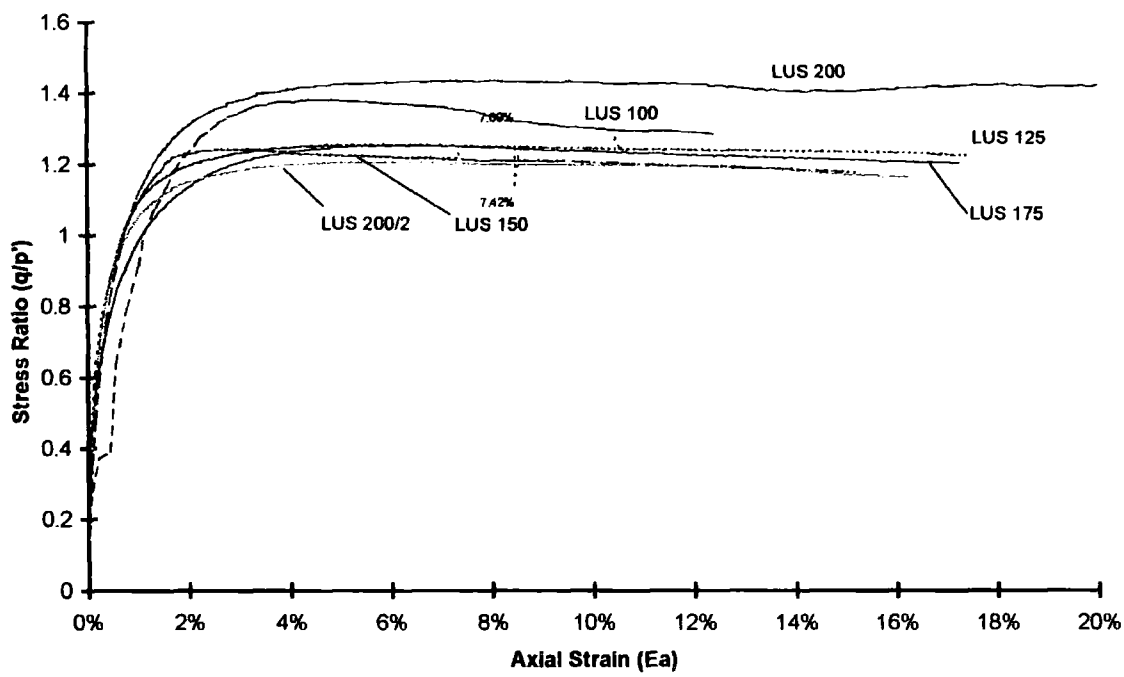

Figure 5-41 Stress ratio against strain for LUS'100-200' tests with LUS100 and LUS200 for comparison

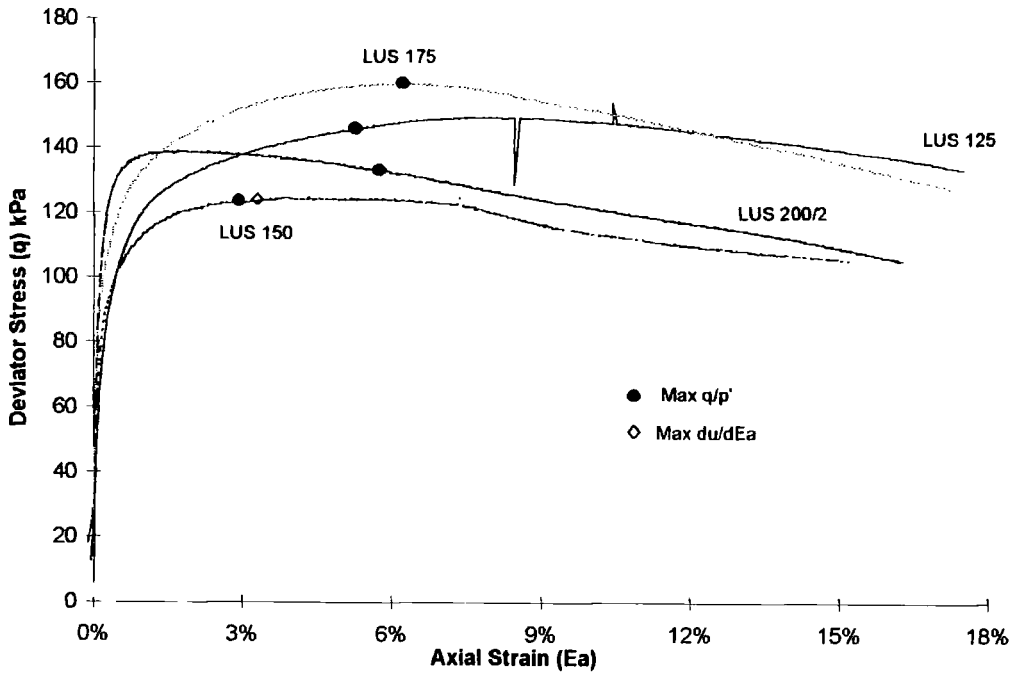

Figure 5-42 Relative position of maximum points for LUS '100-200' test plotted on stress-strain curves

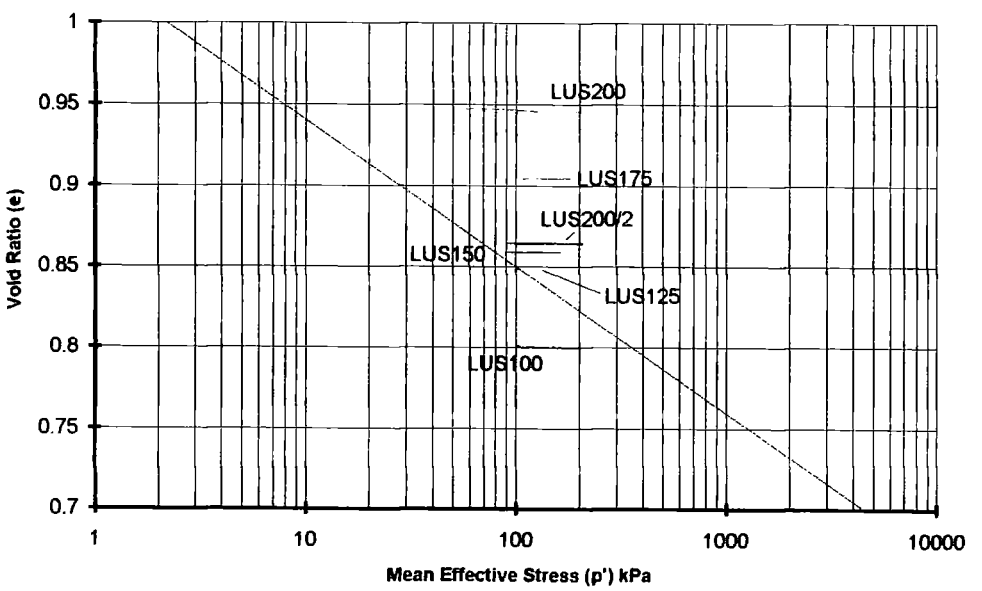

Figure 5-43 Void ratio versus mean effective stress for LUS'100-200' tests

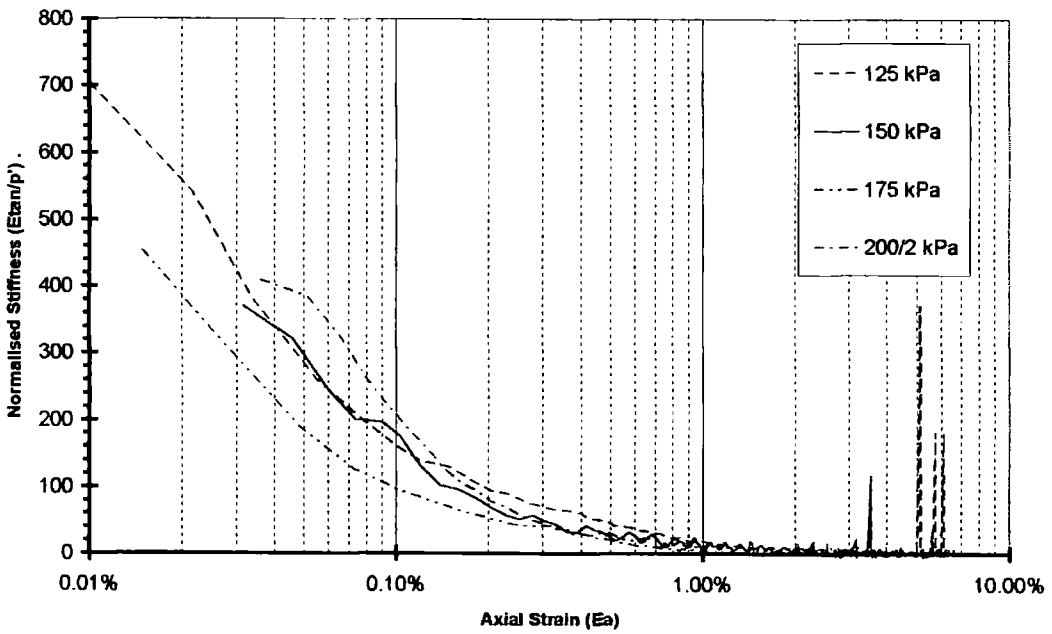

Figure 5-44 Plots of normalised stiffness against strain for LUS'100-200' tests

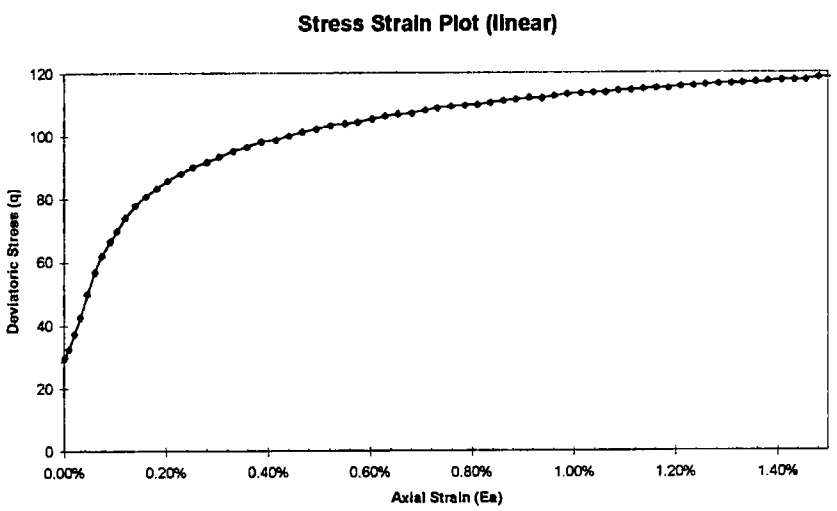

a)

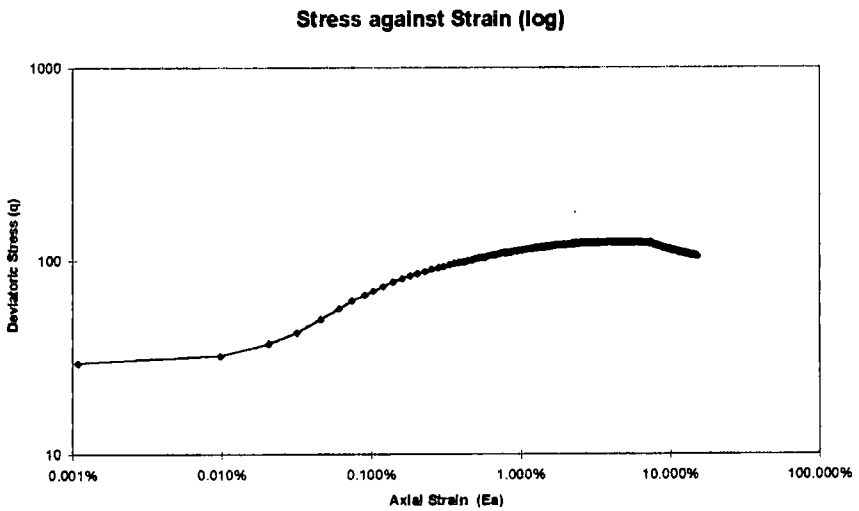

b)

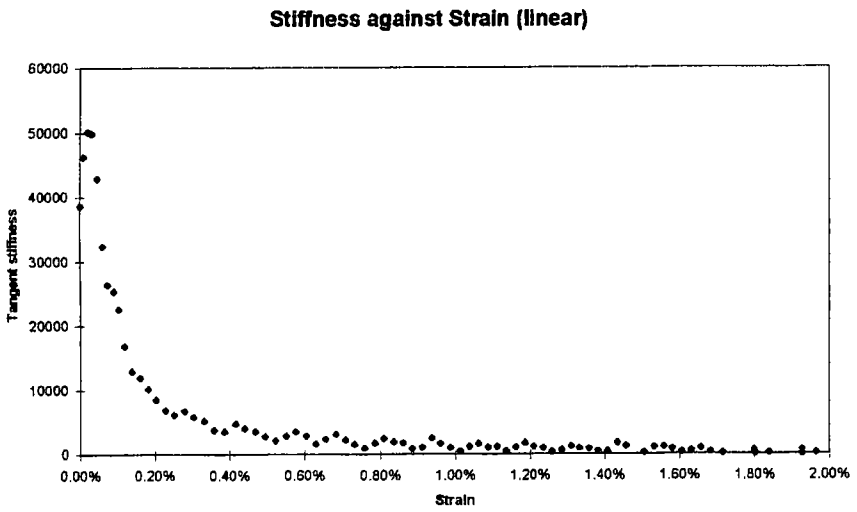

c)

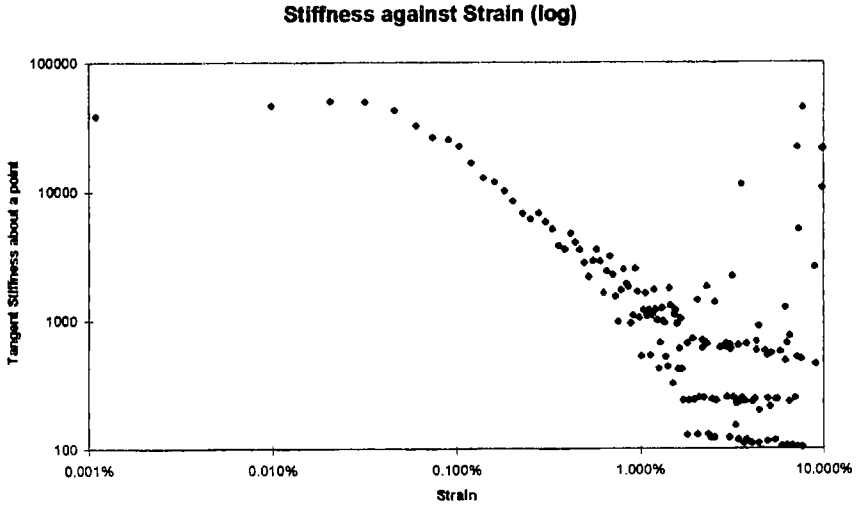

d)

Figure 5-45 Plots of stress against strain (a) normal scales, b) log-log scales) and tangential stiffness against axial strain (c) normal scales, d) log-log scales) for LUS150

5.2.2.3 Depth Profile Tests

The next two groups of undrained tests were designed to study the changes in strength with depth in the lagoon. BS406 was chosen for this study, and at least one specimen was selected from each of the Delft tubes extracted. The tubes were numbered for identification during the original site investigation. It is these numbers that are used in the naming of the tests, replacing the numerical part that represents the confining pressure in the other tests. A higher number indicates a sample from deeper in the lagoon. Four were tested at 75kPa and five were tested at 125kPa. The test at 125kPa for tube 10522 was the same test reported in the previous group named as LUS125.

Test	***depth*** *(m)*	***M/C*** *(%)*	***SG***	$e_{initial}$	e_{consol}
LUS2233	0.9	33.27	2.10	0.737	0.721
LUS7642	2.6	33.41	2.08	0.612	0.601
LUS7887	3.7	38.28	1.98	0.655	-
LUS9351	4.7	36.00	2.24	1.067	1.058
LUS9811	5.7	42.77	2.35	1.167	1.136
LUS10179	6.3	34.41	2.14	0.746	0.722
LUS10458	7.8	40.95	2.01	0.673	0.663
LUS10522	8.7	40.72	2.24	0.929	0.885
LUS10606	9.9	50.55	2.03	1.122	1.073

Table 5-6 Specimen information and parameters for 'Depth Profile' tests

The change in void ratio with depth was plotted in Figure 5-46, where the initial and consolidated void ratios can be compared. The void ratios range from 0.6 to 1.2 with

no clear pattern of change that relates to depth. At 5-6m depth there was a horizon, which is relatively under compacted, compared to layers above. The void ratio reduces again down to 8m depth where there was another rise.

The highest deviator stresses were also plotted against depth in Figure 5-47 and showed the same confused profile with depth. The weakest specimens came from the under compacted layer at 5-6m depth, whilst the strongest specimen came from the denser layers. The exception to this was specimen LUS10606 that, despite having one of the highest void ratios, retained strength similar to specimens at much lower void ratios. The strength of the specimens appeared to be related primarily to their densities. There were however indications that this could not explain the strength of all the specimens.

All the specimens obtained from BS406 can be seen in Plate 5-5. Similar to Plate 5-4 there was a range of colour between the different specimens. LUS9351 was much lighter in colour than LUS10458 and appeared to be made up of much finer grains. The laminations visible in LUS25 were again visible in LUS10606 where they have been offset by the failure surface. Most of the specimens showed evidence of failure surfaces. Some like LUS7642, LUS10179, and LUS10606 had single failure surfaces, whilst others like LUS2233, LUS7887, and LUS10522 had multiple surfaces in different orientations. There was evidence that some of the specimens did not deform evenly throughout the specimen, notably LUS9811 and LUS7642, indicating the presence of weaker layers where deformations had been concentrated

5.2.2.3.1 75kPa Tests

For the tests performed at 75kPa confining pressure the plots of stress against axial strain Figure 5-48 showed a complete range of curve shapes, with no correlation with sample depth. The shallowest sample of this group LUS7887 had a very angular shape with a steep increase in stress, which culminated in a peak failure. The strength then remained reasonably constant until 15% axial strain when it rose to its maximum strength. This was followed by a sudden loss of strength. LUS9811 had a stiff initial response to axial loading reaching a maximum strength of less than one quarter that of LUS7887, by 0.5% axial strain. This was followed by a steady reduction in strength for the remainder of the test. LUS10458, after a similar stiff initial response, showed a gradual reduction in stiffness as it approached its maximum strength. The test was stopped at 15% axial strain before a maximum strength was reached. The deepest sample of this group, LUS10606, also had an initial stiff response to axial loading reaching its maximum strength at 4% axial strain. This was then followed by a gradual reduction in strength towards a constant level by the end of the test at 25% axial strain.

The variation in stress strain curves was repeated in the pwp response plotted against axial strain, Figure 5-49. After the initial compression, LUS7887 showed a marked reduction in pwp, which leveled out as the strength reached its first peak. Pore pressure began to reduce further as the sample reached its maximum strength at which point the corresponding fall in strength was matched with a sharp rise in pore pressure. LUS9811 had a very rapid increase in pore pressure at the beginning, followed by a

slight reduction to a near constant 40 kPa for the remainder of the test. LUS10458 had a similar initial increase in pore pressure to LUS9811; which was followed by a decrease in pore pressure, to an overall loss in pore pressure by the end of the test where it was still falling. LUS10606 had a similar initial increase in pwp to LUS10458 but reached a slightly higher pressure. It also decreased more rapidly than LUS10458, reaching a minimum point at 6% axial strain before increasing again towards a near constant pore pressure 25kPa above its initial pressure.

The stress paths plotted in p'-q stress space (Figure 5-50) for LUS7887, LUS9811, & LUS10606 all showed behaviour similar to the low pressure tests of the first group, where the stress paths passed above the trend of the stress path tails before curling round to the right. LUS10458 showed a different shape to the other three. It did not extend as far as the other three into stress space before curling to the right. The stress path then continued to move in this direction to the end of the test. This was similar to the stress path of LUD25 in Figure 5-27. As no maximum strength was reached before the end of the test, the stress path continued to rise at a constant stress ratio of 1.2. The stress ratio for LUS10458 was significantly different from the other three tests in the group

The plots of q/p' vs. Ea (Figure 5-51) for these tests showed the distinction between the stress ratio of LUS10458 and the others. LUS10458 had the lowest ratio in the group of 1.2 and showed a gradual reduction in the ratio after reaching a maximum. The other tests all showed significant peaks in the ratio. LUS10606 had the highest

stress ratio of 2.0, which reduced to an ultimate ratio of 1.4. LUS9811 reached a value of 1.8 and LUS7887 reached 1.6. All three show similar ultimate stress ratios of about 1.4

The plots showing the maximum points relative to the stress strain plots for these tests Figure 5-52 showed the three relationships seen before. In specimens LUS9811 and LUS10606 the points of $(q/p')_{max}$ preceded the $(du/dEa)_{max}$ point, as seen in other specimens that are considered to be bonded. The two points coincided in LUS10458 indicating that there were no bonding influences on this specimen. For LUS7887 the $(du/dEa)_{max}$ point preceded the $(q/p')_{max}$ point, indicating a possible complex structural influence to the specimens' behaviour. Both maximum points for LUS7887 occurred at lower axial strains when compared to the results from LUS50 and LUS100.

The plots of e vs. log p' (Figure 5-53) split these four tests into two groups of two relative to the CSL, defined from LUD tests (Figure 5-29). LUS7887 and LUS10458 which plotted below behaved in a similar way to other specimens which plotted below the CSL by showing a change in p' towards the CSL. For the tests that plotted above the CSL both decrease in p' towards the CSL initially followed by an increase, which was more significant in LUS10606.

The plot of normalised stiffness against axial strain (Figure 5-54) showed a marked difference between LUS9811 and the other three tests. LUS9811 had a significantly higher stiffness than the other tests, which reduced quickly. The next highest was

LUS7887, which retained a stiffness of 0.8% from 0.5%, before it reduced. LUS10606 showed a steady reduction in stiffness with a small drop at 0.12% before maintaining the constant stiffness loss. LUS10458 showed a gradual change in loss of stiffness from its maximum at 0.22%

5.2.2.3.2 125 kPa Tests

The stress strain plotted for the test performed at 125kPa (Figure 5-55) showed less variation in shape than those at 75 kPa. Again, there was no correlation between sample depth and maximum strength. LUS7642 and LUS10179 both achieved a similar maximum stress level. LUS7642 however was stiffer reaching this stress level at 5% axial strain and maintaining the level until 15% axial strain. LUS10179 reaches its maximum strength at 8% axial strain, followed by a sharp fall in strength once it had reached its maximum. The curve for LUS10179 was very similar to tests LUS50 and LUS100 from the first group. LUS2233 showed a gradual reduction in stiffness from its initial response until it reached its maximum strength at 9% axial strain. This was then followed by constant decrease to two-thirds its maximum strength by the end of the test at 27% axial strain. LUS9351 showed a gradual reduction in stiffness in a similar manner to LUS2233 but reached a maximum stress at only 3% axial strain. Following the maximum, its strength reduced to a near constant level of about half the maximum by the end of the test at 30% axial strain. Test LUS10522 had been described earlier in the second group of tests (Section 5.2.2.2) where it was labelled LUS125. Compared to the rest of this group, LUS10522 had the stiffest response. It

showed a marked change in stiffness to axial loading from its initial sharp rise to the gradual rise after 0.5%, and a fall in strength for the rest of the test, reaching its maximum strength at 8% axial strain.

The response of pwp to axial loading for these tests (Figure 5-56) demonstrated a range of curves showing a reduction in the production of negative pore pressure. LUS7642 had the quickest reduction rate of pore pressure, with a reduction in this rate at the point where the stress-axial strain plot met the upper limit. This is followed by an increase in pore pressure at 15% axial strain. The point of maximum strength coincides with a sharp fall in strength. LUS10179 had the largest negative pore pressure, followed by an increase at 8% axial strain, which correlated to the loss of strength. LUS2233 also showed a pwp decrease but at a much-reduced rate compared to the other two tests. It also showed a change to increasing pore pressure as the sample reaches its maximum strength. LUS10522 had a similar pattern to LUS2233 with a much less significant reduction in pore pressure. All four of these tests had similar levels of initial pore pressure increases before the previously described reductions. The peak of the initial increase occurred at less strain, with the increase in rate of pore pressure decreasing. LUS9531 had a higher value of initial pore pressure increase than the other four tests. It also did not undergo any decrease in pore pressure upon reaching a change in rate, but continued to increase in pwp. There was a slight variation in rate at the point corresponding to maximum strength in the plot of stress against axial strain.

The results of the change in pwp against axial strain were mimicked in the stress paths plotted in p'-q stress space (Figure 5-57). The tests that had large reduction in pore pressure showed the greatest stress. As the reduction in pore pressure reduced so does the maximum level of stress, wa not related to the samples relative depth. LUS9351 had a different stress path to the others and only showed a slight change in direction upon reaching the trend indicated by the stress paths tail before changing direction and moving with decreasing stress towards the origin.

Unlike the specimen tested at 75 kPa in the plot of q/p' vs. Ea (Figure 5-58) there were no significant peak ratios. Instead, the curves were similar to LUS10458 with gradual changes. LUS10522 showed a slight variation from the others in the group by maintaining a near constant value of 1.25. The others showed a gradual reduction in the stress ratio with increasing axial strain. The highest stress ratio was reached by LUS7642 of 1.45, reducing to 1.3. LUS9351 had the next highest of 1.35, followed by LUS10179 at 1.30 and the lowest LUS2233 at 1.20.

For three of these tests (LUS2233, LUS7642, LUS10179) the point of $(du/dEa)_{max}$ preceded that of $(q/p')_{max}$ in Figure 5-59 where they were plotted relative to the stress strain curves. This indicated that there was a possible influence from the specimens structure on their behaviour. The two remaining tests showed a coincidence of the points, indicating that their behaviour was unbonded. In the case of LUS9351 the coincidence of the points occurred after the maximum stress, whereas in other tests the coincidence occurred at lower strains than the maximum stress.

The plot of e vs. log p' (Figure 5-60) compared the void ratios to the CSL defined by the LUD test (Figure 5-29). Three of the tests plotted below the CSL and showed similar behaviour. Of these three LUS7642 and LUS10179 show relatively large changes in p' towards the CSL whilst LUS2233 had less change towards the CSL and a greater lowering of p'. The two tests above the CSL were LUS9351 and LUS10522. LUS9351 plotted high above the CSL and showed continued lowering of p'. LUS10522 plotted close to the CSL and showed very little change in p' but this may be a feature of the test only being sheared to 18% axial strain compared to about 30% axial strain in other tests.

The normalised stiffness plot for the 125kPa (Figure 5-61) showed a more consistent pattern between the specimens than those tested at 75kPa. LUS10522 had the highest stiffness. LUS2233 and LUS7642 showed similar normalised stiffness responses, and reduced quicker than LUS10522. The quickest stiffness loss occurred in LUS9351. The lowest stiffness was seen in LUS10179.

5.2.2.3.3 Yielding and Bonding for BS406

Using the method outlined in Section 5.1.2, tests LUS9811 and LUS10606 were analysed using the same four methods, plotted in Figures 5-62 & 5-63 respectively, to identify any yielding associated with bonding. The initial yield of LUS9811 at about 0.03% axial strain was evident in the stiffness plots (Fig 5-62c&d) again, but not in the stress-strain plots. The second yield was most noticeable in the stiffness plots but this

time could also be identified in the stress-strain plots (Fig 5-62 a&b) at 0.05% axial strain. Further yielding, as seen in the other bonded specimens were again evident, occurring at axial strains of 0.07%, 0.09%, 0.13% and 0.16%. For LUS 10606 the initial yield at best identified in from the stiffness plots again (Figure 5-63c&d), whilst it was the second yield that was most evident in the stress-strain plots (Figure 5-63 a&b). After the second yield from the stiffness plots other yield points were again visible. Further analysis of the plots indicated another significant yield point, which was best seen in the stress-strain plots and to a lesser extent in the stiffness plots at about 0.85% axial strain. This point seemed to mark the end of period of near consistent stiffness, which was followed by its progressive loss. This yield point was consistent with the proposal by Vaughan (1985) that the second yield point marks the point of increased breakdown in structure when the bond stress equals the bond strength. This would seem to indicate the previously identified yields in LUS 10606 should be considered as the initial yielding where the structure began to be broken down, the first of which may mark a change in its elastic response to loading as identified in unbonded soils by Jardine(1992).

5.2.2.3.4 Summary for BS406

The results from BS406 tests helped to assess the effect of sample depth on the behaviour. The profiles showed a confused pattern of void ratio change and strength with depth. They appear to highlight a relatively under compacted region at 5-6m depth, and another below 8m depth. Despite the lack of a consistent pattern with depth the range in void ratios seen in the specimens has allowed a closer study of the effect of the void ratio on the behaviour. The tests were carried out at the same confining stress level and showed how the variations in void ratio gave the same changes in character seen in the 100-200 kPa group of tests. The 100-200kPa tests showed the change in behaviour with increasing confining pressure. These two groups of tests show that both the pressure change and the void ratio change demonstrate a behavioural change consistent with the relationship::

$$\Gamma = \nu_o + \lambda \ln p'_u \qquad \text{Equ 5-1}$$

Where ν_o is the constant specific volume for the sample during the undrained test, p'_u is the effective mean stress at the critical state, λ is the slope of the critical state line in e-ln p' space, and Γ represents the void ratio for the reference effective mean stress at critical state, as explained further in Atkinson & Bransby (1978).

There is very little evidence of bonding in the fly ash from BS406, with only two of the nine specimens showing any characteristics. The strongest evidence was seen in

LUS10606, which also indicates the form of the bonding within the lagoon. The breakdown of LUS10606 from the particle distribution (Section 3.2.3) highlighted the presence of large flat grains, which were agglomerates of much smaller grains. Since each of the samples was exposed to the same conditions to break them down for the particle distribution, this implies that the bonding in LUS10606 was stronger than in other samples. It also demonstrates that the bonding between particles appears to be confined to certain layers. The large strains seen in LUS10606 may be caused by the deformation of unbonded layers between bonded layers. This would tend to make the sample seem less stiff than might be expected from a wholly bonded sample. It is also possible that a specimen containing bonding may appear to be unbonded if the stress applied in testing is accommodated by the straining in the unbonded layer, leaving the bonded fly ash relatively unstressed.

The bonded specimens also demonstrated a greater volume change in the consolidation stage of the test, compared to the unbonded samples. This suggests that where present, the bonding helped to maintain an open matrix in the unbonded regions around the bonded layers. Where there was no support from the interconnection of bonded layers in the sedimentary pile, the unbonded layers were able to consolidate further.

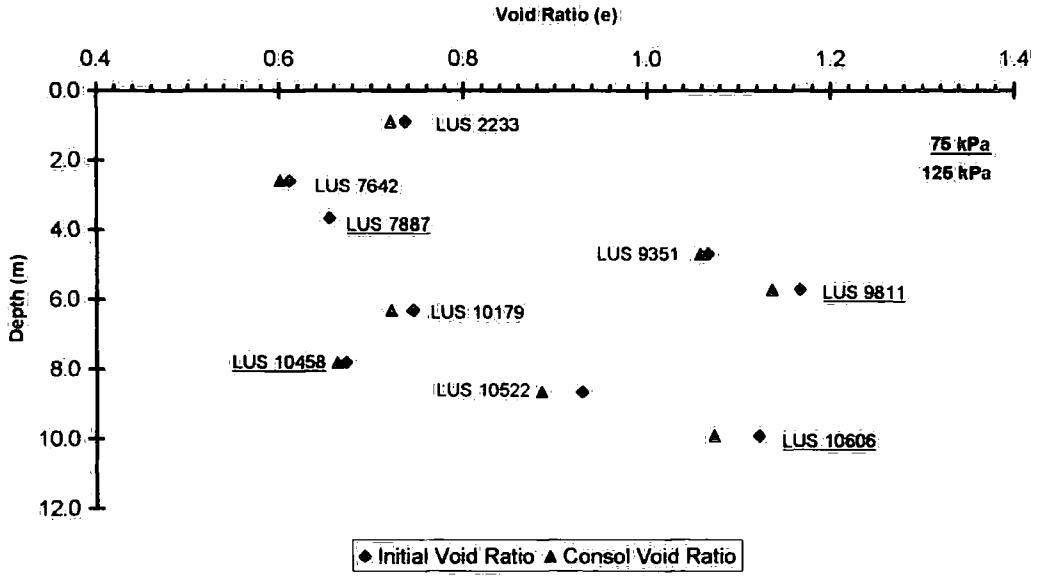

Figure 5-46 The initial and consolidated void ratios for each specimen from BS406 (Table 5-6) plotted relative to their depths in the lagoon

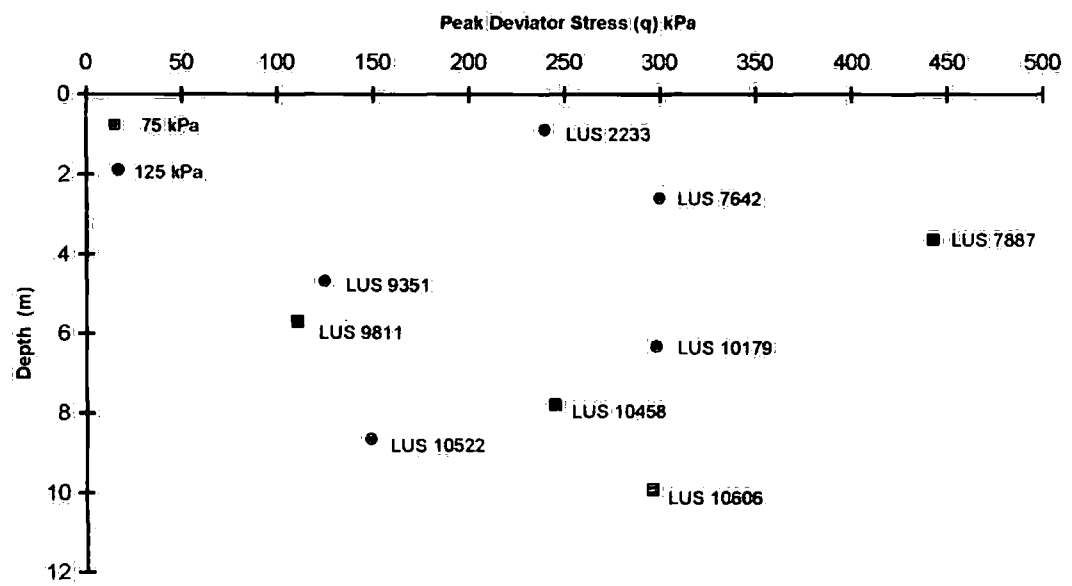

Figure 5-47 Peak stresses against specimen depth for each specimen from BS406 (Table 5-6)

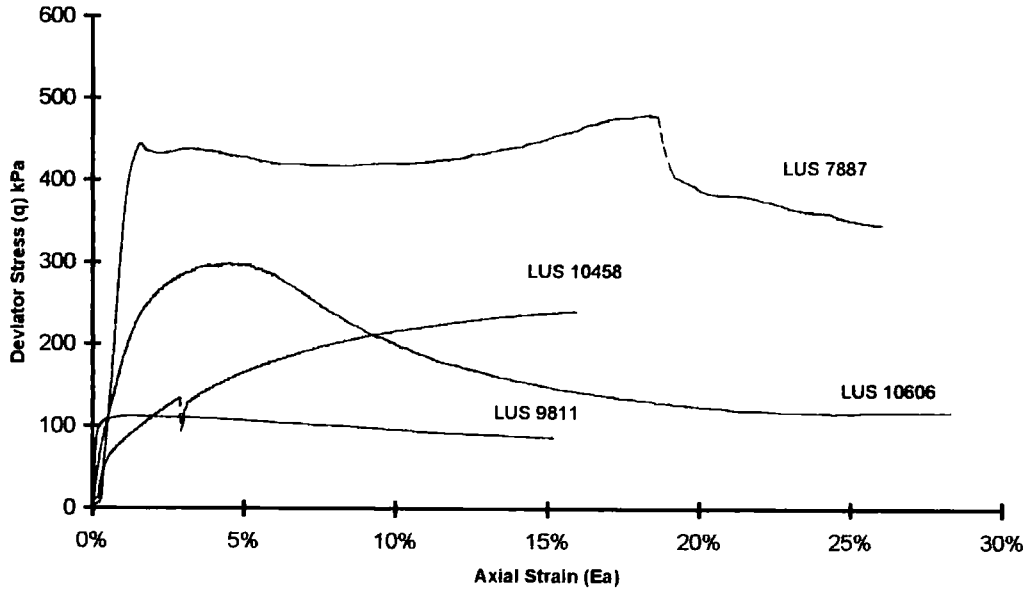

Figure 5-48 Stress against strain for BS406 tests at 75kPa confining pressure

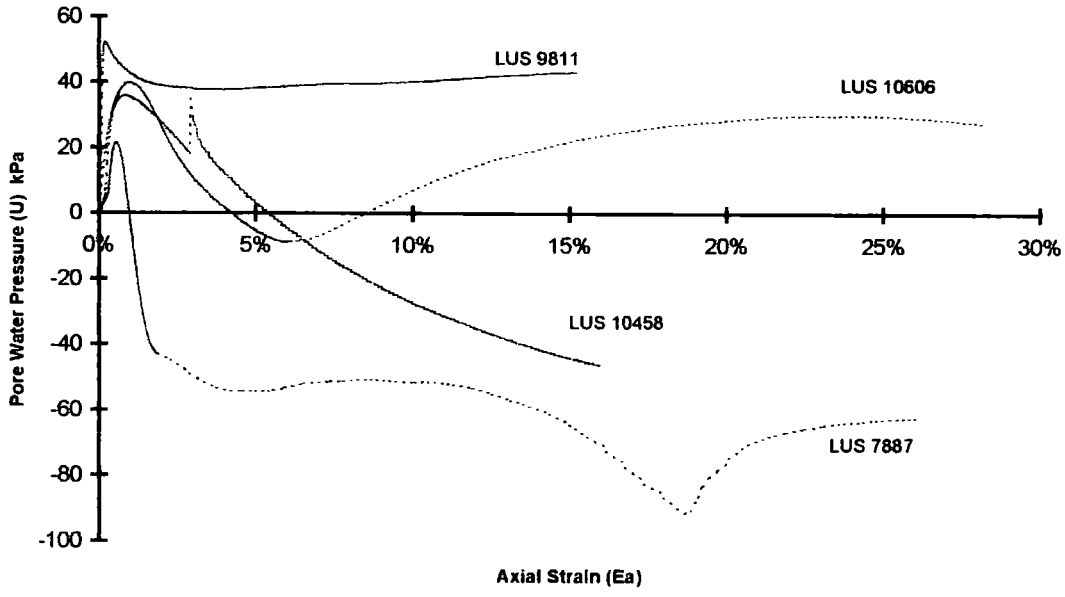

Figure 5-49 Changes in pore water pressure versus axial strain for BS406 tests at 75kPa confining pressure

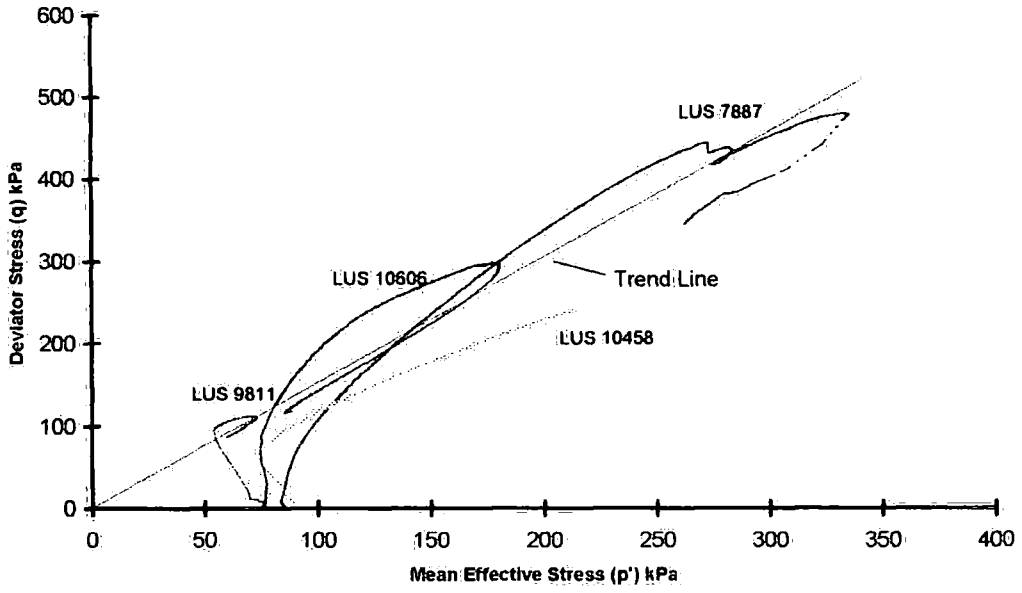

Figure 5-50 Effective stress paths for BS406 tests at 75kPa confining pressure

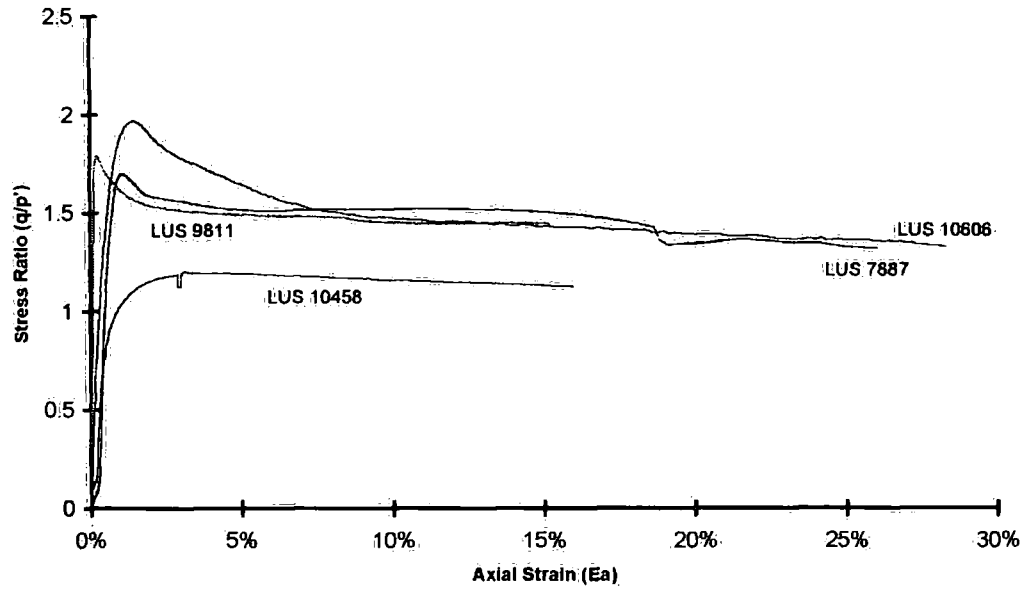

Figure 5-51 Stress ratio versus strain for BS406 tests at 75kPa confining pressure

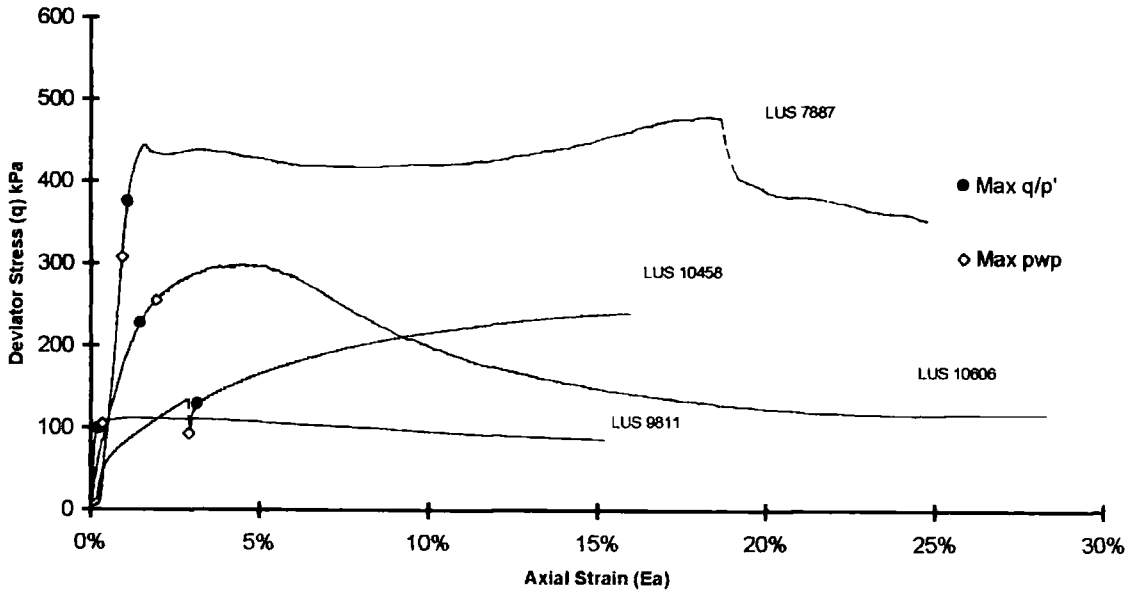

Figure 5-52 Relative position of maximum points for BS406 tests at 75kPa confining pressure plotted on stress-strain curves

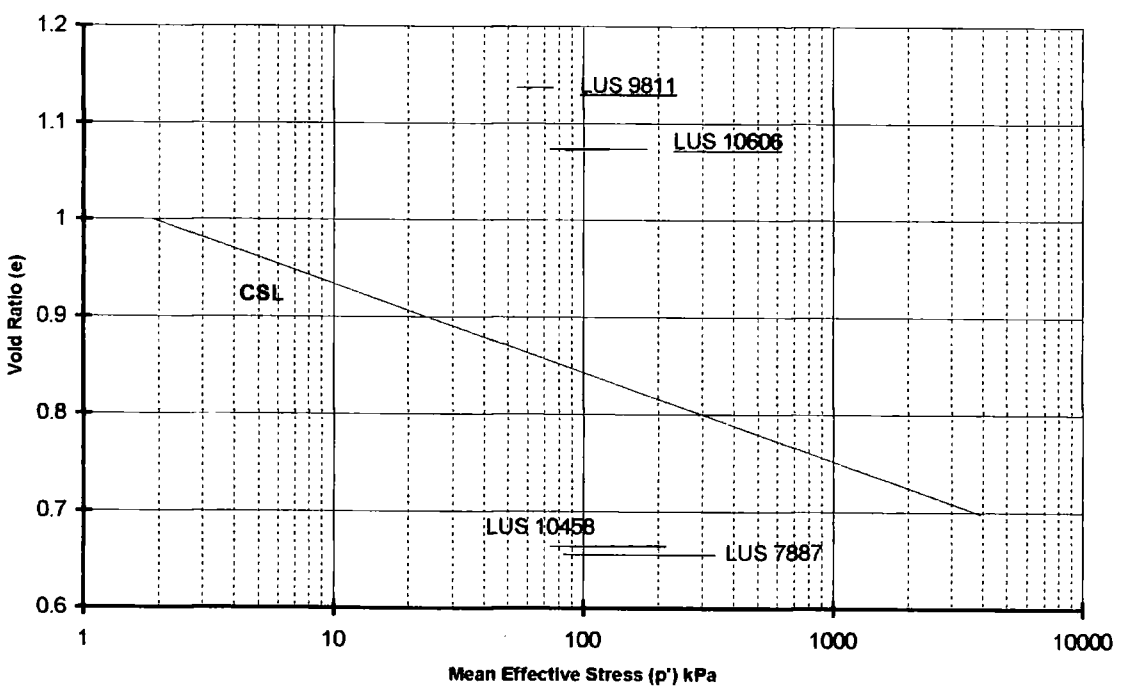

Figure 5-53 Void ratio against mean effective stress plot for BS406 tests at 75kPa confining pressure

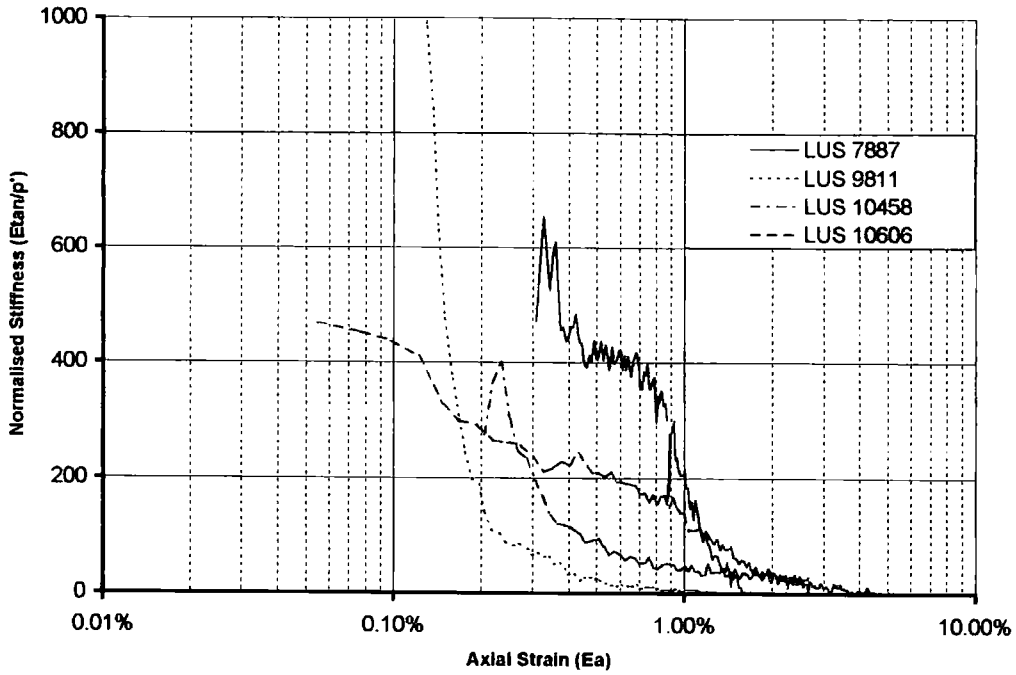

Figure 5-54 Normalised stiffness against strain for BS406 tests at 75kPa confining pressure

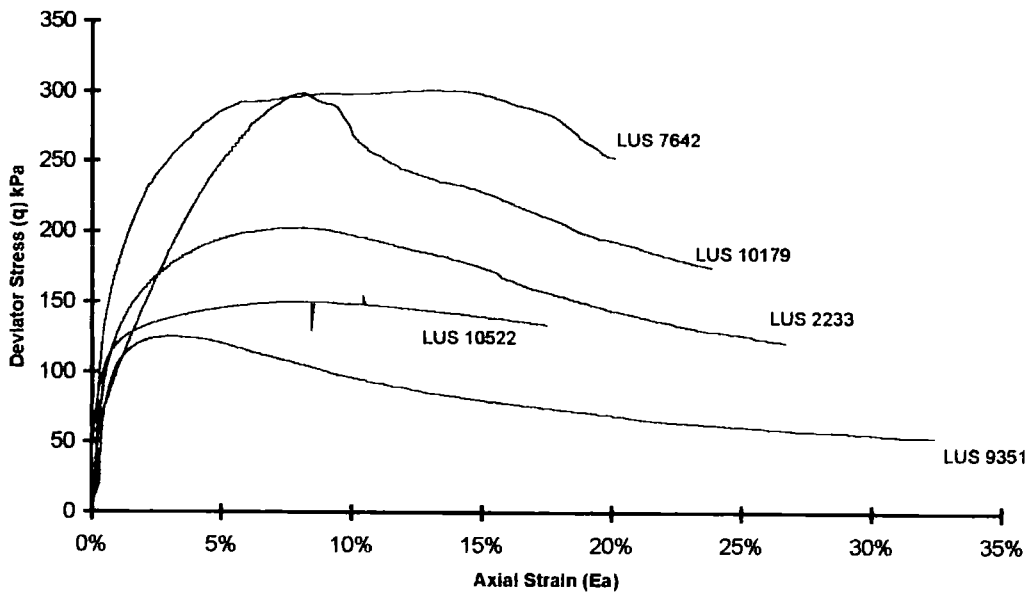

Figure 5-55 Stress against strain for BS406 tests at 125kPa confining pressure

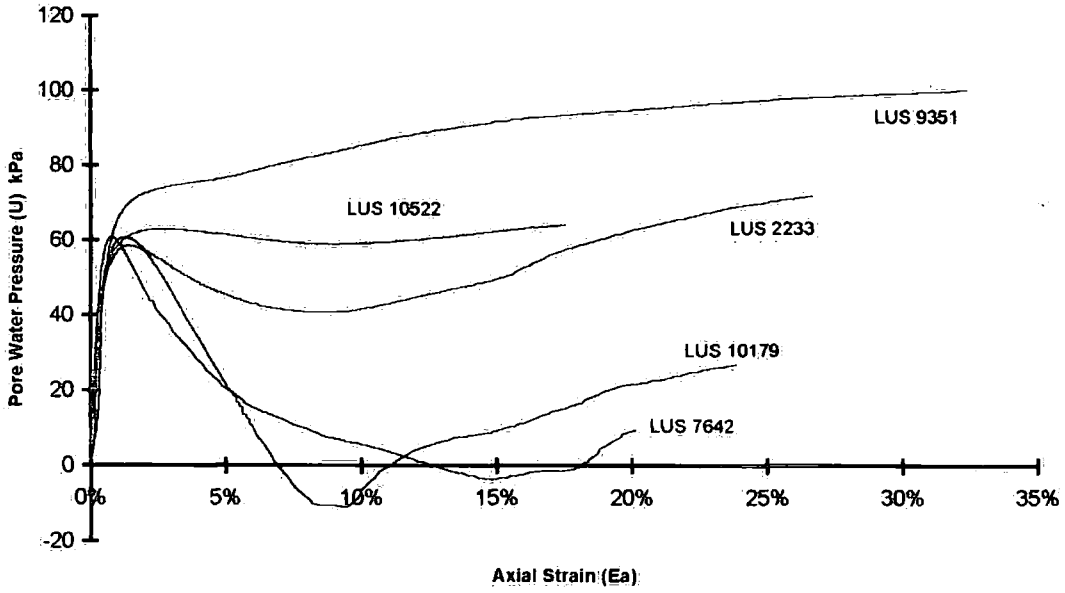

Figure 5-56 Changes in pore water pressure versus axial strain for BS406 tests at 125kPa confining pressure

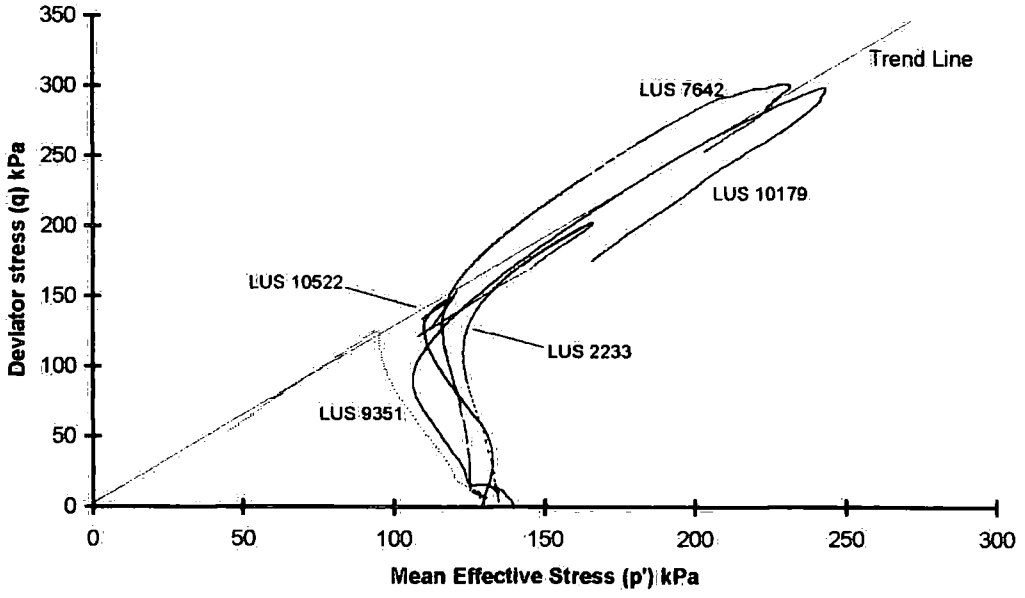

Figure 5-57 Effective stress paths for BS406 tests at 125kPa confining pressure

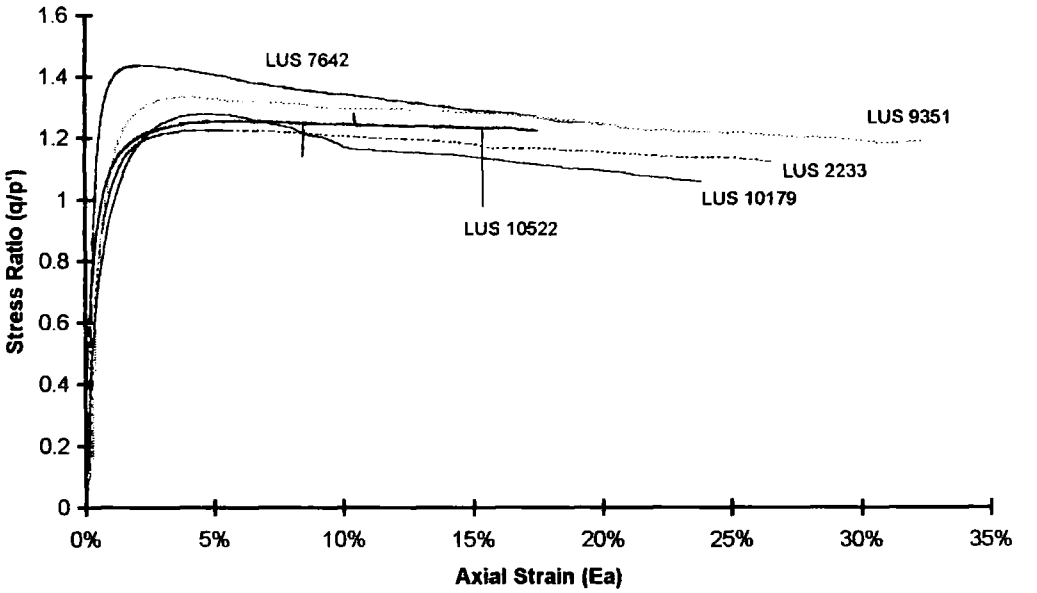

Figure 5-58 Stress ratio against strain for BS406 tests at 125kPa confining pressure

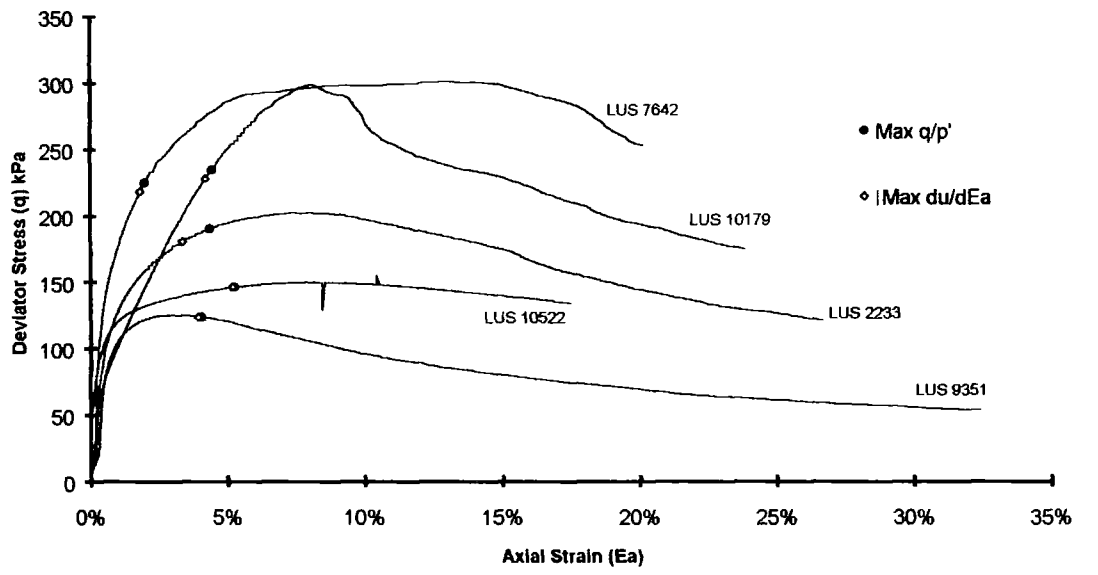

Figure 5-59 Relative position of maximum point for BS406 tests at 125kPa confining pressure plotted on stress-strain curves

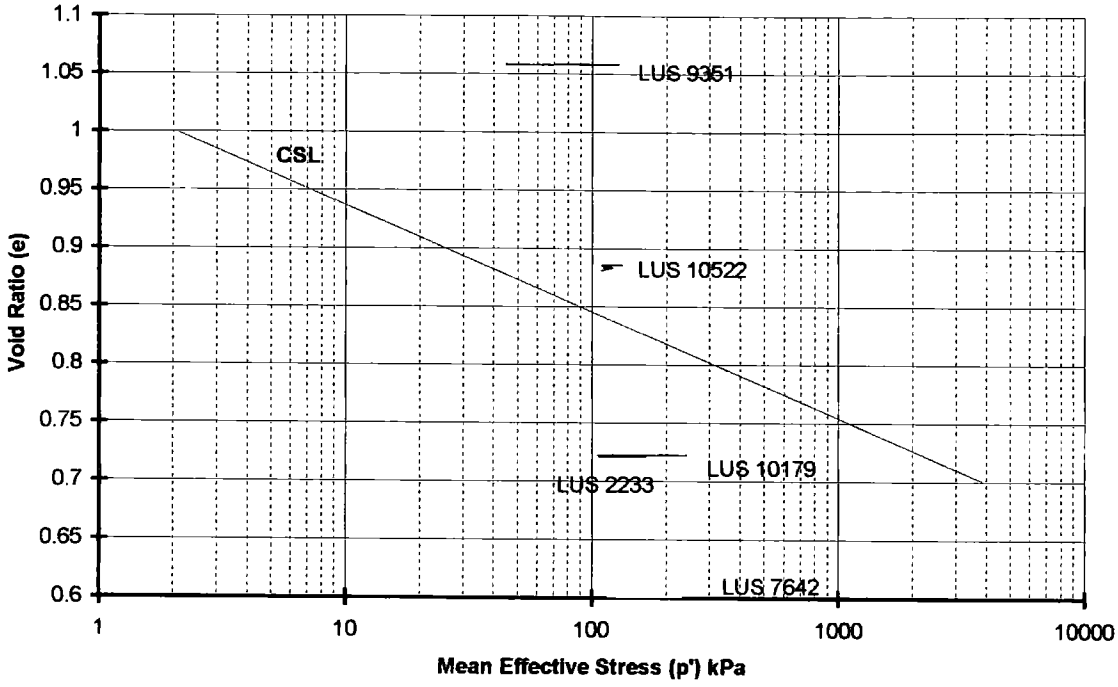

Figure 5-60 Void ratio against mean effective stress for BS406 tests at 125kPa confining pressure

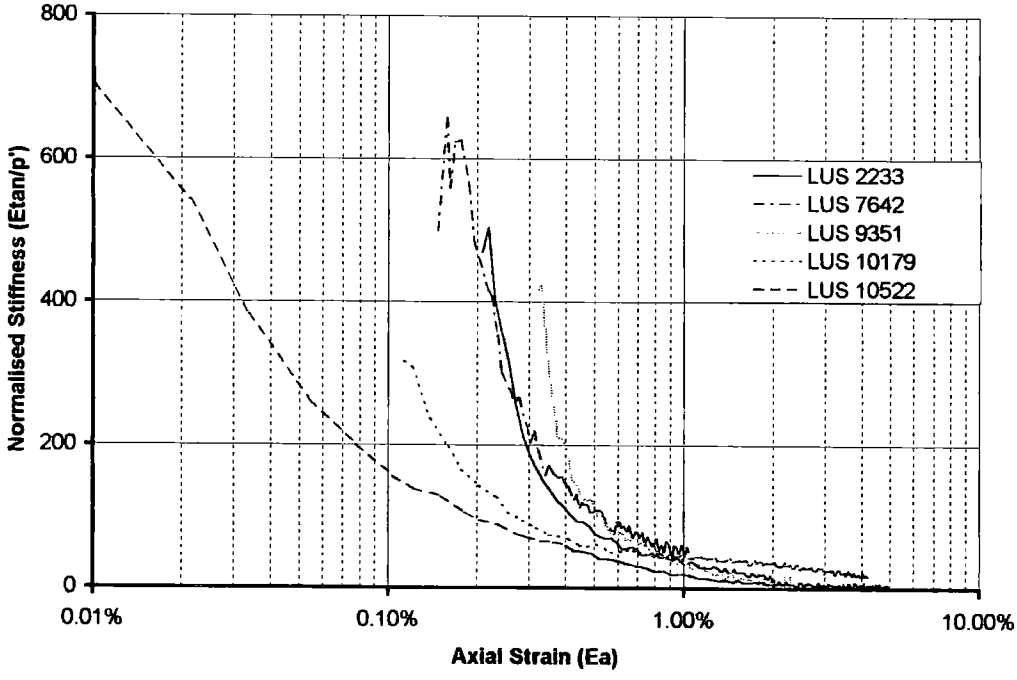

Figure 5-61 Normalised stiffness against strain for BS406 tests at 125kPa confining pressure

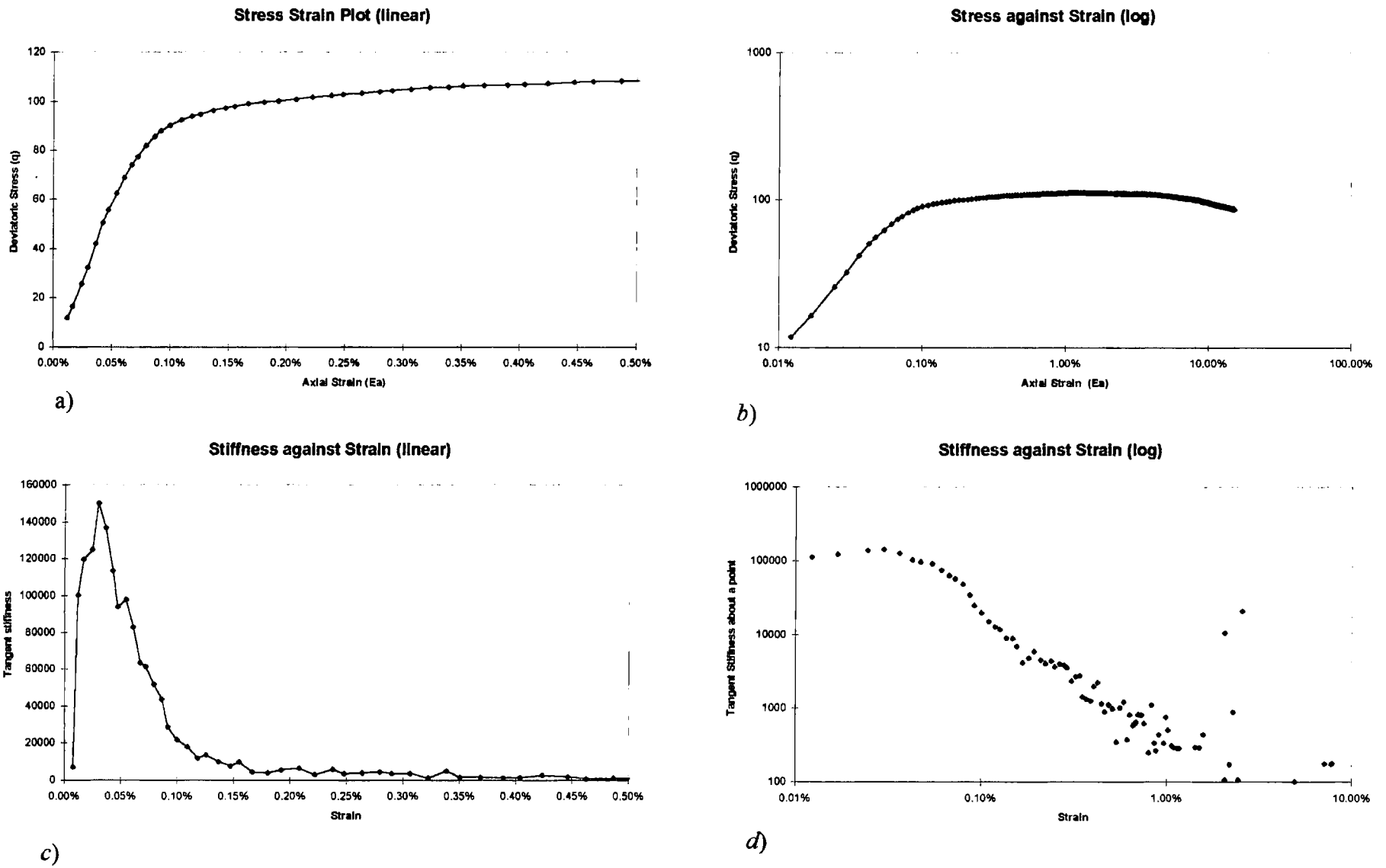

Figure 5-62 Plots of stress against strain (a) normal scales, b) log-log scales) and tangential stiffness against axial strain (c) normal scales, d) log-log scales) for LUS9811

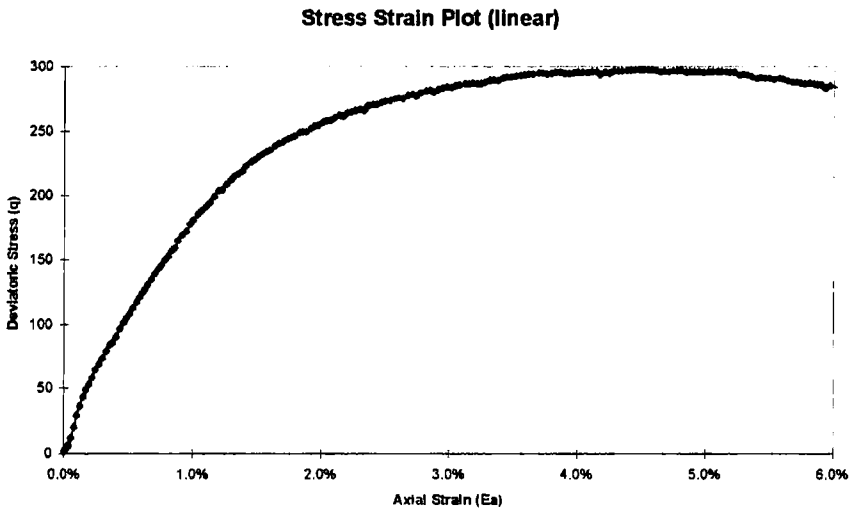

a)

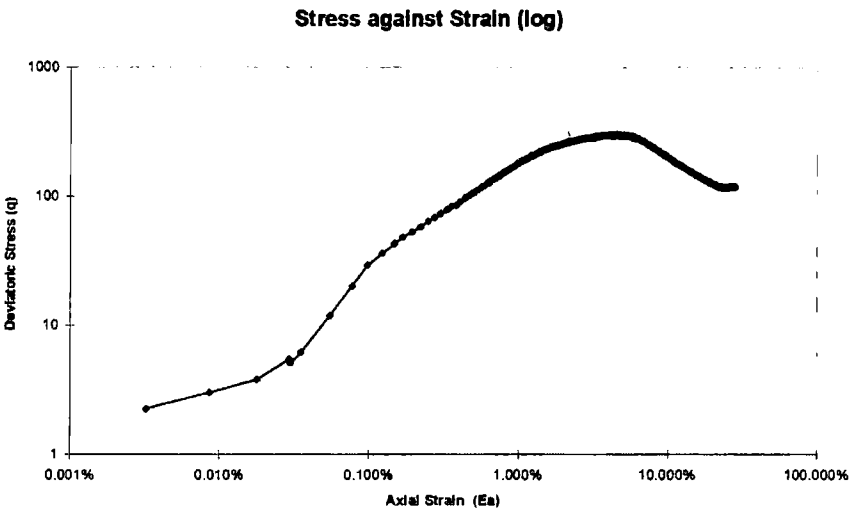

b)

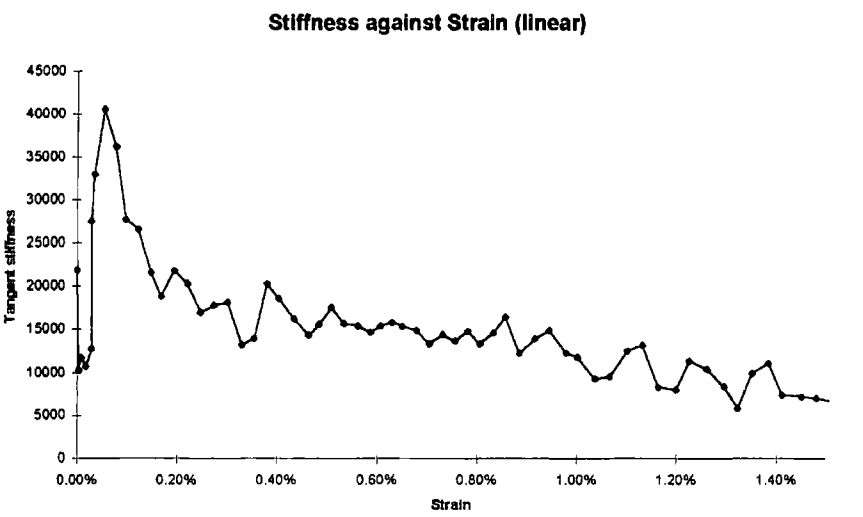

c)

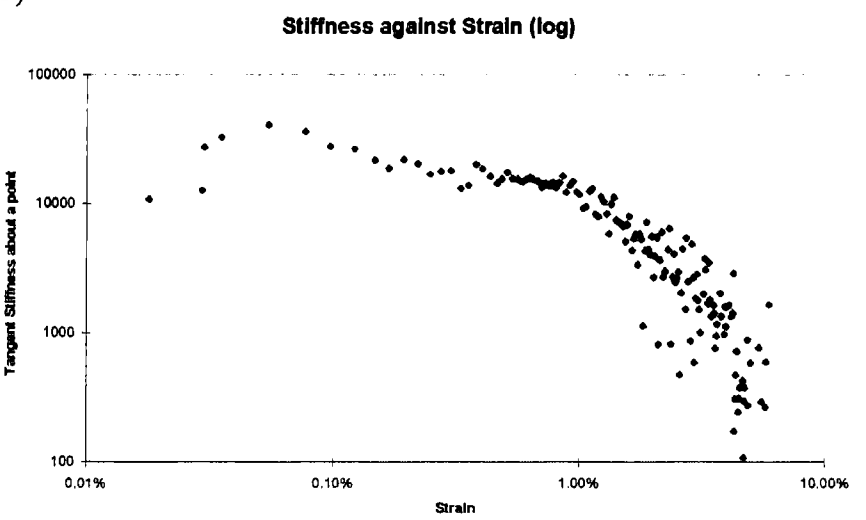

d)

Figure 5-63 Plots of stress against strain (a) normal scales, b) log-log scales) and tangential stiffness against axial strain (c) normal scales, d) log-log scales) for LUS10606

5.2.2.4 Discussion

Results of tests on the undisturbed samples showed two major influences on the sample strengths when compared to the results for remoulded samples. The remoulded samples represent the lagoon ash with all the layering effects removed, all the bonding broken down, a normalising of the particle distribution, and a standardised void ratio. Pozzolanic activity was present in some of the undisturbed specimens but the main behavioural influence is due to void ratio and the build up of negative pore water pressure giving greater strengths. The wide variations in the void ratio at different horizons in the lagoon do not allow a consistent profile with depth to be made.

The low number of undisturbed specimens displaying bonded characteristics did help to explain the change in behaviour seen to occur between 100 and 200 kPa confining pressure. The results showed that below 100 kPa the behaviour is brittle. This was best seen by the stress ratio curves (Figures 5-33, 5-41, 5-51 & 5-58), which show strong peak ratios for tests confined at 100kPa and below. At first a confining pressure of 100 kPa appeared to mark the onset of change from dilatant to compacting behaviour shown by the results of specimen from tube 10522 (Section 5.2.2.2). Any pozzolanic bonding in the specimen does not appear to play any significant role in this, although the highest pressure used on any of the undrained bonded specimens was 150kPa. Bonding was observed under drained conditions at confining pressures above 200kPa indicating that this change might not be a result of the loss of bonding.

5.2.2.4.1 Comparison of Tests on Bonded and Unbonded Specimens

A comparison was made between results from undrained tests on bonded and remoulded specimens in order to consider further the influence of bonding. As with the drained tests not all of the undisturbed specimens demonstrated evidence of a bonded structure. Distinguishing the bonded undisturbed specimen from the unbonded ones was based on their behaviour relative to the CSL and the relative position of the maximum points. The majority showed no indication of bonding.

Bonded LUS Specimen
LUS25
LUS150
LUS9811
LUS10606

Table 5-7 Specimens where bonding was identified for undrained conditions.

5.2.2.4.2 Maximum Points

For the maximum points observed in the LUS tests (section 5.2.2) the relative positions of the points appeared to be linked to the nature of the undisturbed specimen tested. The coincidence of the points was seen in some specimens indicating no bonding was present. These were usually normally consolidated or only slightly overconsolidated and formed from a small number of layers. Where the point of $(q/p')_{max}$ precedes $(du/dEa)_{max}$ the presence of pozzolanic bonding was suspected to be responsible for the yielding and production of negative pore pressures that were

observed. These two combinations fit with the predicted behaviour seen in the maximum points for drained conditions. For heavily overconsolidated specimens which developed large negative pore pressures the $(du/dEa)_{max}$ preceded that of $(q/p')_{max}$. The non-coincidence of the points indicated influences on the behaviour additional to frictional contact. The most likely influencing factor was the layering within the specimen. LUS50 demonstrated how some layers can act as slip surfaces between two more resistant layers (Plate 5-4). Bonding was suggested when the $(q/p')_{max}$ precedes $(du/dEa)_{max}$ and may occur here. In these tests, the pozzolanic bonding was broken down at low axial strains. This is not the case for all the heavily consolidated specimen where $(q/p')_{max}$ occurs at strains of 2% and over for internal stain devices and about 5% for external devices.

In the drained tests the undisturbed specimens, although stiffer than the remoulded specimens, proved to have little additional strength. For the undrained conditions the undisturbed specimens demonstrated a considerable strength increase over the remoulded boundary for small void ratios. This was due to the build up of pore water pressures. The bonded specimens, with the exception of LUS10606, showed only a small increase above the remoulded boundary and where present, appeared to vary in strength. For the most part the additional strength from bonding was small, and was much smaller than those attained in the heavily overconsolidated specimen. For these denser specimens, the development of large negative pore water pressures may be masking the influences of the weaker bonding.

5.2.2.4.3 Bond Yielding

By combining yield points of all the bonded samples identified from the undisturbed specimens (Table 5-7) it was possible to outline loci for both the first and second yields in stress space for undrained conditions (Figure 5-64). The first yield locus occurred across a low stress level, changing very little. Second yield plotted roughly parallel to the first yield locus, only crossing the remoulded boundary at very low stresses. With the exception of the potential second yield for LUS10606 the rest of the other yields observed demonstrate a pattern similar to those of the first and second loci. Following the approach used in the drained specimen, zone 1 is probably up to about 25 kPa where the second yield occurs near to the boundary. As test LUS150 represents the highest pressure for the undrained bonded specimens tested there is no way of estimating the location of the transition from zone 2 to zone 3.

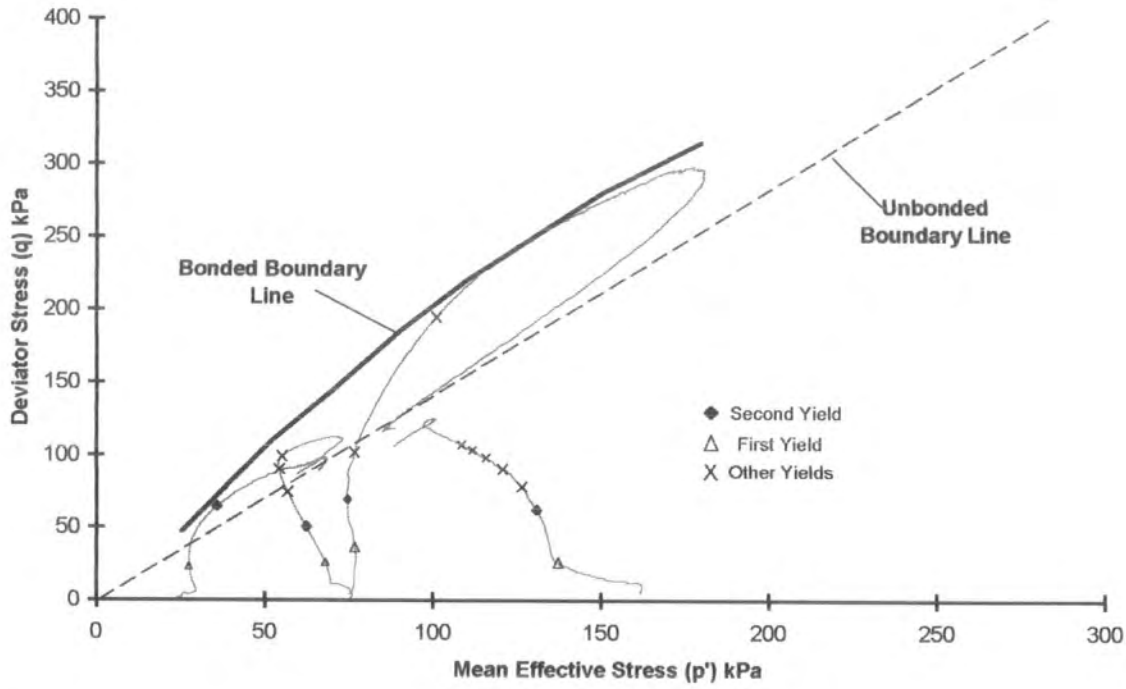

Figure 5-64 Yields plotted in stress space for undrained tests on lagoon fly ash

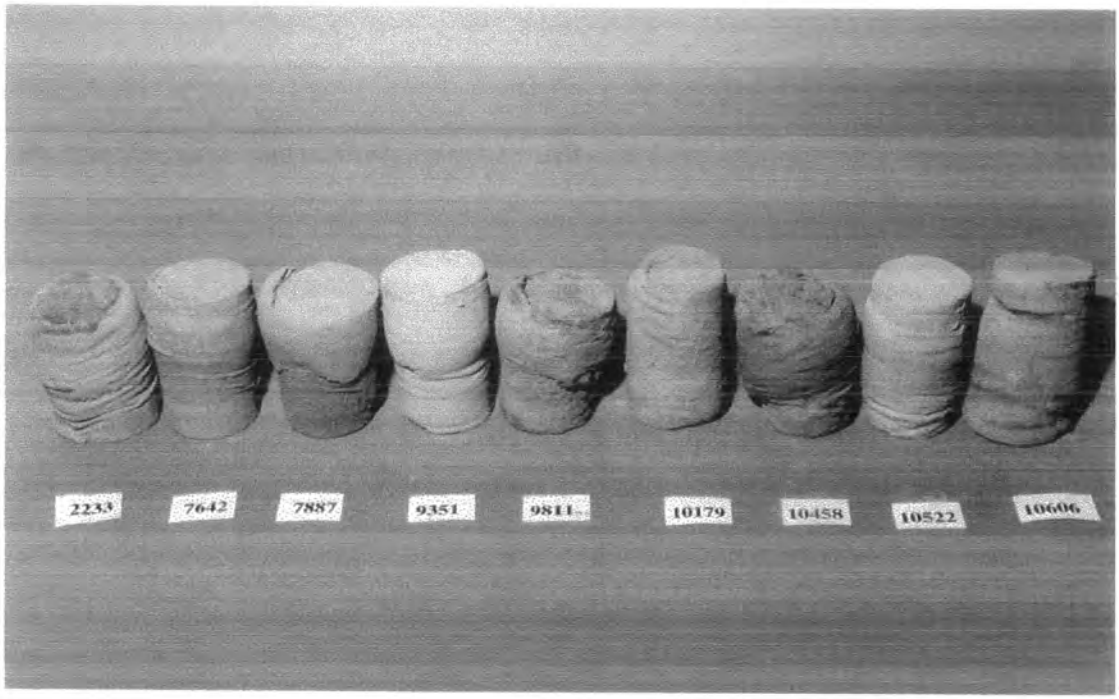

Plate 5-5 Specimens from BH406 after undergoing triaxial compression

5.3 Consolidation

Information for the consolidation characteristics of the lagoon ash has been obtained from four oedometer tests on remoulded and undisturbed samples. The extent of these tests was confined by the weight available for loading.

Four oedometer tests were performed on fly ash from the lagoon. Two of the tests were performed on undisturbed samples cut from tube 9541 (BS405; depth 3.14 - 4.14 m), whilst the other two tests used specimens formed from remoulded material of tube 7642 (BS406; depth 2.03 -3.03 m). The undisturbed specimens were cut from competent sections of the Delft tube containing no layers. They were initially trimmed to the approximate dimensions of the oedometer ring. The ring was then eased down over the sample. Trimmings were removed and used for establishing moisture content and specific gravity. The remoulded specimens were formed using two different methods, described fully in Section 4.2.6.3, to obtain specimens with different void ratios. The loose sample was formed from dry fly ash poured into the ring. It was designed to produce a curve for the normal consolidation of the sample, which could then be used to compare the other tests against. The layered remoulded specimen was designed to have a void ratio closer to that of the undisturbed samples.

5.3.1 Remoulded Samples

The results for the loose remoulded sample showed that its consolidation follows an almost linear path in the plot of void ratio against log stress (Figure 5-65). As there had been no previous stress history, the near linear portion represents a close approximation to normal consolidation behaviour of the fly ash. This line may be considered to represent the Normal Consolidation Line (NCL) for the material. The path of the layered remoulded sample shows only slight consolidation initially. The consolidation increased as it approaches the curve of the loose sample. The curve for the compacted layered remoulded specimen indicated a convergence, at stresses higher than those tested, with the curve of the loose remoulded specimen.

5.3.2 Undisturbed samples

The two undisturbed samples in Figure 5-66 have similar initial void ratios, but showed different reactions to the axial stress. LS1 showed little volume change with early loading. However as the load increased above 100 kPa LS1 began to show more axial strain. The curves appeared to converge with the line indicated from the remoulded samples. LS2 also had a little more volume change during the early loading stages, but did not show the same increase in axial strain seen in LS1 above 100 kPa. The curve for LS2 passed over the NCL indicated from the loose sample. This indicated the presence of bonding between the particles of the specimen.

5.3.3 Discussion

The results of the two remoulded specimen seem to outline the normal consolidation for the lagoon ash. Although the two lines do not coincide, there is a significant convergence of the LD plot to the loose sample plot.

There is not a consistent picture for the undisturbed specimens. LS1 shows a convergence to the extrapolation of the normal consolidation line. Its initial behaviour is stiff, but at higher vertical stresses it deforms more. There is no indication of any additional influence to the structure of the lagoon fly ash. LS2 does not show the same pattern of deformation as LS1. It has an overall stiffer response to loading and shows little axial strain. The plot for LS2 passes outside the normal consolidation line indicated by the other tests into the area of the e-log p' space where normally consolidated samples cannot exist. The apparent pre-consolidation of the sample may be due to the pozzolanic activity of the fly ash causing bonding between particles. This gives a quasi- pre consolidation pressure as described by Vargas (1953) in his study of weathered Granites. The different behaviour of the two undisturbed samples, which originate from the same Delft tube, indicates that bonding is not consistent throughout the lagoon and may be confined to localised areas.

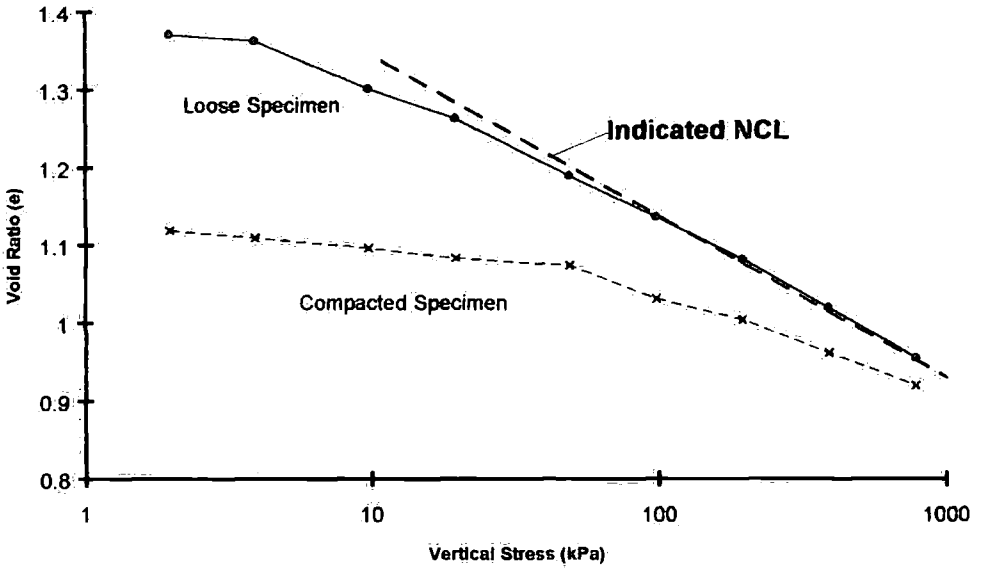

Figure 5-65 Consolidation curves for specimens of remoulded lagoon fly ash

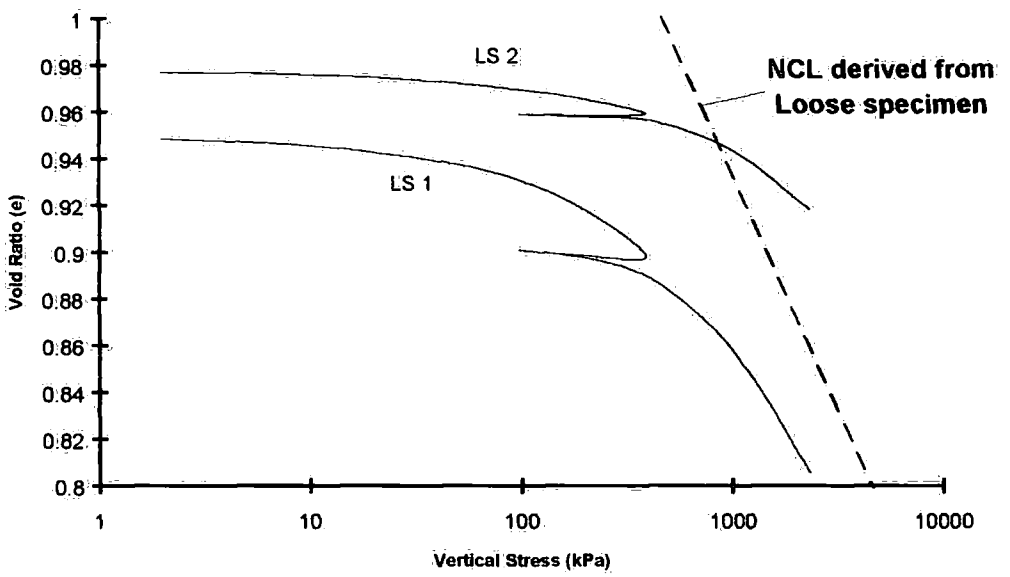

Figure 5-66 Consolidation curves for undisturbed lagoon fly ash specimens

5.4 Discussion of the behaviour of lagoon fly ash in triaxial tests

5.4.1 A comparison of Drained and Undrained results

The results of the drained and undrained tests showed different characteristics. These were most noticeable in the failure boundaries and the yield loci. Comparison of the boundary lines for the tests in p' - q stress space in Figure 5-67 shows the boundary line for the undrained tests to be steeper than that of the drained tests. This was more noticeable at higher pressures and can be characterised by the stress ratio plot of all the remoulded specimens. The difference was also characterised by the friction angles calculated. These can be compared to friction angles taken from the literature on fly ash and similar materials in Table 5-8. The stress ratio plot (Figure 5-68) showed that whilst the drained tests were close to an ultimate stress ratio of 1.1 the undrained tests were more widely spread between 1.1 and 1.4. The gradient of the line in p'-q stress space is normally defined as M (where q'=Mp' Atkinson (1987)) and is considered to represent a soil constant. These results would indicate that there is not a single value of M for the lagoon fly ash, but rather a range of 1.1 - 1.4. This range seen in the remoulded specimens was also seen in the undisturbed specimens (Figure 5-69). The range of stress ratios demonstrate the variability of the fly ash in the lagoon. This had already been identified from the index tests, notably the specific gravities and particle distributions. Therefore it is likely that the apparent difference in characteristics

between the drained and undrained boundaries was probably a product of the variability of the lagoon ash, but further tests would required to confirm this.

TEST	Friction Angle
LDD	28
LUD	34.6
Leonard & Bailey (1982) Drained	38
Leonard & Bailey (1982) Undrained	43
Toth	35
Gray & Lin (1972)	38 – 43
Goh & Tay (1993) – Municipal Waste	45
O'Rouke (1989) – Volcanic Soil	36-40

Table 5-8 Friction angles from the fly ash literature

5.4.2 Soil constants for fly ash

If the value of M was variable, there may be variations in the other critical soil parameters. In the case of the critical state line defined from the remoulded specimens the drained and undrained tests demonstrated a near common CSL (Figure 5-70). However the definition of this line is open to some debate based upon the results from the consolidation tests. It had been noted by Atkinson & Bransby (1978), Atkinson (1994) and Wood (1991) that the normal consolidation line and critical state lines were usually found to be parallel. Also the line of one dimensional consolidation tests was parallel to these lines and to be found at some point between the two. With this in mind it was possible to compare the one-dimensional consolidation line to the critical state lines from triaxial testing as shown in Figure 5-71. These plots show that the

gradients of the lines are far from parallel, suggesting that one or other is in error. As the one-dimensional consolidation line was based essentially on only one test it might reasonably be assumed that this was the line in error, although the other one-dimensional tests appear to agree with it. However the critical state lines identified in the triaxial tests were interpreted from the paths of the tests in void ratio-stress space with no firm evidence as to the slope. So if it is assumed that the one-dimensional line does indeed indicate a better representation of the slope for the CSL should this also relate to the data from the triaxial drained and undrained tests?

The LDD results (Figure 5-72) indicate that the new CSL could reasonably be applied to the data although its exact position may lie within a band between LDD25 and LDD100. Tests LDD25 show a trend roughly parallel to the new CSL, as do LDD100 and LDD400. The new CSL applied to the LDS data (Figure 5-73) gives a slightly better fit with respect to LDS50, LDS100 and LDS 700. This plot indicates that the position of the new CSL is towards the right of the band identified by the LDD tests. The new CSL however does not fit well with all the LUD data (Figure 5-74), specifically in tests LUD50 and LUD200. It is worth noting that these two tests were reasonably significant in defining the previous CSL with the shallower gradient and might be expected to be the source of error. Despite a lack of agreement with the LUD tests, the new CSL fits the LUS data for tests '25-800' (Figure 5-75a), LUS tests '100-200' (Figure 5-75b) and LUS 'Depth Profile' tests (Figure 5-75c). They also appear to have more relevance to these tests where there is a wider spread of void ratios, as their plots now finish closer to the CSL.

As demonstrated by the consolidation information the data from the triaxial tests alone were insufficient to define the critical state line. Although the triaxial data indicated a reasonable credible CSL with a good degree of agreement between drained and undrained test, it was open to interpretation. The consolidation tests helped to resolve some of the uncertainty by identification of the slope of the normal consolidation curve. A review of the triaxial data together with this new information led to another more credible CSL for the lagoon fly ash, based upon Equ 5-1, see Table 5-9.

Parameter	Value
Γ	1.26
λ	0.157
M	1.0 - 1.4

Table 5-9 Soil Constant parameters for Brotherton Ings lagoon fly ash

5.4.3 Pozzolanic Bonding in the fly ash

5.4.3.1 Identification of bonding

A major objective of the testing program was to study the influence of pozzolanic bonding on the stiffness and strength. The specific characteristics of the pozzolanic bonding however were over-shadowed by the question of whether bonding was present in the lagoon specimens at all. The results presented in this chapter would suggest that the pozzolanic bonding was more often not present. Only half of the drained undisturbed specimens and just four of the eighteen undrained specimens

demonstrated behaviour that may be attributed to pozzolanic bonding. Under undrained conditions however there may be a possibility that large negative pore pressures may be masking the influence of the bonding or by destroying it at low confining pressures.

The infrequency of bonded specimens suggests that bonding was probably very weak and not widely spread throughout the fly ash pile in the lagoon. There was further evidence of the sporadic distribution of the pozzolanic activity in the depth profile tests using specimens from BS406. These tests showed no consistent change with depth that may have indicated that curing time or conditions were a factor in its distribution (Figure 5-47). This contradicts the suggestion by Indraratna et al (1991) that considerable cementation can be expected at the bottom of fly ash lagoons due to natural compaction of moist fly ash.

The reason why so few of the undisturbed specimens appeared to be bonded may be attributed partly to the methods used to identify bonding characteristics. If the tests did not meet these criteria then the specimens were considered to be unbonded. The use of maximum points and of the behaviour of bonded specimens relative to the CSL gave consistent indications. However, the specimens found to be bonded tended to plot on the wet side of the CSL indicating their relatively high void ratios. Those with lower void ratios plotting on the dry side of critical may have had their bonding characteristics masked by those of overconsolidation. In the use of the maximum points some of the undrained specimens demonstrated the reverse relationship where

the maximum change in pore water pressure occurred prior to the maximum stress ratio (Figure 5-34). This would seem to indicate that there were additional influences acting on the soil matrix. This is another area, which requires additional research to establish the full mechanics of the behaviour of the ash.

5.4.3.2 Layering

The pozzolanic activity observed in the undisturbed specimen seemed to indicate a layered nature to the bonding. In the four specimens taken from Delft tube 10522, only LUS150 appeared to be bonded. All four specimens came from within a depth range of 1m, this time from a depth of 8-9m in the lagoon. The localised nature of the pozzolanic bonding was seen again in the oedometer tests on two undisturbed specimen (Figure 5-66). The behaviour of LS1 was confined by the same limiting characteristics affecting the remoulded specimens whilst LS2 did show signs of bonding and was able to exceed these limiting factors. The difference between the two specimens was surprising as they originated from the same tube, having been sampled at a depth of 3-4m.

The layered nature of the bonding within the fly ash was highlighted well by the large grains observed in the breakdown of LUS10606 (Figure 3-10). The largest grains were composed of aggregations of many much smaller grains and were platey and needle-like in shape, which suggests strongly that the bonding was localised to within specific layers. These layers were probably sandwiched between unbonded layers,

which mask their influence on the specimen's behaviour, indicating that bonding was very localised.

This layering of the structure fits well with the way the lagoons were filled up in periodic layers, and also the laminations observed in many of the specimens. The results indicate the localisation of bonding suggesting that the majority of curing occurred soon after deposition, when there has been little chance for the reactants to leach away.

5.4.3.3 Yielding

The small number of bonded undisturbed specimens identified made characterisation of the pozzolanic activity difficult, but there were enough specimens to establish yielding patterns. Establishment of the various yield points from the data involved a number of different methods, which could be cross-referenced for validity. No one method proved itself to be any better than the others, although the use of tangential stiffness was more useful when identifying small changes, specifically for the initial yields. The use of log-log plots was suggested by Vaughan (1985) and Malandraki & Toll (1994). Whilst these plots showed some potential when analysing small strains, some characteristics of the log- log scales introduced some ambiguity. Previous bonded soil studies (Vaughan *et al*, 1988, Macarini, 1988 and Bressani, 1990) had identified two significant stages in yielding. The second of these usually occurred at the point where the plot was curving most, which made its determination very difficult. The results of the fly ash differ from the standard 2-yield model, since a number of yield points were

identified in the majority of specimens. This raised the question as to whether there were characteristics which might give a clearer definition of the breakdown of bonded soils. However it should remembered that there is no evidence of a consistent bonding framework within the undisturbed fly ash and that these additional yields may be an indication of the internal structure of the specimens themselves. It is far more likely that the multiple yields observed in these specimens were a function of the complex interaction of different layers.

The layered nature of the bonding suggested by other tests was also suggested by the yield loci identified for initial and secondary yields. The yields for the undrained tests are significantly smaller than those identified in the drained tests (Figure 5-76). However, both the yield loci obtained from both testing conditions were flat and roughly parallel to the stress axis. Leroueil & Vaughan (1990) remarked that an isotropic structure generally shows a yield curve centred around the normal consolidation K_o axis, whilst those with an anisotropic fabric tend to centre on the isotropic stress axis as shown in Figure 5-77. The yield loci for the lagoon fly ash indicate that the material has a strong anisotropic fabric, which agrees well with the observed laminations seen in the photographs of the specimens, especially LUS25 in Plate 5-4. As any bonding appears to be discrete within certain layers, the multiple yields may be associated with yielding of different layers at different points. The 'first yield' probably represents the onset of bond breakdown as suggested by Vaughan (1988). The 'second yield' is not necessarily the second yield in its normal definition, but may be the most significant yield point after the initial yield. These hypotheses are

highly speculative. However the identification of several yields appears to indicate a series of laminations parallel to the first yield.

5.4.3.4 Comparison to other fly ash research

Unfortunately there were insufficient specimens to allow determination of the strength characteristics of the pozzolanic activity. The drained tests suggest that there is little strength advantage in the undisturbed fly ash over the remoulded material. However LUS10606 shows that the pozzolanic reaction does have the potential for much higher strengths. Unfortunately this was the only specimen observed which demonstrated any significant strength gain from the reaction. The remaining strength increases were very slight when compared to results from the literature. Indraratna *et al* (1991) performed some drained and undrained triaxial tests on fly ash from disposal dumps (Figure 5-78) which showed strengths that were comparable with those seen in the corresponding stress-strain plots (Figures 5-1, 5-6, 5-21, & 5-30). Whilst stress paths from undrained tests on fly ash shown in Figure 5-79 are compared to the LUD boundary. The 100 kPa test agrees with the LUD boundary whilst the 200 kPa test shows greater strength.

Unfortunately there is no specific chemical data for each specimen tested. Such data would have allowed for comparisons to be made between the strengths of different specimen. It would also have helped to identify those specimens that had the potential to have pozzolanic bonding. The evidence form the limited chemical compostion data

5.4.1 Summary

The pozzolanic activity seen in previous studies on fly ash is present to a limited degree in some of the lagoon fly ash samples taken from the Brotherton Ings site. The behavioural characteristics seen in the lagoon fly ash are consistent with those seen in other structured soils. It was possible to identify a CSL and boundary conditions for the remoulded material. Against this the bonded specimens show an increased stiffness and some increased strength. It was even been possible to identify yield loci for the various testing conditions, and a suggestion for the transition between zones. However the bonding is relatively weak, and does not have a major influence on strength. Small strain was seen to be detrimental to the strength of a bonded specimen. The internal strain gauges employed were helpful in detecting this small strain activity. Where bonding occurred the specimen's behaviour was not consistent with its void ratio relative to the defined CSL.

Bonding was not consistent in the lagoon pile, and the formation process of the ash in the lagoon was more typical of a transported sediment than a residual soil. The research by Maccarini (1987) demonstrated that the stress history is not as important to bonded soils as it is to unbonded soils. The results of the depth profiles appear to demonstrate the same feature. The storage time of the tubes may be equated to the exposure of the excavation, and the release of vertical stresses. This would suggest that the pozzolanic activity has the potential to adjust to changing stress conditions. This was not expected especially as the reaction is not reversible and the reactants

cannot be reformed once used. However further research would be required to confirm this.

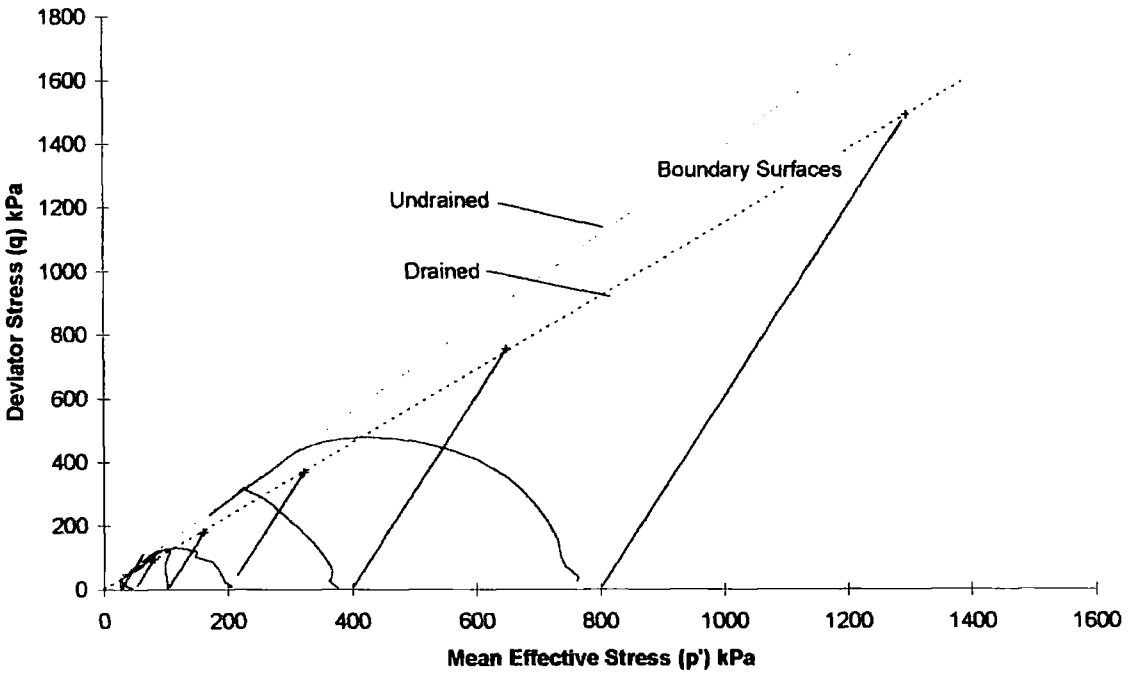

Figure 5-67 Stress paths and boundaries for drained and undrained tests on remoulded lagoon fly ash

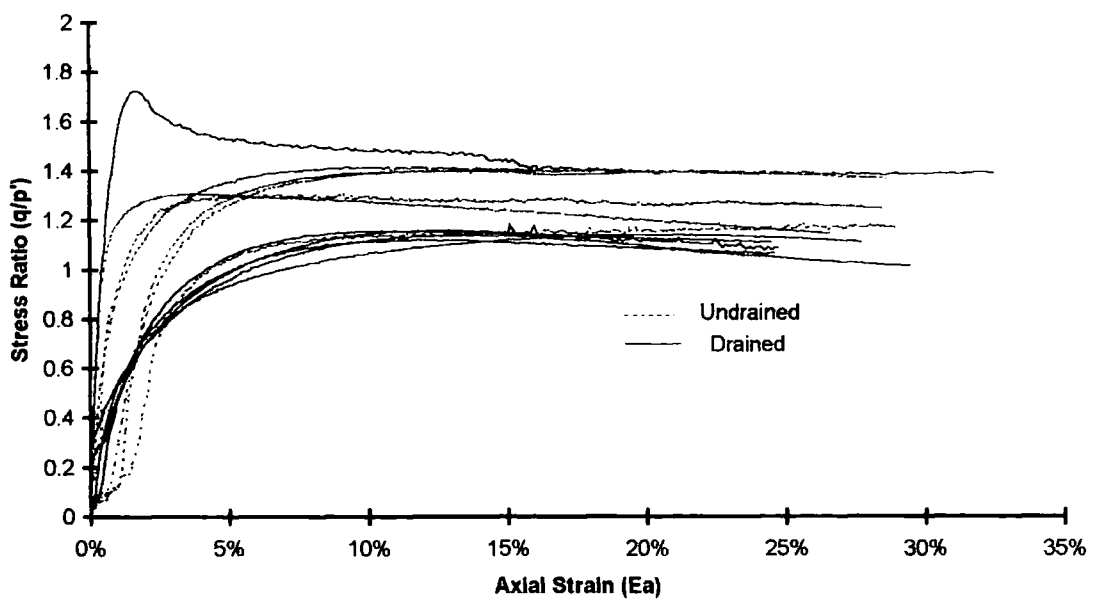

Figure 5-68 Stress ratio against strain plots for all remoulded lagoon fly ash specimen.

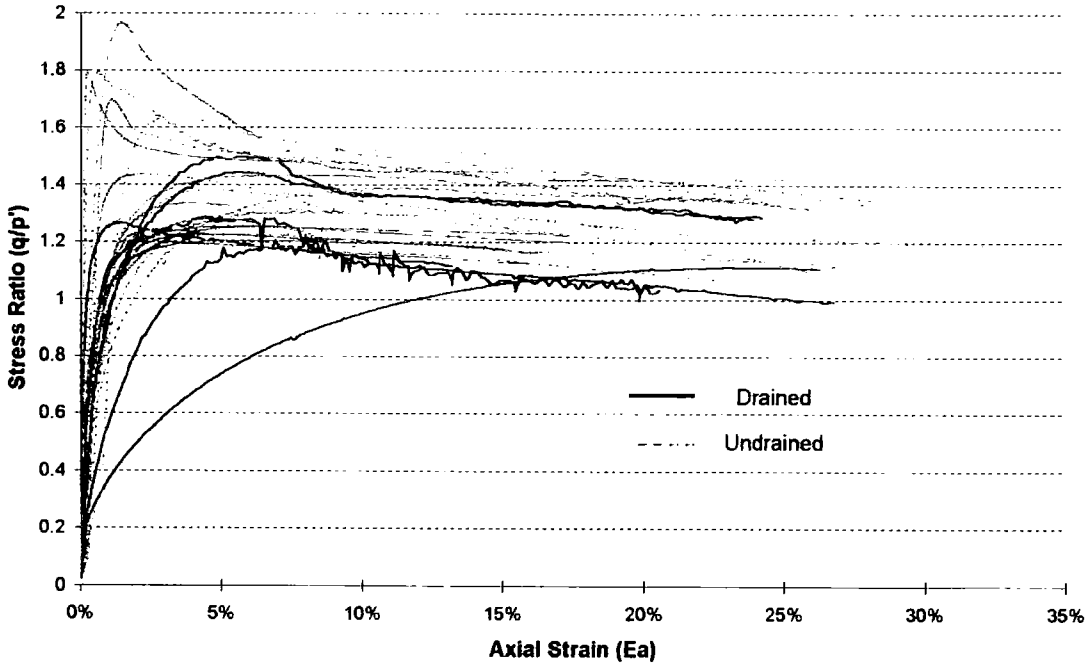

Figure 5-69 Stress ratio against strain plots for all undisturbed lagoon fly ash specimen

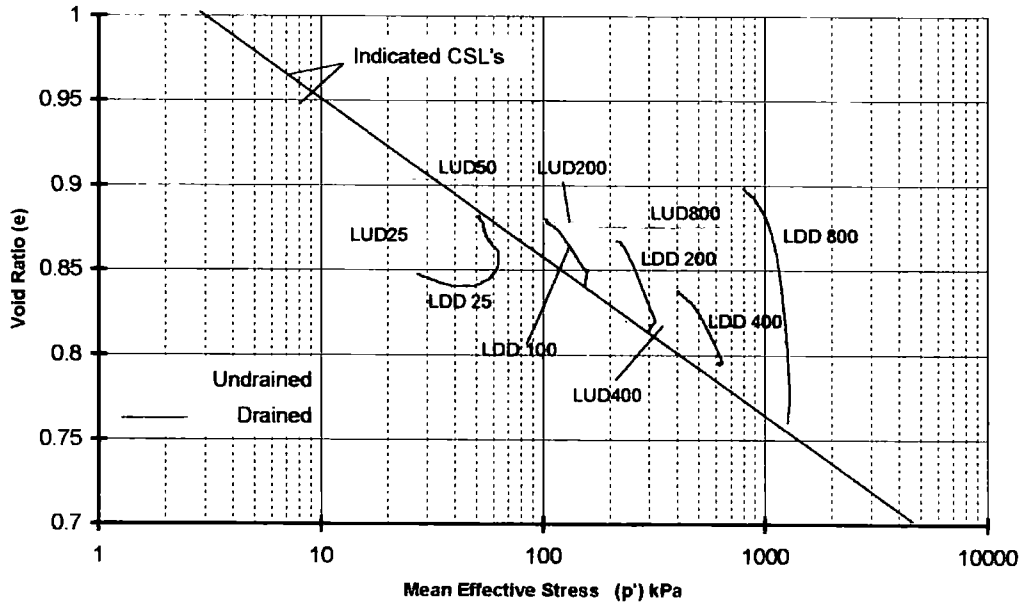

Figure 5-70 Paths of remoulded lagoon fly ash in void ratio - mean effective stress space

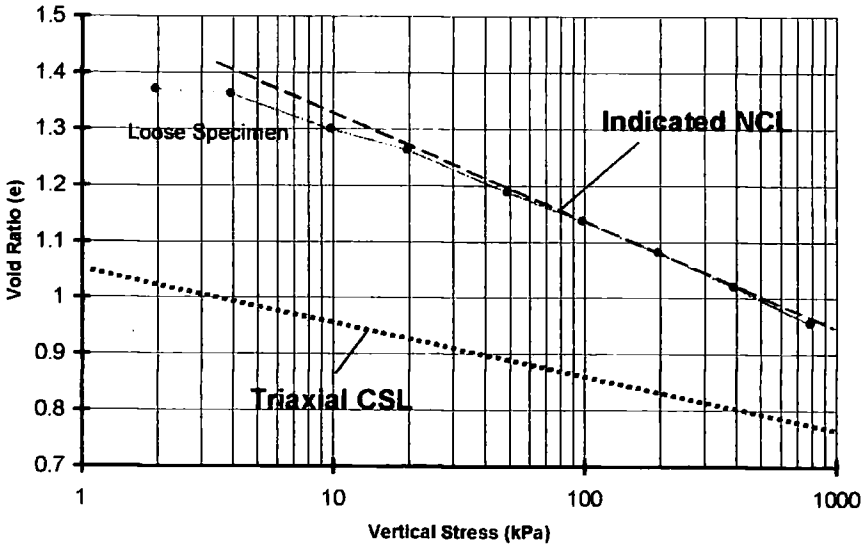

Figure 5-71 Comparison of the inferred critical state line(triaxial) and one-dimensional consolidation line

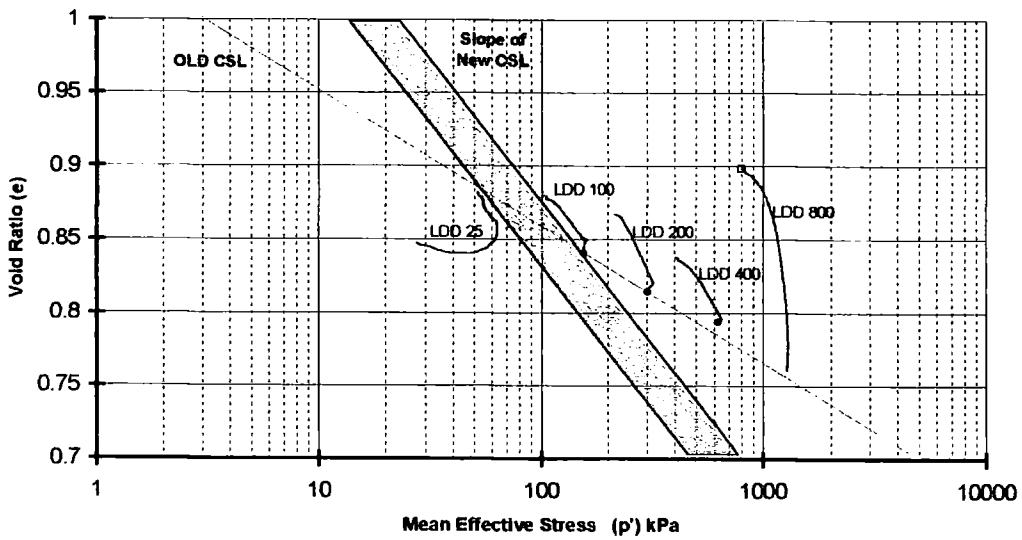

Figure 5-72 Comparison of new CSL to LDD tests

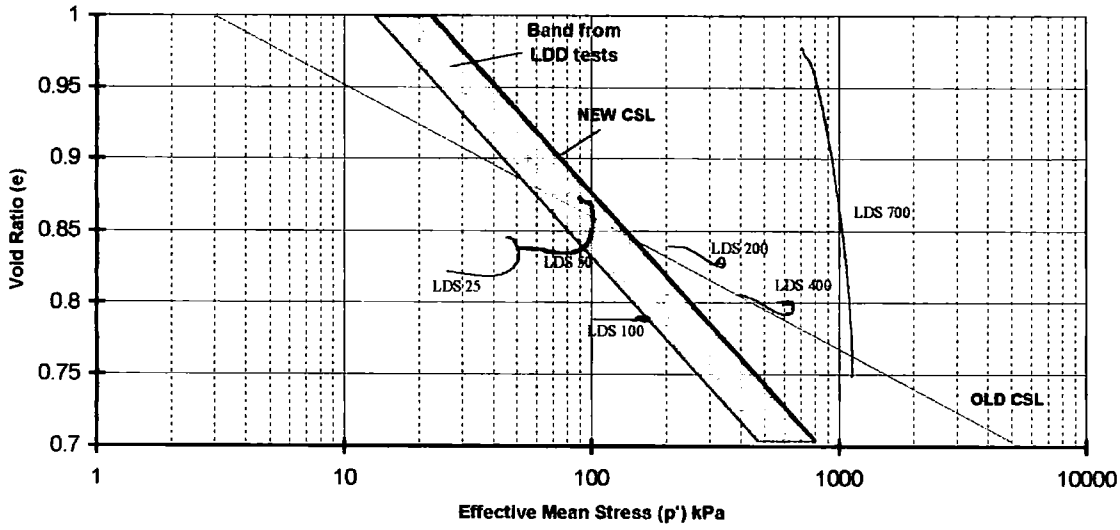

Figure 5-73 Comparison of new CSL to LDS tests

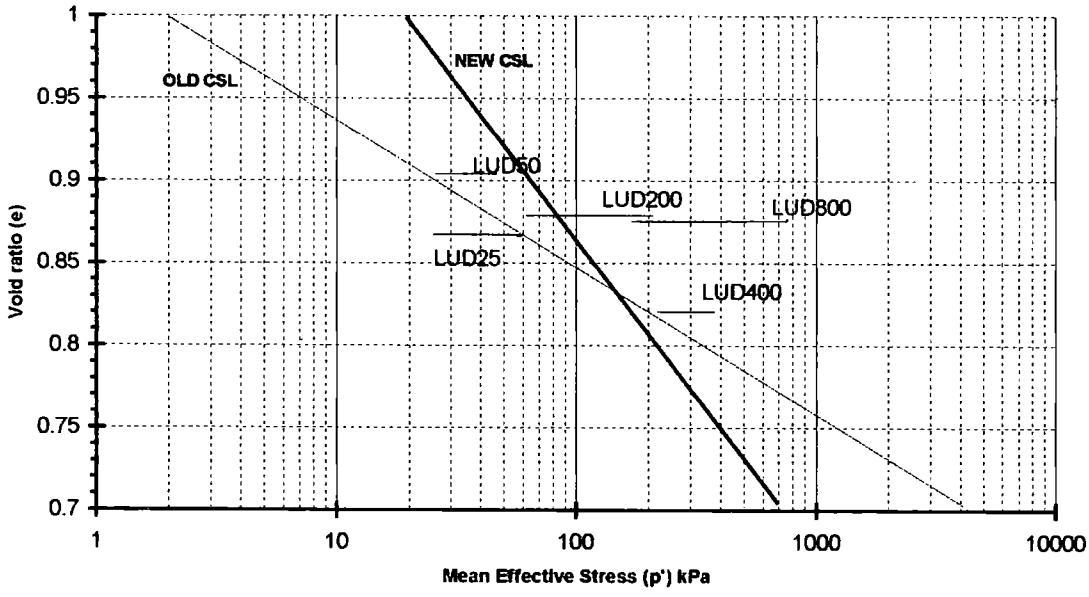

Figure 5-74 Comparison of new CSL to LUD tests

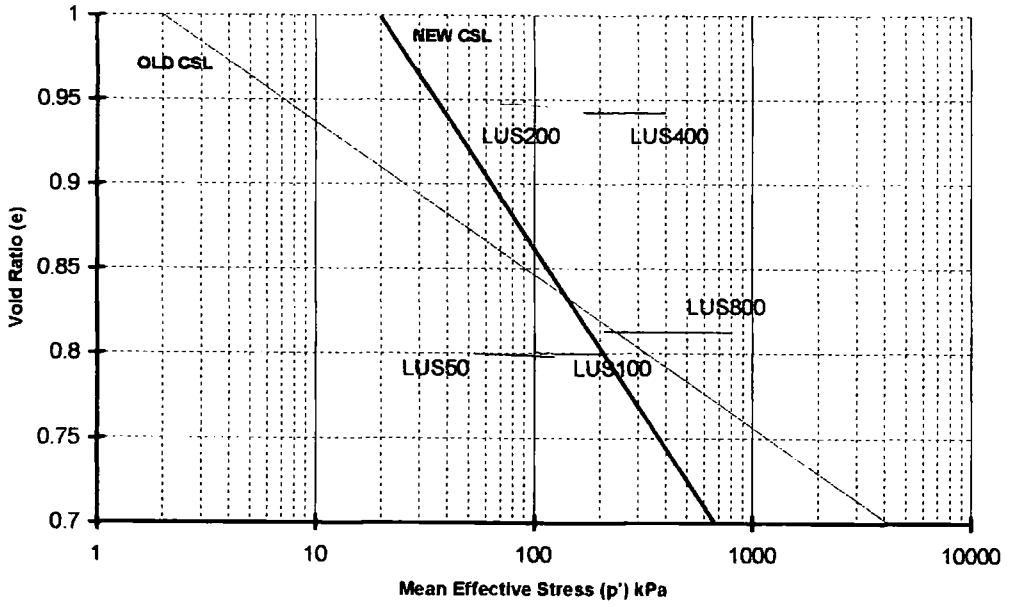

Figure 5-75a Comparison of new CSL to LUS tests '25-800'

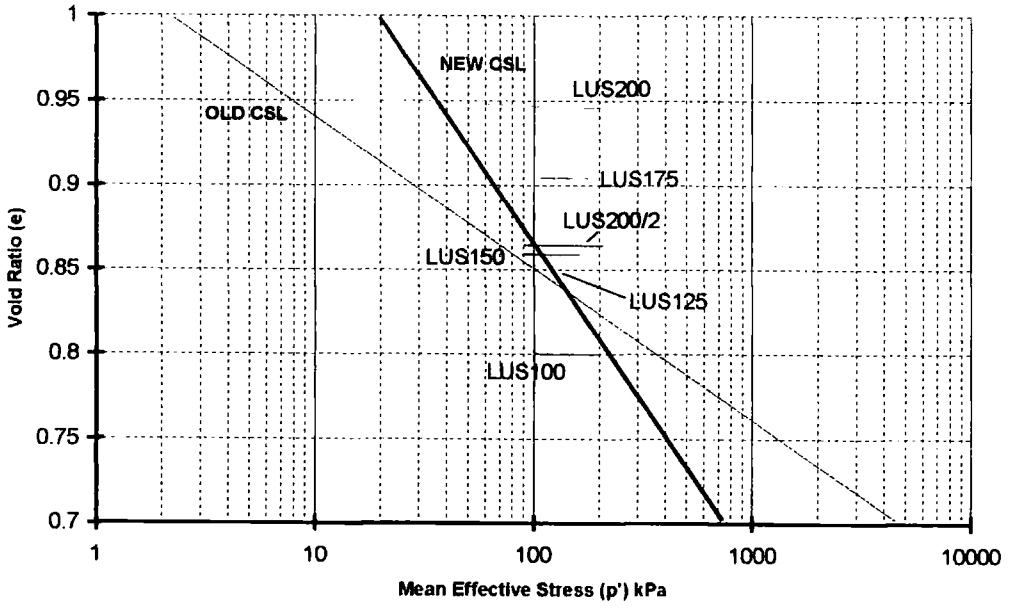

Figure 5-75b Comparison of new CSL to LUS tests '100-200'

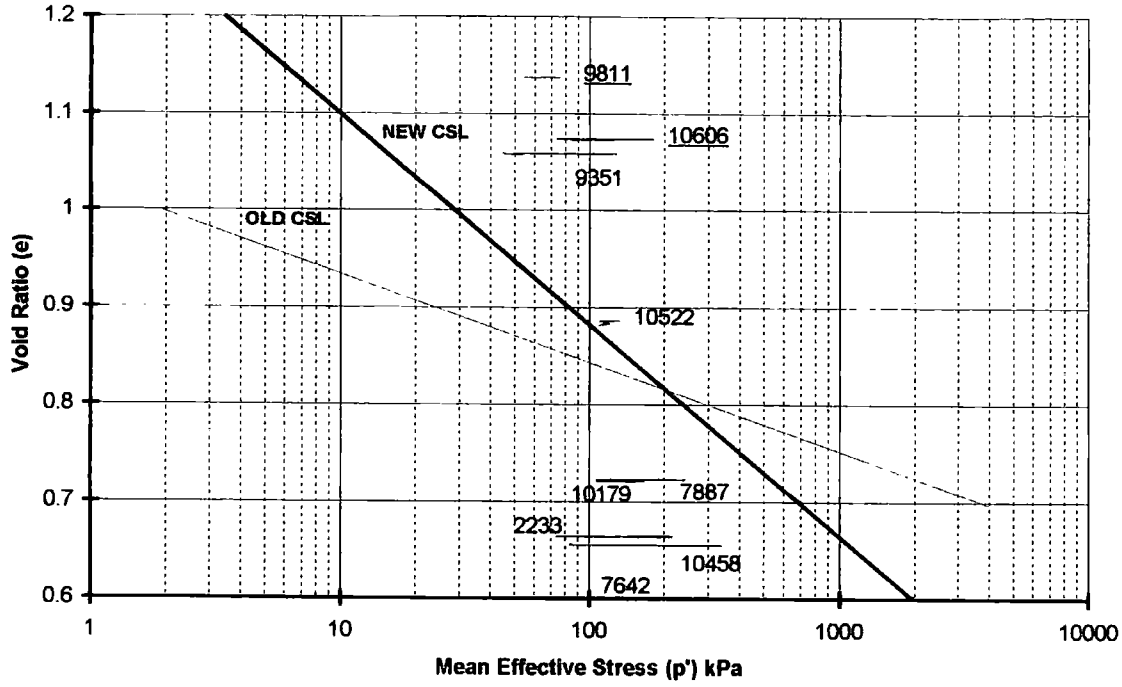

Figure 5-75c Comparison of new CSL to LUS tests 'Depth Profile

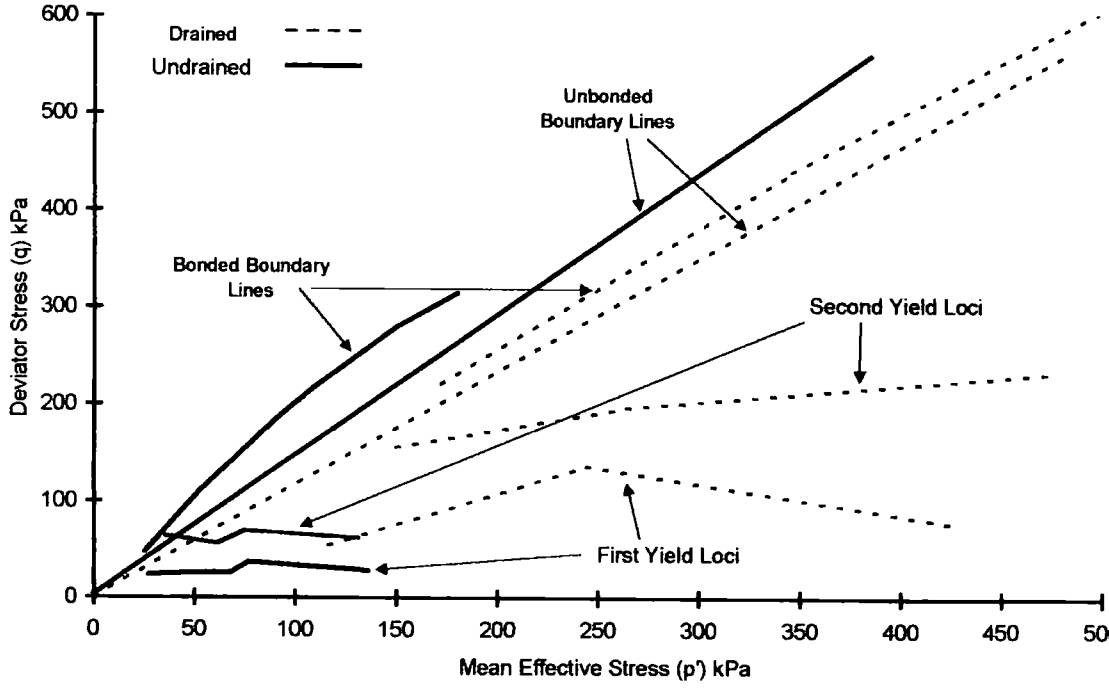

Figure 5-76 Comparison of drained and undrained test yield loci

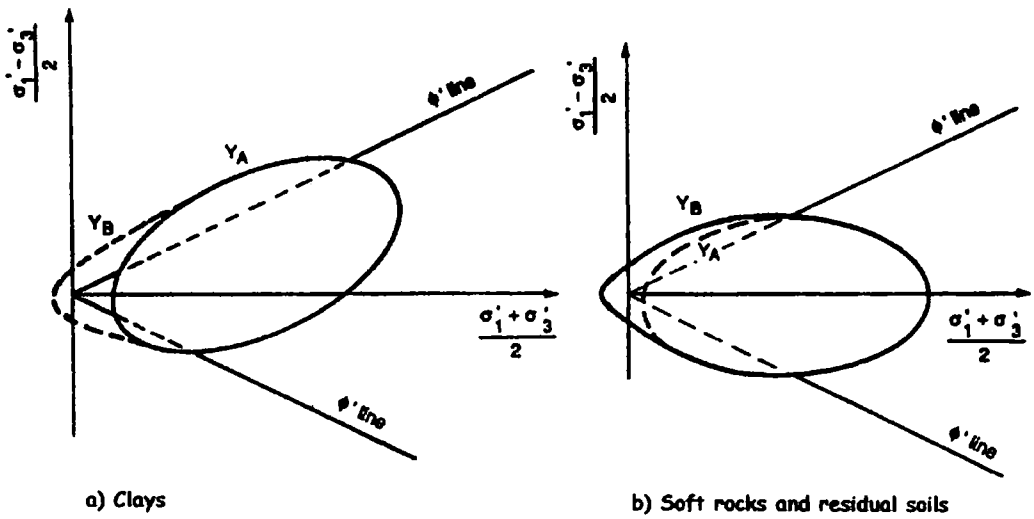

Figure 5-77 Yield curves for structured soils (after Leroueil & Vaughan 1990)

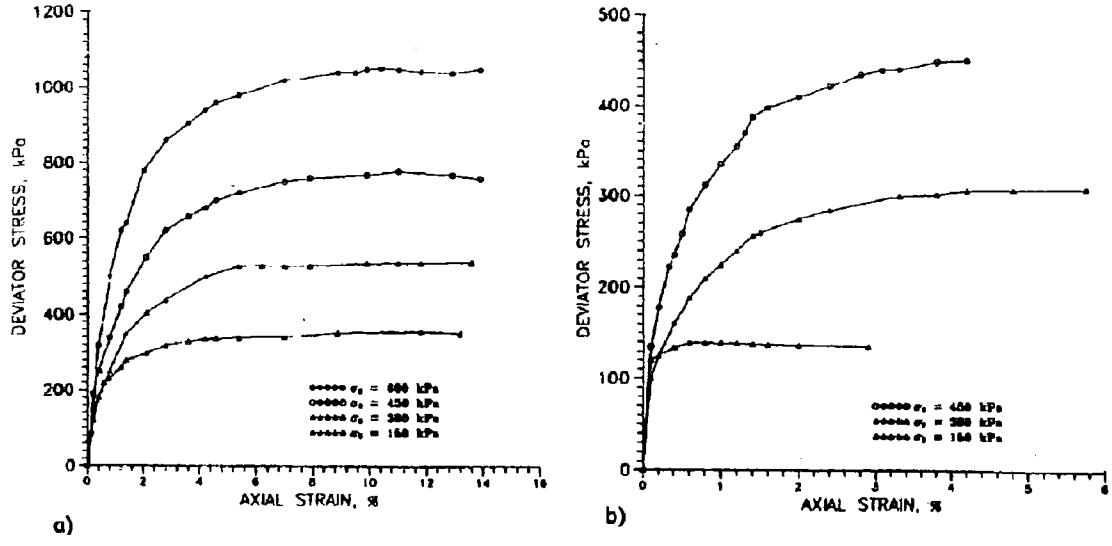

Figure 5-78 Group of triaxial tests (a) Drained & b) Undrained on fly ash after Indraratna et al (1990)

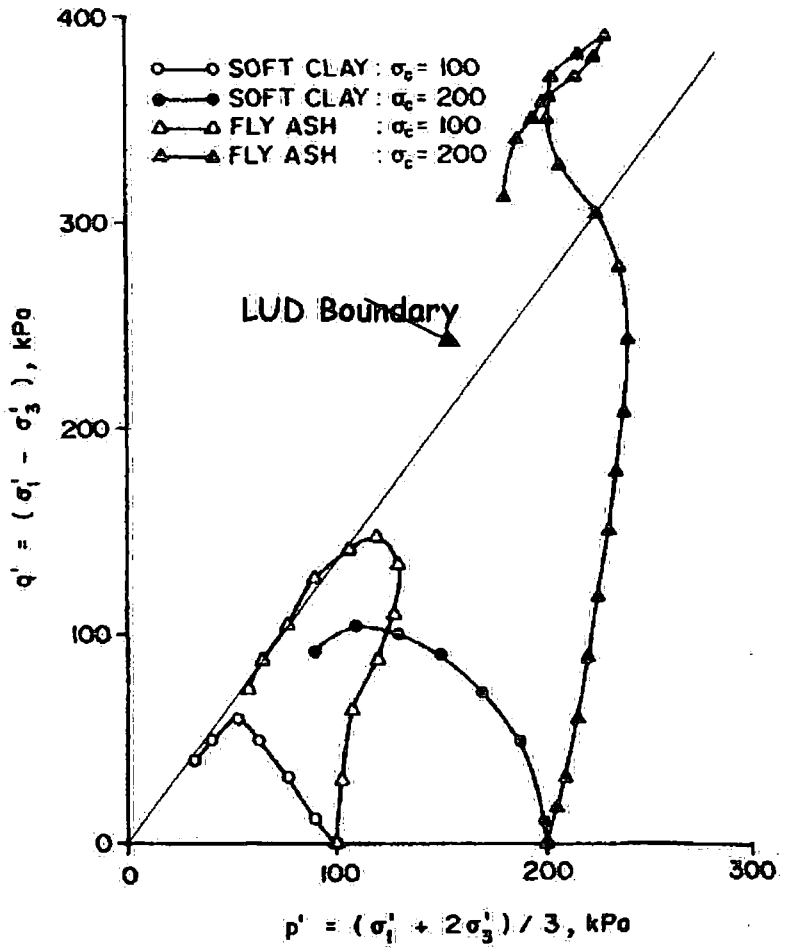

Figure 5-79 Stress paths from undrained tests on Fly ash from a disposal dump (after Indraratna et al 1990) compared to the LUD boundary

6. Lime/Fly Ash Mortar

6.1 Lime/Fly Ash Mortar

The results from tests on the Lagoon Fly Ash material reported in Chapter 5 demonstrated significant variations among different specimens due to the heterogeneity of the fly ash within the lagoon. It was seldom possible to determine the presence of bonding within a particular specimen until the test had been completed and the results analysed. Hence, it was necessary to manufacture mortar specimens in which the pozzolanic reaction had been induced, in order to carry out a controlled study of pozzolanic bonding. By this method the variability in bond strength and sample structure could be reduced and a greater homogeneity within and between specimens achieved. The pozzolanic samples were formed from a standardised fly ash/lime mortar using the method described in section 3.3.1 for both structured and de-structured specimens. A reactive fly ash sample with low self-cementing properties was obtained from Drax power station in North Yorkshire. The fly ash was a bulk sample taken directly from the hopper, which collects dry fly ash from the electrostatic precipitation process.

As with naturally occurring structured soils, the determination of the pozzolanic structural influence was best achieved by relating the behaviour of the structured soil to that of unstructured samples, which matched the structured specimens as closely as possible (except for the bonding between particles). The unstructured specimens were produced

from the same mortar as the structured specimens, except that the mortar was not formed into cylinders. Instead it was left as an uncompacted mass, for the same curing period, to allow the reaction to take place uniformly throughout the soil. The mortar material to be used in the unstructured specimens was left in a mass to prevent the formation of flat-sided particles, produced by the moulding process, which might change the particle interaction behaviour of the unstructured material. The broken down material was moulded into the test specimens immediately prior to the setting up of the apparatus. This was necessary to prevent any further reaction once the specimens were formed. The moulding process is laid out in section 3.4.2. Since the unstructured material consisted of broken down structured mortar the term de-structured was adopted to emphasise that the material had undergone the pozzolanic reaction in its formation.

6.1.1 Curing Time Evaluation

There was no common curing time for the reaction as suggested from previous work but there were many indications of a stepped strength gain for the reaction. The reported curing times vary from 10 days (Gray, 1972), based on cylindrical samples cured at room temperature, up to 200-400 days (Thorne & Watt, 1965) using cubic specimens. There was also a suggestion of a delay at the beginning of the reaction. Tashiro (1994) observed such a delay using variations in resistivity to monitor the reaction.

A series of tests was performed on mortar specimens to identify the effects of curing time on strength. Six specimens were formed from the same batch of mortar using the mould method described in section 3.4.2. They were stored in conditions of 100% humidity, and tested at different times based on weekly intervals. The first specimen was tested on the day of casting, which represented no curing time. The other specimens were tested after curing times of 1, 2, 3, 4, and 8 weeks. These specimens were formed to a void ratio of 0.7. This value was chosen to be similar to the void ratio of samples of lagoon fly ash extracted in the early stages of the test programme. It later became apparent, after the majority of the lagoon tests had been carried out, that a larger void ratio would be required for the research into pozzolanic activity. However, the mortar used in all these tests was uniform, so the results are considered to be a relevant evaluation of the curing time for the mixture. It was considered that the effects of curing would be similar in the specimens formed at larger void ratios.

6.1.2 Results of undrained triaxial tests on mortar specimens.

All tests were carried out using the same triaxial machine (to eliminate potential variations between different machines) and mortar specimens were tested in undrained conditions at 18 %/hour rate of strain. The plots of maximum strength against curing time (Figure 6-1) showed increasing strength with time for the first 4 weeks. However there was no further increase between 4 and 8 weeks. The photographs of the samples (Plate 6-1) show that the sample with no curing time deformed in a ductile manner. The barrelling shape was

'frozen' as the mortar cured after the test. The failure mode quickly became more brittle as the curing time for reaction increased, and the cylindrical shapes of the original specimens were maintained after shearing.

These results showed that the primary strength gain in the specimens was achieved after a curing time of about 4 weeks and appeared to remain constant for up to 8 weeks. These specimens had the same curing time as those of Indraratna *et al* (1991) (Figure 6-2), who reported more rapid initial strength gain. Consequently, it was decided to allow slightly more time for the primary strength gain to finish before testing the specimens. No specimens were left for longer than 8 weeks, because of the lack of information on long term strength gain. All specimens were tested between 6-8 weeks (42-56 days) after formation.

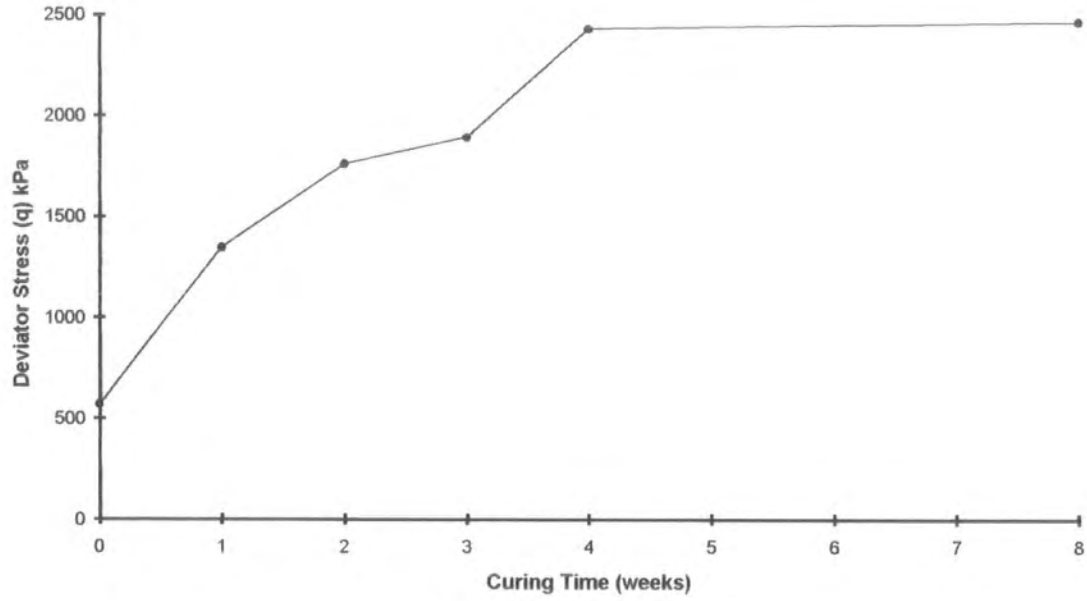

Figure 6.1 Maximum strength against curing time for lime/fly ash mortar specimen

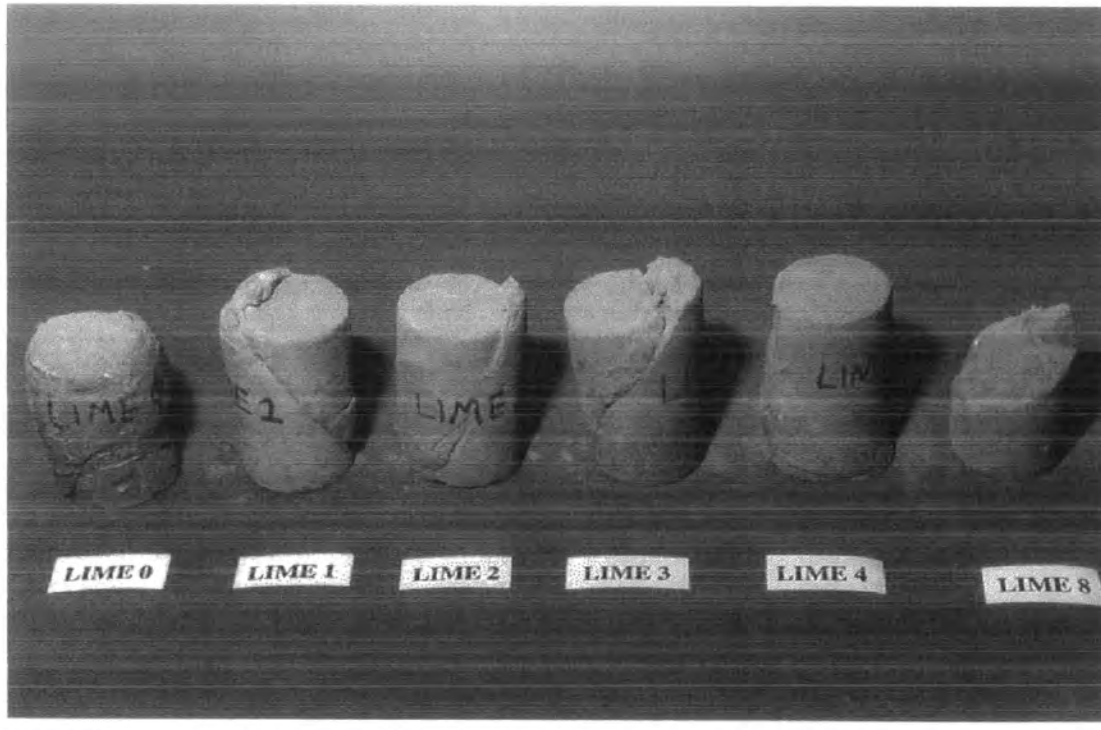

Plate 6-1 Lime/fly ash mortar specimens after undergoing triaxial compression

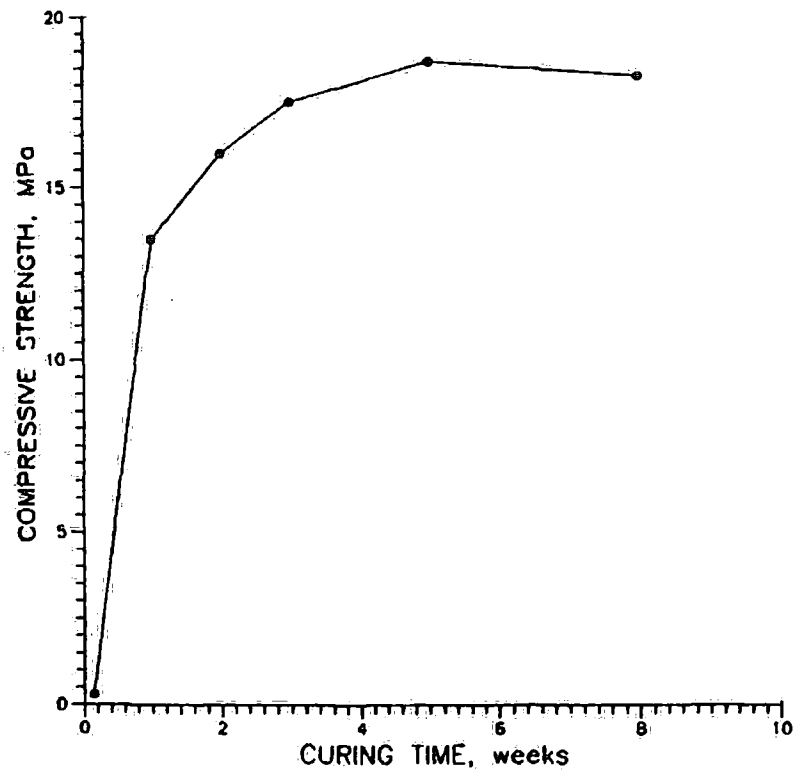

Figure 6-2 Curing Time evaluation by Indraratna et al (1991) showing a similar cure time to that seen in Figure 6-1

6.2 *Drained Triaxial Compression Tests*

6.2.1 De-structured Samples

These samples were formed from the mortar material unused in the formation of the structured samples. The mortar was loose- cured for the same period, and was then broken down. The specimens were formed just prior to each test using the mould method (Section 4.2.6), allowing no time for curing to occur when in the moulded shape. The results on the specimens after testing are shown in Plate 6-2. As with the Lagoon fly ash tests, tests were performed at the deformation rate of 13.72 mm/hour.

Structured Test	Moisture Content	Void Ratio [Initial]	Void Ratio [Consolidated]
MDD25	20.00%	0.948	0.940
MDD50	16.38%	0.930	
MDD100	17.78%	0.970	0.957
MDD200	19.35%	0.971	0.943
MDD400	19.35%	0.962	0.895
MDD700	19.35%	0.923	0.824

Table 6-1 Parameters for MDD specimens

The plots of stress against axial strain (Figure 6-3) show increasing strength with increasing confining pressure. Each sample showed high initial stiffness, followed by a smooth shallow peak, and finally a gradual loss in strength. MDD25 was the only sample to show a peak strength followed by a rapid loss in strength, occurring at 0.7% axial

strain. MDD50 and MDD100 both showed losses in stiffness at small strains followed by an almost constant strength for the remainder of the tests, taken to about 18% axial strain. Maximum strength values were reached at 7% and 9% axial strains respectively. MDD200 and MDD400 showed less significant changes in stiffness and reach maximum strengths at 14% and 16% axial strains respectively. MDD700 demonstrated a more gradual change in stiffness over the test than the other specimens, reaching a maximum strength at 14% axial strain.

The plots of volumetric strain against axial strain (Figure 6-4) show a change in behaviour from MDD25 to MDD400 of increasing volume reduction. MDD25, after an initial reduction in volume, dilated to an overall volume increase of 1%. MDD50 showed very little volume change over the duration of the test. It increased by only 0.012%, which was insignificant compared to the other tests. Above 50 kPa at higher confining pressures the tests showed sample compression throughout axial straining, increasing as confining pressure was increased up to 400kPa. The compressions of MDD400 and MDD700 were very similar and or appear to indicate a limit.

The effective stress paths for the tests plotted in p'-q stress space (Figure 6-5) define a slightly curved surface for the maximum stresses. The stress path of MDD25 was similar to that shown by the remoulded samples of the lagoon ash at the same stress level, being nearly as strong as the 50kPa test in the group. The other tests showed increasing strength with increasing confining pressure in a non-linear relationship. As the confining

pressure was increased there was a corresponding decrease in the friction angle, resulting in the slight curvature of the boundary.

The plots of stress ratio with axial strain (Figure 6-6) show a decrease in the stress ratio with increasing confining pressure, which matched the reduction in friction angle seen in the stress paths. The stress ratio was greatest at the lower pressures and least at the higher pressures, with a bunching in the middle between 50 and 200 kPa. The increase in confining pressure was also accompanied by a change in the curve shape. MDS25 had a peaked curve and its maximum stress ratio was higher than the ultimate ratio. As the confining pressure was increased in MDS50 and MDS100 the stress ratio reached, after the initial rapid rise, was close to the maximum and remains relatively constant. As the pressure was increased further the transition from initial straining to the behaviour at larger strains became smoother.

The stiffnesses of the specimens, normalised with respect to mean effective stress, are shown in Figure 6-7. This shows a reduction in stiffness with increasing confining pressure from MDD25 to MDD200. Above 200 kPa the specimens showed a very similar relationship between normalised stiffness and axial strain.

The de-structured tests can be plotted in e-log p' space (Figure 6-8) in a similar manner to the lagoon tests in Figure 5-5. This plot helps to show a possible CSL for the lagoon ash which must lie on the wet side of MDS25 but on the dryside of the other tests, as marked

on the plot. There was no plot for MDD50 as there was no credible volume change information from the consolidation stage. The CSL has been drawn to pass close to MDD700 and MDS25 at the points where both tests showed a marked change in direction. The remaining tests showed movement towards the line but did not reach it.

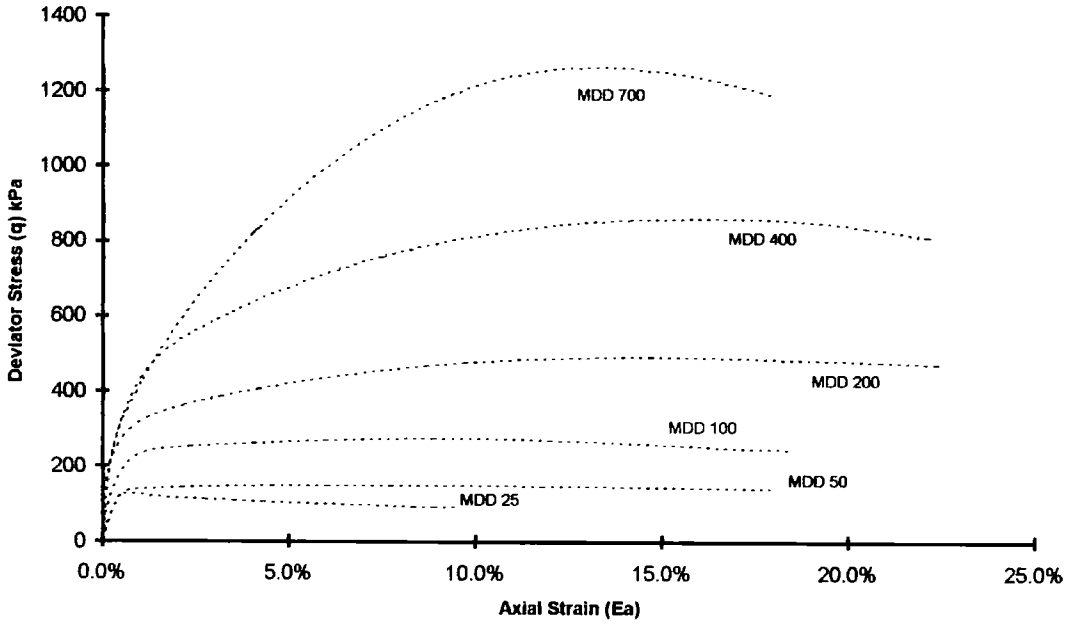

Figure 6.3 Stress against axial strain plot for MDD tests

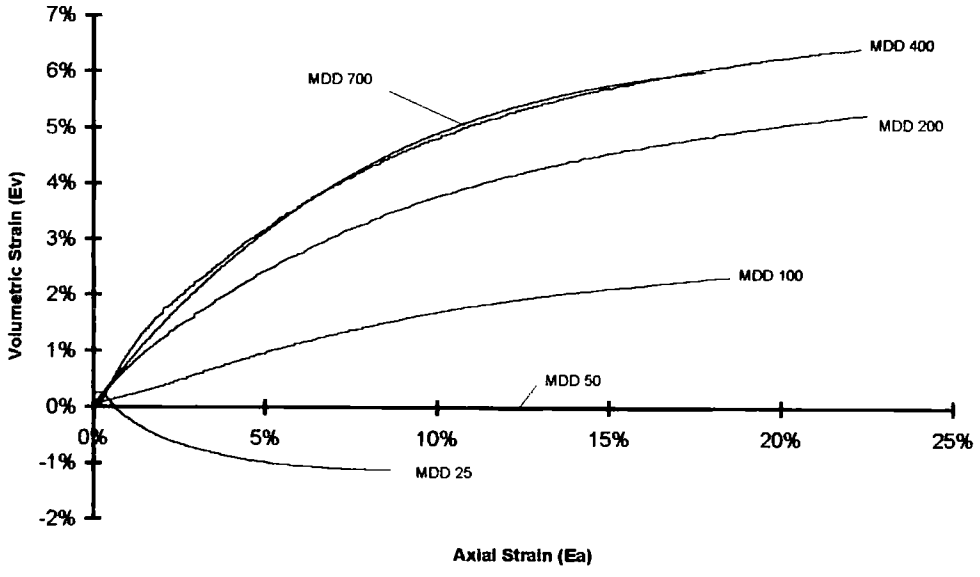

Figure 6-4 Volumetric strain versus axial strain for MDD tests

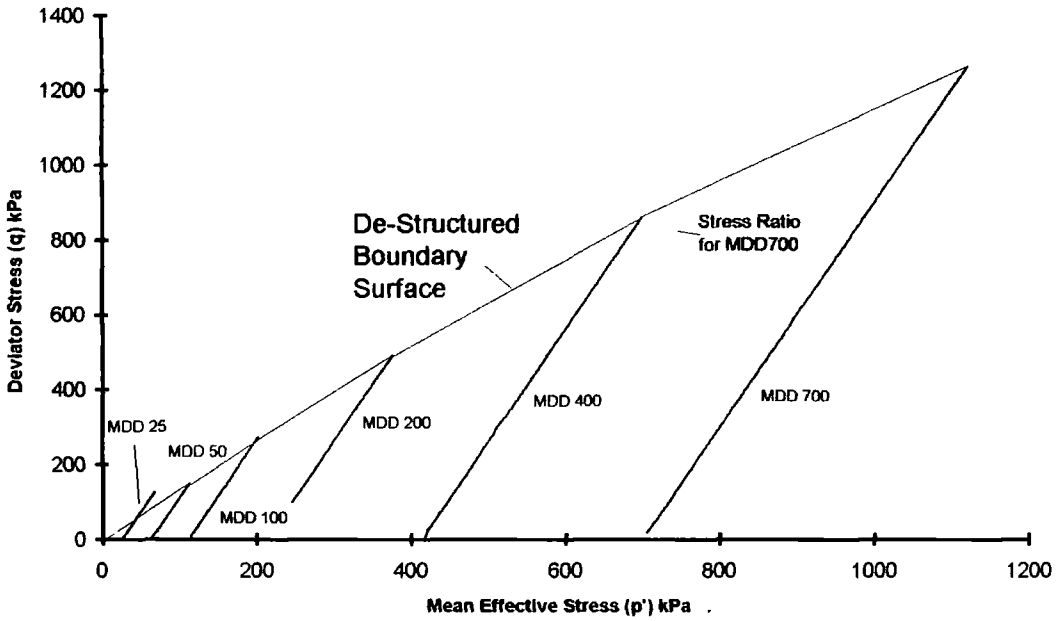

Figure 6.-5 Effective stress paths for MDD tests

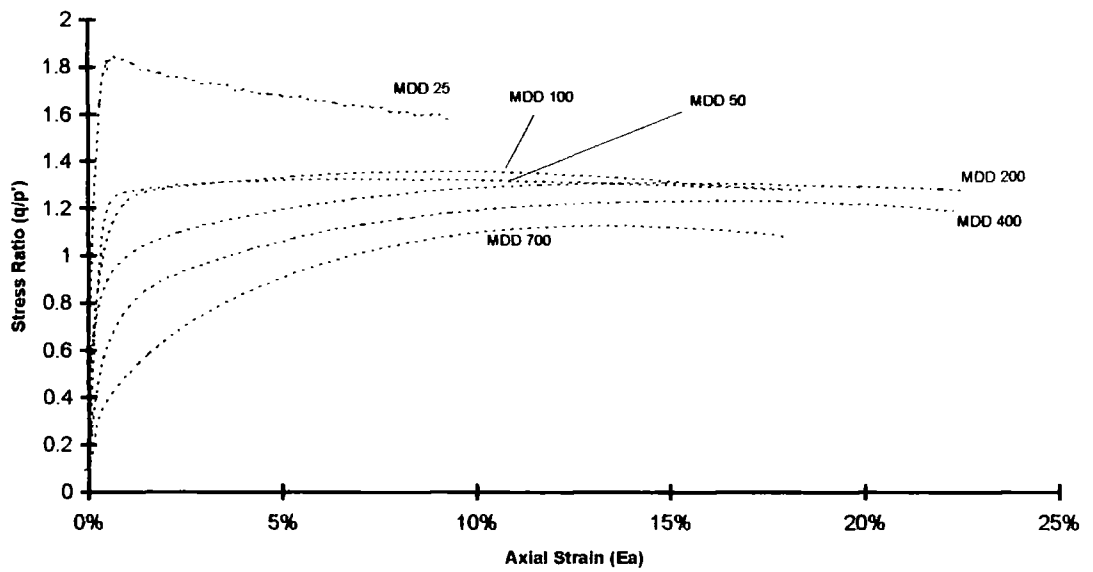

Figure 6.6 Stress ratio against strain for MDD tests

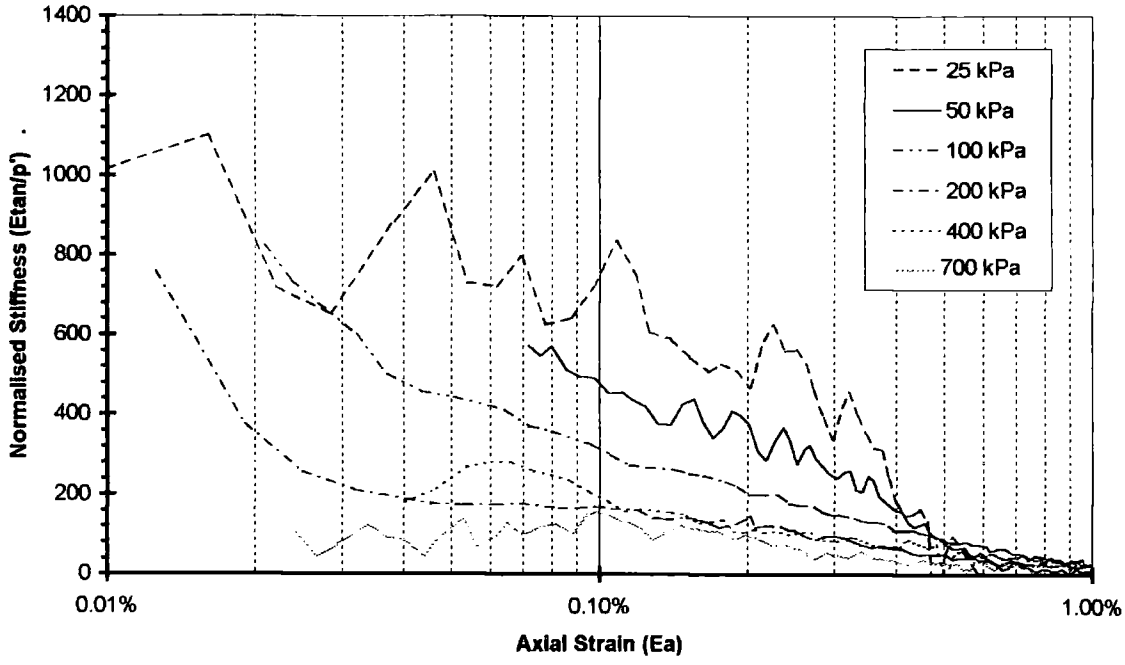

Figure 6.7 Stiffness normalised with respect to mean effective stress against strain for MDD tests

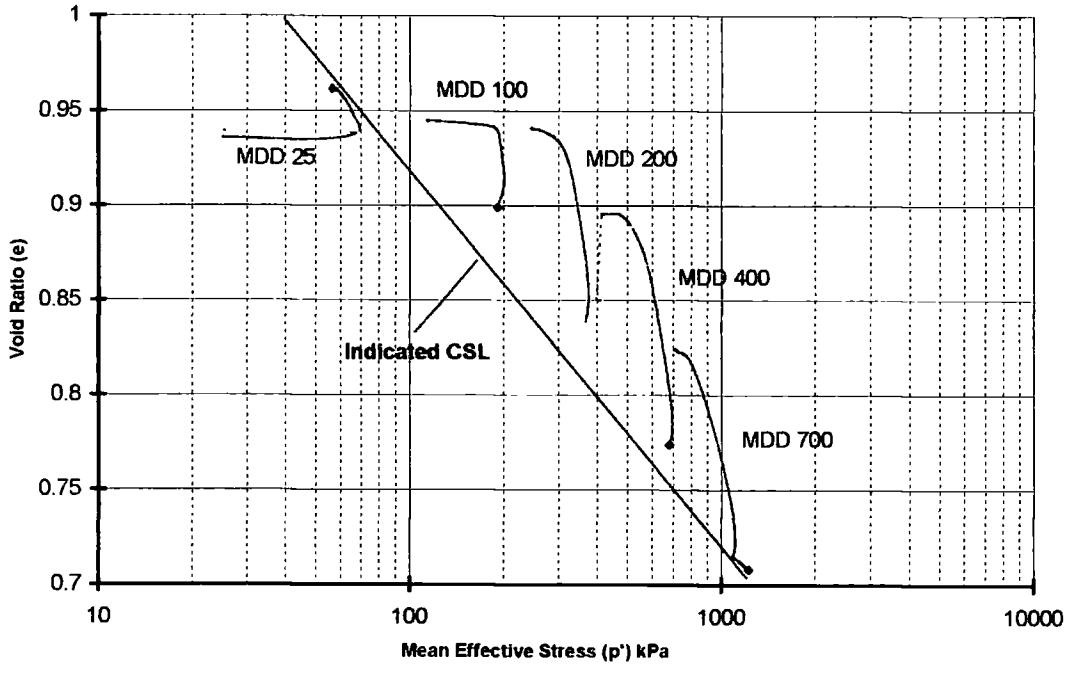

Figure 6.8 Void ratio against mean effective stress for MDD tests

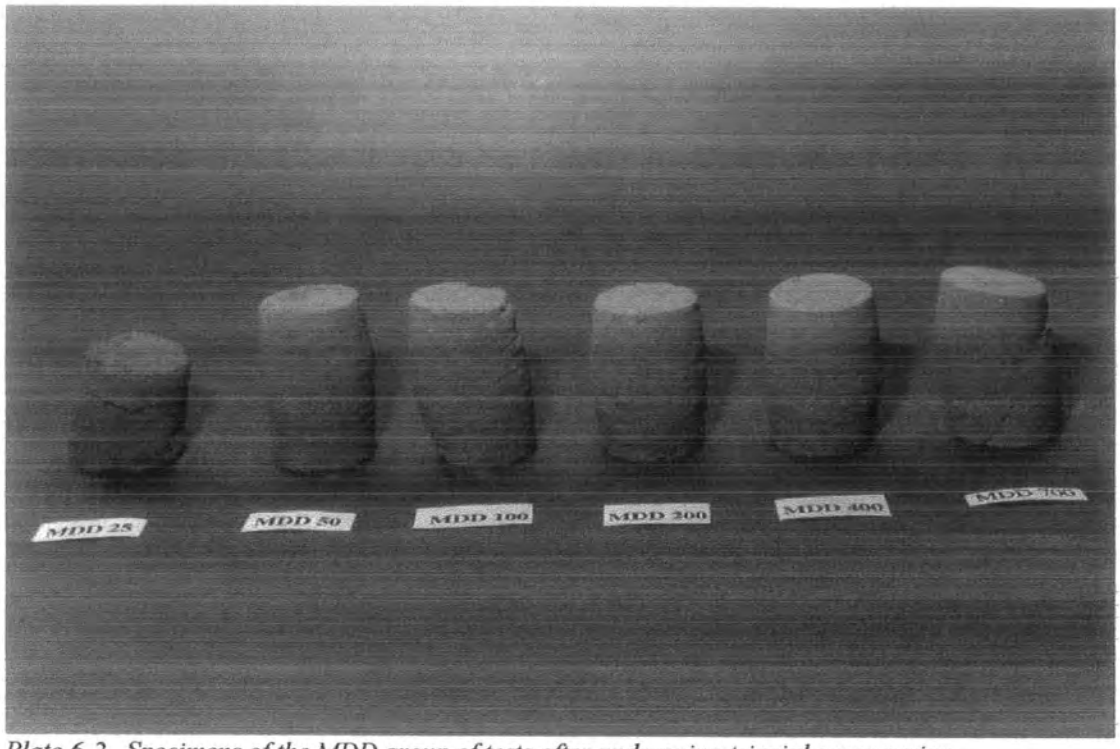

Plate 6-2 Specimens of the MDD group of tests after undergoing triaxial compression

6.2.2 Structured samples

The structured samples used in these tests were all tested within the 6-8 weeks period (42-56 days) of formation, for reasons explained in Section 6.1. They were prepared at a void ratio of about 0.9 to match the higher void ratios seen in the lagoon ash samples. Table 6.2 gives the void ratio and curing time in days for each of the specimens in the group. Some of the specimens are shown in Plate 6-3. All three triaxial machines were used to test the specimens using a deformation rate of 13.72 mm/hour.

Structured Test	Moisture Content	Void Ratio [Initial]	Void Ratio [Consolidated]	Curing Time (Days)
MDS25	18.29%	0.926	0.920	54
MDS50	19.14%	0.942	0.930	48
MDS100	17.15%	0.901	0.918	55
MDS200	17.65%	0.912	0.891	47
MDS300	18.88%	0.953	0.937	54
MDS400	18.80%	0.926	0.926	52
MDS700	18.30%	0.929	0.885	43

Table 6-2 Parameters and curing times for MDS specimens

The stress/axial strain plots (Figure 6-9a), for all of the structured specimens tested under drained conditions, showed very stiff responses to the initial loading. The specimens all yield at axial strains of less than 0.3%. The first 1% strain for each test is presented in Figure 6-8b. The specimens tested at low confining pressures showed a sharp fall in their strengths after reaching a peak, with the ultimate strengths of the specimens increasing

with increasing confining pressure. MDS300 and MDS400 had comparable strength to each other, but MDS400 maintained its strength over a greater range of axial strain than MDS300. MDS700 showed yielding at relatively low stresses at the beginning of the test, after which the specimen had a much lower stiffness. It exceeded the strengths of the other specimens even though the test was finished before a maximum strength was reached.

The volume change with respect to axial strain plots (Figure 6-10) show three phases of behaviour from low to high confining pressures. Initially MDS25 had a small compression before dilating to an increase in the volume of 2%. MDS50 also showed a slight dilation after reaching a peak in compression, but at larger axial strains it began to compress again. MDS100, although it did not compress as much as MDS50, had a similar shape. Above 100kPa there was a change in behaviour and the dilation part seen in the lower pressures was lost, although there was still a significant change in the rate of compression. Tests MDS200, MDS300 and MDS400 all showed similar volume change profiles, reducing in rate at 2% axial strain with very little to separate the three profiles. Above 400 kPa MDS700 had a similar initial rate of volume change except there was no significant reduction in rate at 2% axial strain. Instead, the rate of volume change reduced gradually as axial strain increases.

The stress paths for the structured tests are plotted in p'-q stress space in Figure 6-11. They show a general pattern of increasing strengths with increasing confining pressures. A

boundary line for the structured specimens could be mapped through p'-q stress space, derived from the maximum stress points. The plot for MDS200 fell just short of this boundary and was probably due to a weak specimen. The boundary demonstrated a considerable extension above the strength of the de-structured material in stress space, especially at lower pressures. The difference between structured and de-structured strength became less apparent as the confining pressure increased.

The same method of yield assessment used in the lagoon specimens (section 5.1.2.4) was also applied to the MDS specimens to identify the yield points of the breakdown of bonding (Figure 6-12). In MDS25 the first yield from the stress-strain plot (Figure 6-12a) is not obvious. It would appear that 0.039% axial strain represented a significant change in the plot and might be considered to be the second yield. Finally there appeared to be a yield point at 0.110%, which represented a major loss in stiffness. This might be associated with the total yield of the bonding, observed in the work by Malandraki (1994).

In the plot for MDS50 (Figure 6-13) the yield points were most clearly seen in the stiffness against axial strain plot on non-log scales (Figure 6-13d). The first drop marked the first yield in stiffness at 0.008% axial strain, the second at 0.018%, and another yield at 0.028%. In contrast, the log-log stiffness plot did show the same first and second yields but the third was lost as the graph drops away. The identification of the yields on the stress-strain plots was less obvious but there was a detectable yield at about 0.018%,

which was consistent with the second yield, and was most easily identified in the log-log plot of stress against axial strain.

In MDS100 the non-log stress-strain plot (Figure 6-14a) shows two obvious yield points at 0.047% and 0.18% axial strains. The log-log stress-strain plot however only indicated one yield at 0.018%. For the stiffness plots the non-log plot (Figure 6-14c) was unfortunately hindered by heavy scatter, making a realistic identification of any yield very difficult. However, the log-log plot of stiffness (Figure 6-14d) indicated a first yield at about 0.018% as well as yields at 0.047% and 0.18%. It was also possible to identify yields at 0.029% and 0.14%

The stress-strain plots for MDS200 (Figure 6-15) show relatively smooth curves of decreasing stiffness with no obvious yield points. However, the stiffness plots (Figures 6-15c&d) did allow identification of some yield points. The first was at 0.073% axial strain and a second at 0.116%, with others at 0.20% and 0.29%. The log-log scale indicated a significant loss at 0.29, but in the non-log scale there was little difference between 0.20 and 0.29. This was an indication of the unhelpful distortion of the log scales at this end of the graph.

The stress strain plots for MDS300 (Figure 6-16 a&b) do not show any significant yield points. There does however appear to be an increased loss of stiffness just before 0.1% axial strain. For this test it was the stiffness plots (Figure 6-16 c&d) that gave indications

to of bond yielding. A first yield was identified at 0.019% with other yields at 0.030%, 0.086% and 0.153%. Combining the evidence from the four plots the second yield could be considered to be 0.086% where there was a perceived increase in the rate of stiffness loss identified by the normal stress strain plot (Figure 6-16a).

For MDS400 the stress-strain plot (Figure 6-17) did not show yielding until just before failure at 0.8% in the non-log plot. However, the stiffness plot identified a yield much earlier at 0.01%, most evident in the non-log plot. They also showed the second yield at 0.82% that marked the major lose in stiffness just prior to the specimen's failure. Another yield was apparent at 1.0%

MDS700 (Figure 6-18) showed a significant yield at a very early stage in the stress-strain plot. This was also apparent in the stiffness plot, but there did not appear to be any significant yields after that except at 2%. It might be that the bonds within the specimen yield very early and first and second yield were almost concurrent.

By superimposing the yields identified above onto the stress paths for the MDS tests (Figure 6-19) it was possible to indicate yield loci for first and second yield, as well as a total yield locus. The total yield locus, not observed in the lagoon specimen results, represented the yields observed in 100, 400 and 700 kPa tests, in each of which there appeared to be a hiatus in the stress-strain curves. At higher strains the specimens still showed increasing deviator stress but this was considered to be strain hardening. It was

most obvious in MDS400 (Figure 6-20a). Another good example of total yield is MDS700, which yielded at a very low stress (Figure 6-20b). The yield loci identified were curved, especially the second and total yields. They showed increasing strength for increasing confining pressure before a drop in strength. The second and total yield loci showed a sudden drop for test MDS700. They appeared to be centred around the de-structured boundary.

The plots of stress ratio against axial strain (Figure 6-21) show a decrease in both the maximum stress ratio and the ultimate stress ratio, which can be linked to increasing confining pressure. The lower pressure tests of 100 kPa and below showed a peaked maximum stress ratio at very low axial strains, which decreased with increasing confining pressure. MDS200 and MDS300 showed small peaks at failure followed by near constant stress ratios, whilst MDS400 had the same distinction between the first rapid rise and then near constant residual stress but without the small peak at failure. The highest pressure test, MDS700, demonstrated a marked change at low stress ratio after which the stress ratio increased gradually reaching its maximum at about 11% axial strain.

In tests on lagoon ash samples, the presence of bonding was identified from the points of maximum strength and maximum rate of dilation. This method could be applied to the low-pressure tests of the mortar, which dilated. MDS25 had a significant dilation resulting in an overall increase in volume. MDS50 and MDS100 did show early dilation but had an overall volume reduction. The stress-strain plots for these tests (Figure 6-22) showed the

points of maximum dilation rate and the maximum stress, indicating that the structure was influencing the strength of the material. In the other tests at higher confining pressures there was no dilation of the specimens and hence no point for maximum rate of dilation. However, the peak volume change occurred much later than the peak strength. This suggested that the strength of the samples was still being influenced by the pozzolanic bonding.

Plotting the normalised stiffness of the structured specimens (Figure 6-23) demonstrated that at low confining pressures the structured mortar specimens were very much stiffer than the de-structured specimens. MDS25 and MDS50 had similar stiffnesses, which were quickly lost as the axial strain increased and their failures occurred at less than 0.1% axial strain. As the confining pressure was increased the pozzolanic stiffness reduced further and for MDS700 it had fallen to the level shown by the de-structured samples.

By plotting the structured results in e-log p' space (Figure 6-24) in the same way as the de-structured specimens (Figure 6-8), these results could be compared to the CSL suggested by those results. There were two different responses seen in the structured results relating to the relative starting positions of the specimens in e- p' [log] space. The tests at 100kPa confining pressure and below had very little void ratio change to the point of failure. In the case of MDS25 there was an increase in void ratio, whilst for MDS50 and MDS100 there was no significant change. For the tests at confining pressures over 100 kPa which plot on the wet side of the CSL, there was a slight reduction in the void

ratio up to the point of failure. Failure was then marked by a significant change in direction in the plots and the void ratio began to fall. The behaviour at failure was more abrupt for these structured specimens when compared to the de-structured specimens. The exception was MDS700, which showed the same gradual change seen in MDD700. The CSL defined from the de-structured specimens showed a good correlation to these structured results. It showed a line that matched a trend outlined by tests MDS25 and MDS700 where their plots showed significant direction changes similar to MDS25 & MDS700 of the de-structured tests.

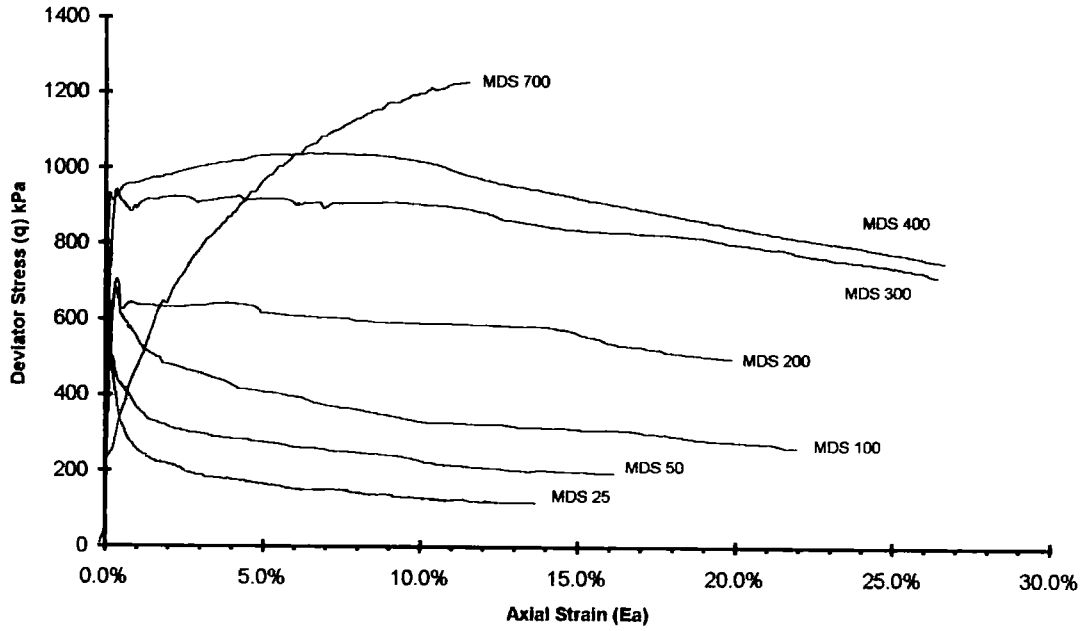

Figure 6.9a Stress against strain plot for MDS tests

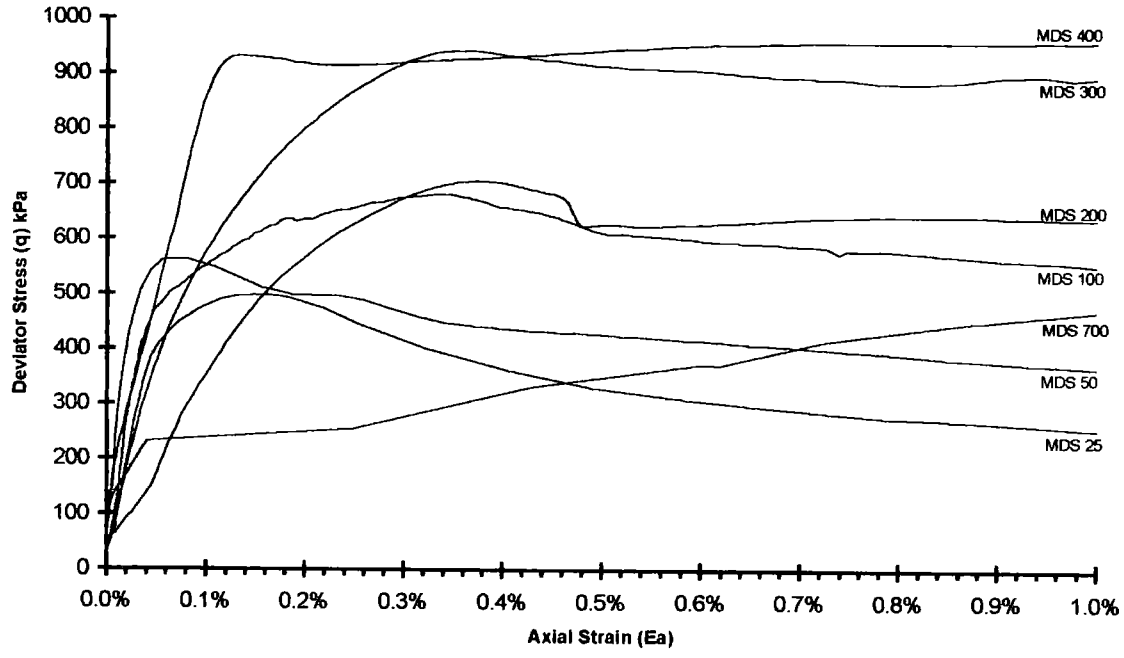

Figure 6-9b Stress-strain plot for MDS tests for the first percent axial strain

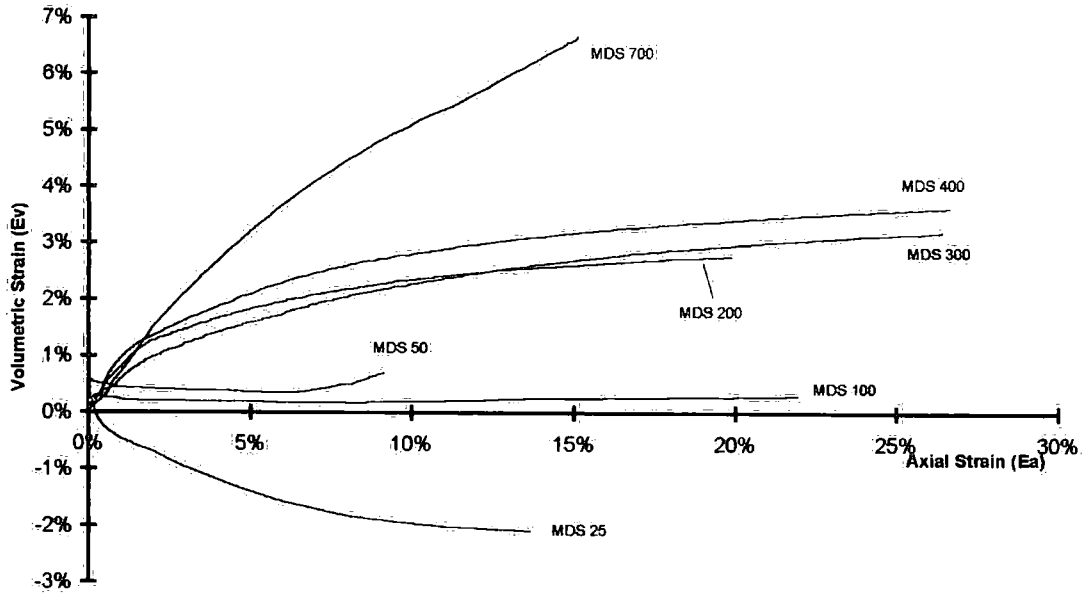

Figure 6-10 Volumetric strain versus axial strain plot for MDS tests

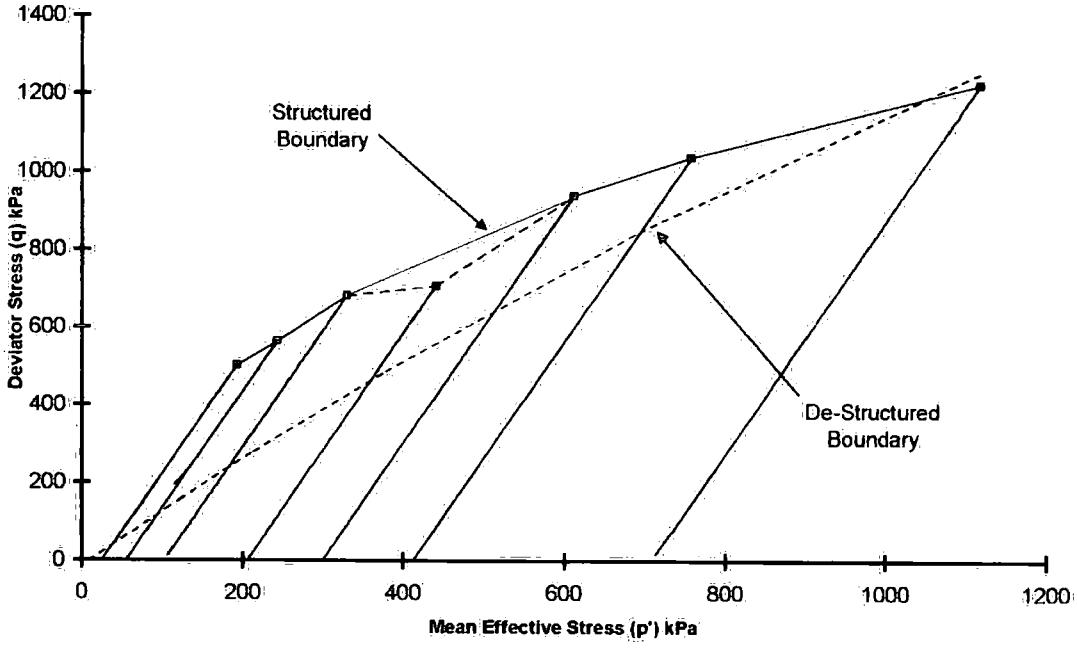

Figure 6-11 Effective stress path plots for MDS tests

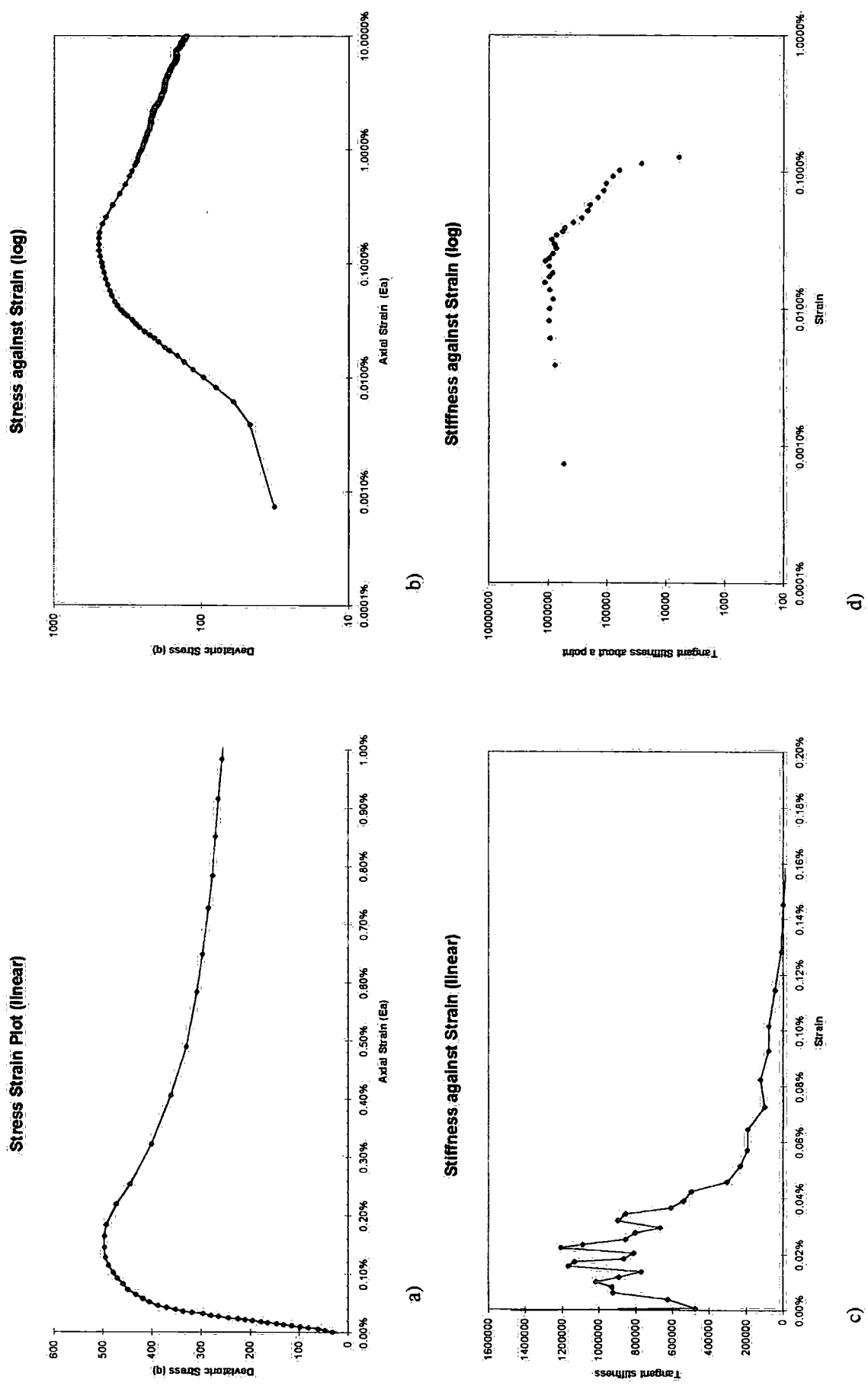

Figure 6-12 Plots of stress against strain (a) normal scales, b) log-log scales) and tangential stiffness against axial strain (c) normal scales, d) log-log scales) for MDS25

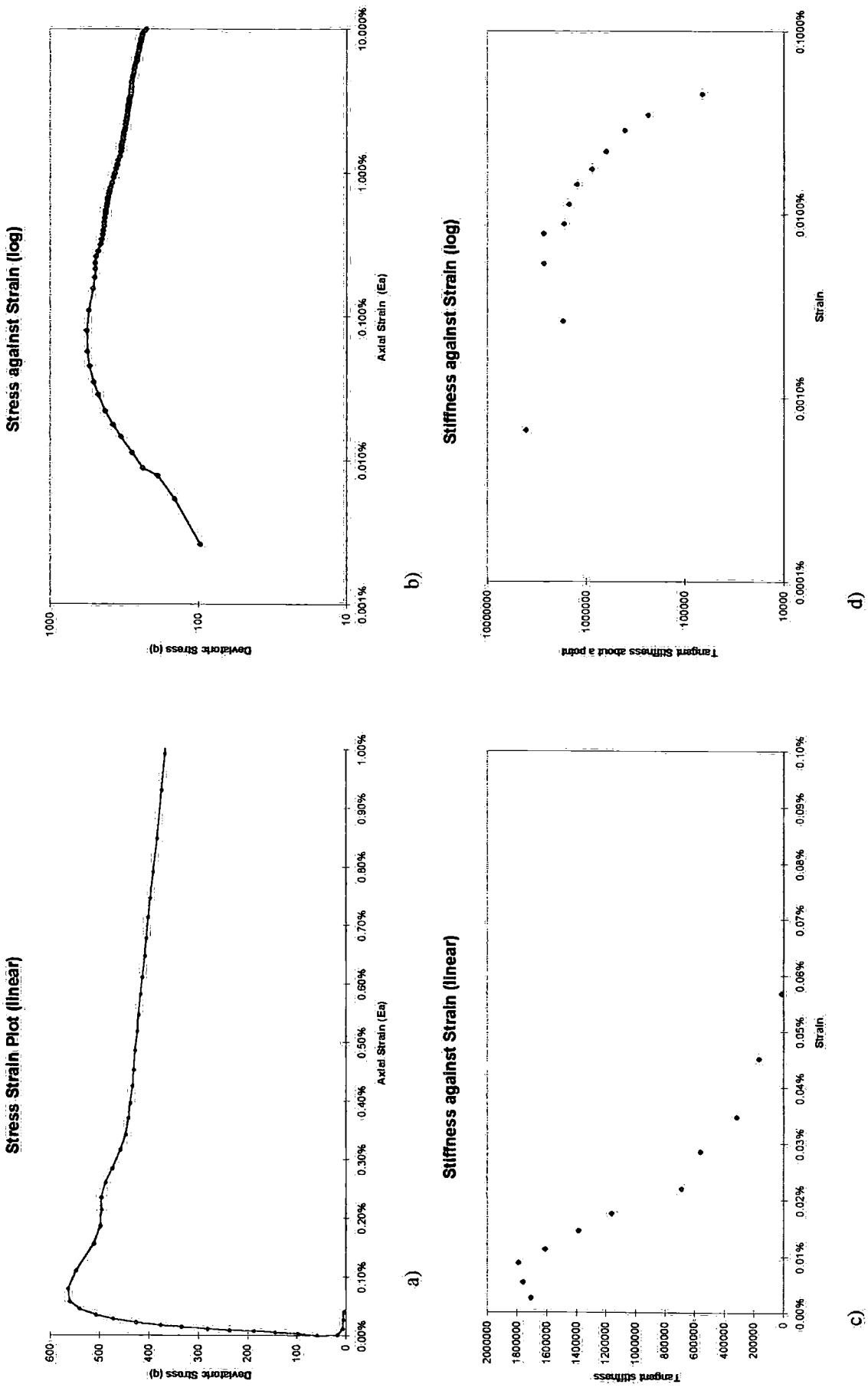

Figure 6-13 Plots of stress against strain (a) normal scales, b) log-log scales) and tangential stiffness against axial strain (c) normal scales, d) log-log scales) for MDS50

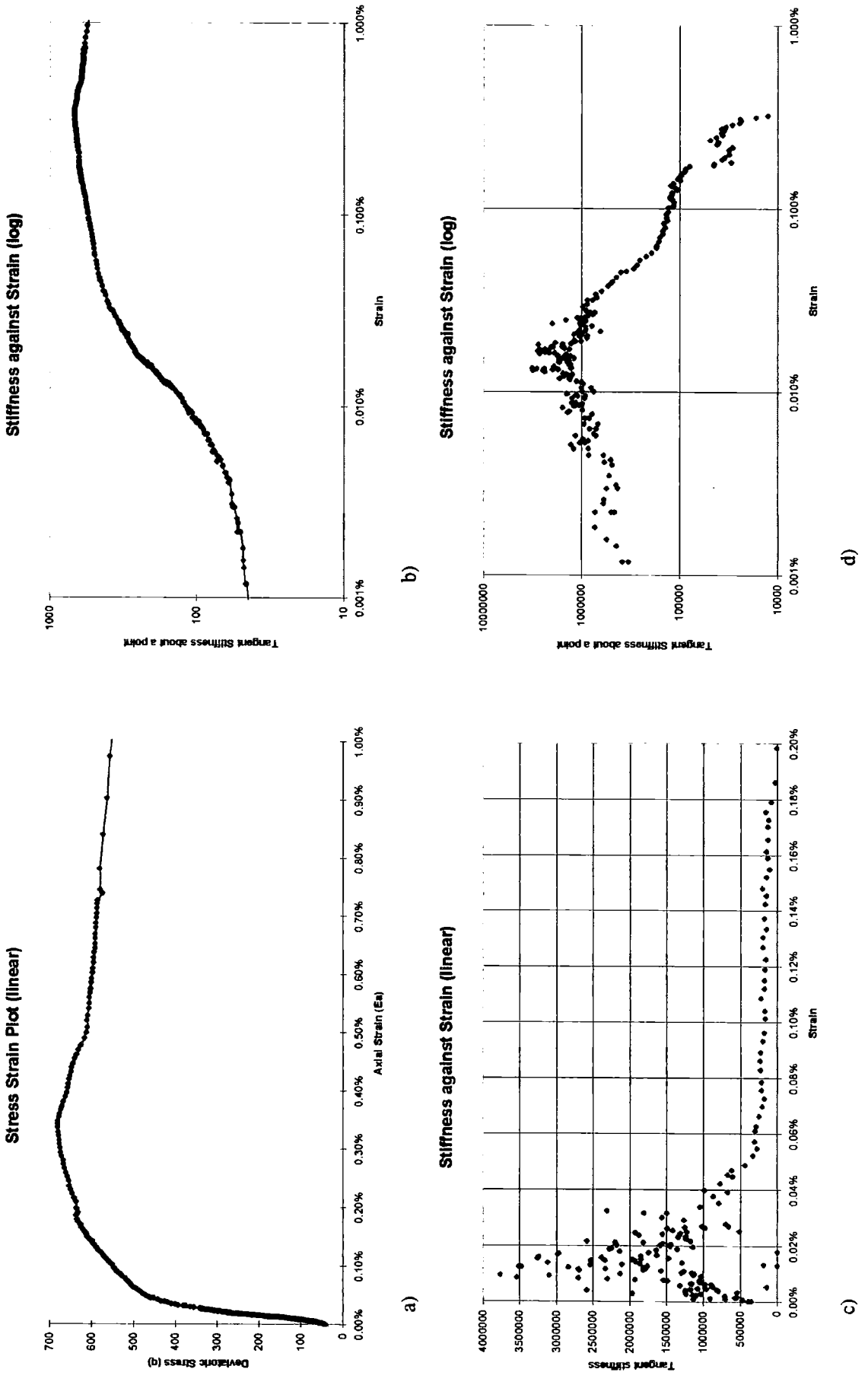

Figure 6-14 Plots of stress against strain (a) normal scales, b) log-log scales) and tangential stiffness against axial strain (c) normal scales, d) log-log scales) for MDS100

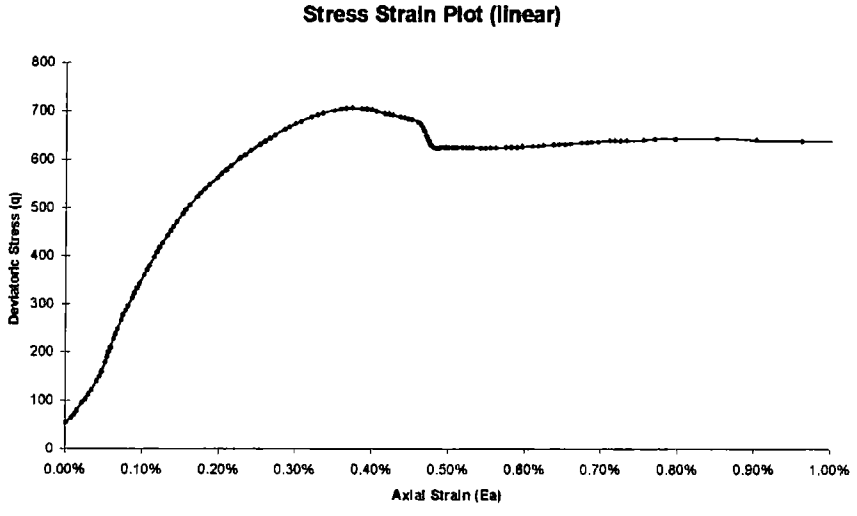

a)

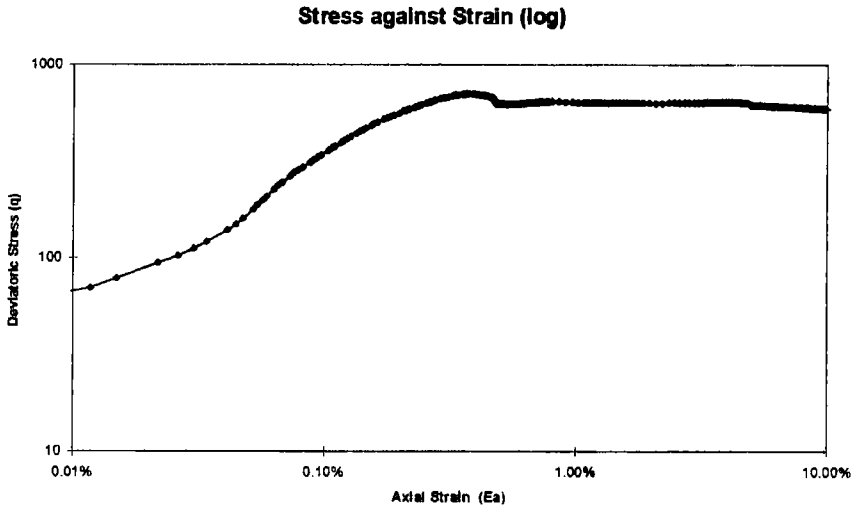

b)

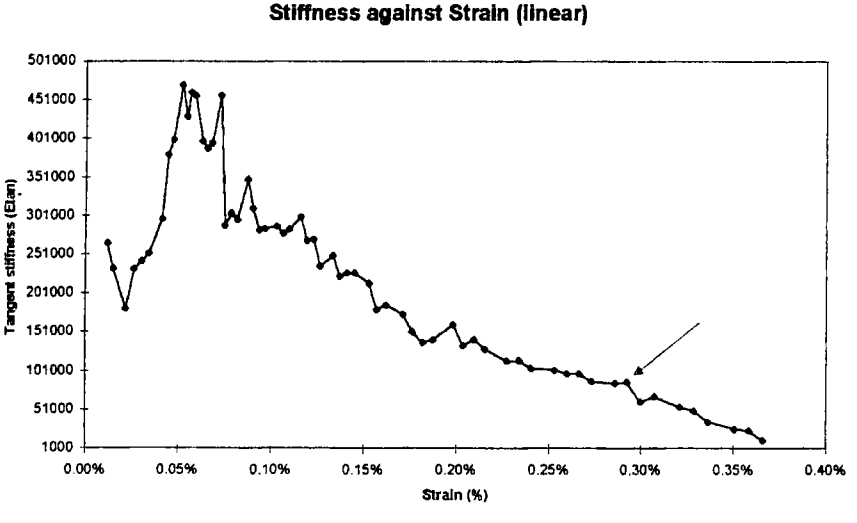

c)

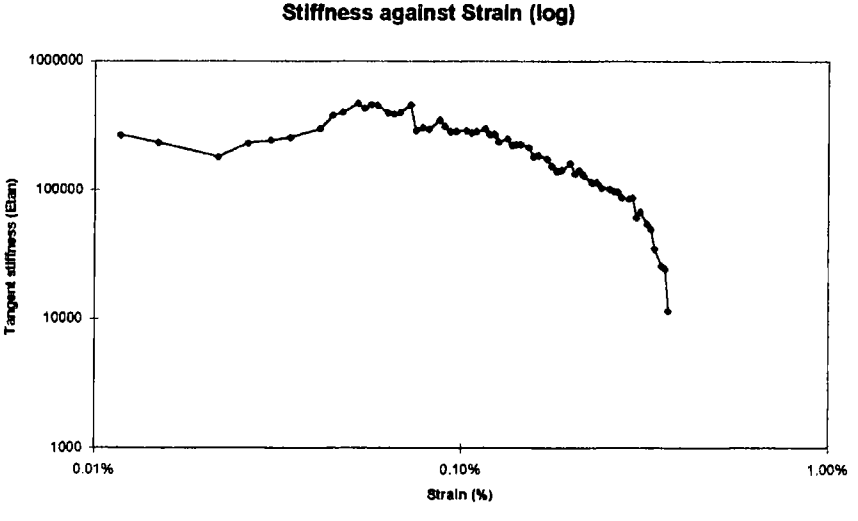

d)

Figure 6-15 Plots of stress against strain (a) normal scales, b) log-log scales) and tangential stiffness against axial strain (c) normal scales, d) log-log scales) for MDS200

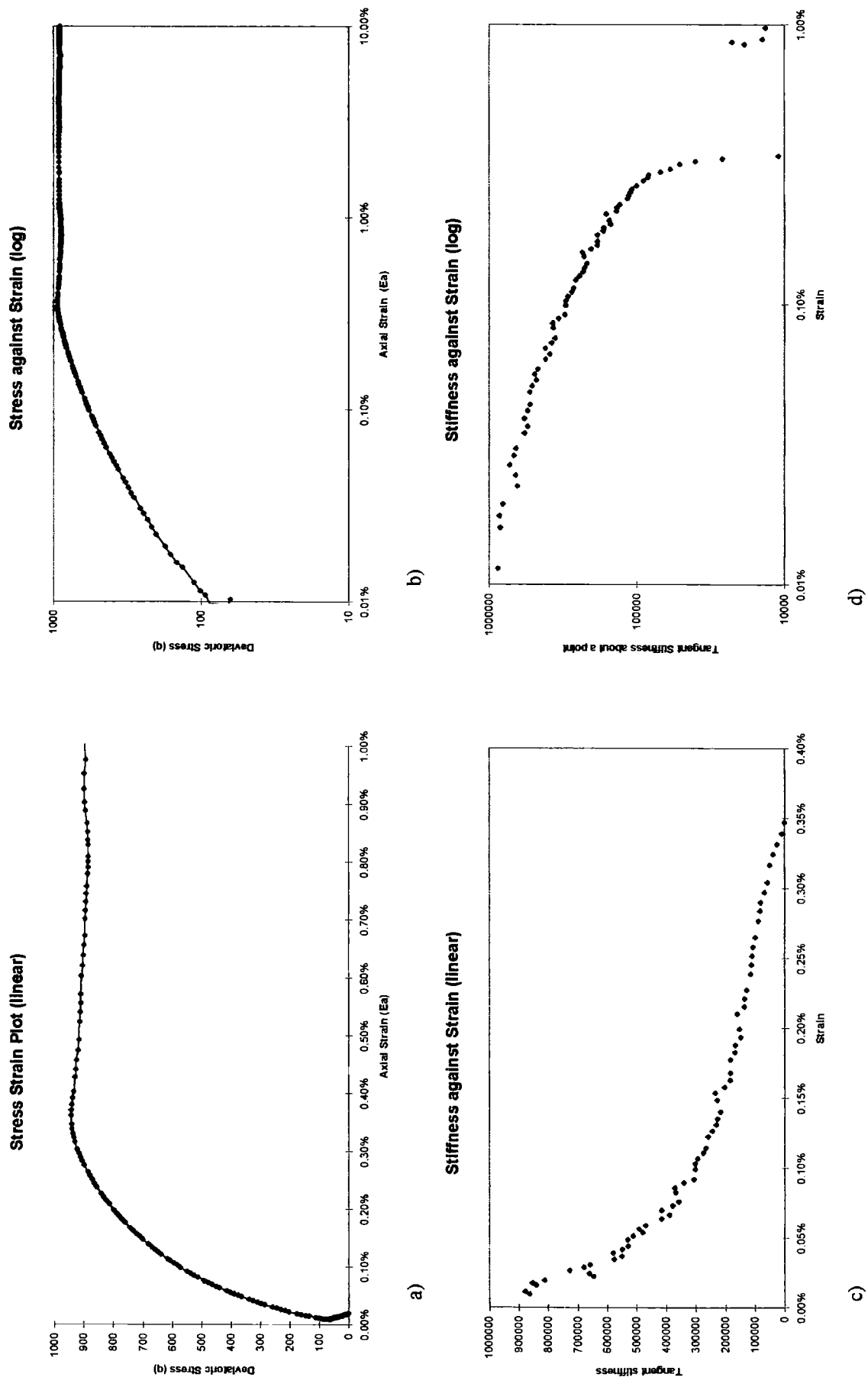

Figure 6-16 Plots of stress against strain (a) normal scales, b) log-log scales) and tangential stiffness against axial strain (c) normal scales, d) log-log scales) for MDS300

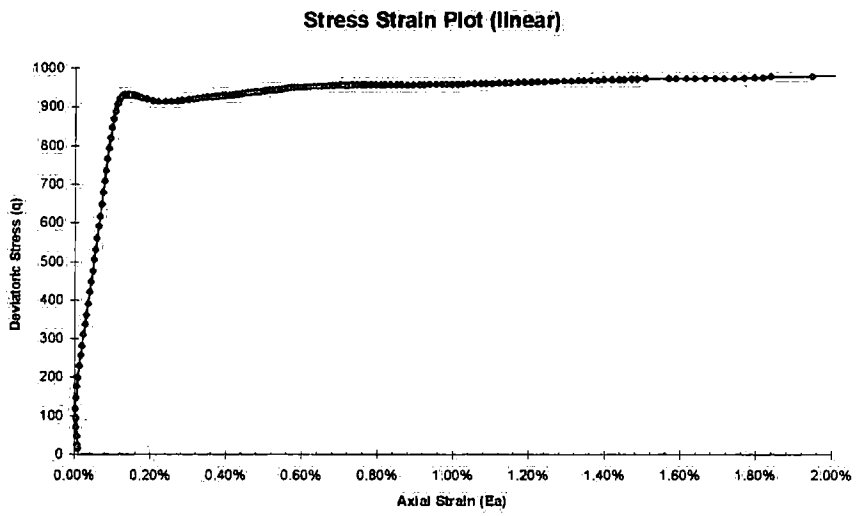

a)

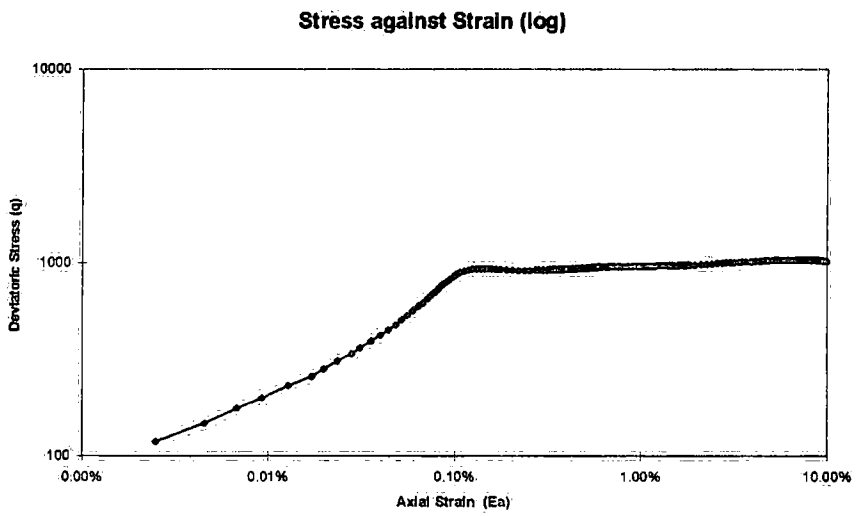

b)

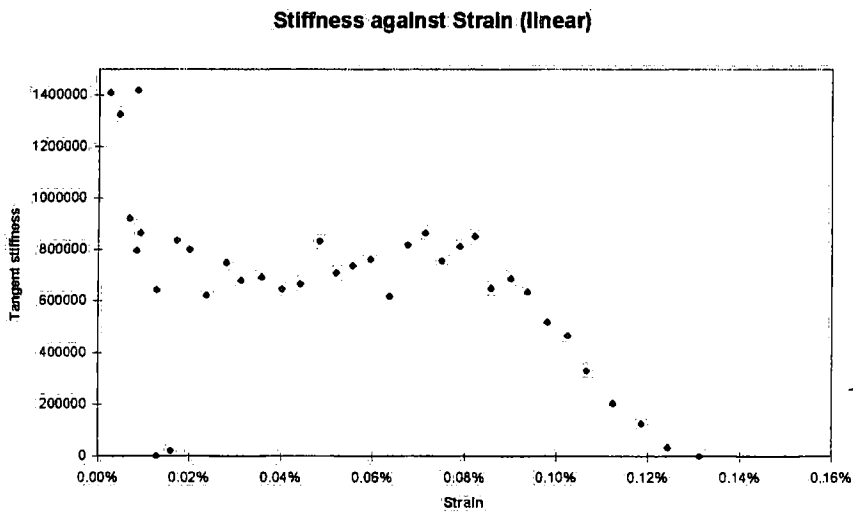

c)

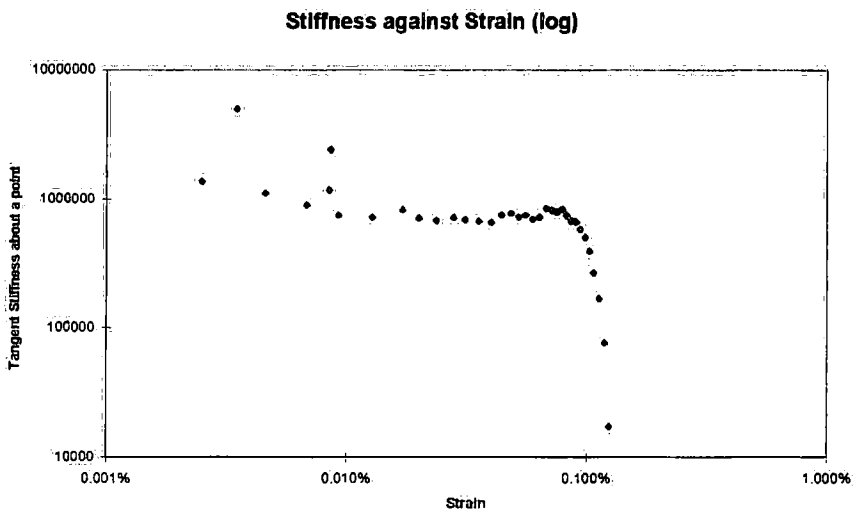

d)

Figure 6-17 Plots of stress against strain (a) normal scales, b) log-log scales) and tangential stiffness against axial strain (c) normal scales, d) log-log scales) for MDS400

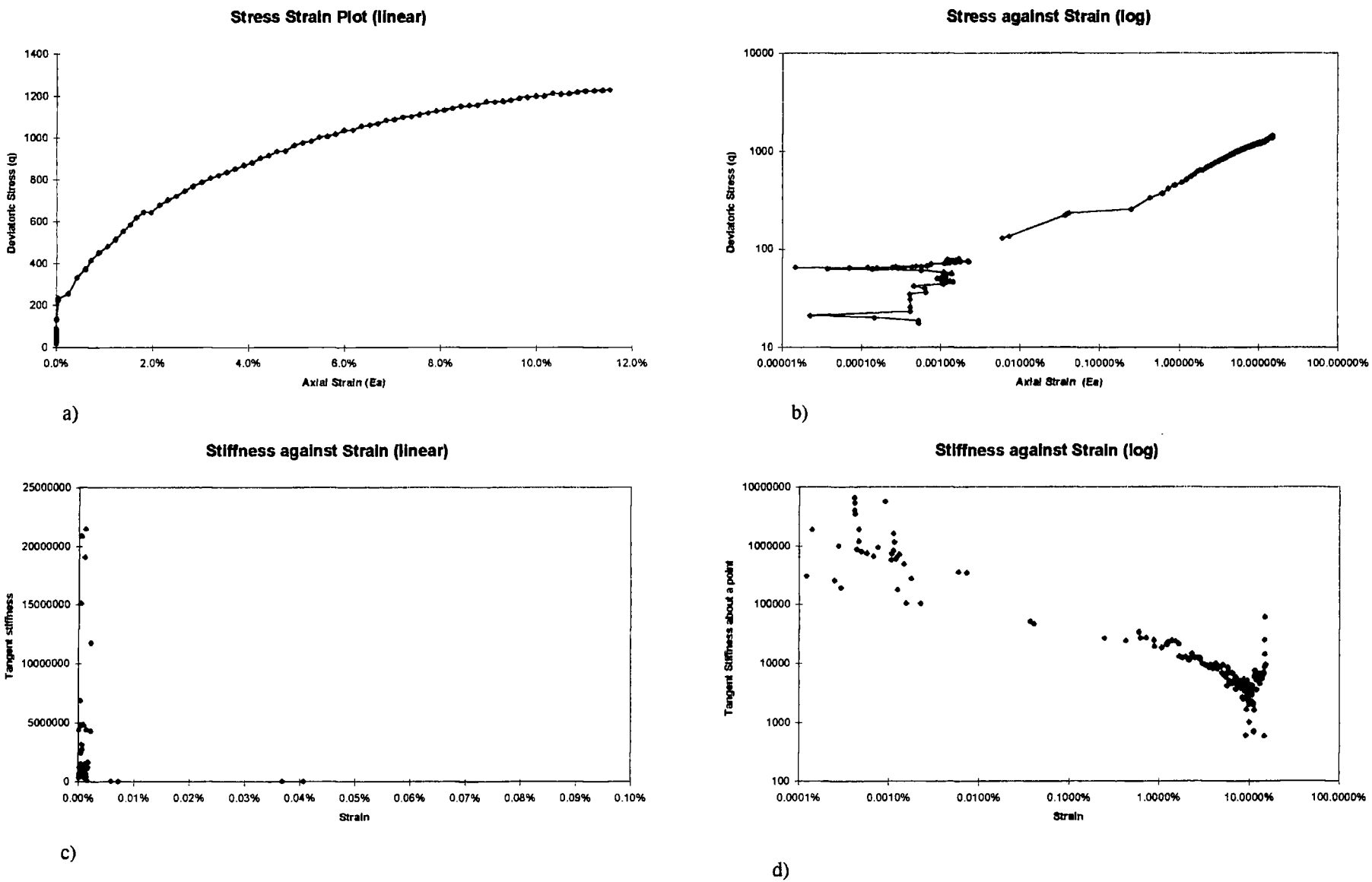

Figure 6-18 Plots of stress against strain (a) normal scales, b) log-log scales) and tangential stiffness against axial strain (c) normal scales, d) log-log scales) for MDS700

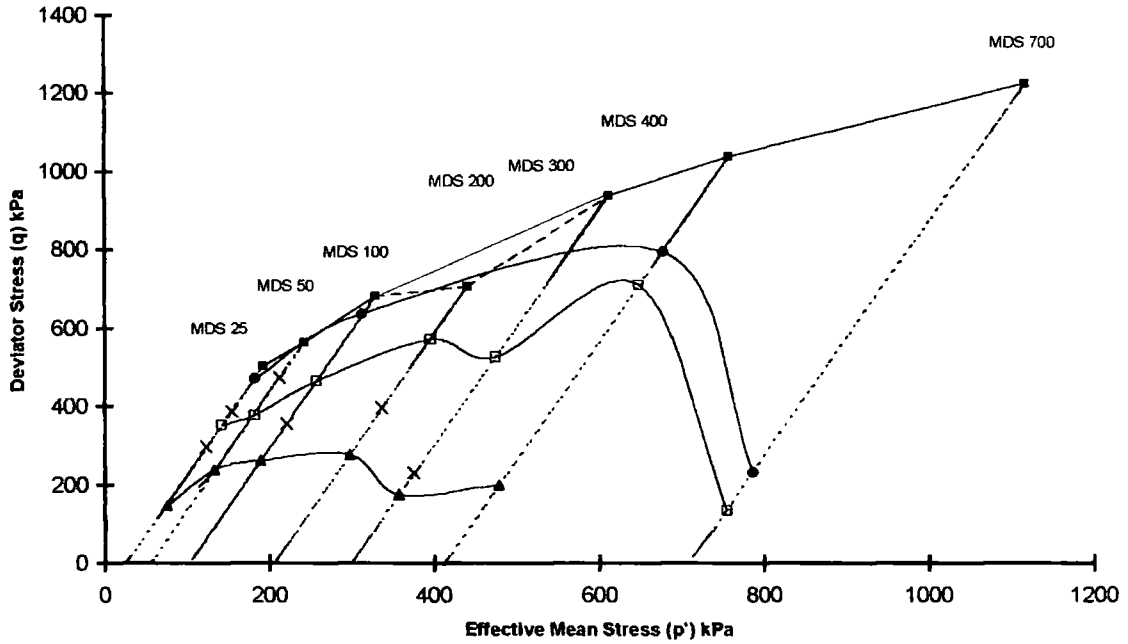

Figure 6-19a Yield points for MDS tests plotted in p'/q stress space relative to their stress paths

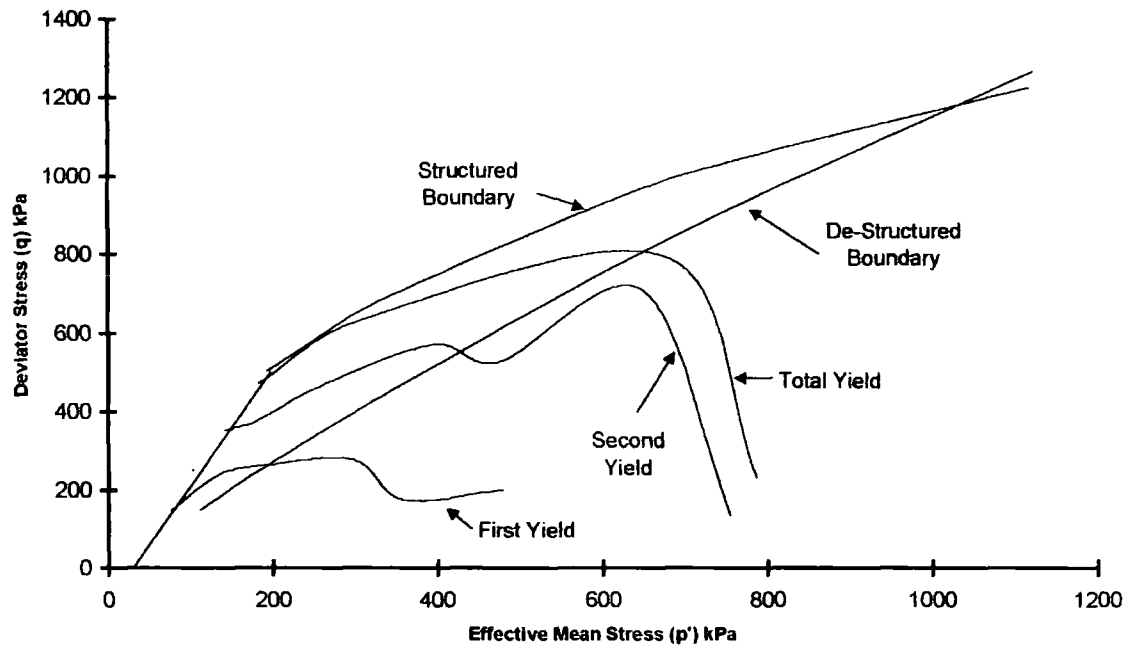

Figure 6-19b Boundary surfaces and yield loci for drained tests on fly ash mortar

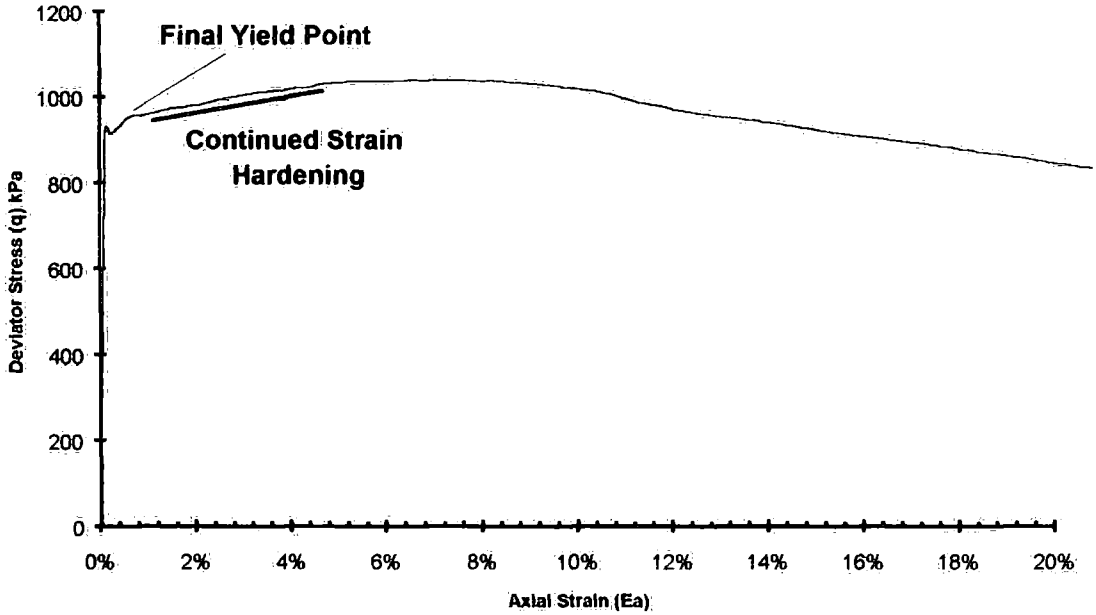

Figure 6-20a Stress-strain plot for MDS400 showing strain development after final bond yielding

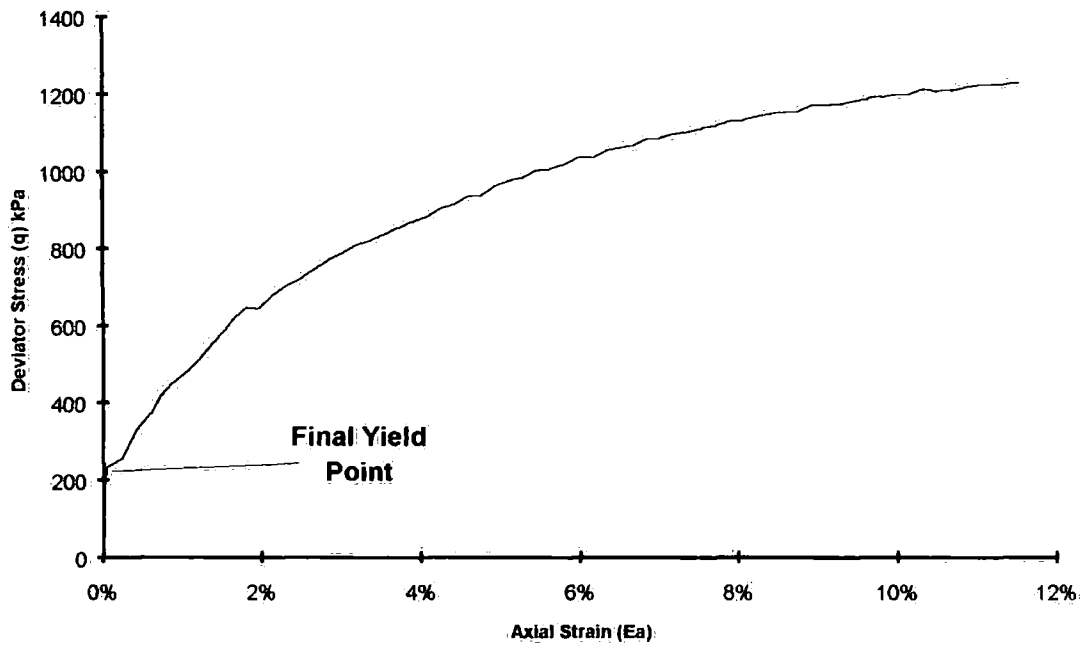

Figure 6-20b Stress-strain plot for MDS700 showing final bond yielding occurring at low stresses

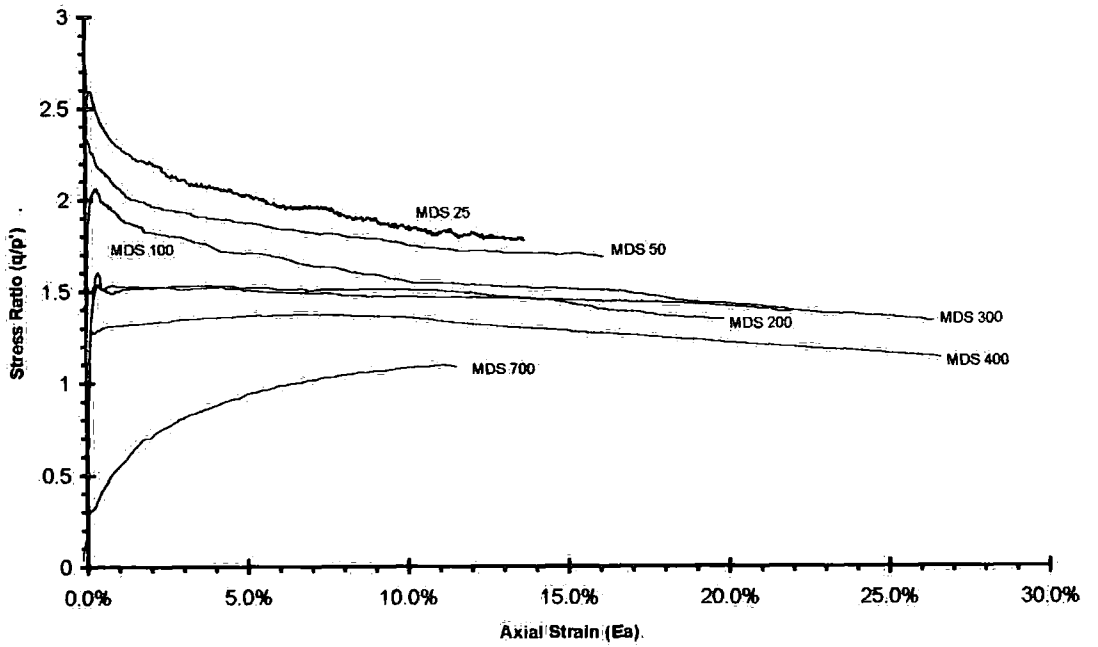

Figure 6-21 Stress ratio against strain plots for MDS tests

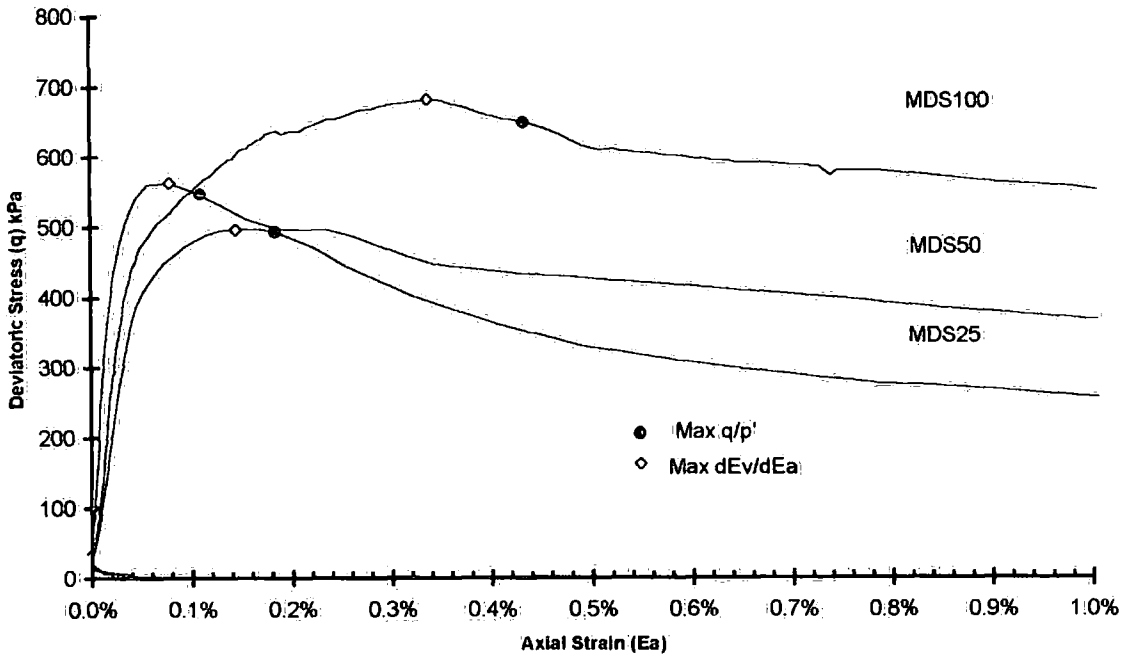

Figure 6-22 Maximum points for MDS25, MDS50 & MDS100 plotted relative to stress-strain curves

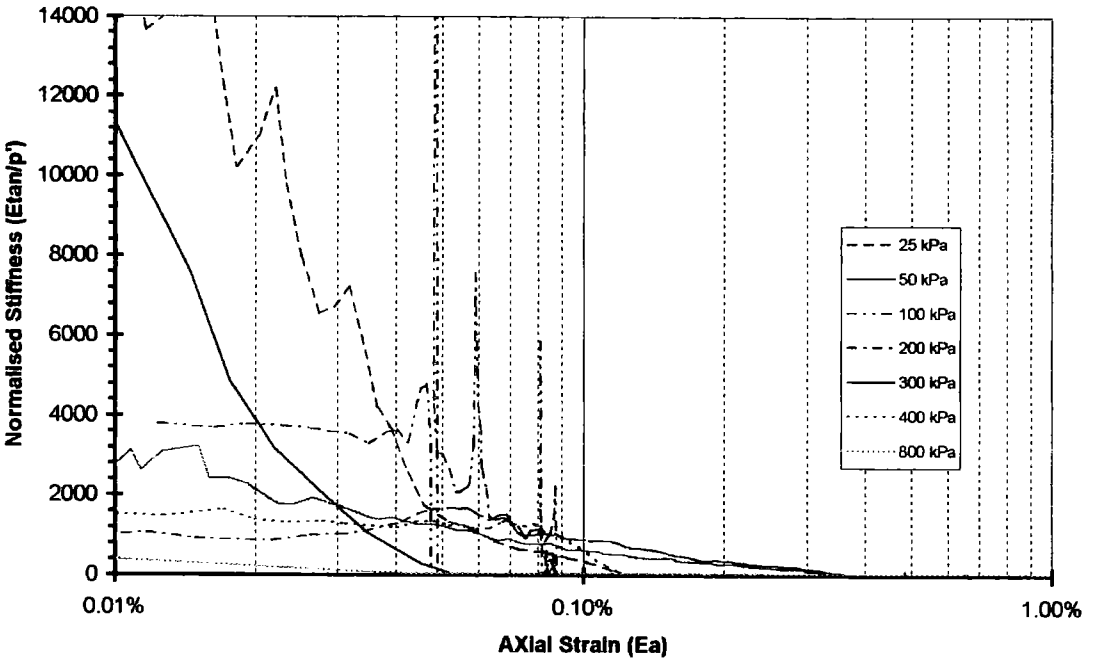

Figure 6-23 Normalised stress against strain plots for MDS tests

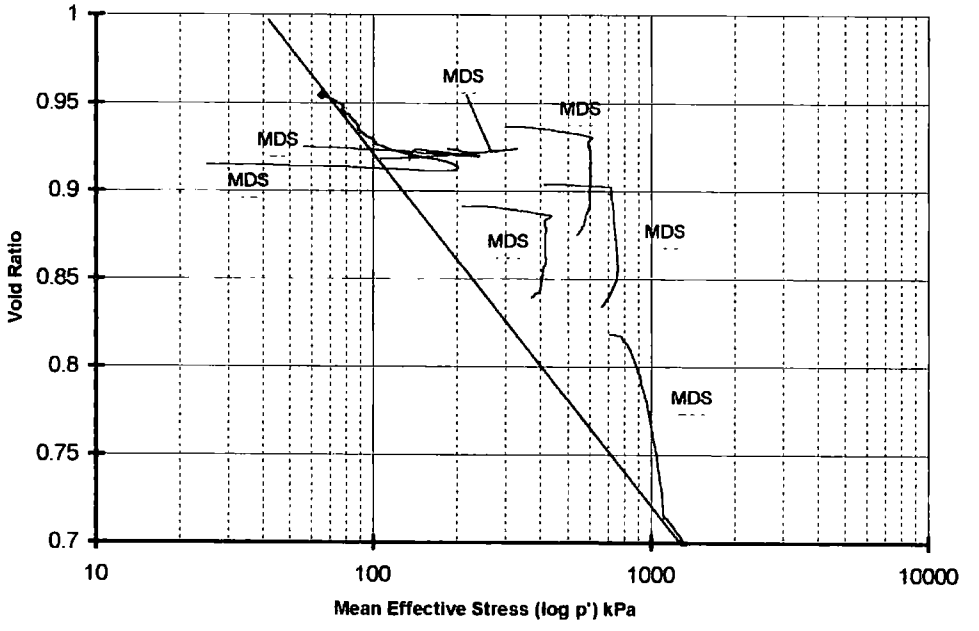

Figure 6-24 Void ratio against mean effective stress plots for MDS tests

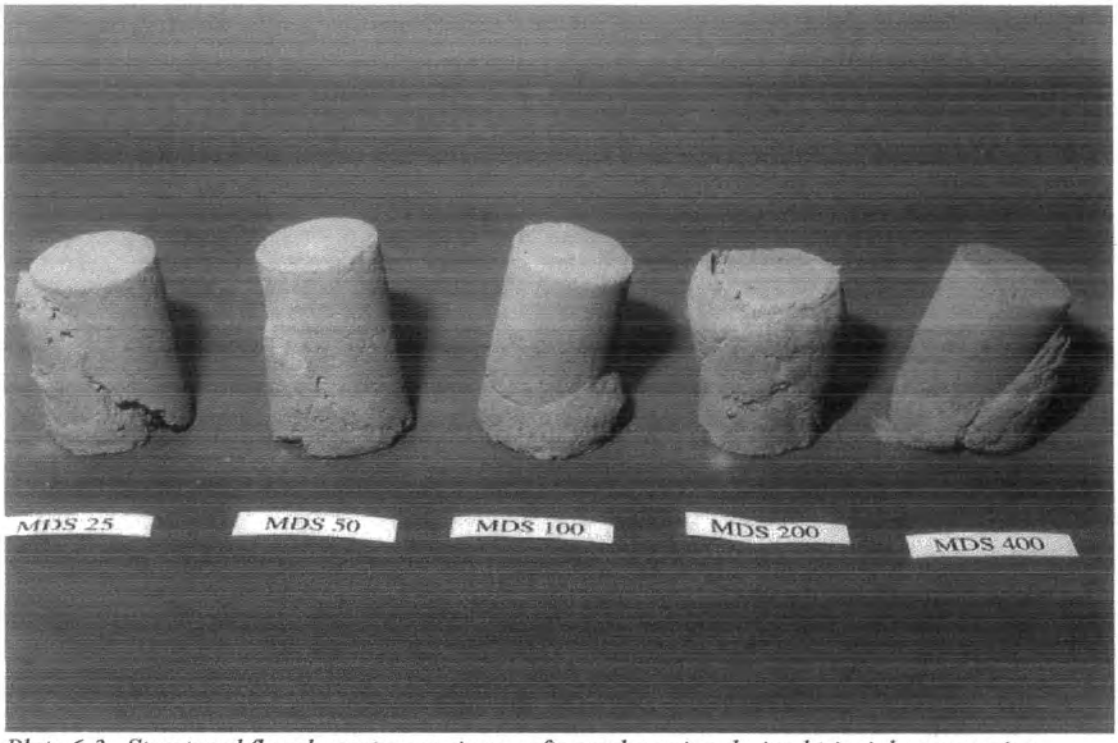

Plate 6-3 Structured fly ash mortar specimens after under going drained triaxial compression

6.2.3 Discussion of Drained Tests

The de-structured specimens were intended to represent the behaviour due to the particle-particle interaction alone. The de-structured specimens demonstrated consistent changes in strength, compression and stiffness with increasing confining pressure, consistent with behaviour of a normally consolidated granular material. The behaviour of the de-structured material in stress space, however, was different from the pattern seen in the remoulded lagoon ash (Figure 5-3). The boundary for a true remoulded material should be linear. However the boundary seen in the MDD plots (Figure 6-5) was curved. The most probable explanation was the presence of some pozzolanic bonding remaining after the de-structuring process. The evidence for this lies in the particle distributions for de-structured and structured mortar specimens when compared to the particle distribution of the original Drax ash (Figure 3-11). Both curves showed an overall increase in the size of the particles, some of which were considerably bigger. These larger grains identified in the particle size distribution must be composed of the smaller fly ash particles aggregated together by the pozzolanic reaction seen in the micrograph Plate 3-4. This was good evidence that the material used in the de-structured samples had not had all the pozzolanic bonding removed in the process of breakdown by hand and continued to breakdown further with increased stress. This was graphically shown in the stress ratio plots for the de-structured specimens (Figure 6-6) and also for the structured material (Figure 6-21). They showed reduced bond strength with increased confining pressure. Since both the structured and de-structured specimens showed the same breakdown, the curvature in the

de-structured boundary was relevant to the structured specimens as it represented the breakdown of the bonding in between the aggregated clumps. It did not however represent the true difference between the fully bonded and fully remoulded specimens. The de-structured material represents an intermediate stage of de-structuring for the structured material with the bonding between the aggregated clumps removed.

The structured specimens showed a different picture of strength behaviour compared to the de-structured specimens. At the lowest pressure of 25 kPa both the structured and de-structured samples demonstrated a peaked strength with increased axial loading (Figure 6-25a). There was a large difference in the maximum strengths and the axial strains at which the failure occurred. The bonding from the mortar gave a significantly higher strength at this pressure over the de-structured material. However, the extra strength was lost at large strains. At larger strains, the ultimate strength of the structured specimens began to converge with the ultimate strength of the de-structured samples. This occurred as the bonding was gradually broken down with the movement of the particles as the specimen deformed.

At 100 kPa (Figure 6-25b), the bonding still added to the strength of the specimen, but was again broken by large axial strain. Both the de-structured and the structured samples showed a less brittle response to loading compared to the lower pressure tests. The structured specimen showed a gradual reduction in strength for the remainder of the test as it approached that shown by the de-structured specimen. The de-structured specimen

showed a more constant strength after the initial gain in strength. The bonding was still affecting the strength of the structured specimen, although there appeared to be a greater influence due to unbonded particle contacts

At the highest pressure of 700kPa (Figure 6-25c), the stress-strain plots for the structured and de-structured samples were very similar. There was negligible difference in strength between the two. This indicated that the structural influence had virtually been lost and there was negligible effect on the sample's strength, now controlled by the interactions of the particle aggregates. The structured sample did show yield at low stress, which was not seen, in the de-structured sample, which had a more progressive loss in stiffness throughout the test. The behaviour of these two specimens was more ductile than seen at the lower confining pressures and they both showed maximum strengths occurring at much larger strains. In the structured specimen, the bonding influence was lost at very low deviator stress at the yield point and the behaviour at higher strain was due entirely to the unbonded particle-particle contact interaction.

The influence of bonding was shown to be greater at lower pressures (Figure 6-25a), but its effects could also be seen at the higher pressures tested, despite the increasing dominance of the frictional contact strength of the de-structured material (Figure 6-25b). Even at the higher pressures the loss of bond strength was apparent by the significant change in stiffness at low stresses in MDS700 (Figure 6-25c). The strength of the structured specimens also appeared to be affected more by the straining of the specimens,

and the extra strength gained was easily lost with large strains. This was demonstrated by the convergence of the ultimate strengths of structured and de-structured specimens tested under the same conditions.

Fewer yields were identified for the MDS specimens than in the lagoon specimens. Also from these yields it was possible to suggest a total yield locus as shown by Malandraki. These yields represented a change in character of the stress-strain curves from stiff responses to much more gradual increases in strength. At this point the bonding had been totally destroyed and the strength of the specimen was due to particle –particle interaction. This continued increase in strength might be associated with strain hardening, best seen in MDS 400 (Figure 6-20a)

Data from both the structured and de-structured specimens could be combined to identify a common surface in void ratio/stress space, in a similar manner to the lagoon drained tests (Figure 6-24). The structured specimens were characterised by the sharp fall in the void ratio associated with the failure of the specimen. There was little change in void ratio up to the yield point as the mean stress increased, after which the void ratio decreased rapidly with little change in mean stress. The de-structured specimens showed a more gradual change between these two states (Figure 6-8). For some structured and de-structured specimens there was a noticeable change in the direction of the path. Furthermore, there was a trend of the path's new direction, which appeared to be consistent with the CSL. The CSL could be defined by the parameters in Equ 5-1, and

listed in Table 6-3. The other soil constant was the stress ratio M. The mortar test results showed a wider variation of M than the variation observed for the lagoon fly ash. This variation occurred because of the much greater pozzolanic influence in the mortar specimens tested at low confining pressures. As indicated in the boundary for the de-structured mortar specimens, and in the particle distribution curves for the mortar specimens, the reaction in the mortar material caused the aggregation of fly ash particles. During testing, the breakdown of the bonding between the aggregations occurred first, at lower stresses, followed later by the breakdown of the aggregations themselves. In Figure 6-22 for the structured mortar, the value of the stress ratio fell with increased axial strain. This was most probably due to the breakdown of the aggregated particles with the increased strain. This was also seen in the de-structured results, (Figure 6-6) although it was less clear. It was clear that at high strains the variation in the value of M would be significantly less. Both the structured and de-structured specimens however did show a lower stress ratio limit of about 1.0 for the highest-pressure tests.

Parameter	Value
Γ	**2.26 ± 0.01**
λ	**0.075**
M	**1.0 - 1.9**

Table 6-3 - *Soil Constant parameters for the Lime/Fly Ash mortar*

The results from the MDS tests could be used as further evidence to indicate the presence of bonding in LDS100. The LDS tests at confining pressures of 100kPa and below all showed behaviour consistent with an origin on the dry side of the CSL. However, the

evidence from the maximum points for LDS100 indicated that it was a bonded specimen whilst LDS25 and LDS50 were not. A significant issue was the near constant void ratio seen in the MDS test that originated on the dry side of critical, whilst the MDD tests showed void ratio changes also seen in LDS25 and LDS50. The similarity between LDS100 and the mortar specimen was another indication of its bonded nature.

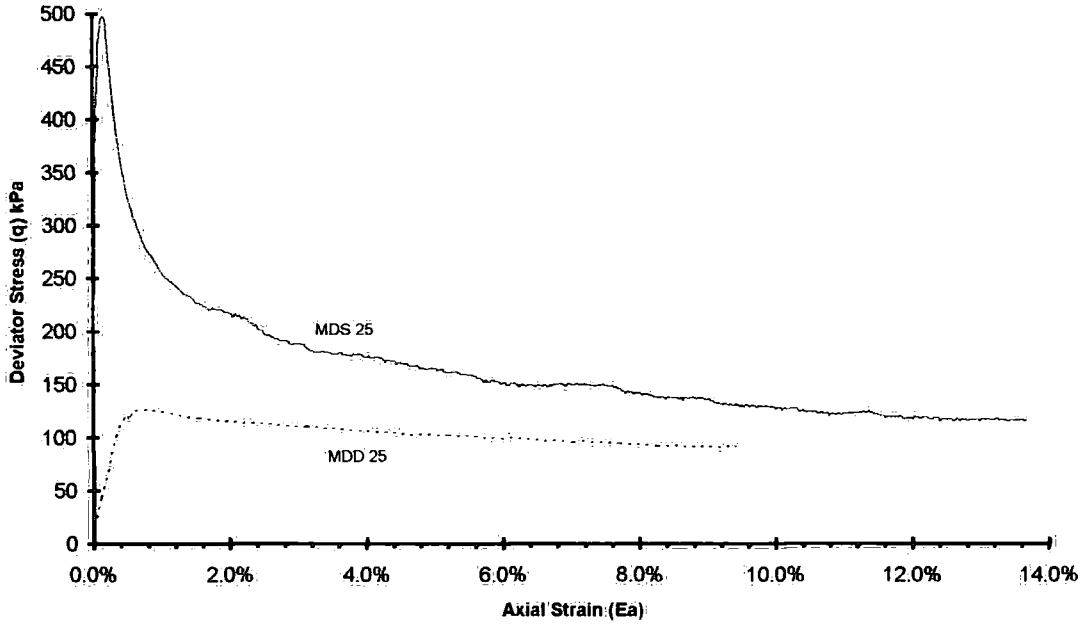

Figure 6-25a Comparison of stress-strain curves for structured and de-structured fly ash mortar specimen tested at 25kPa confining pressure

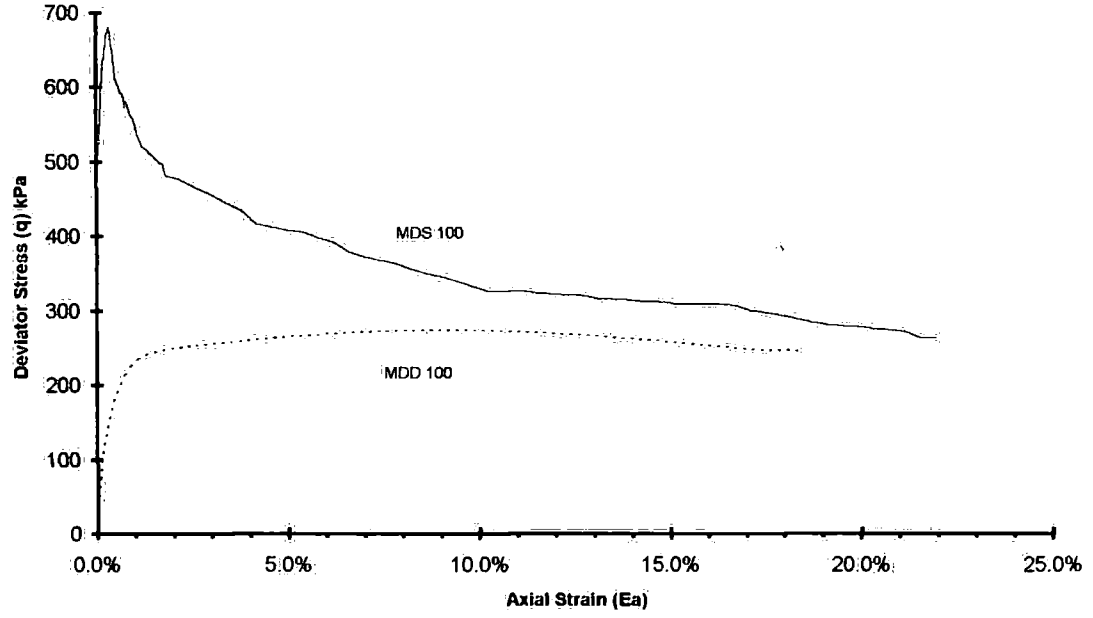

Figure 6-25b Comparison of stress-strain curves fly ash mortar specimen tested at 100kPa confining pressure

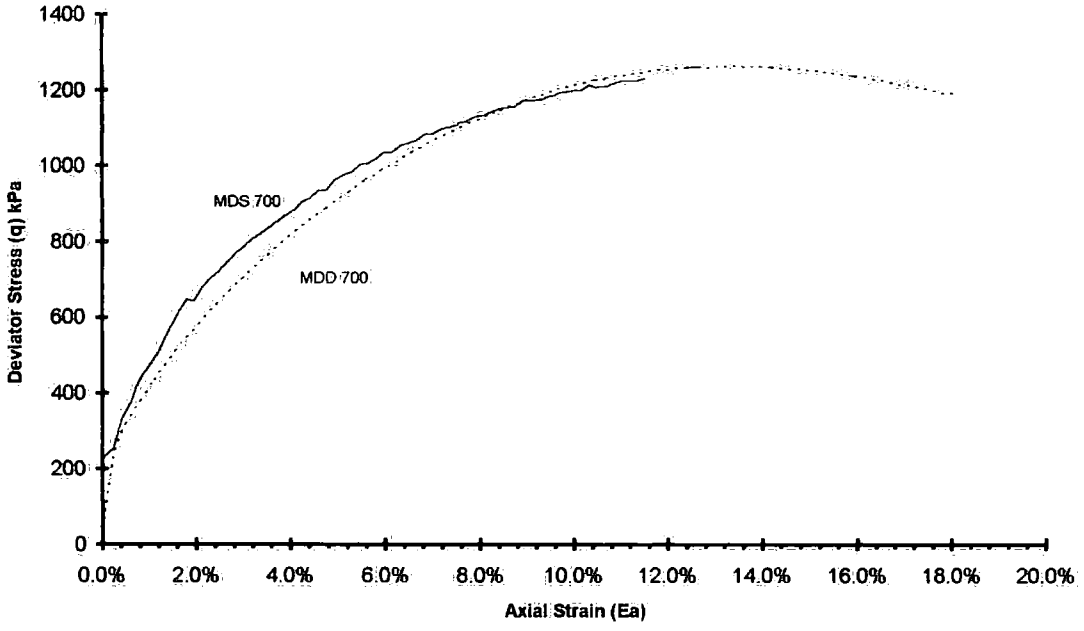

Figure 6-25c Comparison of stress-strain curves fly ash mortar specimen tested at 700kPa confining pressure

6.3 *Undrained tests*

6.3.1 De-structured samples

The de-structured samples were formed in the same manner as the specimens used in the drained tests (7.2.1) four of which are shown in Plate 6-4. Problems with the screw pumps during the high pressure tests meant that a stable pressure of 700 kPa could not be achieved. The highest test pressure possible for the de-structured material under undrained conditions was 500 kPa.

Structured Test	Moisture Content	Void Ratio [Initial]	Void Ratio [Consolidated]
MUD25	20.06%	0.918	0.906
MUD50	20.06%	0.906	0.887
MUD100	19.95%	0.919	0.863
MUD200	19.95%	0.947	0.870
MUD400	18.78%	0.936	0.866
MUD500	18.78%	0.932	0.875

Table 6-4 Parameters for MUD specimens

The plots of stress against axial strain (Figure 6-26) show that most specimens reach a peak strength, accompanied by a significant reduction in strength after further axial strain. The change from increasing to decreasing stress was a more gradual process than the sharp yields seen in the drained tests on structured samples (Section 6.2.2). The peak strength occurred at about 1% axial strain for most specimens, except for MUD50, which

peaked at only 0.2% axial strain. The post peak reduction in strength became proportionally bigger with increased confining pressure.

The plot of change in pore water pressure against axial strain (Figure 6-27) showed that all the samples increase in pore water pressure with increasing axial strain. The initial increase in pore water pressure occurred within the first 1% of axial strain for all tests, while the deviator stress was increasing. For most tests, after the initial increase, the rate of change in pore water pressure decreased to a relatively low rate of increase until the end of shearing.

All of the de-structured specimens showed similar stress path shapes in p'-q stress space (Figure 6-28). The paths defined a common bounding surface for the de-structured material under undrained conditions. This bounding surface could not be defined by a straight line but appeared to be a shallow curve, and more nearly linear than the boundary from the drained tests. The stress paths could be considered in two parts based on pre and post peak strength. In the first part of the test the stress increased to a maximum, and in the second part the stress reduced as the stress path passed through this maximum. The second parts of the stress paths for these specimens all showed the same behaviour of increasing pore water pressure with decreasing strength. MUD200 and tests at lower pressures had relatively large changes in pore water pressure and their paths were well to the left of the initial main stress (they followed almost constant σ_1'). In 400 kPa (MUD400) the initial stress path followed a path much closer to constant p', with a lower

rate of change in pore water pressure. In MUD500 the rate of change in pore water pressure was lower still and the stress path showed increasing p' to the right of the initial mean stress (close to constant σ_3').

The plot of q/p' stress ratio against axial strain (Figure 6-29) showed a rough trend of increasing stress ratio with increasing confining pressure at 10% axial strain. However, this trend was lost upon further strain as the ratios for MUD25 & MUD100 continued to increase and the values for the other tests reduced slightly. This would seem to indicate the lack of any significant trend in the de-structured material with respect to confining pressure in these results.

Plots of the stiffness normalised with respect to the confining pressure against the axial strain (Figure 6-30) showed no discernible pattern relating the effects of pressure to the samples' stiffness. The reduction in the stiffness with increasing axial strain showed a constant reduction over the tests to the point of failure at about 0.5% axial strain.

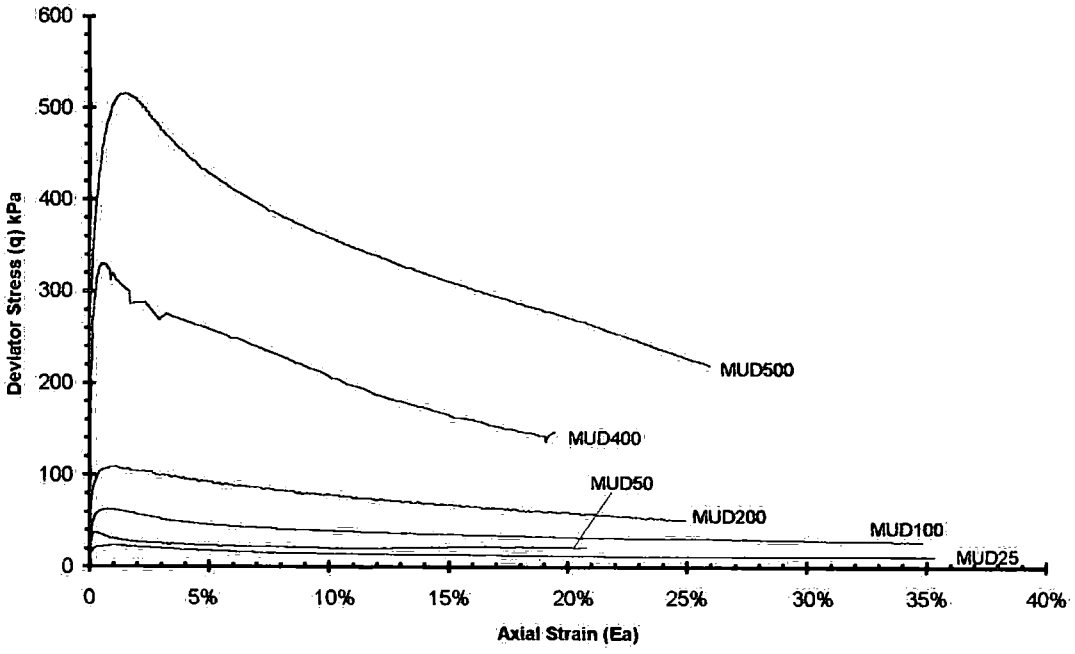

Figure 6-26 Stress against strain plots for MUD tests

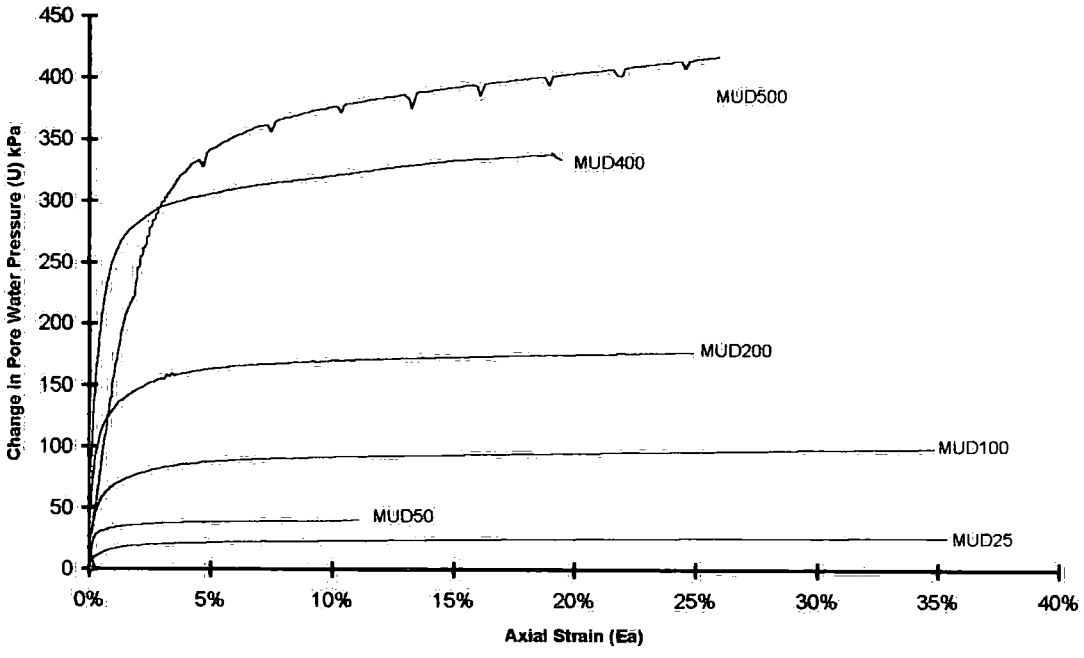

Figure 6-27 Changes in pore water pressure versus strain plots for MUD tests

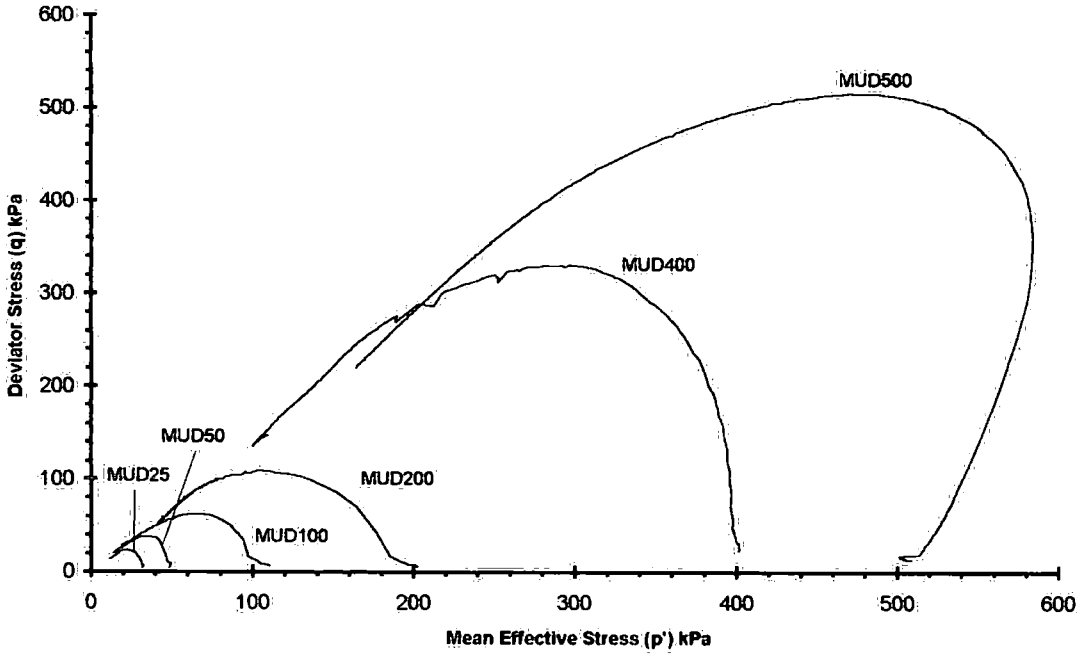

Figure 6-28 Effective stress paths plots for MUD tests in stress space

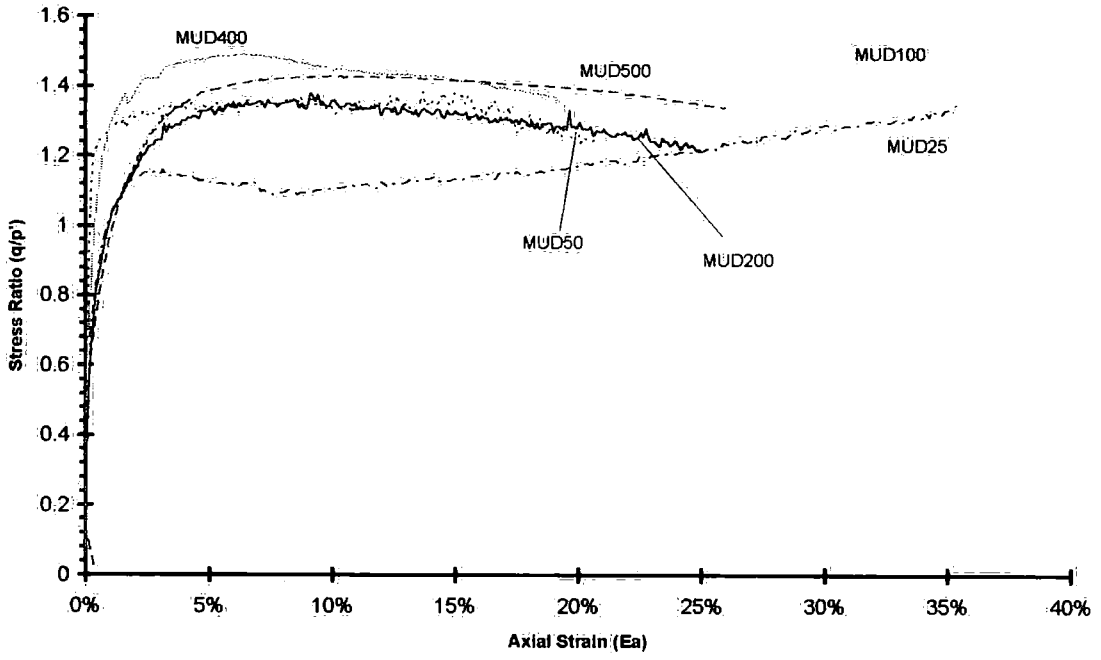

Figure 6-29 Stress ratio against strain plots for MUD tests

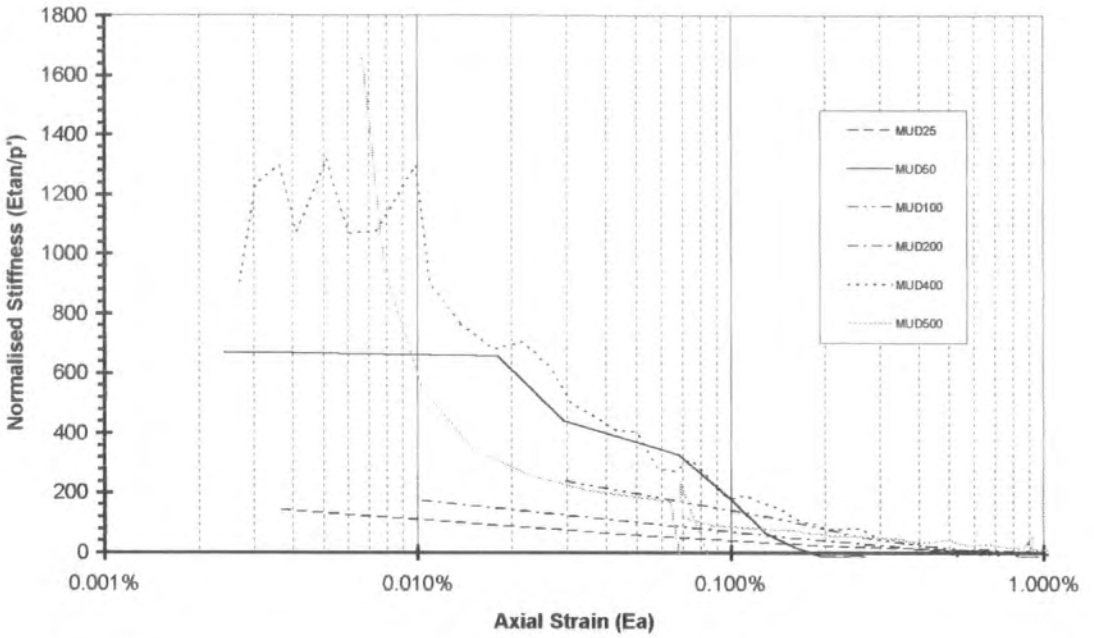

Figure 6-30 Normalised stiffness against strain plots for MUD tests

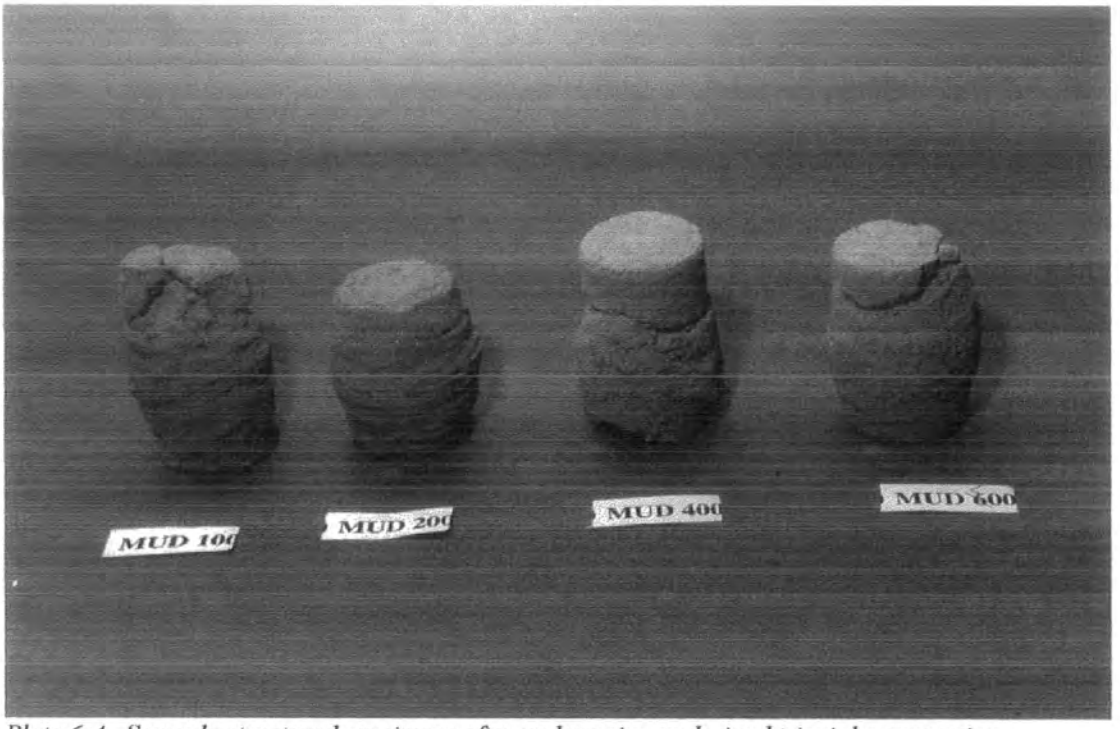

Plate 6-4 Some de-structured specimens after under going undrained triaxial compression

6.3.2 Structured Samples

The structured samples were all prepared in the same manner as the structured samples used in the Drained tests (section 6.2.2) and are shown in Plate 6-5. The initial properties are listed in table 6-5 below.

Structured Test	Moisture Content	Void Ratio [Initial]	Void Ratio [Consolidated]	Curing Time (Days)
MUS25	**16.90%**	**0.915**	**0.910**	**53**
MUS50	**17.71%**	**0.937**	**0.926**	**45**
MUS100	**18.44%**	**0.920**	**0.910**	**48**
MUS200	**18.60%**	**0.933**	**0.902**	**43**
MUS400	**18.52%**	**0.927**	**0.897**	**43**
MUS800	**18.80%**	**0.931**	**0.881**	**42**

Table 6-5 Parameters for MUS specimen and curing times

For two of the tests MUS800 and MUS200 the internal strain measuring devices were unavailable, and the plot of stress again axial strain (Figure 6-31) demonstrated the difference in the response to loading of the external devices compared to the internal devices used in the other tests of the group. The difference between the two methods was graphically demonstrated in a plot of stress against axial strain for MUS50 for the two methods (Figure 6-32). This was also shown in an unload-reload cycle at the start of MUS100 (Figure 6-33) where the comparative reactions of the two displacement measurement methods were plotted together. Where the internal devices were used in the

undrained group of tests the peak strengths occurred at about 1% axial strain, whereas for MUS600 and MUS200 the peak strength occurred at around 3% axial strain.

The fall off in strength after the peak was sharper in the tests on the structured samples than the de-structured tests under the same conditions (Figure 6-26). Below a mean effective stress of 200 kPa the peak strength of these specimens (MUS25 & MUS100) shared a similar level of stress, with MUS50 showing a slightly lower strength. There was also evidence of a constant ultimate strength level for each test. This behaviour was not seen in the de-structured specimens, which showed consistent rates of strength loss after failure. The ultimate strengths for MUS50, MUS100, and MUS200 were similar and were joined by MUS800 at 25% axial strain. For MUS25 and MUS400 the ultimate strengths were slightly higher.

The changes in pore water pressure against axial strain (Figure 6-34 & 6-35) for these specimens showed a change in behaviour between 100kPa and 200 kPa. The low pressure tests (Figure 6-34) showed a significant reduction in pwp after an initial rapid increase. The decreases in the three tests MUS25, MUS50, MUS100 were relatively similar and it was the rapid increase that separates the plots, which increased with increasing confining pressure.

The higher pressures tests were plotted in Figure 6-35. By MUS200 the change in pore water pressure had recovered to the same level seen in MUD200, its de-structured

equivalent (see Figure 6-27). It had only a slight decrease in pore water pressure after the initial increase (Note the response appeared 'slower' than the other tests due to the use of external strain measurements). The structured specimens tested at higher pressures also had equivalent pore water pressure changes to the de-structured samples. This could be related to the confining pressure being applied. This indicated that the specimens at the higher pressures were deforming in a similar manner to the de-structured specimens

The stress paths for the structured specimens plotted in p'-q stress space (Figure 6-36) showed a change in stress path behaviour between 100 and 200 kPa. The lower pressure tests showed decreasing pore water pressure, and the tests at higher pressures showed increasing pore water pressure throughout the tests, which could be related to the pwp plots of Figures 6-34 & 6-35. The strengths of all the specimens passed well above the boundary surface indicated by the de-structured specimens. Upon failure of the specimens, the stress paths dropped towards the de-structured boundary, as the bonding broke down. However, they did not reach the boundary surface at the same points as the de-structured specimens.

The tails of the stress paths showed different patterns to those seen with the lagoon fly ash. The lower pressure tests showed very small changes in p' as the strength decreased post-peak. The stress paths fell nearly vertically in p'-q stress space towards the trend indicated by the higher pressure structured tests. They were irregular, marked by fluctuations along directions of constant stress ratio. The fluctuations might be associated

with progressive failure as the specimen began to deform along an uneven shear surface. The tails of the higher-pressure tests appeared to follow a rough trend towards the origin at a slightly higher friction angle than the de-structured tests.

The plots of stress ratio against axial strain (Figure 6-37) showed a distinction between the low pressure tests up to 100 kPa, marked by their peaked maximum, and higher pressure tests, which showed a rise to the maximum but show no distinct peak ratio. This was consistent with the change in the stress path shapes. There were no obvious trends linking stress ratio to confining pressure as seen in the drained tests on mortar material.

The plots of normalised stiffness against axial strain (Figure 6-38) showed only the tests where internal strain measuring devices were used. The plots demonstrated the reduction in stiffness response with increasing confining pressure. At low pressure, MUS25 did not show the highest stiffness (due to insufficient data), although it did remain stiffer for longer. As the pressure was increased further, the rate change in stiffness remained relatively constant for MUS50 & MUS100. Above this pressure there was a marked reduction in the stiffness, and the stiffness in MUS400 reduced to a level similar to its de-structured equivalent (see Figure 6-30).

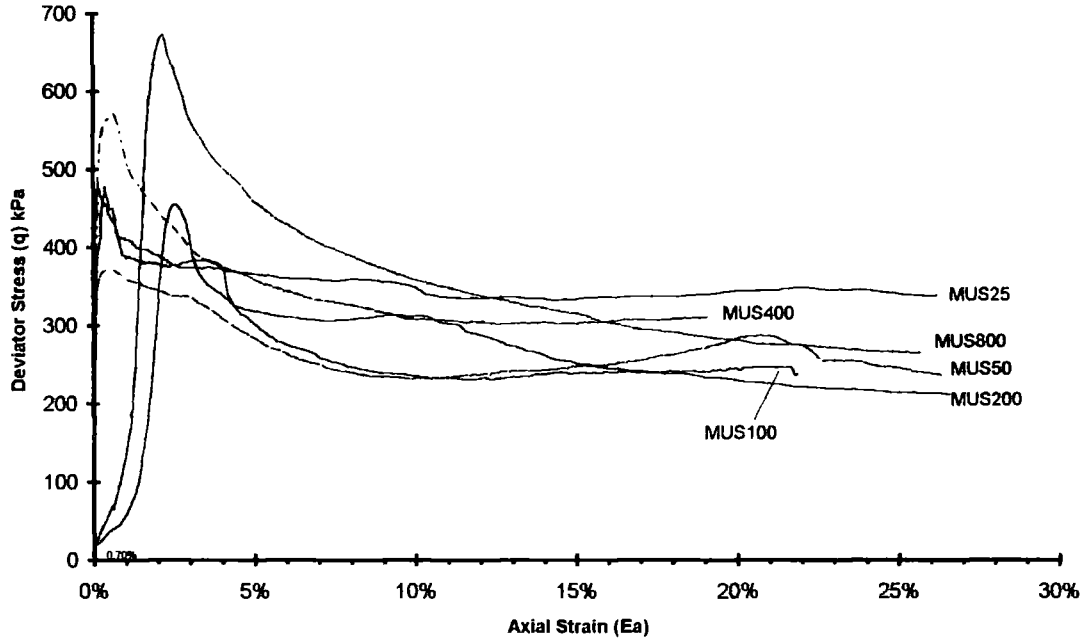

Figure 6-31 Stress against strain plots for MUS tests

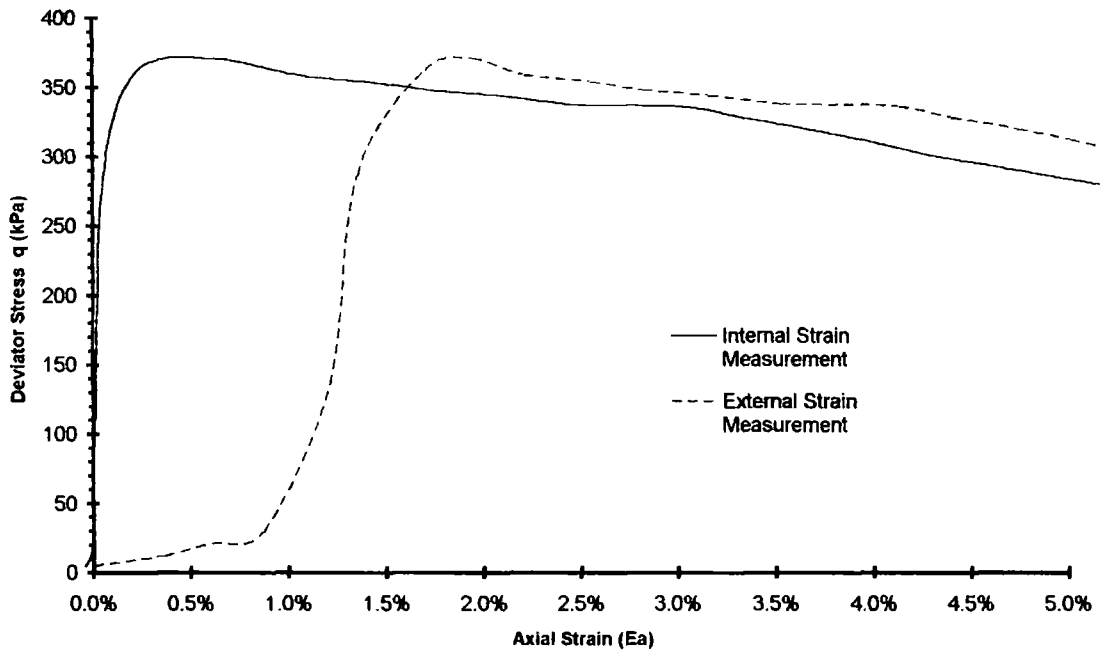

Figure 6-32 The difference between internal and external strain measurement when considering small strains (<1.0%) in LUS50

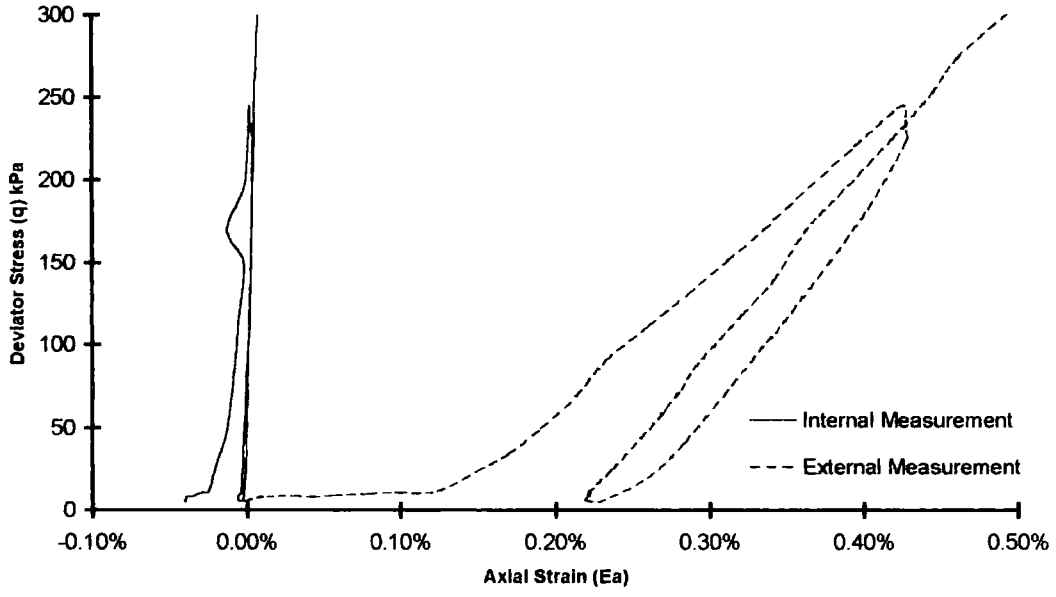

Figure 6-33 The difference between internal and external strain measurements of a small unload/reload cycle at the beginning of LUS100

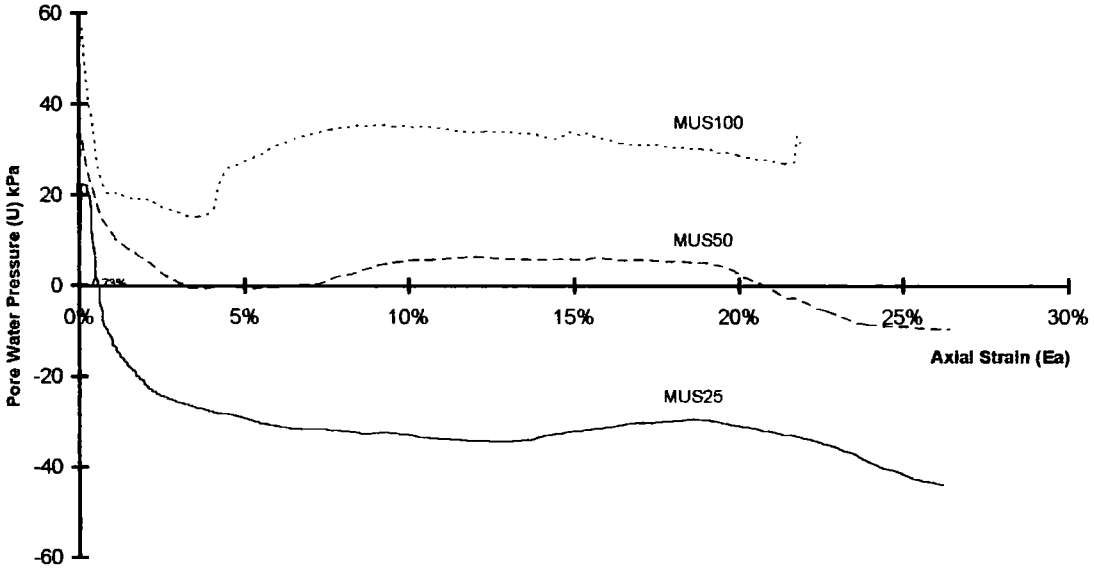

Figure 6-34 Changes in pore water pressure against strain plot for tests at 100kPa confining pressure and below

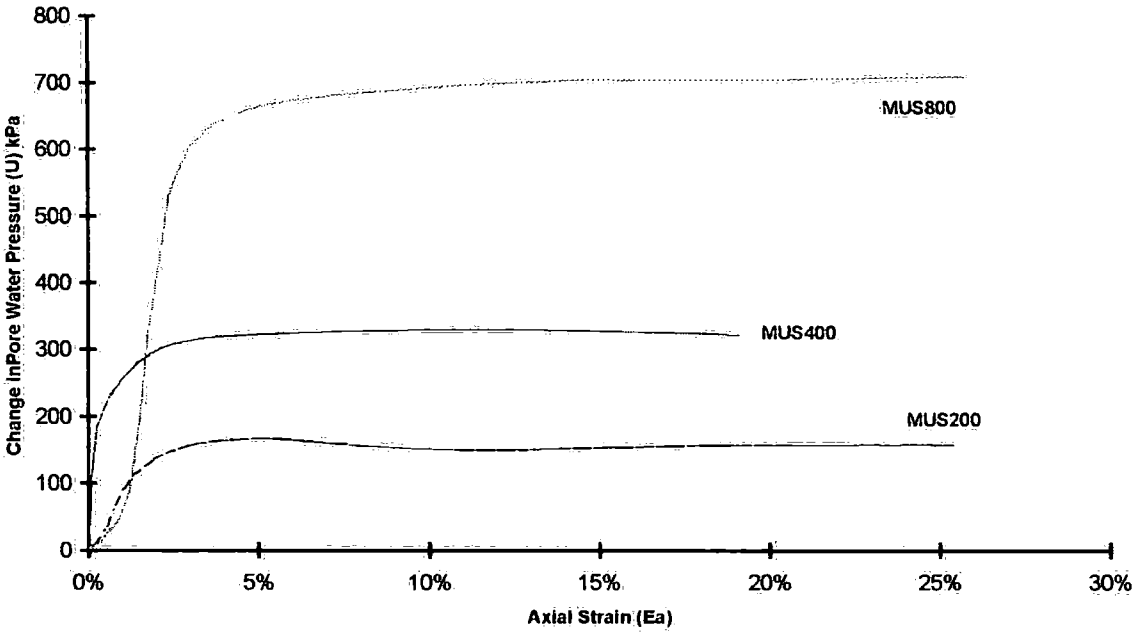

Figure 6-35 Changes in pore water pressure against strain plot for tests at 200kPa confining pressure and above

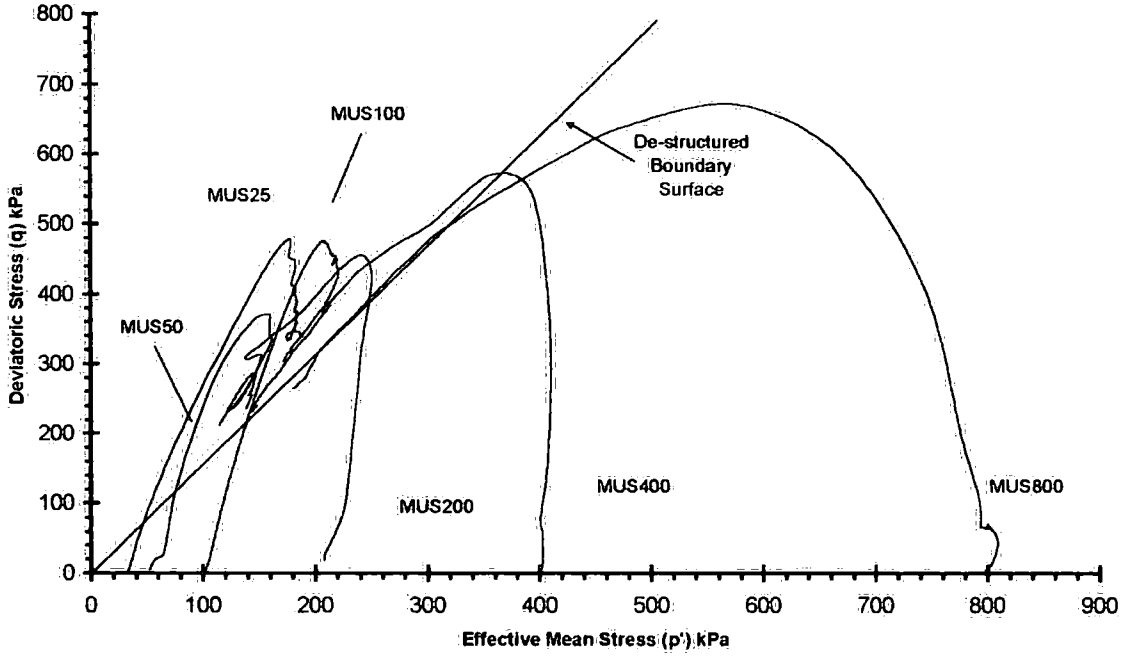

Figure 6-36 Effective stress paths for MUS tests

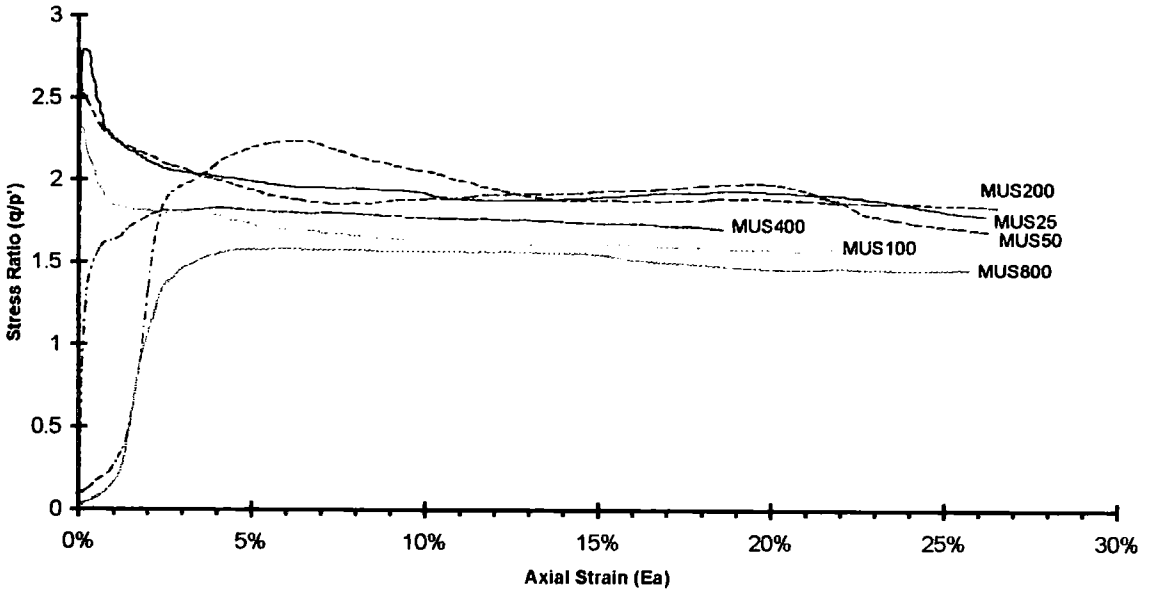

Figure 6-37 stress ratio against strain plots for MUS tests

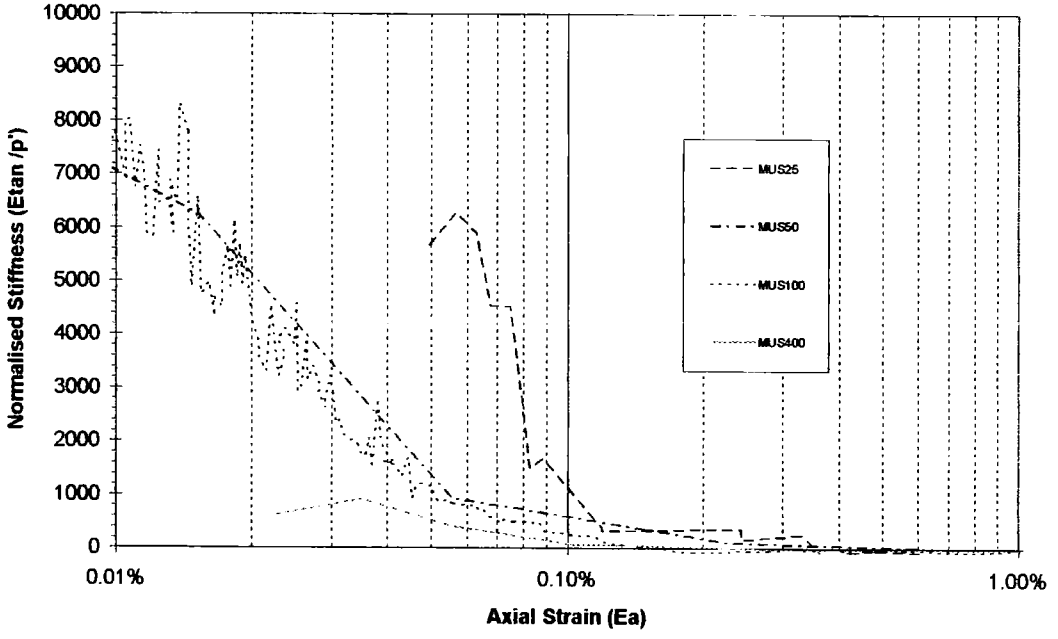

Figure 6-38 Normalised stiffness plots for MUS tests fitted with internal strain measuring devices

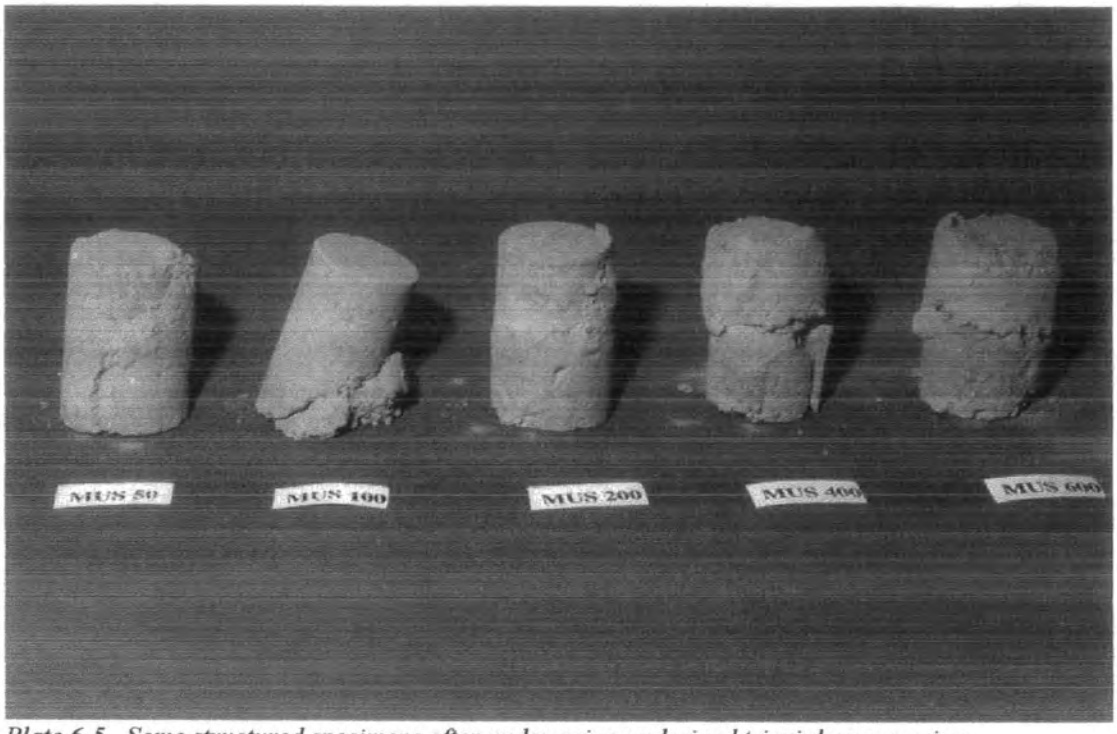

Plate 6-5 Some structured specimens after under going undrained triaxial compression

6.3.3 Discussion of Undrained Tests on Mortar Specimens

The structured specimens showed increased strength when compared to the de-structured specimens, the difference being greater at low confining pressures. The strength difference between the two decreased as the confining pressure increased. At 25 kPa (Figure 6-39) the structured sample demonstrates a peak strength, which occurred at a lower axial strain than in the de-structured specimen, followed by a sharp reduction to a near constant level for the remainder of the test up to 28% axial strain. The de-structured sample in comparison had a very low strength of only 5% of the structured sample. It too showed a post maximum strength reduction, but the change was more gradual as it reached an ultimate strength by the end of the test. The ultimate strengths of the structured samples were significantly higher than the strengths of the de-structured samples, despite having higher void ratios.

At a confining pressure of 100 kPa (Figure 6-40) the de-structured sample achieved 13.5% of the strength of the structured specimen. The structured specimen showed a greater reduction in post peak strength but there was still a large difference in the ultimate strengths.

At a higher confining pressure of 400 kPa (Figure 6-41) the de-structured specimen showed more than 50% of the strength of the structured specimen. Despite the large post

peak strength reduction in the structured sample, there was still no convergence of the ultimate strengths of the structured and de-structured specimens.

Tests at higher confining pressures showed a progressive reduction in the influence of bonding on the behaviour. At low pressure the bonding had a significant influence on the specimen's strength.

The differences in ultimate strength were probably due to the different pwp responses. The structured samples continued to dilate after failure, causing negative pore water pressures, which increased the friction between particles. The difference in ultimate strengths reduced with increasing confining pressure, as the effects of bonding were reduced.

Due to the sandy/silt size nature of fly ash particles the build up in negative pore pressure had a significant effect on the strength of the structured specimens. The de-structured specimens did not show the same degree of build up in negative pore pressure for these void ratios. As both structured and de-structured samples were formed by the same process and to the same void ratio they would be expected to have similar pore sizes. However, the negative pore pressures recorded in the tests suggest that the structured material had smaller pore spaces. The change in pore size must be linked to the pozzolanic activity, which was the main difference between the two specimen types. The pozzolanic reaction forms calcium silicate hydrate needles. These extend into the pore

space, binding particles together where they contact and furring up the open surfaces. The occurrence of needle growth into the pore space has been noted previously (e.g. Helmuth (1989), Ying (1992)). These fine needles were probably lost in the de-structuring process, and did not influence the behaviour of the de-structured specimens. This meant that if there was any pozzolanic activity within the compacted ash, its strength might be influenced by rapid loading, which might damage the needle-like forms and so cause smaller pore voids.

In the structured results there was an apparent change in behaviour between 100 & 200 kPa. This was seen in the plots of pore water pressure against axial strain, stress paths in stress space and stress ratios against axial strain (Figures 6-34, 6-36 & 6-37 respectively). No such change was observed in the de-structured tests and so it might be assumed that this was a function of the pozzolanic bonding present in the structure and missing in the de-structured soil. This difference was also seen in the lagoon specimens and investigated in the LUS 100-200 group of tests (Section 5.2.3)

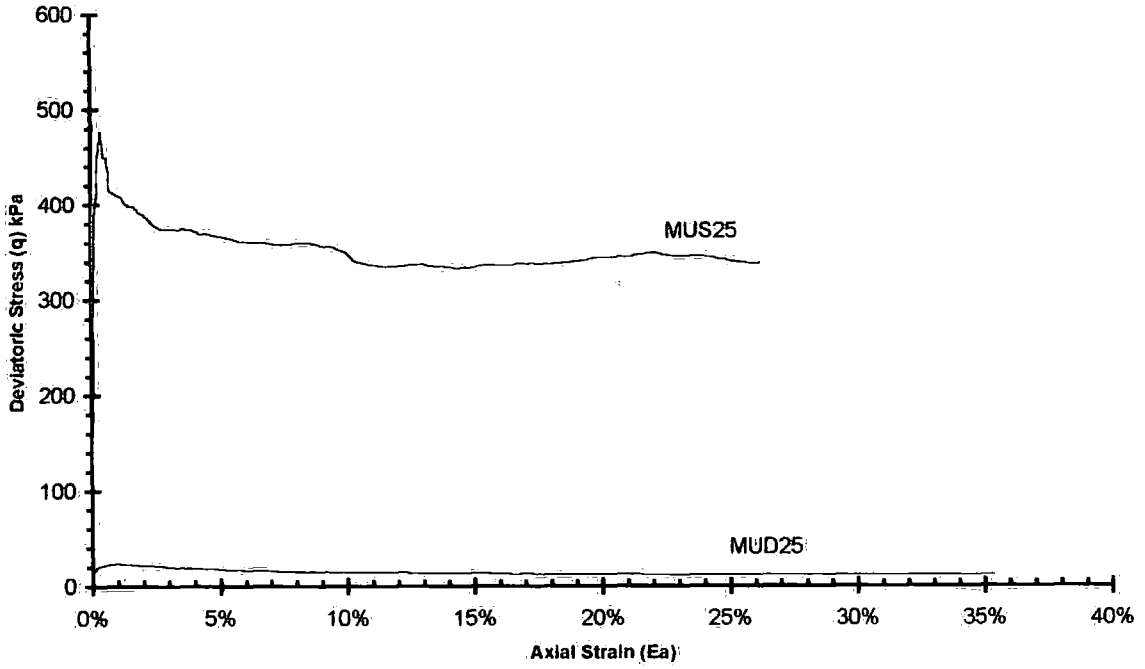

Figure 6-39 Comparison between structured and de-structured stress-strain curves for specimen tested at 25kPa confining pressure

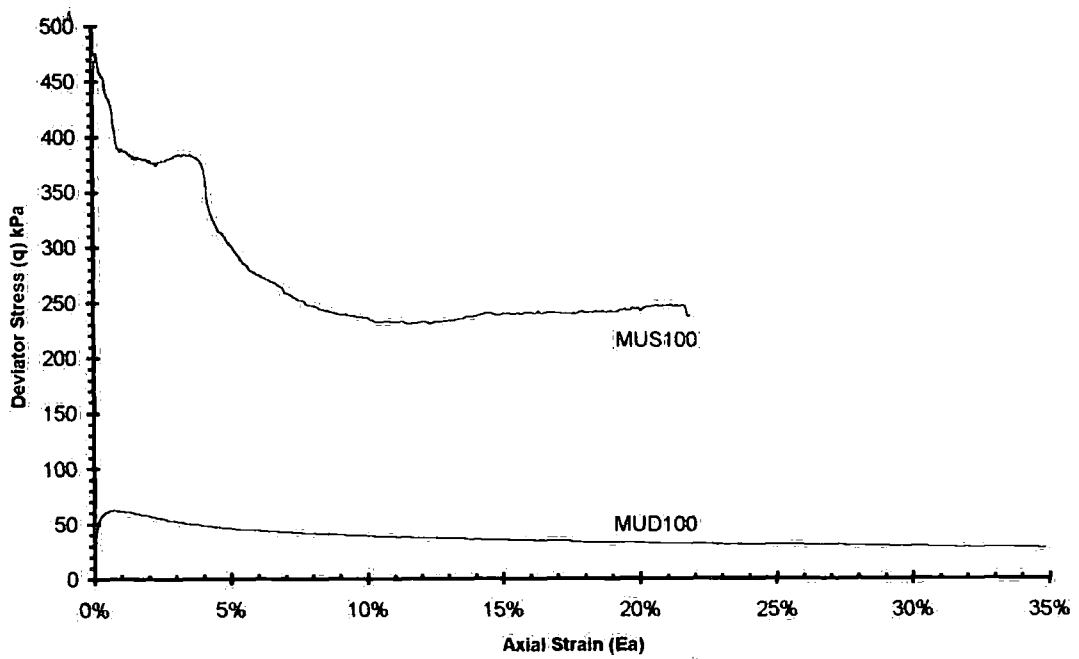

Figure 6-40 Comparison between structured and de-structured stress-strain curves for specimen tested at 100kPa confining pressure

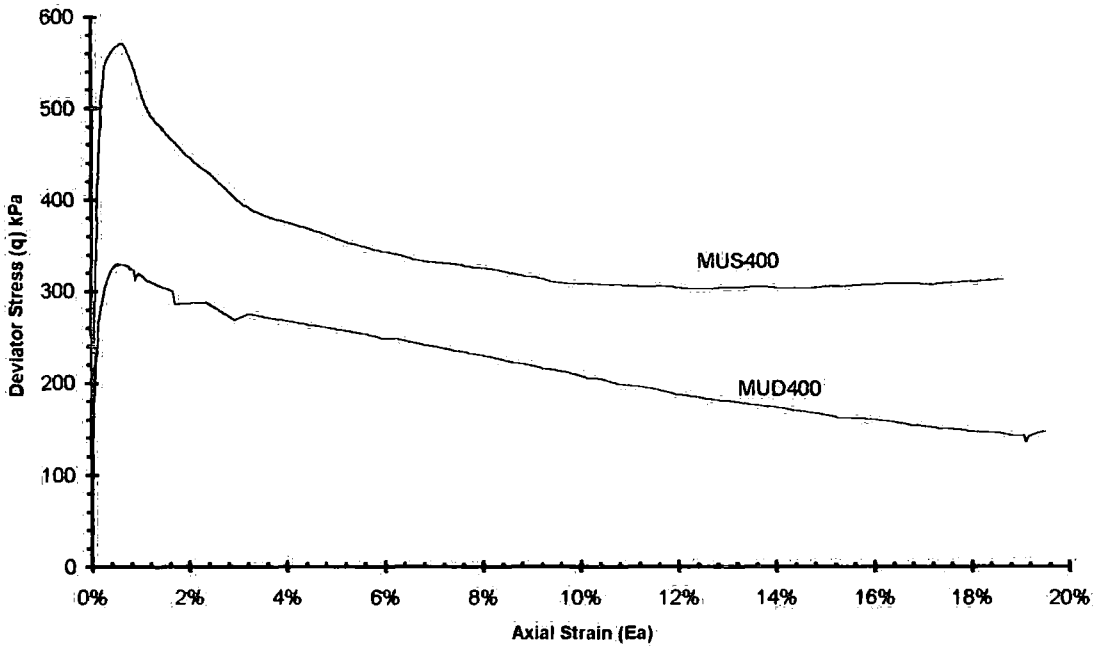

Figure 6-41 Comparison between structured and de-structured stress-strain curves for specimen tested at 400kPa confining pressure

6.4 Discussion of tests on Mortar Specimens

Comparisons between the test results of structured and de-structured specimens under both drained and undrained testing conditions has demonstrated the full potential influence of pozzolanic activity on the behaviour of the fly ash. The pozzolanic bonding has had its greatest influence at low confining pressures, where there has been a significant increase in the material's strength and stiffness. These were subsequently lost with increased axial straining of the specimens.

The reduction in the structural influence with increasing confining pressures has been demonstrated well by the normalised stiffness plots (Figures 6-7, 6-22, 6-30 & 6-38). These have been normalised with respect to the confining pressure and show the de-structured material as having very low stiffness.

Both the drained and undrained tests for the de-structured material showed a slight curvature to the boundary surface (Figures 6-5 & 6-28 respectively). The curvature was most noticeable in the drained test and was linked with the reduction in stress ratio with increasing confining pressure. This was the result of breakdown of discrete aggregations of grains, which remained after the de-structuring process. In the undrained tests there was no obvious consistent reduction in stress ratio with confining pressure. These undrained tests showed that the material underwent a significant loss in strength with

increasing axial strain due to pore pressure increases, which was not seen in the corresponding drained tests.

The two test conditions could also be differentiated by the boundary surfaces of the structured specimens (Figure 6-42). The build up in pore water pressure in the undrained specimens had a significant effect on the structure. At low pressures the peak strength remained relatively constant. It was only at higher confining pressures above 200 kPa that the peak strength began to increase. This was likely to be caused by the increasing influence of the particle-particle friction to the specimen's strength at these higher pressures. At lower pressures, negative pore water pressures developed after initial pore water pressure rise. When there was no longer the reduction in pore water pressure between 100 and 200kPa a small fall in strength was observed. The amount of structural breakdown was increased as confining pressure increased, which was shown in the reduction in the stress ratio from MUS200-MUS800 (Figure 6-37). This pattern of behaviour contrasted well to the gradual changes seen in the drained tests.

At larger axial strains, under drained conditions, the strengths of the structured specimens closely resembled those of the de-structured material. This is an indication of the degradation of the bonding within the structured specimens. This was not the case for the undrained specimens, where the structured specimens remained significantly stronger than those made of de-structured material, due to the effects of pore water pressure. The structured and de-structured specimens had different stress paths and met the boundary at

different points (Figure 6-43), which accounted for the different ultimate strengths. At higher confining pressures the influence of the structure on the strength and the stiffness was reduced, and at 700 kPa, in drained conditions, there was no strength advantage provided by the pozzolanic bonding (Figure 6-25c). However the bonding still affected the response of the specimens to loading, which could be seen by the stiffer response of MDS700.

From the results of tests under drained conditions, areas in stress space were outlined where the material could be described as being either in the stable region or in the region of potential collapse (Figure 6-45). The stable region was the area below the boundary line for the de-structured material, and the potential collapse region was the area in stress space between the boundary surfaces defined for the de-structured and structured materials Only the pozzolanic activity allowed the material to exist in this region. The potential collapse region for the undrained tests was much reduced and related to confining pressures below 200 kPa. This is the same region where the pore pressures are considered to influence the pozzolanic bonding most. So the detrimental effects of pore pressures in the undrained tests reduces its sphere of influence.

6.4.1 Relationships between test on mortar and lagoon fly ash specimens

The purpose of the programme of tests on mortar specimens was to provide an assessment of the full potential of pozzolanic bonding of fly ash. The formation and pozzolanic bonding of the mortar specimens was standardised by careful control of the lime content, curing time and void ratio. Variations in bonding, fabric, and the presence of random laminations had restricted the scientific study of the pozzolanic influences in the lagoon ash specimens. Strength gain from bonding was very substantial in the mortar compared to its weakness and randomness in the lagoon ash samples. However the de-structuring process was only partially effective in the case of mortar specimens, which still contained bonding in the form of discrete aggregates of grains. Whereas the de-structuring (remoulding) of the lagoon ash samples appeared to be complete

The strength gain from bonding reduced with increasing confining pressures in a consistent pattern for both mortar and lagoon ash samples (see Figure 6-45). The break-down of this pozzolanic bonding appeared to be a function of confining pressure, irrespective of the bonding strength. Results of undrained triaxial tests showed smaller pozzolanic strength gains than were achieved in drained tests, for both mortar and lagoon ash materials. Leonards & Bailey (1982) hypothesized that failure to expel air, trapped by irregular particle shapes and holes and crevices within the fly ash particles, may contribute to the bleeding and pumping phenomena they observed. These same irregular pore spaces can also be considered to be present within the specimens used in this research. In the

undisturbed lagoon material pore sizes were smaller because of layering and the features outlined by Leonards and Bailey above. In the mortar specimens there was not the same layering but there was the growth of crystals into the pore spaces restricting their size. The destructive effects of pore pressure on bonding may have been due to smaller irregular pores restricting the movement of water through the specimens.

Both lagoon ash and mortar specimens showed multiple yielding and not the characteristic two-stage yielding often used by other authors. Multiple yielding of the lagoon ash specimens was due to sequential breakdown of different layers whilst the multiple yields seen in the mortar specimens were probably due to the non-uniform nature of the bonding framework. It was still possible to identify the more classic 'first yield' and 'second yield', which could be ascertained from major changes in the stress-strain curves. The clearer information from the mortar tests allowed the identification of a total yield in some tests, which was not possible from the lagoon material.

The results demonstrated differences in the internal structure of the bonding between the two different fly ash forms. The lagoon specimens were heavily laminated and their anisotropic nature was characterised by slightly curved yield loci roughly parallel to the mean effective stress axis. The mortar specimens were designed to be homogeneous and isotropic. This was shown by their yield loci, which were convex curves characteristic of bonded isotropic soils

A CSL was identified for the lagoon material, based on results of oedometer and triaxial tests. Triaxial test results on mortar specimens showed a fair agreement with the CSL, indicating that the CSL might apply to the fly ash generally, although no other such information could be found in the literature. Tests conducted at up to 800kPa confining pressure failed to reveal a sharp modification to the CSL at high pressure as has been suggested by Been *et al* (1992).

Other research into fly ash mostly centres on its use as an additive to cement as well as its use as a fill material and stabilizer for soft clay soils. When its pozzolanic activity is studied most authors use unconfined tests to quickly assess the effects from changes in constituents or curing times or conditions. There are some triaxial tests that allow for some comparisons to be made to the results of this research.

In Section 5.4.3.4 the results of the lagoon undrained tests were compared to those of similar tests by Idraratna et al (1991). They showed a close resemblance of their residual behaviour but slightly higher strengths. When compared to the mortar material for the same testing conditions (Figure 6-46) the mortar specimens were significantly stronger. This is most probably due to the different chemical compositions of the two fly ashes or the method of formation. The increased strength of the mortar specimens over the Indraratna tests are overshadowed by the strength of fly ash specimens tested by Yang (1992). Figure 6-47 shows the significantly greater strength and stiffness of the Yang tests over those of both the mortar and lagoon specimens at the same confining pressures.

This comparison demonstrates the wide variations possible in the potential strength gains for one fly ash to another. This indicates that the variations seen in the undisturbed lagoon specimen represent only part of the problems that may arise when comparing different fly ash. The results of the mortar tests however show that by using a consistent source of material the underlying characteristics can be better defined.

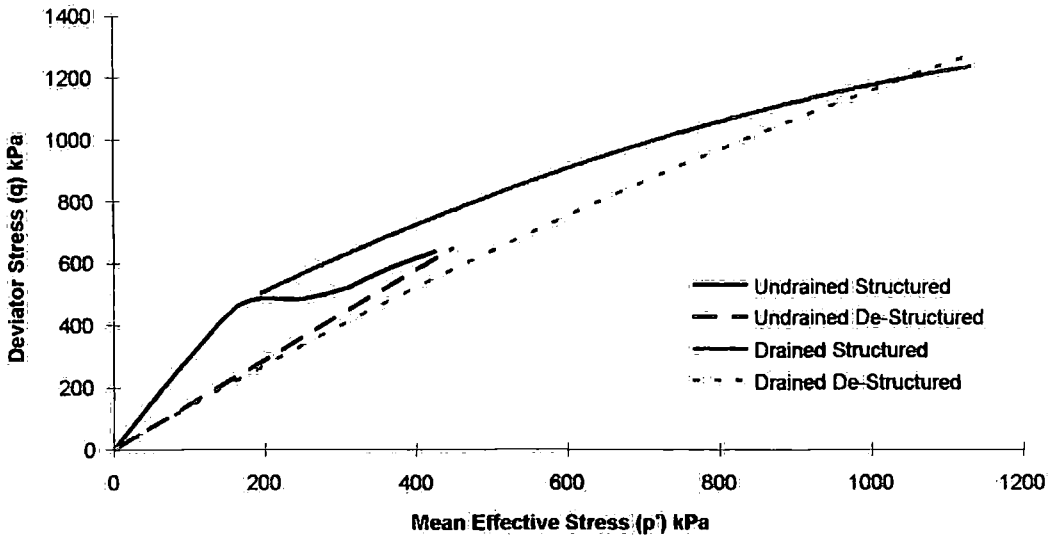

Figure 6-42 Comparison between the boundary surfaces for the two triaxial testing conditions

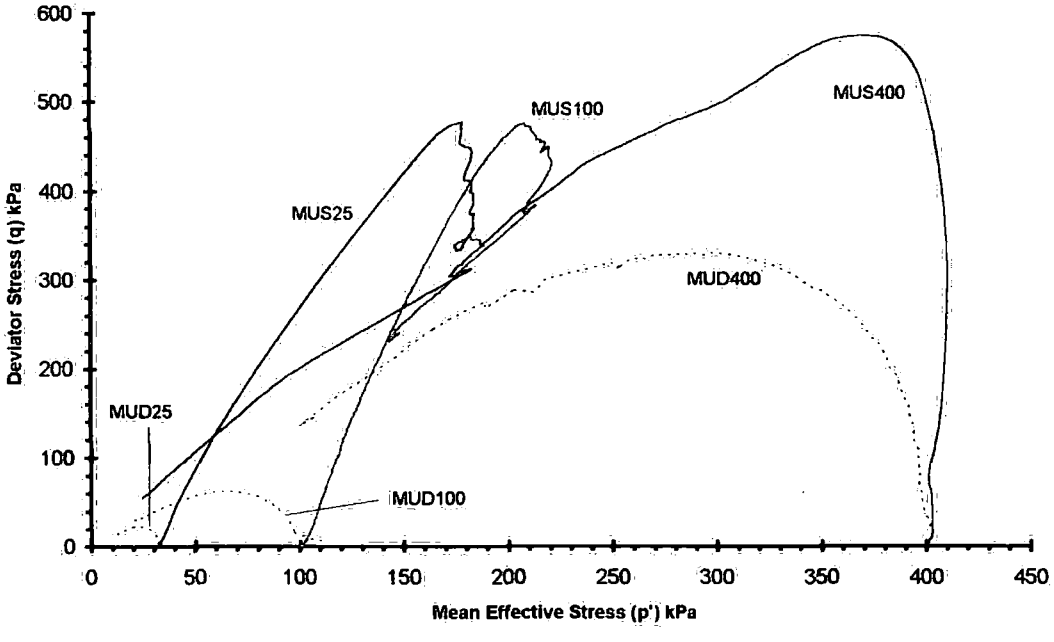

Figure 6-43 Comparison de-structured stress paths and structured stress paths for undrained triaxial tests on fly ash mortar specimen

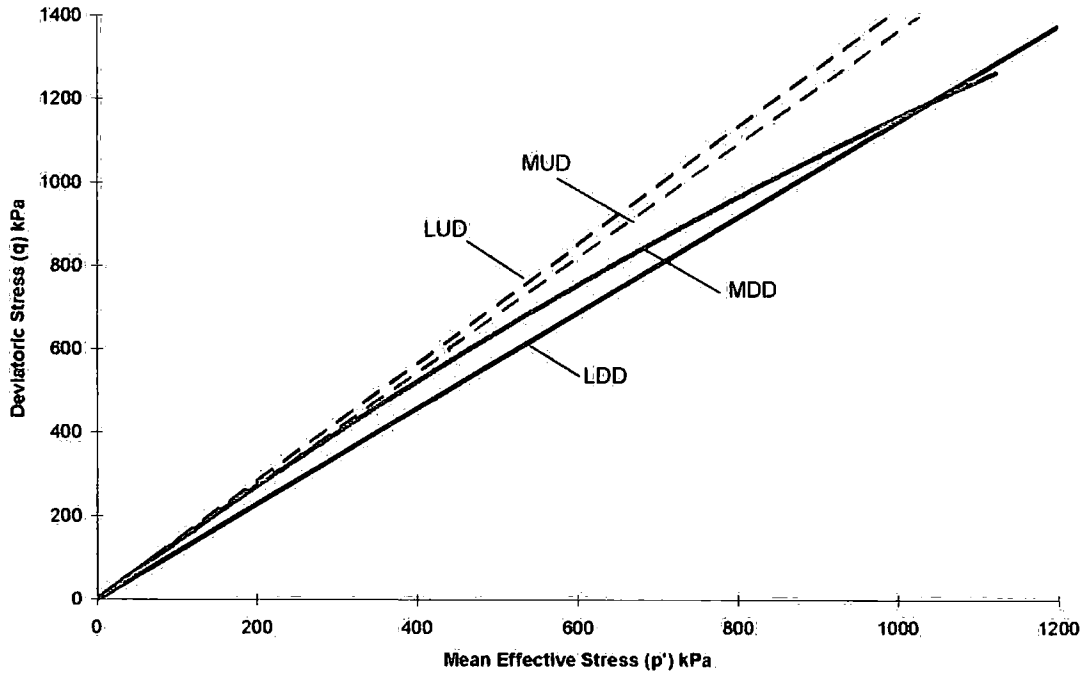

Figure 6-44 Boundary surfaces for fly ash specimens under drained triaxial conditions

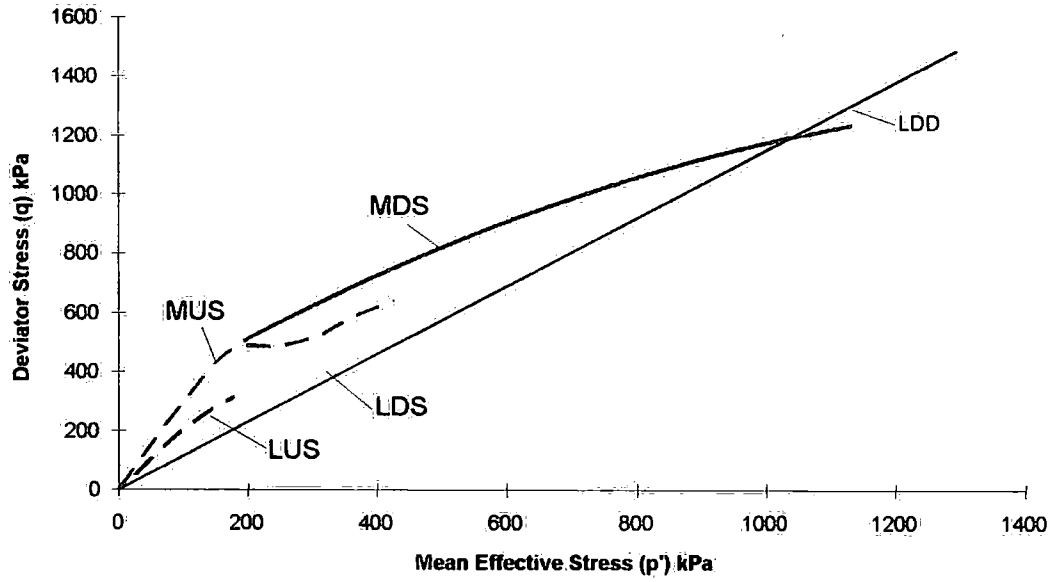

Figure 6-45 Boundary surfaces for bonded specimen

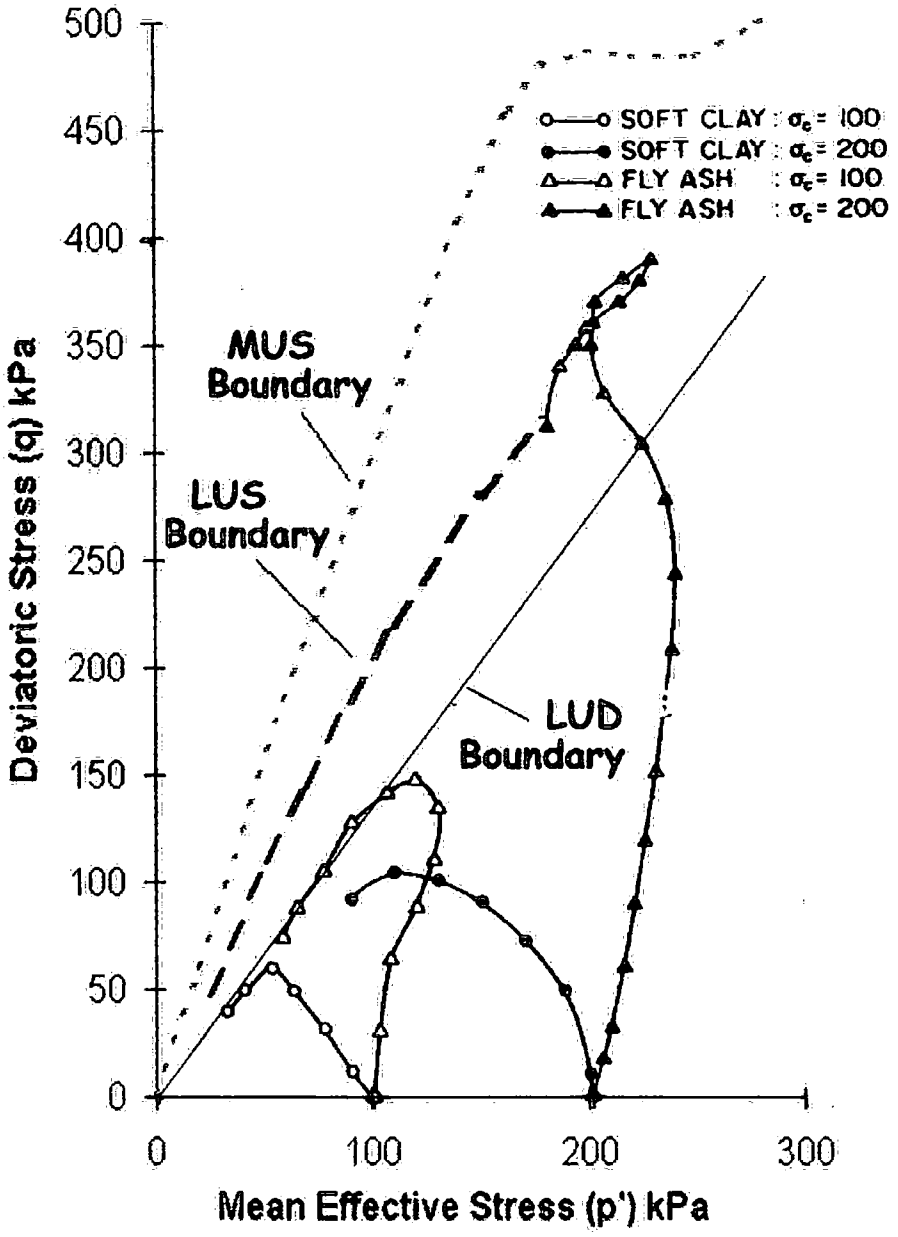

Figure 6-46 Comparison of the boundaries derived for LUD, LUS and MUS tests against test result by Inraratne et al (1991)

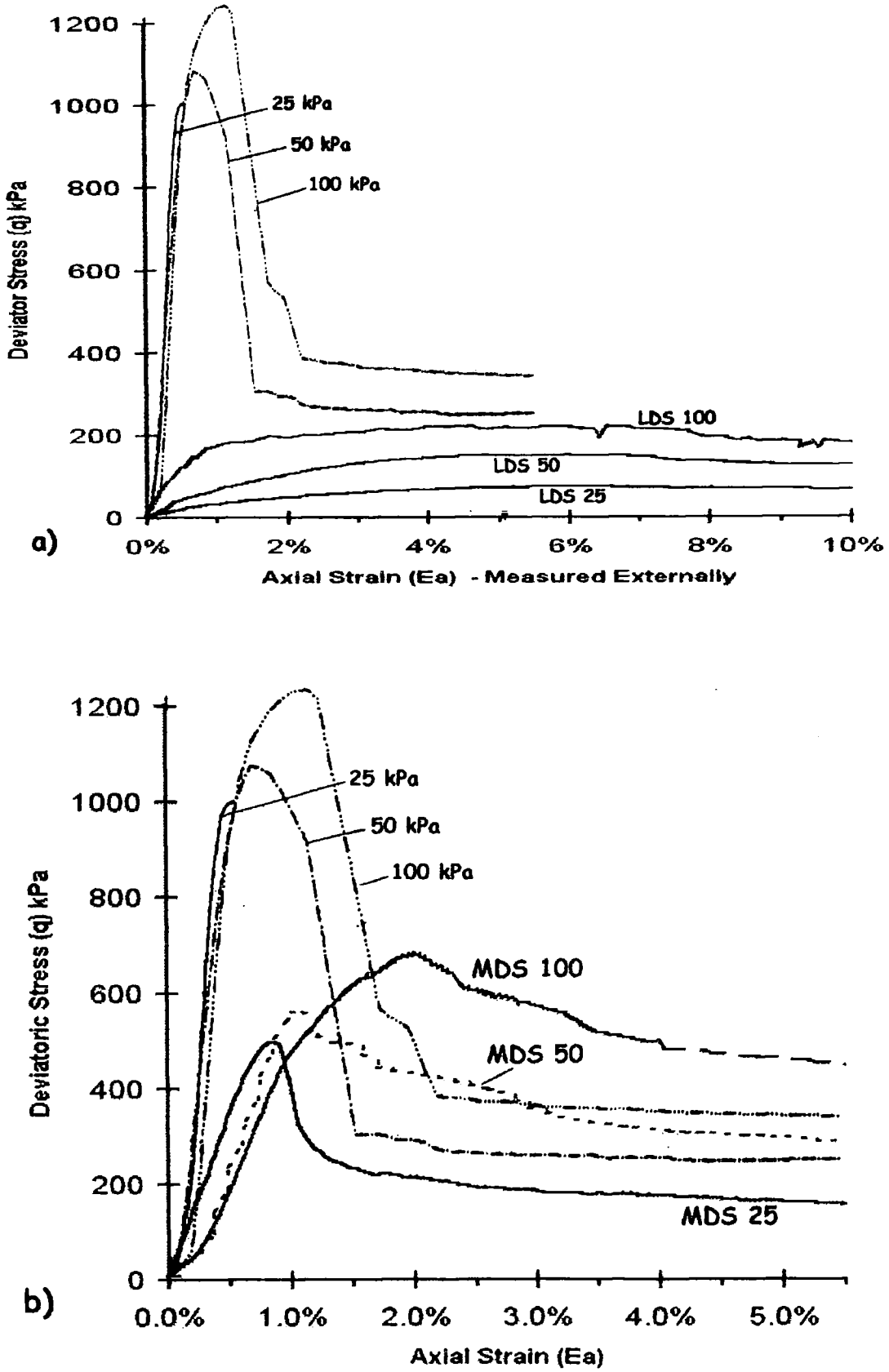

Figure 6-47 Comparison of a) LDS tests and b) MDS tests at equivalent confining pressures to the stress-strain plots for fly ash specimens of dry fly ash from Blyth power station (compacted to 95% dry of its optimum moisture content and allowed to cure for 2 months (Yang 1992)).

7. Conclusions

7.1 Lagoon fly ash at Ferrybridge

The primary aim of this research was to assess the pozzolanic activity, thought to be widespread throughout the pfa lagoons, at Ferrybridge. In addition the pozzolanic effects were to be characterised for comparison with the behaviour of other soils previously studied for their bonding characteristics.

The results of triaxial, oedometer and index tests on specimens of fly ash originating from lagoon 5L at Brotherton Ings demonstrated that there were signs of pozzolanic activity. However, the effects of the pozzolanic action were weak, showing only small gains in strength and stiffness, with small reductions in ductility. In addition, the activity was sporadic within and between samples, and usually occurred in thin weak horizons. It is probable that the pozzolanic activity was confined to specific horizons because of the formation of the lagoon from a number of discrete outwash events.

Tests on remoulded fly ash specimens showed consistent changes in strength, volume change and changes in pore water pressure. In stress space the tests defined linear boundaries with equivalent friction angles of 28° and 34.6° for drained and undrained conditions respectively. By combining results of triaxial and oedometer tests of remoulded specimens it was possible to define the linear critical state line for the lagoon fly ash.

Of the 24 triaxial specimens tested during this phase of the work only 7 were characterised as possessing pozzolanic activity that had influenced their character and strength. Despite the limited number of triaxial tests on pozzolanic-affected samples, it was possible to demonstrate the response of these bonded specimens over a range of confining pressures from 50 kPa to 800kP. At low confining pressures bonded undisturbed specimens were seen to be stronger, stiffer and more brittle than the remoulded counterparts. With increased confining pressure the bonded undisturbed specimens became more ductile and showed less gain in stiffness and strength. At 800 kPa there was little to distinguish between the undisturbed and remoulded specimens. At this confining pressure the pozzolanic bonding had negligible effect and the material can be considered as being unbonded.

In the study of bond yielding a number of different identification methods were employed. The results showed that no one of the methods could be used to assess yielding adequately on its own. It was possible to map the yielding of pozzolanic bonding in stress space. The first and second yield loci indicated that the bonding in the lagoon specimens had an anisotropic nature. This anisotropy can be associated with the layered structure of the undisturbed material. In the majority of the triaxial tests many yield points were observed, which showed their uneven nature as different areas of the specimen yielded at different stress levels

Drained and undrained triaxial tests were conducted on undisturbed, bonded specimens, at the same strain rates. Only a limited number of undrained test results

was achieved. At confining pressures below 200 kPa the pore water pressure in the undrained tests appeared to reduce the bonding influence significantly.

7.2 Artificial fly ash – lime specimens

During the first phase of the work, on samples of lagoon fly ash, pozzolanic activity was found to be weak and randomly dispersed, within laminations. Only a small number of the lagoon fly ash specimens demonstrated pozzolanic activity. In consequence, the project was extended to a study of the full potential of pozzolanic activity, by the manufacture and testing of artificial specimens of a mortar of fly ash and hydrated lime.

Mortar specimens were found to attain a relatively stable state after curing in 100% humid conditions for 6-8 weeks. Triaxial tests were conducted on bonded and on de-structured specimens. The bonded specimens showed significant gains in strength and stiffness, which were much greater than those on the lagoon ash. The triaxial tests on bonded specimens again demonstrated the effects of confining pressure. The bonding was observed to be degraded by confining pressures of 800 kPa, in a similar fashion to tests on lagoon ash. This suggests an upper limit for the pozzolanic bonding.

Results of undrained and drained triaxial tests on mortar specimens showed that the pore water pressures in the undrained tests reduced the influence of bonding. These were also seen in the lagoon fly ash tests and suggest this is a feature of fly ash.

The critical state parameters derived from the lagoon fly ash were shown to fit the triaxial results of the mortar specimens as well, suggesting that the critical state parameters defined could be applied to fly ash in general.

De-structured specimens formed of broken down fly ash/lime mortar were used to characterise the unbonded material. Unfortunately the de-structuring process used did not remove all pozzolanic bonding from the mortar, as was achieved in the remoulded lagoon fly ash. Instead partial bonding remained in the form of aggregated clumps of grains, which degraded with increasing confining pressure.

Although the mortar specimens had critical state parameters similar to those of the lagoon ash, there were some major differences between the two materials.

The yield patterns observed for the mortar specimens showed an isotropic nature to the bonding framework, indicating that the bonding was distributed uniformly throughout the specimens. It was also possible to identify a total yield locus for the mortar specimens, which could not be identified for the lagoon ash specimens. The yield loci showed that bonding within the structured specimens was isotropic

7.3 Suggestions for further work

This research has identified a number of areas for further investigation, which include;

i) A more systematic study of storage lagoons to investigate patterns of pozzolanic bonding within them

ii) A series of one-dimensional consolidation tests to to study the cosolidation characteristics of fly ash.

iii) An investigation into the effect of excess pore water pressures on pozzolanic bonding and how it reduces its influence in stress space

iv) A study of the relationship of the points of maximum stress ratio$(q/p')_{max}$ and maximum rate of change in pwp $(du/dEa)_{max}$ to help understand their relevant positions to one another.

v) An investigation to find the best method for breaking down pozzolanic bonding within bonded fly ashes.

vi) An investigation into better methods of forming artificial pozzolanically bonded fly ash specimens and how best to achieve consistent void ratios.

vii) A study of the potential of using fly ash samples, cured under pressure, to investigate the effects of pressures release on weakly bonded soils when removed from the ground for laboratory testing.

References

Ackerly, S.K., Hellings, J.E., and Jardine, R.J., (1987), *"Discussion on 'A new device for measuring local axial strains on triaxial specimens'."*, Geotechnique, Vol.37, No.3, pp413-417

Alarcon-Guzman, A., and Leonards, G.A., (1988), *"Undrained monotonic and cyclic strength of sands"*, Journal of Geotechnical Engineering and American Society of Civil Engineers, Vol.114, No.10, pp1089-1109

Allman, M.A. and Atkinson, J.H. (1992) *"Mechanical properties of reconstituted Bothkennar soil"*, Geotechnique, Vol.42, No.2, pp289-301

Atkinson, J.H. (1994), *"An introduction to the mechanics of soils and foundations"*, London New York : McGraw-Hill

Atkinson, J.H. and Bransby, P.L. (1978) *"The mechanics of soils"*, London: McGraw-Hill

Atkinson, J.H. and Evans, J.S. (1985), *"The measurement of soil stiffness in the triaxial apparatus - discussion"*, Geotechnique, Vol.35, No.3, pp378-382

Ball, M., (1995) Brotherton Ings Site Engineer, personal communication.

Been, K., Jefferies, M.G., and Hachey, J., (1991), *"The critical state of sands"*, Geotechnique, Vol.41, No.3, pp365-381

Begemann, H.K.S.Ph, (1961), *"A new method for taking samples of great length"*, Proceedings of the International Conference on Soil Mechanics and Foundation Engineering, Paris, Vol.1, pp437-440

Bishop, A.W. and Wesley, L.D. (1975), *"An introduction to the mechanics of soils"*, London : McGraw-Hill

Bressani, L.A. (1990), *"Experimental properties of bonded soils"*, PhD Thesis, University of London

Bressani, L.A., and Vaughan, P.R., (1989), *"Damage to soil structure during triaxial testing"*, 12th International Conference on Soil Mechanics and Foundation Engineering, Rio, Brazil

Bullen & Partners Consultant Engineers, (1996), *"A1 motorway Ferrybridge to Hook Moor section - Geotechnical Interpretative Report"*, Vol.4, Highways Agency

Burland, J.B. (1989), *"9th Laurits-Bjerrum-Memorial-Lecture - small is beautiful - the stiffness of soils at small strains"*, Canadian Geotechnical Journal, Vol.26, No.4, pp499-516

Carson, P.A. and Mumford, C.J. (1994), *"Hazardous Chemical Handbook"*, Oxford: Butterworth-Heinmann

Cassagrande, A., (1988), *"Liquefaction and cyclic deformations of sands"*, Proceedings of the 5th Pan American Conference on Soil Mechanics, Buenos Aires, Vol.5, pp80-113

Castro, G. (1969), *"Liquifaction of Sand"*, PhD thesis, Division of Engineering and Applied Physics, Harvard University

Clark, R.G., Haws, E.T. and Stephen, M.. (1985), *"Mining subsidence beneath pfa disposal lagoons at Brotherton-Ings, Yorkshire"*, 3rd Int. Conf. on Ground Movement and Structures, Ch.57, pp281-297

Clayton, C.R.I., Hight, D.W. and Hopper, R.J. (1992), *"Progressive destructuring of Bothkennar clay - implications for sampling and reconsolidation procedures"*, Geotechnique, Vol.42, No.2, pp219-239

Clough, G.W., Sitar, N., Bachus, R.C. and Rad, N.S. (1981), *"Cemented sands under static loading"*, Journal of Geotechnical Engineering-ASCE, Vol.107, No.GT6, pp799-817

Coop, M.R., and Atkinson, J.H., (1993), *"The mechanics of cemented carbonate sands"*, Geotechnique, Vol.43, No.1, pp53-67

Cuccovillo,T. and Coop, M.R., (1993) *"The influence of bond strength on the mechanics of carbonate soft rocks"*, Proc. of an Int. Symp on the geotechnical engineering of hard soils/soft rocks, Vol.1, pp447-456

Cuccovillo,T. and Coop, M.R., (1997), *"Yielding and pre-failure deformation of structured sands"*, Geotechnique, Vol.47, No.3, pp491-508

Das, B.M., Yen, S.C., and Dass, R.N., (1995), *"Brazilian tensile-strength test of lightly cemented sand"*, Canadian Geotechnical Journal, Vol.32, No.1, pp166-171

Exploration Associates, (1995), *"A1 motorway Ferrybridge to Hook Moor- Factual Report on Ground investigation"*, Report 133083,

Foundation and Exploration Services Limited (1992), *"Deparment of Transport Brotherton Ings PFA Lagoons, Castleford, West Yorkshire - Factual report on site investigation"*, Contract No: 2045.

Gray, D.H., and Lin, Y.K., (1972), *"Engineering properties of compacted fly ash"*, Proceedings of the American Society of Civil Engineers, Vol.98, No.SM4, April

Goh, A.T.C., and Tay, J, (1990), *Municipal solid-waste incinerator fly ash for geotechnical application"*, Journal of Geotechnical Engineering, Vol.119, No.5, May, pp811-825

Hardin, B.O., (1987), *"1-D strain in normally consolidated cohensionless soils"*, Journal of Geotechnical Engineering of the Ammerican Society of Civil Engineers, Vol.113, No.12, pp1449-1467

Head, K.D., (1982), *"Manual of soil laboratory testing"*, Vol.3, London: Pentech Press

Helmuth, R.A., (1987), *"Fly ash in cement and concrete"*, Portland Cement Association, USA

Hight, D.W., Bond, A.J., and Legge, J.D., (1992), *"Characterization of the Bothkennar clay - an overview"*, Geotechnique, Vol.42, No.2, pp303-347

Hjelmar, O., (1990), *"Leachate from land disposal of coal fly ash"*, Waste Management & Research, Vol.8, pp429-449

Indraratna, B., Balasubramaniam, A.S., and Khan, M.J., (1995), *"Effect of fly-ash with lime and cement on the behavior of a soft clay"*, Quarterly Journal of Engineering Geology, Vol.28, Pt2, pp131-142

Indraratna, B., Nutalaya, P., Koo, K.S., and Kuganenthira, N., (1991), *"Engineering behavior of a low-carbon, pozzolanic fly-ash and its potential as a construction fill"*, Canadian Geotechnical Journal, Vol.28, No.4, pp542-555

Ingles, O.G., (1962), *"Bonding Forces in Soils"*, Australian Road Research Board Proc., Vol.1, Part.2, pp999-1047

Jardine, R.J., Symes, M.J., and Burland, J.B., (1984), *"The measurement of soil stiffness in the triaxial apparatus"*, Geotechnique, Vol.34, No.3, pp323-340

Jardine, R.J., (1992), *"On the kinematic nature of soil stiffness"*, Soils and Foundations, June

Jefferies, M.G., Rogers, B.T., Stewart, H.R., Shinde,S.B., James, D.A., and Williams-Fitzpatrick, S., (1988), *"Island construction in the Canadian Beaufort Sea"*, ASCE Speciality Conference on Hydraulic Fill Structures, Fort Collins, CO., pp810-883

Kuerbis, R., Negussey, D., and Vaid, Y.P., (1988), *"Effect of gradation and fines content on the undrained response of sand"*. ASCE Speciality Conference on Hydraulic Fill Structures, Fort Collins, CO., pp330-345

Leddra, M.J., Jones, M.E., and Goldsmith, A.S., (1993), *"Compaction and shear deformation of a weakly-cemented, high porosity sedimentary rock"*, The engineering geology of weak rocks, Rotterdam: Balkema, Vol.1, pp 45-54

Leonards, G.A., and Bailey, B., (1982), *"Pulverized coal ash as structural fill"*, Journal of the Geotechnical Engineering Division-ASCE, Vol.108, No.4, pp517-531

Leroueil, S., Magnan, J-P., and Tavenas, F., (1990), *"Embankments on soft clays"*, New York : Ellis Horwood

Leroueil, S., and Vaughan, P.R., (1990), *"The general and congruent effects of structure in natural soils and weak rocks"*, Geotechnique, Vol.40, No.3, pp467-488

Liu, M.D., and Carter, J.P., (1999), *"Virgin compression of structured soils"*, Geotechnique, Vol.49, No.1, pp43-57

Ma, W.P., Liu, C.L., Brown, P.W., and Komarneni, S., (1995), *"Pore structures of fly ashes activated by $Ca(OH)_2$ and $CaSO_4 \cdot 2H_2O$"*, Cement and concrete research, Vol.25, No.2, pp417-425

Maccarini, M., (1987), *"Laboratory studies of a weakly bonded artificial soil"*, PhD Thesis, University of London

Malandraki, V., (1994), *"The engineering behaviour of a weakly bonded artificial soil"*, PhD Thesis, University of Durham

Malandraki, V.and Toll, D.G., (1994) *"Yielding of a weakly bonded artificial soil"*, Proc. of the Int. Symp. on Pre-failure deformation characteristics of geomaterials, pp315-320

Manz, O.E., (1984), *"Lime-Fly Ash Stabilization for Road Building"*, Proc. 2nd International Conference on Ash Technology and Marketing, Vol.2, pp505-512

McCarthy, G.J., Johansen, D.M., Thedchanamoorthy, A., Steinwand, S.J., and Swanson, K.D., (1988), *"Characterization of North American Lignite Fly Ashes - II XRD Mineralogy"*, Mat. Res. Soc. Symp. Proc., Vol.113, pp99-105

Minwick, L.J., and Miller, R.H., (1952), *"Lime-Fly-Ash-Soil Compositions in Highways"*, Proc. Highway Research Board, pp511-528

Nagaraj, T.S., Pandian, N.S., and Narasimha, P.S.R., (1998), *"Compressibility behaviour of soft cemented soils"*, Getechnique, Vol.48, No.2, pp281-287

Novello, E.A., and Johnston, I.W., (1995), *"Geotechnical materials and the critical state"*, Geotechnique, Vol.45, No.2, pp223-235

Ohtsuki, H., Nishi, K., Okamoto, T. and Tanaka, S., (1981), *"Time dependent characteristics of strength and deformation of a mudstone"*, Proceedings of the Symposium on Weak Rocks, Tokyo, Vol.1, pp173-180

O'Rourke, T.D., and Crespo, E, (1988), *"Geotechnical Properties of Cemented Volcanic Soil"*, Journal of Geotechnical Engineering, Vol.114, No.10, pp1126-1147

Poulos, S.J., (1981), *"The steady state of deformation"*, Journal of Geotechnical Engineering of the American Society of Civil Engineers, Vol.17, GT5, pp553-562

Rahardjo, H., Lim, T.T., Chang, M.F., and Fredlund, D.G., (1995), *"Shear-strength characteristics of a residual soil"*, Canadian Geotechnical Journal, Vol.32, No.1, pp60-77

Rao, S.M., Sridharan, A., and Ramanath, K.P., (1995), *"Collapse behavior of an artificially cemented clayey silt"*, Geotechnical Testing Journal, Vol.18, No.3, pp334-341

Roscoe, K.H., Schofield, A.N., and Wroth, C.P., (1958), *"On the yielding of soils"*, Geotechnique, Vol.8, No.1, 22-53

Schlorholtz S., Bergeson K., and Demirel T., (1988), *"Monitoring Fluctuations in the Physical and Chemical Properties of High-Calcium Fly Ash"*, Mat. Res. Soc. Symp. Proc., Vol.113, pp107-116

Sangrey, D.A., (1972), *"Naturally cemented sensitive soils"*, Geotechnique, Vol.22, No.1, pp139-152

Saxena, S.K., and Lastrico,R.M., (1978), *"Static Properties of Lightly Cemented Sand"*, Journal of Geotechnical Engineering-ASCE, Vol.104, No.12, pp1149-1164

Schofield, A.N. and Wroth, C.P., (1968) *"Critical state soil mechanics"*, London: McGraw-Hill

Sharma, R.C., Jain, N.K., and Ghosh, S.N., (1992), *"Semi-Theoretical method for the assessment of reactivity of fly ashes"*, Cement and Concrete Research, Vol.23, pp41-55

Sherwood, P.T., (1995), *"Alternative materials in road construction : a guide to the use of waste, recycled materials and by-products"*, London: Thomas Telford

Sherwood, P.T., (1993), *"Soil stabilization with cement and lime"*, London : HMSO

Shi, C.J., and Day, R.L., (1995), *"Acceleration of the reactivity of fly-ash by chemical activation"*, Cement and Concrete Research, Vol.25, No.1, pp15-21

Sivapullaiah, P.V., Prashanth, J.P., and Sridharan, A., (1995), *"Optimization of lime content for fly-ash"*, Journal of Testing and Evaluation, Vol.23, No.3, pp222-227

Sladen, J.A., D'Hollander, R.D., Krahn, J., and Mitchell, D.E., (1985), *"Back analysis of the Nerlerk berm liquefaction slides"*, Canadian Geotechnical Journal, Vol.22, No.4, pp579-588

Smith, P.R., Jardine, R.J., and Hight, D.W., (1992), *"The yielding of Bothkennar clay"*, Geotechnique, Vol.42, No.2, pp257-274

Soil Mechanics Limited, (1996), *"A1 motorway Ferrybridge to Hook Moor supplementary ground investigation"*, Report No.7939

Stevenson, R.J., Collier, J.C., Crashell, J., and Quandt, L.R., (1988), *"Characterization of North American Lignite Fly Ashes I - Chemical Variation"*, Mat. Res. Soc. Symp. Proc., Vol.113, pp87-98

Stroud, M.A., (1971), *"The behaviour of sand at low stress levels in the simple shear apparatus"*, PhD thesis, University of Cambridge, UK

Sutherland, H.B., and Finlay, T.W., (1964), *"A Laboratory Investigation of the Age Hardening Characteristics of Pulverised Fuel Ash"*, University of Glasgow, Dept of Engineering, Research Contract: 01038, Vol.1,

Sutherland, H.B., Finlay, T.W., and Cram, I.A., (1968), *"Engineering and Related Properties of Pulverised Fuel Ash"*, Journal of the Institute of Highway Engineers, Issue.June, pp19-27

Swamy, R.N., (1993), *"Fly-ash and slag - standards and specifications - help or hindrance"*, Materials and Structures, Vol.26, No.164, pp600-613

Tashiro, C., Ikeda, K., and Inoue, Y., (1994), *"Evaluation of pozzolanic activity by the electric-resistance measurement method"*, Cement and Concrete Research, Vol.24, No.6, pp1133-1139

Tatsuoka, F., Sakamoto, M., Kawamura, T., and Fukushima, S., (1986), *"Strength and deformation characteristics of sand in plane strain compression at extremely low pressures"*, Soils Foundations, Vol.26, No.1, 65-84

Taylor, D.W., (1948), *"Fundamentals of soil mechanics"*, New York: John Wiley

Thorne, D.J., and Watt, J.D., (1965), *"Composition and Pozzolanic Properties of Pulverised Fuel Ash I - Composition of fly ashes from some British Power stations and Properties of their Component Particles"*, Journal of Applied Chemistry, Vol.15, pp585-594

Thorne, D.J., and Watt, J.D., (1965), *"Composition and Pozzolanic Properties of Pulverised Fuel Ash II - As determined by crushing strength tests on Lime mortars"*, Journal of Applied Chemistry, Vol.15, pp595-604

Toll, D.G., (1993) *"A computer control system for stress path triaxial testing"*, 5th Int. Conf. on Civil and structural engineering computing, Edinburgh, pp107-113

Toll, D.G. and Malandraki, V., (1993) *"Triaxial testing of a weakly bonded soil"*, The engineering geology of weak rocks, Rotterdam: Balkema, Vol.1, pp817-823

Toth, P.S., Chan, H.T., and Cragg, C.B.(1988), *"Coal ash as structural fill, with special reference to Ontario experience"*, Canadian Geotechnical Journal, Vol.25, pp694-704

Uriel, S., and Seranno, A.A. (1973), *"Geotechnical Properties of two collapsible Volcanic Soils of Low Bulk Density at the Site of two Dams in Canary Islands (Spain)"*, 8th Int. Conf. on Soil Mech. FE, Vol.42, No.4, pp257-264

Vaid, Y.P., Chung, E.K.F., and Keubris, R.H., (1990), *" Stress path and steady state"*, Canadian Geotechnical Journal, Vol.27, No.1, pp1-7

Vargas, M., (1953), *"Some Engineering Properties of Residual Clay Soils Occuring in Southern Brazil"*, Proc. 3rd Int. Conf. Soil Mechanics, Vol.1, pp39-62

Vaughan, P.R., and Kwan, C.W., (1984), *"Weathering, structure and in situ stress in residual soils"*, Geotechnique, Vol.34, No.1, pp43-59

Vaughan, P.R., (1985), *"Mechanical and hydraulic properties of insitu residual soils"*, 1st Int. conf. in Geomechanics in TTropical Lateritic and Saprolitic Soils, Vol.session 2, No.3, pp231-263

Vaughan, P.R., Maccarini, M., and Mokhtar, S.M., (1988), *"Indexing the engineering properties of residual soil"*, Quarterly Journal of Engineering Geology, Vol.21, pp69-84

Wallace, K.B, (1973), *"Structural behaviour of residual soils of the continually wet Highlands of Papua New Guinea"*, Geotechnique, Vol.23, No.2, pp203-218

Watt, J.D., and Thorne, D.J., (1966), *"Composition and Pozzolanic Properties of Pulverised Fuel Ash III - As determined by Chemical Methods"*, Journal of Applied Chemistry, Vol.16, pp33-39

Wesche, K., (1994), *"Fly Ash in Concrete - Properties and Performance"*, Rilem, Chapman & Hall

Wood, D.M., (1992), *"Soil behaviour and critical state soil mechanics"*, Cambridge : Cambridge University Press

Wroth, C.P., and Bassett, R.H., (1965), *"A stress-strain relationship for the shearing behaviour of a sand"*, Geotechnique, Vol.15, No.1, pp32-56

Yang, Y., (1992), *"Study of the Mechanical Properties of Pulverised Fuel Ash for Use in Geotechnical Applications"*, PhD Thesis, University of Newcastle upon Tyne.

Zhu, F.Y., Clark, J.I., and Paulin, M.J., (1995), *"Factors affecting at rest lateral stress in artificially cemented sands"*, Canadian Geotechnical Journal, Vol.32, No.2, pp195-203